THE STRUCTURE OF TEMPERATURE AND HUMIDITY TURBULENT FLUCTUATIONS IN THE STABLE SURFACE LAYER

A Dissertation
Presented to the Faculty of the Graduate School
of Cornell University
in Partial Fulfillment of the Requirements for the Degree of
Doctor of Philosophy

by

Nelson Luís Dias

January 1994

THE STRUCTURE OF TEMPERATURE AND HUMIDITY FLUCTUATIONS IN THE STABLE SURFACE LAYER

Nelson Luís Dias, Ph.D.

Cornell University 1994

Most of the information regarding the behavior of scalars in the turbulent atmospheric boundary layer is derived from temperature measurements. It is generally assumed that other scalars behave "in the same way", i.e., that they have the same statistical behavior and turbulent transport properties as temperature. Both theoretical and experimental evidence has been presented in the literature suggesting that this simple picture might not be valid under stable stratification conditions. The evidence, however, is often contradictory (for instance, the ratio of the eddy diffusivities of heat and water vapor has been found to be both larger and smaller than one in different experiments). Under the validity of Monin-Obukhov similarity conditions (stationarity and surface uniformity), the budgets for the turbulent temperature and humidity variances and covariance are used to show that they indeed have a similar behavior, with very small discrepancies due to their different molecular diffusivities. Besides explicitly assessing the molecular effects, it is also shown how earlier theoretical analysis can be reconciled. Analysis of atmospheric turbulence data measured during nocturnal periods confirms this similarity, except in one night when large-scale advective processes associated with frontal activity cannot be ruled out. It is also shown that the dimensionless temperature and humidity statistics are essentially constant with stability, validating the hypothesis of vertical homogeneity under stable conditions. Analogous results are obtained from spectral analysis, which also shows how part of the experimental discrepancies may be attributed to the spatial separation of the temperature and humidity sensors. Higher-order scalar cospectra (whose integral yields the third moment) are calculated for the first time, and shown to follow a Kolmogorov-Corrsin type of power law in the wavenumber, with a -2 exponent. Radiative effects on the temperature spectra are also studied; it is shown that under common conditions close to the surface, radiation has a very minor effect; non-dimensionalization of the temperature spectral budget on the other hand discloses a simple dimensionless parameter which can be readily used to estimate the importance of radiation on an individual basis.

BIOGRAPHICAL SKETCH

The author was born in Rio de Janeiro, Brazil, in 1961. As he grew up in that city, he can remember his fascination with the tropical thunderstorms, the waves breaking at the beach, and the turbulent creeks winding their way down the steep slopes of the green mountains that come so close to the sea that they touch it, making Rio such a beautiful and unique place. At the age of 17, he had to choose between studying Literature or Engineering. He chose the second, partly to follow his father's steps, and partly because he suspected that the poems he wrote might not be a solid foundation for his livelihood. He graduated in 1984 as a Civil Engineer from the Federal University of Rio de Janeiro (UFRJ), where he also got a M.Sc. in Civil Engineering in 1986. Between 1985 and 1989, he worked as a researcher at the Electric Energy Research Center (CEPEL), a lecturer of Fluid Mechanics at the Brazilian Army's Military Institute of Engineering (IME), a lecturer of Transport Phenomena in the School of Engineering of UFRJ and was a member of the faculty of the Graduate School of Engineering of UFRJ. He came to Cornell in August, 1989, to pursue a Ph.D. degree in Civil and Environmental Engineering. He has a few other interests in life: good Literature and History books, Bossa Nova and Rock and Roll music, going to the beach in São Pedro and Cabo Frio (small cities to the north of Rio), and preparing *Caipirinha*, a drink made with cachaça (a spirit distilled out of sugar cane), sugar, lime and ice. And every now and then, when the situation is conducive to it, he still writes poems.

Amanhã será um lindo dia
da mais louca alegria
que se possa imaginar

Amanhã redobrada a força
prá cima que não cessa
há de vingar

Amanhã mais nenhum mistério
acima do ilusório
o astro-rei vai brilhar

Amanhã a luminosidade
alheia a qualquer vontade
há de imperar
há de imperar

Amanhã está toda a esperança
por menor que pareça
que existe é prá vicejar

Amanhã apesar de hoje
será a estrada que surge
prá se trilhar

Amanhã mesmo que uns não queiram
será de outros que esperam
ver o dia raiar

Amanhã ódios aplacados
temores abrandados
será pleno
será pleno

Guilherme Arantes

Em memória de Nelson Mariano Costa, vovô Nelson, Vovoieco, Voieco: suas estórias fantásticas de Fords Bigode e nuvens de gafanhotos nas fazendas de sua infância, e do Rio do começo do século XX ainda vivem na minha lembrança. Seu exemplo de vida também.

ACKNOWLEDGEMENTS

Dr. Wilfried Brutsaert advised this research, as well as all of my activities as a graduate student at Cornell, with a mix of gentleness and understanding of human inevitable limitations (in this case, mine), and a firm adherence to scientific rigor. It has been a privilege, and a pleasure, to have his guidance.

Dr. Zelman Warhaft cooperated closely with most aspects of this research as a Minor advisor. The results in Chapter 3, the spectral analyses in Chapter 5, and the decision to study radiation in Chapter 6, owe much to our discussions about the possible causes of dissimilarity between scalars.

Drs Timothy Healey and John Lumley, also in my Special Comitee as Minor advisors, were always extremely kind and helpful.

Dr. Marvin Wesely of Argonne National Laboratories provided the turbulence data for the analyses in Chapters 4 and 5. I am indebted to his generosity as well as patience in dealing with my neophyte questions. Dr. Richard Hart, also at ANL, endured an exhaustive exchange of electronic mail with me, while I was trying to find my way through the intricacies of turbulence data analysis.

Dr. Leo Fritschen made his raw Bowen-ratio measurements available to this research, helping in no small way to the data analysis of Chapter 4.

Cameron Wilkens was always eager to answer all my questions about computers and programs. Thanks to him, the data I analyzed were transferred from tapes to disks to disquettes, safely and skillfuly.

Chia-Ren Chu was extremely helpful in pointing me to Bendat and Piersol's book on random data analysis.

All of the staff of Hollister Hall provided a very good working enviroment, where the help needed often came together with smiles and friendliness.

Many friends made life in Ithaca a lot more human and nice, in various languages and accents: Gustavo and Nilza Bodstein, Ísis and Geraldo Rodrigues, Renato and Laura Mattos, Márcia Araújo, Ney and Lélia Oliveira, Heinz and Diva Fill, Marcelo Borba and Anne Keple, Christian Alcalá, Casey Carlstrom, Nuria Hernandez-Mora, not only for the fun we had in parties, barbecues and beers in the Chapter House, but also for the support in difficult times.

And far from here, in the Southern Hemisphere, there were also many people providing the love and strength to carry on: my family (in particular sister "Mary Rose") and so many friends, Guilherme Aboim, Delmiro Torreão, Rodolfo Aboim, Lilian and Marcelo Ribeiro Campos, Fernando and Marisa Vasconcellos. With you, I never lost my "South".

For all the duration of my studies in Ithaca, I was supported by the Brazilian Government, through CNPq (Conselho Nacional de Desenvolvimento Científico e Tecnológico).

TABLE OF CONTENTS

LIST OF TABLES

Chapter 2

Chapter 3

Chapter 4

LIST OF FIGURES

Chapter 6

UNITS, NOTATION AND SYMBOLS

The SI (*Système International*) system of units is used throughout, with two exceptions. Some temperatures are given in degrees Celsius (°C) and specific humidity in grams of water vapor per kilogram of air. This happens mainly in the tables of Chapter 4. In the equations and text, however, SI units are strictly adhered to. In both figures and tables, I follow Adkins's (1987, p. viii) "solidus notation": any physical quantitiy is expressed as the product of a pure number and a unit, such as in

$$\overline{u} = 2.7\,\mathrm{m\,s^{-1}} ,$$

so that in headers of tables and axis labels the units are indicated as $\overline{u}$ / $\mathrm{m\,s^{-1}}$, $\overline{\theta}$ / °C , p / Pa, etc. In some cases, the same symbol is used for different quantities or purposes, such as k as an index (e.g., x_k) and k as wavenumber, or u as velocity and u as a dummy integration variable. Hopefully, the context in which a symbol appears is always clear enough so as to make its meaning unambiguous. A list of the symbols used in this work follows.

Lowercase roman letters

a generic turbulence quantitiy (velocity, temperature, humidity, etc.)

a constant in the expression for the absorption coefficient β_μ in the continuum range

a_j constant in the Malkmus expression for Goody's random line model

$\overline{a}$ mean (in the turbulence sense) of a

$\overline{\overline{a}}$ mean (in the turbulence sense) of a at a second point in space

a' fluctuation (in the turbulence sense) of a

a'' fluctuation (in the turbulence sense) of a at a second point in space

a_* turbulence scale of a

a'_i high-pass filtered data at 0.005 Hz

$\widetilde{a}_i$ low-pass filtered data at 0.005 Hz

$\breve{a}'_j$ high-pass filtered low-freqeuncy data at 0.005 Hz

$\widetilde{\breve{a}}_j$ low-pass filtered low-frequency data at 0.005 Hz

b generic turbulence quantitiy (velocity, temperature, humidity, etc.)

b constant in the expression for the absorption coefficient β_μ in the continuum range

b_j constant in the Malkmus expression for Goody's random line model

c generic turbulence quantitiy (velocity, temperature, humidity, etc.)

c velocity of light in the vacuum

c constant in the expression for the absorption coefficient β_μ in the continuum range

c a parameter in $H(x)$

c_p specific heat of air at constant pressure

c_I closure constant in spectral model for the w, u cospectrum

c_{II} closure constant in spectral model for the w, θ cospectrum

e vapor pressure

e' twice the turbulence kinetic energy

f a generic distribution to be Fourier-transformed

f dimensionless frequency

f two-point cross-covariance in Appendix C

$f_{0,ab}$ position parameter for the dimensionless cospectrum of a, b

f_e low-wavenumber solution of turbulence kinetic energy and temperature spectra

g acceleration of gravity

g two-point cross-covariance in Appendix C

g_i acceleration of gravity in the i-th direction

g_u high-wavenumber solution of turbulence kinetic energy spectrum

g_θ high-wavenumber solution of temperature spectrum

h Planck's constant

i $\sqrt{-1}$

$\mathbf{k}$ wavenumber vector

k_k k-th component of $\mathbf{k}$

k the norm of $\mathbf{k}$

k Boltzmann's constant

ℓ_h local lenght scale (see equation (2.16))

m a parameter in $H(x)$

m_a sample mean of a'_i

n cyclic frequency

n a parameter in $H(x)$

$\mathbf{n}$ a matrix of frequencies

p pressure

p probability of occurence of a value larger than u in a statistical test

p a parameter in $H(x)$

p_* pressure turbulence scale

q specific humidity

$\partial q'$ fluctuating vertical humidity gradient

q_* specific humidity turbulence scale

$\mathbf{r}$ position vector

r distance in space, the norm of $\mathbf{r}$

r_{ab} correlation coefficient between a', b'

r_l l-th component of $\mathbf{r}$

$\mathbf{s}$ direction vector in space

s_k k-th component of $\mathbf{s}$

$s^2_{a,1}$ sample variance of a'_i (see equation (4.4))

$s^2_{a,2}$ sample variance of a'_i (see equation (4.5-a))

t time

u horizontal velocity, longitudinal to the mean wind direction

u quantile of a normal probability distribution used in hypothesis testing

$\partial u'$ fluctuating strain rate in the plane xz

u_i generic turbulence quantity (see equation (2.5))

u_* friction velocity

$\widehat{u}_i$ the Fourier transform of u'_i

v horizontal velocity, transversal to the mean wind direction

w vertical velocity

w_* convective velocity scale

$\mathbf{x}'$ a first point in space

$\mathbf{x}''$ a second point in space

x horizontal coordinate axis longitudinal to the mean wind direction

x $\eta/(20\eta_P)$

x_i coordinate axis in the i-th direction

y horizontal coordinate axis transversal to the mean wind direction

z vertical coordinate axis

z_i height of the atmospheric boundary layer

Uppercase roman letters

A_a dimensionless standard deviation of a'

$A_\perp$ an element of area in space

B_μ Planck's blackbody function

Bo_f flux Bowen ratio

Bo_g gradient Bowen ratio

C integration constant

C capacitance of a circuit

C_H heat transfer coefficient

$C_{i,j}(\mathbf{k})$ cospectrum of u_i', u_j': the real part of $\Phi_{i,j}(\mathbf{k})$

D integration constant

E water vapor surface flux

$E_e(k)$ shell average of twice the turbulence kinetic energy spectrum $\Phi_e(\mathbf{k})$

$E_{i,j}(k)$ shell average of $C_{i,j}(\mathbf{k})$ in wavenumber space

$F(x)$ dimensionless spectral radiative dissipation function

F_a conversion constant for an integer-to-real transformation of turbulence data

$F_{i,j}(k_1)$ one-dimensional (wavenumber) cross-spectrum of u_i', u_j' (superscripts c and q indicate the cospectrum and the quadrature spectrum, respectively)

$\mathcal{F}[\cdot]$ Fourier transform

G ground heat flux

$G(x)$ $x^{-5/3}F(x)$

G_a conversion constant for an integer-to-real transformation of turbulence data

H heat surface flux

$H(x)$ integral of $G(x)$

$\tilde{H}(t)$ an approximation to $H(x)$

H_v virtual heat surface flux

I_a 16-bit integer storage value of a turbulence measurement

I_μ intensity of radiation at wavenumber μ

J_μ thermal emission function

K starting length of averaging for the linear filter in equation (4.3)

K_E eddy diffusivity of water vapor

K_F eddy diffusivity of a, associated with flux F

K_H eddy diffusivity of heat

L latent heat of evaporation

L linear filter width in equation (4.3)

L_B length of a block for the calculation of spectra

L_q Obukhov's stability length for humidity effects

L_{θ_v} Obukhov's stability length for temperature and humidity effects

L_θ Obukhov's stability length for temperature effects

M sample size in the calculation of statistics for a short run

M_v molecular mass of water vapor

N total duration (in points) of a short run

$N(k)$ spectral radiative dissipation function

N_A Avogadro's number

N_* dimensionless parameter describing the relative importance of radiative and turbulent heat transfer

N_∞ asymptotic value of $N(k)$ as $k \uparrow \infty$

Re_* Reynolds number

$P[\cdot]$ notation for probability of an event

Pe_*^θ Péclet number for temperature

Pe_*^q Péclet number for humidity

$Q_{i,j}(\mathbf{k})$ quadrature spectrum of u_i', u_j'; the negative of the imaginary part of $\Phi_{i,j}(\mathbf{k})$

R resistance of a circuit

$\mathbf{R}$ radiative flux vector

R_k k-th component of $\mathbf{R}$

R_n net radiation at the surface

R_v gas constant for water vapor

$\mathbf{S}_{a,b}$ a matrix of cross-spectral densities

$S_{i,j}(n)$ one-dimensional (frequency) cross-spectrum of u_i', u_j' (superscripts c and q indicate the cospectrum and the quadrature spectrum, respectively)

T period

T thermodynamic temperature

T time constant of a linear filter, R–C circuit

T_W period associated with low-frequency data, collected once every $T_W = 0.5$ s

T_μ transmission at wavenumber μ

$\overline{T}_\mu(r)$ average transmission over wavenumber range $\Delta\mu$ centered on μ

$\overline{T}'_\mu(r)$ first derivative of $\overline{T}_\mu$ with respect to r

$\overline{T}''_\mu(r)$ second derivative of $\overline{T}_\mu$ with respect to r

$T_{i,i}(k)$ fluctuating strain rate spectral transfer of u_i

$\mathcal{T}$ characteristic time for the atmospheric boundary layer in Moeng and Wyngaard's pressure closure

$\mathcal{T}$ averaging time required to obtain a certain accuracy in the estimation of third moments

U a random variable

$U_{i,i}(k)$ mean strain rate spectral transfer of u_i

W linear filter width in equation (4.7-a)

$V(t)$ potential difference in an R–C circuit

X starting length of averaging for the linear filter in equation (4.7-c)

Y linear filter width in equation (4.7-c)

Lowercase greek letters

α an integration variable used in Appendix B

α_{ij} inertial subrange Kolmogorov "constant" for the E_{ij} cross-spectrum

α_{ij}^1 inertial subrange Kolmogorov "constant" for the F_{ij}^c one-dimensional cospectrum

β function of ϕ_τ, ϕ_H and ζ in spectral model (see equation (6.36))

β a parameter used in Appendix B

β_P Planck's coefficient

β_μ absorbing coefficient at wavenumber μ

$\delta(\cdot)$ Dirac's delta function

δ_{ij} Kronecker's delta

ϵ desired accuracy in the estimation of third moments

ϵ_{ij} viscous dissipation of the covariance of u_i, u_j

ϵ_e viscous dissipation of turbulence kinetic energy

ϵ_{Ri} radiative dissipation of u_i

$\epsilon_{T\theta}$ total (viscous plus radiative) dissipation of temperature variance

$\varepsilon(t)$ electromotive force in an R–C circuit

ζ Monin-Obukhov similarity variable for stability

ζ_q Monin-Obukhov similarity variable for stability due to humidity

ζ_R Schertzer and Simonin's radiative dimensionless parameter

ζ_θ Monin-Obukhov similarity variable for stability due to temperature

η dimensionless wavenumber

η_1 dimensionless wavenumber corresponding to the x_1 direction

η_P dimensionless Planck wavenumber

θ potential temperature

θ_v virtual potential temperature

θ_* temperature turbulence scale

θ_{v*} virtual temperature turbulence scale

$\partial\theta'$ fluctuating vertical temperature gradient

$\partial\theta'_v$ fluctuating vertical virtual temperature gradient

$\vartheta_{i,j}$ phase function between u'_i, u'_j

κ von Kármán's constant

λ wavelength associated with a period T by Taylor's hypothesis

λ radiative wavelength

μ radiative wavenumber

ν_u molecular diffusivity of momentum in the air

ν_v molecular diffusivity of momentum in the air

ν_w molecular diffusivity of momentum in the air

ν_θ molecular diffusivity of heat in the air

ν_q molecular diffusivity of water vapor in the air

ξ position vector of a second point in space, in Appendix C

ξ_i i-th component of ξ

π the number $3.141592\ldots$

ρ air density

ρ_a density of absorbing material

ρ_v water vapor density

σ Stefan-Boltzmann's constant

σ_a standard deviation of a'

τ momentum surface flux

τ_i integral time scale of a process

$\widetilde{\tau}$ constant in Moeng and Wyngaard's (1986) pressure closure

$\tau_{a,b}$ dimensionless fluctuating strain rate spectral transfer

$\upsilon_{a,b}$ dimensionless mean strain rate spectral transfer

ϕ_{ab} Monin-Obukhov dimensionless function for the covariance of a, b

ϕ_{abc} Monin-Obukhov dimensionless function for the third moment of a, b, c

$\phi_{p\partial a}$ Monin-Obukhov dimensionless function for the covariance of pressure with the gradient of a

ϕ_F Monin-Obukhov dimensionless gradient for $\overline{a}$, associated with the flux F

ϕ_E Monin-Obukhov dimensionless gradient for humidity

ϕ_H Monin-Obukhov dimensionless gradient for temperature

ϕ_{H_v} Monin-Obukhov dimensionless gradient for virtual temperature

$\phi_{\epsilon_{ab}}$ Monin-Obukhov dimensionless function for the dissipation of the covariance of a, b

$\phi_{\epsilon_{R\theta}}$ dimensionless dissipation of temperature variance due to radiation

$\phi_{\epsilon_{T\theta}}$ dimensionless dissipation of temperature variance due to radiation and molecular diffusion

χ an integration variable used in Appendix B

$\psi_{a,b}(\eta)$ dimensionless cospectrum of a, b

$\psi^1_{a,b}(\eta)$ dimensionless one-dimensional cospectrum of a, b

ω solid angle in space

Uppercase greek letters

$\Gamma_{i,j}$ coherence between u'_i, u'_j

$\Phi_{i,j}(\mathbf{k})$ cross-spectrum between u'_i, u'_j

Φ_{F12} an integral associated to the Monin-Obukhov similarity functions ϕ_F between two levels, see equation (4.10)

Chapter 1
INTRODUCTION

This thesis deals with the turbulent transport of heat and water vapor close to the surface of the Earth under stable conditions, i.e.; when the potential temperature increases with height in the air above the surface, implying a downward heat flux (actually, the *virtual* heat flux and temperature, as defined in chapter 2). It is very common for stable conditions to be associated with an upward water vapor flux, so that heat and water vapor are transported in opposite directions. In this case, some theoretical and experimental analyses have cast doubt on the equality of the turbulent transport properties of these two scalars: it has been hypothesized that their "eddy diffusivities" of semi-empirical turbulence theory might not be equal. More generally, they would be "dissimilar" in the sense of their dimensionless turbulent statistical properties being different. Furthermore, it is known that long-wave radiation affects the equations for the mean and the variance of the temperature field, but not their counterparts for the humidity field, and this effect could be important in nocturnal periods. These questions are dealt with here both from the point of view of theory and available equations and that of statistical analysis of field data. We will show that there is strong evidence of perfect similarity between the temperature and humidity fields, and that some of the discrepancies observed in the data can be attributed to instrumental limitations.

1.1 The physical importance of evaporation in stable conditions

The main objective of hydrologists dealing with the aerial part of the hydrologic cycle is to estimate precipitation and evaporation to/from the Earth's surface and water bodies accurately. Evaporation, or surface water vapor flux, is closely linked to surface heat and momentum fluxes, and it is usually necessary to estimate them together. Even though most of the water vapor and heat exchanges over land occur in unstable atmospheric conditions during the day, there are many cases when it is important to study stable conditions. We cite, as examples, large-scale advection of warm air masses, local advection of warm air over colder surfaces, such as irrigation projects surrounded by arid land or lakes, and nocturnal periods.

Thus, the arrival of a warm front and the maintenance of a temperature inversion in the atmosphere for a long period of time, of the order of days, can significantly worsen the air quality in urban and industrial regions, since a stable atmosphere reduces the rate at which pollutants are transported upwards and diffused in the atmosphere.

The quantification of evaporation from vegetated land surfaces and lakes has been the object of continuing study (Penman, 1948; Harbeck, 1962; Brutsaert and Yeh, 1970; Katul and Parlange, 1992), and in arid or semi-arid regions, where availability of water may be severely restricted, it may well be critical. Yet it is exactly in this situation that the advection of warm air can create a locally stable atmosphere.

As for the nocturnal evaporation, it represents a small but important fraction of the total, as Sugita and Brutsaert (1991) have shown: correcting their evaporation figures calculated from radiosoundings during the day to take into account the nocturnal fluxes did improve their estimates compared to 24-hour totals calculated by surface flux stations.

It is also worth mentioning that many greenhouse gases are released in the Atmospheric Boundary Layer (ABL) to diffuse later into the free atmosphere above, and this process is qualitatively similar to that described earlier, whereby water vapor and heat fluxes have opposite directions. In the case of trace gases, their flux at the *top* of the ABL is still "positive" (upwards), whereas the existence of a strong temperature inversion capping the ABL usually implies a negative (downwards) heat flux from the free atmosphere into the ABL, which is of the order of 20% to 40% of the surface heat flux during the day (Deardorff, 1974; Driedonks and Tennekes, 1984; Kustas and Brutsaert , 1987; Stull, 1988).

From the point of view of practical applications, the question of whether or not heat and humidity are similar is therefore extremely important: often, results obtained from temperature measurements are assumed to hold for humidity as well. This hypothesis is also at the heart of most procedures used for calculating surface fluxes other than the direct measurement by the eddy correlation method:

the energy-budget Bowen ratio method, the variance method and several of the heat and mass-transfer methods all rely on the idea that the two scalars are similar (Angus and Watts, 1984; Wesely, 1988; Eichinger *et al.*, 1993).

1.2 A review of experimental and theoretical facts regarding the similarity of heat and water vapor in stable condtions

Stable conditions occur most commonly during the night, when radiative cooling of the surface produces a temperature inversion in and above the surface layer (the layer where the turbulent fluxes do not vary by more than 10% of their surface values). Under these condtitions, it is usually more difficult to estimate fluxes than during the day, i.e., the empirical relationships for dimensionless functions exhibit more scatter for stable than unstable conditions (Brutsaert, 1982, p. 71). This can be attributed in part to the order of magnitude of the nocturnal fluxes (about 10% of the daily values), which is much closer to the expected absolute error of the instruments. Not only that, until now the development of fast-response humidity instruments has lagged behind that of temperature sensors, with the result that in many cases humidity fluctuations and humidity turbulent fluxes have not been measured at all. In the face of this, most of the early studies about water vapor in the surface layer either assumed it to be similar to temperature, or found little difference between them (Phelps and Pond, 1971; Dyer, 1974; Champagne *et al.*, 1977).

During the last 20 years, some theoretical and experimental evidence of dissimilarity between heat and water vapor has been brought up. Warhaft (1976) studied the budgets of temperature and humidity fluxes with the help of closures for the pressure-scalar correlation terms. He suggested that the eddy diffusivities for heat and humidity could be different if the correlation coefficient between temperature and humidity fluctuations were not equal to ± 1. Then, Verma *et al.* (1978) and Lang *et al.* (1983a) measured different eddy diffusivities for heat and humidity; however, the results of Verma *et al.* contradict Warhaft's theory, while those of Lang *et al.* agree only qualitatively. To make the situation a bit more confused, there are also theoretical results pointing to the perfect similarity between heat and humidity: Hicks and Everett (1979) noted that Verma *et al.*'s results could at least be partially explained by different zero-plane displacement heights for the two scalars and measurements too close to the canopy; Brost (1979) pointed out that by using higher-order turbulence closures for the temperature and humidity variance and covariance equations, one is led to the conclusion that the correlation coefficient between heat and humidity is immaterial, and that the eddy diffusivities are equal. Then, Hill (1989a, 1989b) showed that if Monin-Obukhov similarity theory holds for any scalar *and* linear combination of scalars in the surface layer, then the similarity functions for all scalars are equal, and their correlation coefficient is either $+1$ or -1. Bertela (1989), who investigated the apparent failure of the Bowen-ratio method to perform well in some cases involving both stable and unstable conditions, attributed it to local advection. Furthermore, if one considers the radiative term which appears in the variance budget for temperature but not for humidity, then it is clear that radiation can be a source of dissimilarity. Coantic and Simonin (1984) have argued that radiative effects can be important in stable nocturnal boundary layers when the intensity of turbulence (as measured by the turbulence kinetic energy) is small.

To summarize, even though there are two cases (to the author's knowledge) of different eddy diffusivities for heat and humidity actually measured, there are physical causes such as advection or different displacement heights that might explain them, whereas the theoretical framework about the similarity of scalars has been somewhat confusing, with less than unanimous results.

Finally, it is important to assess the behavior of temperature and humidity keeping in mind the wealth of physical phenomena associated with scalars under stable conditions. Examples are the existence of a buoancy subrange (Bolgiano, 1959; Weinstock, 1978; Chiba, 1989), intermittency of turbulence (Kondo *et al.*, 1978; Kunkel and Walters, 1982; Nappo, 1991), interaction with radiation (Brutsaert, 1972; Coantic and Simonin, 1984), scalar mean profiles (Swinbank and Dyer, 1967; Sheppard *et al.*, 1972), spectral behavior as a function of stability (Kaimal *et al.*, 1972; Kaimal, 1973; Priestley and Hill; 1985, Rees, 1991; Wang and Mitsuta, 1991), local advection (Lang *et al.*, 1983b), the effect of topography on the scalar fields (Raupauch *et al.*, 1992) and the overall evolution of the nocturnal stable boundary layer (Kurzeja *et al.*, 1991; Wittich, 1991).

1.3 Outline of work

We have tried to summarize, so far, the most important questions dealt with in this research. Chapter 2 lays down the theoretical aspects of atmospheric turbulence in terms of the equations for mean quantities, for second moments and for spectra and cross-spectra. There, we unify the semi-empirical approach to spectral and cospectral shapes in the atmospheric boundary layer that was proposed a long time ago by Kaimal *et al.* (1972), Wyngaard and Coté (1972) and Kaimal (1973), and improved upon by Moraes and Epstein (1987). Chapter 2 also contains a novel (to the author's knowledge) study of the behavior of higher-order scalar cospectra in the inertial subrange: the time-honored predictions of Kolmogorov (1941) and Corrsin (1954) for the turbulence kinetic energy and scalar spectra is extended to these higher-order cospectra (whose integral yields the third moments of the scalars). A -2 power law in wavenumber k is predicted, which finds confirmation in Chapter 5.

In Chapter 3, we study the controversy about the similarity of temperature and humidity from a theoretical point of view. We use the variance and covariance budgets for temperature and humidity, to show that they indeed are "similar" in the sense defined above, except for slight differences induced by the different molecular diffusivities; in so doing, it is also possible to reconcile some apparent contradictions between earlier works.

Chapter 4 presents an extensive analysis of turbulence data in stable conditions. We used turbulent records of vertical and horizontal wind speed, temperature and humidity measured during nocturnal periods by a team of Argonne National Laboratory (ANL) led by Dr. Marvin Wesely, which were gratiously made available for this research. There, we make an in-depth analysis of those similarity functions that can be calculated with data measured at one level only; we confirm the simple forms of the scalar budgets predicted for homogeneous turbulence and often assumed in stable conditions, and that temperature and humidity indeed show a high degree of similarity, except for one of the nights analyzed.

Chapter 5 presents the results of the spectral analysis of turbulence data from 36 52-min periods measured during 6 nights in August, 1989. In this analysis, we have been able to detect dissimilarities between temperature and humidity on the night of August 03rd, in connection with the passage of a front. For the remaining nights, however, temperature and humidity spectra and cospectra with vertical velocity are remarkably similar. The coherence between them is also very close to +1, and the phase to $\pm 180^\circ$, as predicted by Hill (1989a) and in chapter 3. Although coherence falls off in the higher-frequency range, this can be attributed to the spatial separation of the sensors. Indeed, CO_2 coherence spectra measured elsewhere (Montcrieff *et al.*, 1992) by two co-located sensors measuring the *same* scalar, whose correlation with itself, obviously, is 1, show the same behavior. Finally, the prediction that higher-order scalar cospectra have an inertial subrange with a slope of -2, developed in chapter 2, is confirmed with temperature data.

In Chapter 6, we perform a somewhat after-the-fact investigation on how much radiative effects can change the above picture of perfect similarity. A simple spectral model is used to calculate dimensionless temperature spectra as a function both of stability and radiative parameters; in rendering the spectral equations dimensionless we arrive at two dimensionless parameters which describe the influence of radiation and present their interpretation as the ratio of two physical processes, as is usual. Moreover, formerly complicated equations for the radiative terms are greatly simplified into dimensionless empirical functions, which allows most of the results to be presented in analytical form. The main conclusion in this chapter is that radiation is unlikely to play an important role in the stable surface layer, but in any case we show how the importance of radiation can easily be assessed by one of the aforementioned dimensionless parameters.

Chapter 7 summarizes the results and presents some further comments and recommendations for future research.

Appendix A presents the connection between a linear recursive filter and an analog sensor with limited time response.

Appendix B presents a derivation of the spectral radiative dissipation function extensively used in chapter 6.

Appendix C presents a derivation of two-point equations of turbulent flow.

Chapter 2
ATMOSPHERIC TURBULENCE

This chapter contains most of the theoretical framework for turbulence in the stable surface layer relevant to this research. The equations for means and second moments of turbulent quantities, which are standard, are written down in a compact notation used, in a different context, by Kader (1993). We introduce formally the usual Monin-Obukhov assumptions of stationarity and surface uniformity. The turbulent scales u_*, θ_* and q_* for velocity, temperature and humidity are then defined, and the corresponding dimensionless equations and Monin-Obukhov similarity functions are obtained. We then proceed to define cross-spectra and spectra, and their corresponding equations in homogeneous turbulent flow. The inertial subrange relationships are reviewed, and some results are extendend for the cospectrum of the fluctuation of a scalar and its square; these spectral relationships are also cast in dimensionless form, with some new predictions for dimensionless cospectra, and all dimensionless spectra and cospectra in the inertial subrange are shown to depend on a few similarity functions.

2.1 The equations of turbulent flow in the surface layer

The physical quantities usually measured in the atmosphere close to the surface are wind velocity with components (u, v, w), potential temperature θ and specific humidity q. We shall assume that both θ and q are active scalars, being responsible for changes in the air density ρ. That effect is incorporated into the equations by means of the virtual potential temperature

$$\theta_v \equiv \theta(1 + 0.61q) \; . \tag{2.1}$$

From here on, we will often refer to θ and θ_v as "temperature" and "virtual temperature" only, dropping the adjective "potential". Notice that close to the surface potential temperature and temperature are nearly identical. In some cases, when the *absolute* temperature is needed, it will be refered to explicitly and denoted by T. If a is any of the variables above, we adopt the Reynolds decomposition

$$a(t) = \overline{a}(t) + a'(t) \tag{2.2}$$

where the turbulent fluctuations $a'(t)$ are assumed to be a stationary process with zero mean (Lumley and Panofsky, 1964; Lumley, 1970a; Tennekes and Lumley, 1972; Todorovic,1990). The corresponding view of $a'(\mathbf{r})$ as a homogeneous stochastic process in space will be adopted when working with spectral equations. From (2.1) and (2.2) the virtual temperature fluctuations are

$$\theta_v' = (1 + 0.61\overline{q})\theta' + 0.61\overline{\theta}q' \tag{2.3}$$

if products of fluctuations are neglected.

In addition to the fluctuations of (u, v, w), θ, q and θ_v, it is also necessary to consider the fluctuations of some derived quantities, such as the fluctuation of twice the turbulence kinetic energy e'; the fluctuating strain rate in the plane xz $\partial u'$; the fluctuating vertical temperature gradient $\partial\theta'$, the fluctuating vertical humidity gradient $\partial q'$ and the fluctuating vertical virtual temperature gradient $\partial\theta'_v$:

$$e' \equiv u'u' + v'v' + w'w' \tag{2.4-a}$$

$$\partial u' \equiv \left(\frac{\partial u'}{\partial z} + \frac{\partial w'}{\partial x}\right) \tag{2.4-b}$$

$$\partial\theta' \equiv \frac{\partial \theta'}{\partial z} \tag{2.4-c}$$

$$\partial q' \equiv \frac{\partial q'}{\partial z} \tag{2.4-d}$$

$$\partial\theta'_v \equiv \frac{\partial \theta'_v}{\partial z} \; . \tag{2.4-e}$$

The equations for mean quantities and covariances in the atmosphere are well known (Stull, 1988). We adopt the following convention:

$$u_1 = u \qquad x_1 = x \tag{2.5-a}$$

$$u_2 = v \qquad x_2 = y \tag{2.5-b}$$

$$u_3 = w \qquad x_3 = z \tag{2.5-c}$$

$$u_4 = \theta \qquad x_4 = 0 \tag{2.5-d}$$

$$u_5 = q \qquad x_5 = 0 \; . \tag{2.5-e}$$

We will also denote the molecular diffusivities of momentum, heat and water vapor by $\nu_u = \nu_v = \nu_w$, ν_θ and ν_q, respectively. It is then possible to write *all* equations for the mean quantities as

$$\frac{\partial \overline{u}_i}{\partial t} + \overline{u}_k \frac{\partial \overline{u}_i}{\partial x_k} + \frac{\partial \overline{u_i u_k}}{\partial x_k} = -\frac{1}{\overline{\rho}} \frac{\partial \overline{p}}{\partial x_i} + g_i + \nu_{u_i} \frac{\partial^2 \overline{u}_i}{\partial x_k \partial x_k} - \delta_{i4} \frac{1}{\overline{\rho} c_p} \frac{\partial \overline{R}_k}{\partial x_k} \tag{2.6}$$

where g_i is the acceleration of gravity in the direction of x_i, R_k is the component of the radiative flux vector in the direction x_k, p is pressure and the Coriolis acceleration, which is very small close to the surface, is neglected. We also adopt the convention that a repeated index k or l in a term implies summation for $k = 1, 2, 3$, $l = 1, 2, 3$. On the other hand, the appearance of a repeated i or j *does not* imply summation in the ensuing equations in this chapter. Notice that Kronecker's delta δ_{i4} indicates that the divergence of the mean radiative flux appears in the equation for $u_4 = \theta$ only. The equations for the fluctuations are

$$\begin{aligned} \frac{\partial u'_i}{\partial t} + \overline{u}_k \frac{\partial u'_i}{\partial x_k} + u'_k \frac{\partial \overline{u}_i}{\partial x_k} + \frac{\partial u'_i u'_k}{\partial x_k} &= -\frac{g_i}{\overline{\theta}_v} \theta'_v - \frac{1}{\overline{\rho}} \frac{\partial p'}{\partial x_i} + \nu_{u_i} \frac{\partial^2 u'_i}{\partial x_k \partial x_k} \\ &+ \frac{\partial \overline{u'_i u'_k}}{\partial x_k} - \delta_{i4} \frac{1}{\overline{\rho} c_p} \frac{\partial R'_k}{\partial x_k} \; . \end{aligned} \tag{2.7}$$

Continuity of the mean and fluctuating fields is expressed by

$$\frac{\partial \overline{u}_k}{\partial x_k} = 0 \tag{2.8-a}$$

$$\frac{\partial u'_k}{\partial x_k} = 0 \; . \tag{2.8-b}$$

The equations for the covariances $\overline{u'_i u'_j}$ can be obtained multiplying (2.7) by u'_j, exchanging the subscripts i and j, summing the two resulting equations and averaging:

$$\begin{aligned} \frac{\partial \overline{u'_i u'_j}}{\partial t} + \overline{u}_k \frac{\partial \overline{u'_i u'_j}}{\partial x_k} + \frac{\partial \overline{u'_i u'_j u'_k}}{\partial x_k} &= -\overline{u'_i u'_k} \frac{\partial \overline{u}_j}{\partial x_k} - \overline{u'_j u'_k} \frac{\partial \overline{u}_i}{\partial x_k} + \\ &- \frac{1}{\overline{\theta}_v} \left[g_i \overline{u'_j \theta'_v} + g_j \overline{u'_i \theta'_v} \right] - \left(\overline{\frac{\partial p'}{\partial x_i} u'_j} + \overline{\frac{\partial p'}{\partial x_j} u'_i} \right) \\ &- 2\epsilon_{ij} - \delta_{j4} \epsilon_{Ri} - \delta_{i4} \epsilon_{Rj} \; . \end{aligned} \tag{2.9}$$

where the terms representing viscous dissipation are

$$\epsilon_{ij} = \frac{(\nu_{u_i} + \nu_{u_j})}{2} \overline{\frac{\partial u'_i}{\partial x_k} \frac{\partial u'_j}{\partial x_k}} \tag{2.10}$$

and the radiative dissipation is

$$\epsilon_{Ri} = \frac{1}{\overline{\rho} c_p} \overline{u'_i \frac{\partial R'_k}{\partial x_k}} \; . \tag{2.11}$$

In (2.9), when $i = j$ it is understood that no sum is implied, and the resulting equations will then mean the turbulent budget for the variance of u_i. Then, one can also set $l = i = j$, obtaining an equation for the budget of $\overline{u_l u_l}$ with l summed from 1 to 3, which is twice the mean turbulence kinetic energy $\overline{e'}$:

$$\overline{e'} = \overline{u'u' + v'v' + w'w'} \; . \tag{2.12}$$

The rate of dissipation of turbulence kinetic energy ϵ_e is given by (2.10) for $l = i = j$. The presence of the radiative terms introduces a "radiative dissipation" as the last term in (2.9). Radiative effects in (2.11) will be present and may be important (among others) in the cases $i = j = 4$ (temperature variance budget), $i = 4$, $j = 5$ (temperature-humidity covariance budget) and $i = 3$, $j = 4$ (vertical heat flux budget).

2.2 Stationarity, surface uniformity and homogeneity

The equations presented in section 2.1 can be considerably simplified for many practical situations in the surface layer. We shall adopt the assumptions that the mean fields and turbulence are quasi-stationary and that the surface is uniform, so that $\partial(.)/\partial t = \partial(.)/\partial x = \partial(.)/\partial y = 0$ in the equations above. Under these assumptions, and neglecting the effects of molecular diffusion in (2.6), this equation then indicates that the turbulent fluxes do not vary with height which is an approximation valid only in the surface layer (Brutsaert, 1982 p. 54; Stull, 1988 pp. 51–56):

$$\frac{\partial\, \overline{w'u'}}{\partial z} = 0 \tag{2.13-a}$$
$$\frac{\partial\, \overline{w'\theta'}}{\partial z} = 0 \tag{2.13-b}$$
$$\frac{\partial\, \overline{w'q'}}{\partial z} = 0 \tag{2.13-c}$$
$$\frac{\partial\, \overline{w'\theta_v'}}{\partial z} = 0\ . \tag{2.13-d}$$

where the last equation, dealing with the *virtual* heat flux, is a consequence of (2.3). Under the above assumption of constant turbulent fluxes with height, the surface fluxes of momentum, heat, water vapor and virtual heat are

$$\tau = -\overline{\rho}\,\overline{w'u'} \tag{2.14-a}$$

$$H = \overline{\rho} c_p\, \overline{w'\theta'} \tag{2.14-b}$$

$$E = \overline{\rho}\,\overline{w'q'} \tag{2.14-c}$$

$$H_v = \overline{\rho} c_p\, \overline{w'\theta_v'} = \overline{\rho} c_p \left[(1 + 0.61\overline{q})H + 0.61\overline{\theta}E\right]\ . \tag{2.14-d}$$

With the same hypothesis of stationarity and surface uniformity one obtains, from (2.9),

$$0 = -\,\overline{w'u'}\,\frac{\partial\,\overline{u}}{\partial z} - \frac{1}{2}\frac{\partial\,\overline{w'e'}}{\partial z} + \frac{g}{\overline{\theta}_v}\,\overline{w'\theta_v'} - \frac{1}{\overline{\rho}}\frac{\partial\,\overline{w'p'}}{\partial z} - \epsilon_e \tag{2.15-a}$$
$$0 = -\,\overline{w'w'}\,\frac{\partial\,\overline{u}}{\partial z} - \frac{\partial\,\overline{w'w'u'}}{\partial z} + \frac{g}{\overline{\theta}_v}\,\overline{u'\theta_v'} + \overline{\frac{p'}{\overline{\rho}}\left(\frac{\partial\,u'}{\partial z} + \frac{\partial\,w'}{\partial x}\right)} - 2\epsilon_{wu} \tag{2.15-b}$$

$$0 = -\,\overline{w'w'}\,\frac{\partial\,\overline{\theta}}{\partial z} - \frac{\partial\,\overline{w'w'\theta'}}{\partial z} + \frac{g}{\overline{\theta}_v}\,\overline{\theta'\theta'_v} + \frac{\overline{p'}}{\overline{\rho}}\frac{\overline{\partial\,\theta'}}{\partial z} - 2\epsilon_{w\theta} - \epsilon_{Rw} \tag{2.15-c}$$

$$0 = -\,\overline{w'w'}\,\frac{\partial\,\overline{q}}{\partial z} - \frac{\partial\,\overline{w'w'q'}}{\partial z} + \frac{g}{\overline{\theta}_v}\,\overline{q'\theta'_v} + \frac{\overline{p'}}{\overline{\rho}}\frac{\overline{\partial\,q'}}{\partial z} - 2\epsilon_{wq} \tag{2.15-d}$$

$$0 = -2\,\overline{w'\theta'}\,\frac{\partial\,\overline{\theta}}{\partial z} - \frac{\partial\,\overline{w'\theta'\theta'}}{\partial z} - 2\left(\epsilon_{\theta\theta} + \epsilon_{R\theta}\right) \tag{2.15-e}$$

$$0 = -2\,\overline{w'q'}\,\frac{\partial\,\overline{q}}{\partial z} - \frac{\partial\,\overline{w'q'q'}}{\partial z} - 2\epsilon_{qq} \tag{2.15-f}$$

$$0 = -\,\overline{w'\theta'}\,\frac{\partial\,\overline{q}}{\partial z} - \overline{w'q'}\,\frac{\partial\,\overline{\theta}}{\partial z} - \frac{\partial\,\overline{w'\theta'q'}}{\partial z} - 2\epsilon_{\theta q} - \epsilon_{Rq}\;. \tag{2.15-g}$$

Notice that the pressure terms for the budgets of momentum, heat and humidity fluxes are written in a different form from the general budget for $\overline{u'_i u'_j}$ in (2.9): they were rewritten as the sum of a pressure-diffusion and a redistribution term, with the former neglected by an order-of-magnitude analysis (Stull, 1988 pp. 136–137). One further, very important simplification is the assumption of homogeneity, which is the counterpart of stationarity for a random function in space. Thus, in homogeneous turbulence all moments $\overline{u'_i u'_j}$, $\overline{u'_i u'_j u'_k}$, $\overline{u'_i u'_j u'_k u'_l}$, …, as well as moments of derivatives such as $\overline{\partial u'_i/\partial x_k\, \partial u'_j/\partial x_k}$ are constant throughout space which immediately implies, in (2.9), that the mean gradients $\partial \overline{u}_i/\partial x_k$ must also be constant (Hinze, 1975 p. 322). Therefore, equations (2.13) would hold by definition and the derivatives with respect to z of the third moments in (2.15) would all be zero.

Now we know that the mean gradients *are not* constant in the surface layer (for instance, in neutral conditions $\partial\overline{u}/\partial z$ varies with the reciprocal of z), so that homogeneity can be at best an approximation; on the other hand, if the turbulent length scales are no larger than the length scales defined locally by

$$\ell_h \equiv \frac{\partial \overline{u}_i}{\partial z} / \frac{\partial^2 \overline{u}_i}{\partial z \partial z} \tag{2.16}$$

it may still be reasonable to assume homogeneity (Hinze, 1975 p. 322; Claussen, 1985a). The question of whether or not the third moments, pressure-velocity and pressure-scalar covariances vary appreciably with height is more difficult to assess. Neglecting third moments is, in a sense, a very simple way of closing the turbulence equations or at least reducing their complexity. It has often been assumed to be true in the surface layer (Fairall and Larsen, 1986). Wyngaard and Coté (1971) observed an imbalance of gradient and buoyant prediction versus dissipation in the turbulence kinetic energy equation (2.15-a), but assumed that gradient production was equal to the dissipation of temperature variance; Bradley *et al.* (1981a) measured the divergence of triple moments $\overline{w'\theta'\theta'}$, concluding that it was small. More recently, some experiments have yielded results suggesting that the so-called transport terms may be important in the TKE equation (Högström, 1990; Frenzen and Voguel, 1992). In the next section, it will be seen that under Monin-Obukhov similarity assumptions, the so-called "z-less" stratification hypothesis is tantamount to assuming homogeneity in the z-direction (Wyngaard, 1973), and in Chapter 4 we will use a simple technique due to Wyngaard *et al.* (1978) to show that the variation of third moments with height is indeed negligible in stable conditions during FIFE-89; the behavior of the pressure-correlation terms, however, remains unprobed .

2.3 Turbulence scales and Monin-Obukhov similarity theory

We define the turbulence scales u_*, θ_*, q_*, θ_{v*} in terms of vertical surface fluxes according to

$$u_* a_* \equiv \pm \overline{w'a'} \tag{2.17}$$

where a is any of the corresponding quantities above, the minus sign holding for $a = u$ and the plus sign holding for the remaining. For θ_{v*}, from (2.3):

$$\theta_{v*} = (1 + 0.61\overline{q})\theta_* + 0.61\overline{\theta} q_* \tag{2.18}$$

whereas for pressure we define

$$p_* \equiv \overline{\rho} u_*^2 \tag{2.19}$$

Monin-Obukhov similarity theory (MOS) (Obukhov, 1946; Businger and Yaglom, 1971) describes all mean and statistical properties of the surface layer in dimensionless form with the use of these scales, plus a "natural" length scale z which is the height above the surface. The independent variable is

$$\zeta \equiv -\frac{\kappa g \theta_{v*} z}{\overline{\theta}_v u_*^2} \equiv \frac{z}{L_{\theta_v}} \tag{2.20}$$

where $\kappa = 0.41$ is von Karman's constant and L_{θ_v} is Obukhov's stability length. Using (2.1), it is possible to write ζ as

$$\zeta = \zeta_\theta + \zeta_q \equiv -\frac{\kappa g \theta_* z}{\overline{\theta} u_*^2} - \frac{0.61}{1 + 0.61\overline{q}} \frac{\kappa g q_* z}{u_*^2} \equiv \frac{z}{L_\theta} + \frac{z}{L_q} \tag{2.21}$$

which shows the separate effects of temperature and humidity on the stratification of the atmosphere. For the mean gradients, MOS predicts

$$\pm\frac{\kappa z}{a_*}\frac{\partial \overline{a}}{\partial z} = \phi_F(\zeta) \tag{2.22}$$

where the plus sign holds for $a = u$, and the minus sign for the remaining quantities; the subscript F represents any of the fluxes appearing in (2.14) for the corresponding quantity a, and ϕ_F must be determined by experiment, in principle for each quantity a. For moments of order 2 and 3, with a and b representing generic turbulence quantities,

$$\frac{\overline{a'b'}}{a_* b_*} = \phi_{ab}(\zeta) \tag{2.23-a}$$

$$\frac{\overline{a'b'c'}}{a_* b_* c_*} = \phi_{abc}(\zeta)\ . \tag{2.23-b}$$

Notice how, if $\phi_{ab}(\zeta)$ is known, it is possible, say, to estimate u_* from $\overline{w'w'}$, θ_* from $\overline{\theta'\theta'}$ and q_* from $\overline{q'q'}$. This is the basis of the so-called variance method, whereby the fluxes in (2.14) can be indirectly estimated by variances alone, without the need to calculate covariances (Tillman, 1972; Ariel and Nadezhina, 1976; Hicks, 1981; Wesely, 1988; Weaver, 1990; Gao *et al.*, 1991; Lloyd *et al.*, 1991; De Bruin *et al.*, 1993; Lee and Black, 1993). In the data analyzed in Chapter 4 we will see how, under stable conditions, this aspect of MOS needs some more study: the plots corresponding to $\phi_{\theta\theta}$ and ϕ_{qq} are somewhat too scattered, even though the *mean* values obtained for them are still quite reasonable. Also, in Chapter 6 we will show how a "theoretical" $\phi_{\theta\theta}$ can be obtained from a spectral model which agrees quite well with the observed (mean) behavior.

For the covariances of pressure fluctuations p' and strain rates $\partial a'$ (see (2.4) and (2.19)), the MOS prediction is:

$$\frac{\kappa z\,\overline{p'\partial a'}}{\overline{\rho} u_*^2 a_*} = \phi_{p\partial a}(\zeta) \tag{2.24}$$

and finally, for the rates of dissipation,

$$\frac{\kappa z \epsilon_{ab}}{u_* a_* b_*} = \phi_{\epsilon_{ab}}(\zeta). \tag{2.25}$$

An immediate and important consequence of MOS is that the correlation coefficient r_{ab} between any two turbulent quantities is itself a dimensionless function of stability:

$$r_{ab} \equiv \frac{\overline{a'b'}}{\sqrt{\overline{a'a'}}\sqrt{\overline{b'b'}}} \equiv \frac{\overline{a'b'}/a_* b_*}{\sqrt{\overline{a'a'}/a_* a_*}\sqrt{\overline{b'b'}/b_* b_*}} = \frac{\phi_{ab}}{\sqrt{\phi_{aa}\phi_{bb}}}, \tag{2.26}$$

since the last term on the right-hand side of (2.26) is made up of functions of ζ. In Chapter 4, we will see that, whereas the correlation coefficient between θ and q can be shown to be -1 in a majority of cases in the stable surface layer, the measured correlations $r_{w\theta}$ and r_{wq} show a rather large scatter when plotted against ζ. This is, of course, a consequence of the aforementioned scatter in the functions $\phi_{\theta\theta}$ and ϕ_{qq}.

We now consider the result of making (2.15) non-dimensional. First, note that

$$\frac{\partial(\cdot)}{\partial z} = \frac{\partial(\cdot)}{\partial \zeta L_{\theta_v}} = \frac{1}{L_{\theta_v}}\frac{\partial(\cdot)}{\partial \zeta}. \tag{2.27}$$

We now multiply each equation in (2.15) by κz and divide by the suitable combination of turbulence scales $a_* b_* \ldots$ which makes it dimensionless. The resulting equations (neglecting the radiative terms) are

$$\phi_\tau - \frac{1}{2}\kappa\zeta\frac{\partial\,\phi_{we}}{\partial\zeta} - \zeta - \kappa\zeta\frac{\partial\,\phi_{wp}}{\partial\zeta} - \phi_{\epsilon_e} = 0 \tag{2.28-a}$$

$$-\phi_{ww}\phi_\tau - \kappa\zeta\frac{\partial\,\phi_{wwu}}{\partial\zeta} - \zeta\phi_{u\theta_v} + \phi_{p\partial u} - 2\phi_{\epsilon_{wu}} = 0 \tag{2.28-b}$$

$$\phi_{ww}\phi_H - \kappa\zeta\frac{\partial\,\phi_{ww\theta}}{\partial\zeta} - \zeta\phi_{\theta\theta_v} + \phi_{p\partial\theta} - 2\phi_{\epsilon_{w\theta}} = 0 \tag{2.28-c}$$

$$\phi_{ww}\phi_E - \kappa\zeta\frac{\partial\,\phi_{wwq}}{\partial\zeta} - \zeta\phi_{q\theta_v} + \phi_{p\partial q} - 2\phi_{\epsilon_{wq}} = 0 \tag{2.28-d}$$

$$2\phi_H - \kappa\zeta\frac{\partial\,\phi_{w\theta\theta}}{\partial\zeta} - 2\phi_{\epsilon_{\theta\theta}} = 0 \tag{2.28-e}$$

$$2\phi_E - \kappa\zeta\frac{\partial\,\phi_{wqq}}{\partial\zeta} - 2\phi_{\epsilon_{qq}} = 0 \tag{2.28-f}$$

$$\phi_E + \phi_H - \kappa\zeta\frac{\partial\,\phi_{w\theta q}}{\partial\zeta} - 2\phi_{\epsilon_{\theta q}} = 0\ . \tag{2.28-g}$$

It is particularly interesting to notice how, in neutral conditions, the explicit appearance of ζ "kills" many of the terms. In the TKE dimensionless budget, (2.28-a), the values of ϕ_{we} and ϕ_{wp} become immaterial, unless of course their gradients blow up at $\zeta = 0$. Högström (1990) advanced a somewhat contradictory hypothesis, namely that very close to neutral conditions the divergence of the third moment $\overline{w'e'}$ *is* important. Seen in the light of (2.28), however, and assuming that MOS *does* hold, his suggestion seems less likely.

Finally, consider the further assumption of homogeneous turbulence: it greatly simplifies (2.28), since all the terms involving the derivatives with respect to ζ then drop. Under stable condtions, it has been argued (Wyngaard, 1973) that the restoring buoancy forces limit the scale of vertical movements, so that turbulence should become independent of z, that is to say, effectively homogeneous in the vertical direction. This is called "z-less stratification". Not surprisingly, the velocity and scalar mean gradients then become (asymptotically) linear with z. The so-called log-linear shape of the the dimensionless gradients ϕ_H, ϕ_E has been found to hold even for small (i.e., close to neutral) but finite values of ζ (Brutsaert, 1982 p. 71). In Chapter 4, further experimental support for this assumption in stable conditions is presented by showing that ϕ_{waa} and ϕ_{wwa} ($a = \theta$,q) do not vary with ζ. Under the assumption of homogeneity, the dimensionless budgets become:

$$-\zeta + \phi_\tau - \phi_{\epsilon_e} = 0 \tag{2.29-a}$$

$$-\phi_{ww}\phi_\tau - \zeta\phi_{u\theta_v} + \phi_{p\partial u} - 2\phi_{\epsilon_{wu}} = 0 \tag{2.29-b}$$

$$\phi_{ww}\phi_H - \zeta\phi_{\theta\theta_v} + \phi_{p\partial\theta} - 2\phi_{\epsilon_{w\theta}} = 0 \tag{2.29-c}$$

$$\phi_{ww}\phi_E - \zeta\phi_{q\theta_v} + \phi_{p\partial q} - 2\phi_{\epsilon_{wq}} = 0 \tag{2.29-d}$$

$$2\phi_H - 2\phi_{\epsilon_{\theta\theta}} = 0 \tag{2.29-e}$$

$$2\phi_E - 2\phi_{\epsilon_{qq}} = 0 \tag{2.29-f}$$

$$\phi_E + \phi_H - 2\phi_{\epsilon_{\theta q}} = 0\ . \tag{2.29-g}$$

2.4 Spectra and cross spectra of turbulence

A large part of Chapters 5 and 6 is concerned with theoretical and experimental analyses of spectra and cross spectra. It is convenient to consider them from the standpoint of both time-frequency transformations and space-wavenumber transformations in one and three dimensions. The Fourier transform of a generic distribution f in each case is

$$\mathcal{F}[f(t)] \equiv \int_{-\infty}^{+\infty} e^{-2\pi\, i\, nt}\, f(t)\, dt \tag{2.30-a}$$

$$\mathcal{F}[f(x_l)] \equiv \frac{1}{2\pi} \int_{-\infty}^{+\infty} e^{-\, i\, k_l x_l}\, f(x_l)\, dx_l \tag{2.30-b}$$

$$\mathcal{F}[f(\mathbf{r})] \equiv \frac{1}{(2\pi)^3} \int_{\mathcal{R}^3} e^{-\, i\ (\mathbf{k}\cdot\mathbf{r})}\ f(\mathbf{r})\, d^3\mathbf{r} \tag{2.30-c}$$

where $i = \sqrt{-1}$, n is frequency, k_l is wavenumber in the direction l, $\mathbf{k} = (k_1, k_2, k_3)$ is wavenumber vector and $\mathbf{r} = (x_1, x_2, x_3)$ is the position vector. Allowing f to be a distribution circumvents the problem of convergence of the corresponding integrals when f (which will mean some turbulent fluctuation u'_i) does not decrease rapidly to infinity (Lesieur, 1990 p. 90). This considerably simplifies the formalism that leads to the spectral budget equations, allowing Fourier transforms of the turbulent fluctuations to be taken freely.

For two generic random functions $u'_i(\mathbf{r})$, $u'_j(\mathbf{r})$ representing a pair of turbulent fluctuations in *space*, let

$$\widehat{u}_i(\mathbf{k}) \equiv \mathcal{F}[u'_i(\mathbf{r})] \tag{2.31-a}$$

$$\widehat{u}_j(\mathbf{k}) \equiv \mathcal{F}[u'_j(\mathbf{r})] \tag{2.31-b}$$

$$[\widehat{u_i u_j}](\mathbf{k}) \equiv \mathcal{F}\left[\, [u'_i u'_j](\mathbf{r})\, \right]\ . \tag{2.31-c}$$

We then define the cross-spectrum of u'_i and u'_j by

$$\Phi_{i,j}(\mathbf{k}) \equiv \frac{1}{\delta(\mathbf{0})} \overline{\widehat{u}_i^*\, \widehat{u}_j} \tag{2.32}$$

where a^* means the complex conjugate of the complex number a, and the overbar means expected value over an ensemble of realizations;

$$\delta(\mathbf{k}) \equiv \left(\frac{1}{2\pi}\right)^3 \int_{\mathcal{R}^3} e^{-\, i\, (\mathbf{k}\cdot\mathbf{r})}\, d^3\mathbf{r} \tag{2.33}$$

is Dirac's delta function; its appearance in (2.32) makes $\Phi_{i,j}$ dimensionally consistent (notice how, in $\mathcal{R}^3$, δ has dimensions of volume) and in fact represents a limit process. It can be shown that (2.32) is equivalent to defining $\Phi_{i,j}$ as the Fourier transform of the cross-correlation function in homogeneous turbulence (Lesieur, 1990 p. 109). The choice of this (somewhat more abstract) definition will allow the spectral budgets to be derived rather easily in section 2.5. The corresponding definitions for one-dimensional time processes can be found in Bendat and Piersol (1986 p. 130)

The cross-spectrum between u_i' and the *product* $u_j'u_k'$ is

$$\Phi_{i,jk}(\mathbf{k}) \equiv \frac{1}{\delta(\mathbf{0})} \overline{\widehat{u}_i^* \, [\widehat{u_j u_k}]} \, . \tag{2.34}$$

Notice that cross-spectra are hermitian: $\Phi_{i,j} = \Phi_{j,i}^*$ and $\Phi_{i,jk} = \Phi_{jk,i}^*$. The cospectrum $C_{i,j}$ and the quadrature spectrum $Q_{i,j}$ are the real part and the negative of the imaginary part of $\Phi_{i,j}$,

$$\Phi_{i,j} \equiv C_{i,j} - i \, Q_{i,j} \, , \tag{2.35}$$

with an analogous definition holding for $\Phi_{i,jk}$.

Again, in (2.32), if $i = j$ we interpret it as the definition of the *spectrum* of the variable u_i, whereas if we choose $l = i = j$, then it will represent the spectrum of twice the turbulence kinetic energy.

In practice, obtaining $\Phi_{i,j}(\mathbf{k})$ involves knowledge of the behavior of turbulent fluctuations in 3 dimensions, while classical measurements on micrometeorological masts or with airplanes are one-dimensional in time or space. One way to alleviate this problem is to work with averages over spherical shells in wavenumber space:

$$E_{i,j}(k) \equiv \oint_{|\mathbf{k}|=k} C_{i,j}(\mathbf{k})\, d^2\mathbf{k} \tag{2.36}$$

where $d^2\mathbf{k}$ indicates an element of area on the surface of the sphere with center at $(0,0,0)$ and radius k in wavenumber space. Even then, it is not possible in principle to calculate $E_{i,j}$ without knowledge of the three-dimensional structure of turbulence. The one-dimensional equivalents of $E_{i,j}$ in space and time are obtained from the one-dimensional Fourier transforms defined in (2.30). If u'_i and u'_j are taken as functions of the space coordinate x_l or of time t, one obtains the corresponding one-dimensional spectra of wavenumber k_l and frequency n (Bendat and Piersol, 1986 p.132),

$$F_{i,j}(k_l) \equiv \begin{cases} \frac{2}{\delta(0)} \overline{[\widehat{u}_i^* \, \widehat{u}_j]}(k_l), & k_l \geq 0 \\ 0 & k_l < 0 \end{cases} \tag{2.37-a}$$

$$S_{i,j}(n) \equiv \begin{cases} \frac{2}{\delta(0)} \overline{[\widehat{u}_i^* \, \widehat{u}_j]}(n), & n \geq 0 \\ 0 & n < 0 \end{cases} . \tag{2.37-b}$$

The definitions of $E_{i,j}(k)$, $F_{i,j}(k_1)$ and $S_{i,j}(n)$ above are such that the integrals from 0 to ∞ of the cospectra are equal to the covariance $\overline{u'_i u'_j}$, i.e., if

$$F^c_{i,j} \equiv \mathrm{Re}(F_{i,j}) \tag{2.38-a}$$

$$S^c_{i,j} \equiv \mathrm{Re}(S_{i,j}) \; , \tag{2.38-b}$$

then

$$\overline{u'_i u'_j} = \int_{k=0}^{\infty} E_{i,j}(k)\, dk = \int_{k_1=0}^{\infty} F^c_{i,j}(k_1)\, dk_1 = \int_{n=0}^{\infty} S^c_{i,j}(n)\, dn \; . \tag{2.39}$$

In practice, $F^c_{i,j}(x_1)$ and $S^c_{i,j}(n)$ are often used interchangeably with the help of Taylor's frozen turbulence hypothesis (Lumley and Panofksky, 1964 p.56); if the mean velocity $\overline{u}$ at which the turbulent eddies are advected past a sensor is high enough, then

$$k_1 = \frac{2\pi}{\lambda} = \frac{2\pi}{\overline{u}T} = \frac{2\pi n}{\overline{u}} \tag{2.40}$$

where λ is wavelength and T is period; using (2.40) and (2.39) we obtain

$$\frac{2\pi}{\overline{u}} F^c_{i,j}\left(\frac{2\pi n}{\overline{u}}\right) = S^c_{i,j}(n)\ . \tag{2.41}$$

The coherence function $\Gamma_{i,j}$ between two quantities u'_i, u'_j in the one-dimensional spatial case is

$$\Gamma_{i,j}(k_1) \equiv \frac{F^*_{i,j}(k_1)F_{i,j}(k_1)}{F_{i,i}(k_1)F_{j,j}(k_1)}\ . \tag{2.42}$$

Naturally, there is an equivalent definition in terms of $S_{i,j}(n)$. The coherence function can be interpreted as the square of a *spectral* correlation coefficient; however, notice that it does not give any information about the *phase difference* between u_i and u_j, since both co- and quadrature spectra are present in it; the phase function is the argument of the complex number $F_{i,j}$,

$$\vartheta_{i,j}(k_1) \equiv \arg(F_{i,j})\ . \tag{2.43}$$

For isotropic turbulence, it *is* possible to relate the one-dimensional spectra defined in (2.37) to the three-dimensional average spectra given by (2.36); the relations between one and three-dimensional spectra for the velocity field and a scalar field (for instance temperature) are (Hinze, 1975 pp. 209 and 285):

$$F_{u,u}(k_1) = \frac{1}{2}\int_{k_1}^{\infty}\left(1 - \frac{k_1^2}{k^2}\right)E_e(k)\frac{dk}{k} \tag{2.44-a}$$

$$F_{w,w}(k_1) = \frac{1}{4}\int_{k_1}^{\infty}\left(1 + \frac{k_1^2}{k^2}\right)E_e(k)\frac{dk}{k} \tag{2.44-b}$$

$$F_{\theta,\theta}(k_1) = \int_{k_1}^{\infty} E_{\theta,\theta}(k)\frac{dk}{k}\ . \tag{2.44-c}$$

In isotropic turbulence, however, the cospectra and corresponding covariances in (2.39) are identically zero for $i \neq j$. In the stable surface layer in general the turbulent fluxes are *not* zero, so the hypothesis of isotropy seems a poor one in this context. In fact, there is a need, not yet fully recognized, for developing more realistic models for atmospheric turbulence that take into account anisotropy, such as that of Kristensen *et al.* (1988), which unfortunately does not go so far as to introduce a formulation for the cospectra.

There are a few experiments specifically designed to test the validity of isotropy in the atmospheric boundary layer (Kristensen *et al.*, 1981; Webster and Burling, 1991); it is generally accepted to hold in the high wavenumber range of the spectrum (Kaimal *et al.*, 1972; Van Atta, 1977). Purely isotropic turbulence still accounts for a large part in the current research efforts (Chollet and Lesieur, 1981; Schertzer and Simonin, 1981; Herring *et al.*, 1982; Herring and Métais, 1989; Métais and Herring, 1989), but there have been various efforts to incorporate various degrees of anisotropy and inhomogeneity (Deissler, 1961; Deissler, 1962; Domaradzki and Mellor, 1984; Nagano and Tagawa, 1990).

2.5 Spectral budgets

In much the same way as equations (2.9) describe the budgets of turbulent covariances $\overline{u_i' u_j'}$, it is possible to derive the equations for the cross-spectra $\Phi_{i,j}$. This is not, per se, something new; different versions of the spectral budgets of turbulence kinetic energy and temperature have long been known (Deissler, 1961; Deissler, 1962; Corrsin, 1964; Fox, 1964; Lumley and Panofksy, 1964; Pao, 1965; Hinze, 1975). Yet their use in specific atmospheric contexts has somewhat lagged behind by 10 to 20 years (Straka *et al.*, 1977; Coantic and Simonin, 1984; Claussen, 1985a). The most complete derivations available seem to be those of Deissler (1962) and Hinze (1975); a more concise derivation with a thorough interpretation of the physical meaning of the terms responsible for redistribution of energy (or variance) in wavenumber space can be found in Lumley and Panofsky (1964). In these derivations, *two-point* equations giving the spatial covariance function between two quantities u_i' and u_j'' at two different points in space (hence the double prime in u_j'') are first derived (see Appendix C); the spectral budgets are then obtained by means of Fourier transforms of these cross-covariance functions.

Since the spectral budgets are less common in the literature than equations (2.9), they will be rederived here in full generality for *all* cross-spectra $\Phi_{i,j}$. We will also avoid the two-point equations, whose derivation is long and fastidious, by instead Fourier-transforming the equations for the turbulent fluctuations directly; finally, we will assume the turbulence to be homogeneous.

Thus, consider the Fourier transform of (2.7), where the last term in the right-hand side ($\partial \overline{u_i' u_k'} / \partial x_k$) is *zero* in homogeneous turbulence. Also, we shall admit that the mean quantities vary linearly around the level at which (2.7) is being considered, which we take to be $r_l = 0$ for $l = 1, 2, 3$. Then,

$$\frac{\partial \overline{u}_k}{\partial x_l} = \text{constant} \tag{2.45-a}$$

$$\overline{u}_k = \overline{u}_{k0} + \frac{\partial\,\overline{u}_k}{\partial x_l}\,r_l\;. \tag{2.45-b}$$

We retain the full three-dimensional form above, since it will be useful in the following; for a uniform surface, of course, the constant in (2.45-a) is zero for x_1 or x_2; $\overline{u}_{k0}$ is the value of $\overline{u}_k$ at $r_k = 0$. With these simplifications, (2.7) becomes

$$\frac{\partial\,u_i'}{\partial t} + \left(\overline{u}_{k0} + \frac{\partial\,\overline{u}_k}{\partial x_l}\,r_l\right)\frac{\partial\,u_i'}{\partial x_k} + u_k'\,\frac{\partial\,\overline{u}_i}{\partial x_k} + \frac{\partial\,u_i'u_k'}{\partial x_k} = -\frac{g_i}{\overline{\theta}_v}\theta_v' - \frac{1}{\overline{\rho}}\frac{\partial\,p'}{\partial x_i}$$
$$+\,\nu_{u_i}\frac{\partial^2\,u_i'}{\partial x_k\partial x_k} - \delta_{i4}\frac{1}{\overline{\rho c_p}}\frac{\partial\,R_k'}{\partial x_k}\;. \tag{2.46}$$

Now the Fourier transform of most of the terms above is straightforward, except for $r_l\,\partial u_i'/\partial x_k$ and $\partial R_k'/\partial x_k$. The Fourier transform of the divergence of the fluctuating radiative flux vector is dealt with detail in Appendix B, and is studied in depth in Chapter 6; here, it is sufficient to define

$$\mathcal{F}\left[\delta_{i4}\frac{1}{\overline{\rho c_p}}\frac{\partial\,R_k'}{\partial x_k}\right] \equiv N(k)\delta_{i4}\widehat{u}_i \tag{2.47}$$

where we anticipate that N is a real function of $k = |\mathbf{k}|$ alone due to the assumption of isotropy of the longwave radiative emission. To calculate $\mathcal{F}\left[r_l\partial u_i'/\partial x_k\right]$, first notice the standard relation for the Fourier transform of a partial derivative,

$$\mathcal{F}\left[\frac{\partial}{\partial x_k}f(x_k)\right] = i\,k_k\mathcal{F}\left[f(x_k)\right]\;. \tag{2.48}$$

Then,

$$\mathcal{F}\left[\frac{\partial\,\overline{u}_k}{\partial x_l}r_l\frac{\partial\,u_i'}{\partial x_k}\right] = \frac{1}{(2\pi)^3}\int_{\mathcal{R}^3}\frac{\partial\,\overline{u}_k}{\partial x_l}r_l\frac{\partial\,u_i'}{\partial x_k}e^{-\,i\,(\mathbf{k}\cdot\mathbf{r})}\,d^3\mathbf{r}$$

$$
\begin{aligned}
&= \frac{\partial \overline{u}_k}{\partial x_l} \frac{1}{(2\pi)^3} \int_{\mathcal{R}^3} r_l \frac{\partial u_i'}{\partial x_k} e^{-i\,(\mathbf{k}\cdot\mathbf{r})}\, d^3\mathbf{r} \\
&= -\frac{1}{i} \frac{\partial \overline{u}_k}{\partial x_l} \frac{1}{(2\pi)^3} \int_{\mathcal{R}^3} \frac{\partial u_i'}{\partial x_k} \frac{\partial}{\partial k_l} \left[e^{-i\,(k_l r_l)} \right] d^3\mathbf{r} \\
&= -\frac{1}{i} \frac{\partial \overline{u}_k}{\partial x_l} \frac{\partial}{\partial k_l} \frac{1}{(2\pi)^3} \int_{\mathcal{R}^3} \frac{\partial u_i'}{\partial x_k} e^{-i\,(k_l r_l)}\, d^3\mathbf{r}
\end{aligned}
\tag{2.49}
$$

where the integral in the last line above is the Fourier transform of $\partial u_i'/\partial x_k$; then, using (2.48),

$$
\begin{aligned}
\mathcal{F}\left[\frac{\partial \overline{u}_k}{\partial x_l} r_l \frac{\partial u_i'}{\partial x_k} \right] &= -\frac{1}{i} \frac{\partial \overline{u}_k}{\partial x_l} \frac{\partial}{\partial k_l} \left[i\,k_k \widehat{u}_i \right] \\
&= -\frac{\partial \overline{u}_k}{\partial x_l} \left[\delta_{kl} \widehat{u}_i + k_k \frac{\partial \widehat{u}_i}{\partial k_l} \right] \\
&= -\frac{\partial \overline{u}_k}{\partial x_k} \widehat{u}_i - \frac{\partial \overline{u}_k}{\partial x_l} k_k \frac{\partial \widehat{u}_i}{\partial k_l} \\
&= -\frac{\partial \overline{u}_k}{\partial x_l} k_k \frac{\partial \widehat{u}_i}{\partial k_l}
\end{aligned}
\tag{2.50}
$$

because of continuity of the mean velocity field. The rest of the Fourier transforms of terms in (2.46) can be calculated easily with the help of (2.48); the result is

$$
\begin{aligned}
&\frac{\partial \widehat{u}_i}{\partial t} + \overline{u}_{k0}(\,i\,k_k)\widehat{u}_i - \frac{\partial \overline{u}_k}{\partial x_l} k_k \frac{\partial \widehat{u}_i}{\partial x_k} + \frac{\partial \overline{u}_i}{\partial x_k} \widehat{u}_k + (\,i\,k_k)\widehat{u_i u_k} + \\
&\qquad \frac{g_i}{\overline{\theta}_v} \widehat{\theta}_v + \frac{1}{\overline{\rho}}(\,i\,k_i)\widehat{p} + \nu_{u_i} k^2 \widehat{u}_i + N(k)\delta_{i4}\widehat{u}_i = 0
\end{aligned}
\tag{2.51}
$$

where all terms have been moved to the left-hand side. A totally analogous equation holds, of course, for j instead of i; the complex conjugate (2.51) is

$$
\begin{aligned}
&\frac{\partial \widehat{u}_i^*}{\partial t} - \overline{u}_{k0}(\,i\,k_k)\widehat{u}_i^* - \frac{\partial \overline{u}_k}{\partial x_l} k_k \frac{\partial \widehat{u}_i^*}{\partial x_k} + \frac{\partial \overline{u}_i}{\partial x_k} \widehat{u}_k^* - (\,i\,k_k)\,[\widehat{u_i u_k}]^* + \\
&\qquad \frac{g_i}{\overline{\theta}_v} \widehat{\theta}_v^{\,*} - \frac{1}{\overline{\rho}}(\,i\,k_i)\widehat{p}^* + \nu_{u_i} k^2 \widehat{u}_i^* + N(k)\delta_{i4}\widehat{u}_i^* = 0\,.
\end{aligned}
\tag{2.52}
$$

The remaining is relatively simple: multiply (2.51), with j instead of i, by $\widehat{u}_i^*$, and (2.52) by $\widehat{u}_j$, sum the two resulting equations and take the expected value; then $\Phi_{i,j}$ appears naturally; the result is

$$\frac{\partial \Phi_{i,j}}{\partial t} - \frac{\partial \overline{u}_k}{\partial x_l} k_k \frac{\partial \Phi_{i,j}}{\partial k_l} + \frac{\partial \overline{u}_i}{\partial x_k}\Phi_{k,j} + \frac{\partial \overline{u}_j}{\partial x_k}\Phi_{i,k} + i\, k_k(\Phi_{i,jk} - \Phi_{ik,j}) +$$
$$\frac{1}{\overline{\theta}_v}(g_i \Phi_{\theta_v,j} + g_j \Phi_{i,\theta_v}) + \frac{i}{\overline{\rho}}(k_j \Phi_{i,p} - k_i \Phi_{p,j}) + k^2(\nu_{u_i} + \nu_{u_j})\Phi_{i,j} +$$
$$N(k)\left[\delta_{i4} + \delta_{j4}\right]\Phi_{i,j} = 0\ . \quad (2.53)$$

The spectral budgets are considerably simpler if we assume the usual hypothesis of stationarity and surface uniformity and look at $l = i = j$ (which will give the spectrum of twice the turbulence kinetic energy Φ_e) and $i = j$ for $i = 4$ (temperature spectrum $\Phi_{\theta,\theta}$) and $i = 5$ (humidity spectrum $\Phi_{q,q}$). The pressure terms then drop and, noticing that $\Phi_{i,j} = \Phi_{j,i}^*$, one obtains

$$-\frac{\partial \overline{u}}{\partial z} k_1 \frac{\partial \Phi_e}{\partial k_3} + 2\frac{\partial \overline{u}}{\partial z} C_{w,u} + 2k_k Q_{l,lk} - 2\frac{g}{\overline{\theta}_v} C_{w,\theta_v} + 2\nu_u k^2 \Phi_e = 0 \quad \text{(2.54-a)}$$
$$-\frac{\partial \overline{\theta}}{\partial z} k_1 \frac{\partial \Phi_{\theta,\theta}}{\partial k_3} + 2\frac{\partial \overline{\theta}}{\partial z} C_{w,\theta} + 2k_k Q_{\theta,\theta k} + 2\left[\nu_\theta k^2 + N(k)\right]\Phi_{\theta,\theta} = 0 \quad \text{(2.54-b)}$$
$$-\frac{\partial \overline{q}}{\partial z} k_1 \frac{\partial \Phi_{q,q}}{\partial k_3} + 2\frac{\partial \overline{q}}{\partial z} C_{w,q} + 2k_k Q_{q,qk} + 2\nu_q k^2 \Phi_{qq} = 0 \quad \text{(2.54-c)}$$

which still are, however, differential equations in three-dimensional wavenumber space. In much the same way that was done in the definition of $E_{i,j}$ in (2.36), we define what are called the fluctuating strain rate transfer $T_{i,i}$ and the mean strain rate transfer $U_{i,i}$ (Lumley and Panofsky, 1964 pp. 76–82; Hinze, 1975 p. 336), with obvious equivalent definitions holding for $T_{l,l}$ and $U_{l,l}$:

$$T_{i,i}(k) \equiv 2\oint_{|\mathbf{k}|=k} k_k Q_{i,ik}(\mathbf{k}) d^2\mathbf{k} \quad \text{(2.55-a)}$$
$$U_{i,i}(k) \equiv \oint_{|\mathbf{k}|=k} k_1 \frac{\partial \Phi_{i,i}(\mathbf{k})}{\partial k_3} d^2\mathbf{k} = \frac{\partial}{\partial k}\left[\frac{1}{k}\oint_{|\mathbf{k}|=k} k_1 k_3 \Phi_{i,i}(\mathbf{k}) d^2\mathbf{k}\right] \quad \text{(2.55-b)}$$

where the second equality in (2.55) can be obtained after a long integration in spherical coordinates (Hinze, 1975 pp. 339–340). Upon integration of (2.54) over a spherical shell in wavenumber space we obtain, finally,

$$2\frac{\partial \overline{u}}{\partial z}E_{w,u} - \frac{\partial \overline{u}}{\partial z}U_e + T_e - \frac{2g}{\overline{\theta}_v}C_{w,\theta_v} + 2\nu_u k^2 E_e = 0 \tag{2.56-a}$$

$$2\frac{\partial \overline{\theta}}{\partial z}E_{w,\theta} - \frac{\partial \overline{u}}{\partial z}U_{\theta,\theta} + T_{\theta,\theta} + 2\left[\nu_\theta k^2 + N(k)\right]E_{\theta,\theta} = 0 \tag{2.56-b}$$

$$2\frac{\partial \overline{q}}{\partial z}E_{w,q} - \frac{\partial \overline{u}}{\partial z}U_{q,q} + T_{q,q} + 2\nu_q k^2 E_{q,q} = 0\ . \tag{2.56-c}$$

2.6 Inertial subrange behavior

One of the best known topics in turbulence theory is Kolmogorov's prediction of the behavior of the (turbulence kinetic) energy spectrum in the "inertial" subrange. This corresponds to a range of scales much smaller that those at which turbulence is produced (in our case, by interaction with mean gradients) and yet much larger than those at which energy is dissipated by viscous effects. Therefore, neither variables associated with production nor with dissipation should matter in the inertial subrange, the only relevant ones being the wavenumber k itself and the rate of dissipation of turbulence kinetic energy ϵ_e, here interpreted as an "energy flux" cascading down length scales (Tennekes and Lumley, 1972 pp. 257–261). Corrsin (1951), Lumley (1965), Wyngaard and Coté (1972) and Wyngaard *et al.* (1978) later extended this argument for the behavior of spectra and cospectra of scalars, and for the cospectra of vertical velocity w with u, θ and q.

The forms predicted by dimensional analysis are of course the same for *one-dimensional* (co-) spectra $F_{i,j}(k_1)$, which can be directly compared to measurements. For horizontal and vertical velocity spectra, the inertial subrange behavior is

$$F_{u,u}(k_1) = \alpha^1_{uu}\epsilon_e^{2/3}k_1^{-5/3} \tag{2.57-a}$$

$$F_{w,w}(k_1) = \alpha^1_{ww}\epsilon_e^{2/3}k_1^{-5/3} \tag{2.57-b}$$

where, for isotropic turbulence (Tennekes and Lumley, 1972 p. 273):

$$\alpha^1_{ww} = \frac{4}{3}\alpha^1_{uu} \; . \tag{2.58}$$

For spectra and cospectra of temperature and humidity (Corrsin, 1951; Wyngaard *et al.*, 1978) one has:

$$F_{\theta,\theta}(k_1) = \alpha^1_{\theta\theta}\epsilon_e^{-1/3}\epsilon_{\theta\theta}k_1^{-5/3} \tag{2.59-a}$$

$$F_{qq}(k_1) = \alpha^1_{qq}\epsilon_e^{-1/3}\epsilon_{qq}k_1^{-5/3} \tag{2.59-b}$$

$$F^c_{\theta q}(k_1) = \alpha^1_{\theta q}\epsilon_e^{-1/3}\epsilon_{\theta q}k_1^{-5/3} \; . \tag{2.59-c}$$

Equation (2.59-c), proposed by Wyngaard *et al.* (1978), is particularly important: if temperature and humidity are perfectly correlated or anti-correlated, their quadrature spectrum is zero, and $\alpha^1_{\theta\theta} = \alpha^1_{qq} = \alpha^1_{\theta q}$; thus, the coherence function is flat and equal to +1 throughout the inertial subrange. This will be tested with field data in Chapter 5. For the cospectra with vertical velocity (Lumley, 1965; Wyngaard and Coté, 1972) one has:

$$F^c_{w,u}(k_1) = \alpha^1_{wu} \frac{\partial \overline{u}}{\partial z} \epsilon_e^{1/3} k_1^{-7/3} \tag{2.60-a}$$

$$F^c_{w,\theta}(k_1) = \alpha^1_{w\theta} \frac{\partial \overline{\theta}}{\partial z} \epsilon_e^{1/3} k_1^{-7/3} \tag{2.60-b}$$

$$F^c_{w,q}(k_1) = \alpha^1_{wq} \frac{\partial \overline{q}}{\partial z} \epsilon_e^{1/3} k_1^{-7/3} \; . \tag{2.60-c}$$

In principle, it should be possible to extend the same idea for higher-order cospectra, such as $F^c_{i,jk}$. The situation would be particularly simple for $i = j = k = \theta$ and $i = j = k = q$, if one could assume that $F^c_{i,ii}$ depends on the same variables which determine the spectra $F_{i,i}$, namely the rate of dissipation of turbulence kinetic energy ϵ_e, the rates of dissipation of variance $\epsilon_{\theta\theta}$ and ϵ_{qq} and wavenumber k_1. By means of dimensional analysis we then obtain the following predictions for the inertial subrange:

$$F^c_{\theta,\theta\theta} = \alpha^1_{\theta,\theta\theta} \epsilon_e^{-1/2} \epsilon_{\theta\theta}^{3/2} k_1^{-2} \tag{2.61-a}$$

$$F^c_{q,qq} = \alpha^1_{q,qq} \epsilon_e^{-1/2} \epsilon_{qq}^{3/2} k_1^{-2} \; . \tag{2.61-b}$$

Higher order cross-spectra $F_{i,jk}$ are important for several reasons, even though so far they have received relatively little attention. The integral of the corresponding cospectra is equal to the third moments which appear in the transport equations for covariances: knowledge of their behavior with stability can considerably simplify those equations. Moreover, the quadrature spectra $Q_{i,ik}$ appear explicitly in the spectral budget equations (2.53), so that it may be useful to analyze the behavior of the corresponding one-dimensional cross-spectra.

In Chapter 5, we will show that the prediction of (2.61) is indeed observed in experimental temperature and humidity turbulence data.

In the equations above, α^1_{ij} and $\alpha^1_{i,jk}$ are constants (when $i = j$ for α^1_{ij}) or functions of stability ζ at most (Wyngaard and Coté, 1972); in the following tables we give some values of α^1_{uu}, $\alpha^1_{\theta\theta}$ and α^1_{qq} found in the literature.

Table 2.1 – values of α^1_{uu} found in the literature

Author	α^1_{uu}
Tennekes and Lumley (1972)	0.49
Lumley and Panofsky (1964)	0.46
Brutsaert (1982)	0.50 - 0.55
Fairall and Larsen (1986)	0.52 - 0.54
Kaimal *et al.* (1972)	0.50 - 0.53

2.7 Spectral similarity

We begin by making the spectral budgets for the variances, (2.56), dimensionless, in the same way that was done for the budgets of covariances in section 2.3. Thus, we need to render cospectra, transfer terms and wavenumbers

Table 2.2 – values of $\alpha^1_{\theta\theta}$ and α^1_{qq} found in the literature

Author	$\alpha^1_{\theta\theta}$	α^1_{qq}
Paquin and Pond (1971)	0.83 ± 0.13	0.80 ± 0.17
Wyngaard and Coté (1971)	0.79 ± 0.10	
Champagne *et al.* (1977)	0.82 ± 0.04	
Smedman–Högström (1973)		0.52 ± 0.20
Leavitt (1975)		0.81 ± 0.31
Raupach (1978)		0.88 ± 0.26
Bradley *et al.* (1981)	0.8 ± 0.2	

dimensionless:

$$\frac{kE_{a,b}}{a_* b_*} = \psi_{a,b}(\eta) \tag{2.62-a}$$

$$\frac{\kappa z k T_{a,b}}{u_* a_* b_*} = \tau_{a,b} \tag{2.62-b}$$

$$\frac{kU_{a,b}}{a_* b_*} = \upsilon_{a,b} \tag{2.62-c}$$

$$\eta = \kappa z k \tag{2.62-d}$$

$$\frac{\kappa z u_*}{\nu_u} \equiv \mathrm{Re}_* \tag{2.62-e}$$

$$\frac{\kappa z u_*}{\nu_\theta} \equiv \mathrm{Pe}^\theta_* \tag{2.62-f}$$

$$\frac{\kappa z u_*}{\nu_q} \equiv \mathrm{Pe}^q_* \tag{2.62-g}$$

where of course $\tau_{a,b}$ should not be confused with the momentum flux defined in (2.14).

Multiplying (2.56) by $\kappa z k$, and dividing by a suitable combination of $a_* b_* \ldots$, one obtains:

$$-2\phi_\tau \psi_{w,u} + \tau_e + \phi_\tau \upsilon_e + 2\zeta\psi_{w,\theta} + \frac{2}{\mathrm{Re}_*}\eta^2\psi_e = 0 \qquad (2.63\text{-a})$$

$$-2\phi_H \psi_{w,\theta} + \tau_{\theta,\theta} + \phi_\tau \upsilon_{\theta,\theta} + \frac{2}{\mathrm{Pe}_*^\theta}\eta^2\psi_{\theta,\theta} + 2\frac{\kappa z N(k)}{u_*}\psi_{\theta,\theta} = 0 \qquad (2.63\text{-b})$$

$$-2\phi_E \psi_{w,q} + \tau_{q,q} + \phi_\tau \upsilon_{q,q} + \frac{2}{\mathrm{Pe}_*^q}\eta^2\psi_{q,q} = 0\ . \qquad (2.63\text{-c})$$

The solution of (2.63) with a convenient formulation for the radiative term will be the subject of Chapter 6. We now turn to the particularly simple dimensionless shapes for the inertial subrange. We will need to look at one-dimensional dimensionless cospectra and spectra. The dimensionless wavenumber and frequency in this case are:

$$\kappa z k_1 = \eta_1 \qquad (2.64\text{-a})$$

$$\frac{nz}{\overline{u}} = f \qquad (2.64\text{-b})$$

$$2\pi\kappa f = \eta_1 \qquad (2.64\text{-c})$$

where (2.64-c) comes from Taylor's hypothesis (2.40); also, from (2.41) we obtain

$$\frac{k_1 F^c_{a,b}}{a_* b_*} = \psi^1_{a,b}(\eta_1) = \psi^1_{a,b}(2\pi\kappa f) = \frac{n S^c_{a,b}}{a_* b_*}\ , \qquad (2.65)$$

so that one can use $\psi^1_{a,b}$ interchangeably both for one-dimensional spatial and temporal cospectra. From (2.57) and (2.59) with (2.25), we then find, for the inertial subrange,

$$\psi^1_{u,u}(\zeta; f) = \alpha^1_{u,u}\phi_{\epsilon_e}^{2/3}(2\pi\kappa f)^{-2/3} \qquad (2.66\text{-a})$$

$$\psi^1_{w,w}(\zeta; f) = \frac{4}{3}\alpha^1_{u,u}\phi_{\epsilon_e}^{2/3}(2\pi\kappa f)^{-2/3} \qquad (2.66\text{-b})$$

and

$$\psi^1_{\theta,\theta}(\zeta; f) = \alpha^1_{\theta,\theta}\phi_{\epsilon_e}^{-1/3}\phi_{\epsilon_{\theta\theta}}(2\pi\kappa f)^{-2/3} \tag{2.67-a}$$

$$\psi^1_{q,q}(\zeta; f) = \alpha^1_{q,q}\phi_{\epsilon_e}^{-1/3}\phi_{\epsilon_{qq}}(2\pi\kappa f)^{-2/3} \tag{2.67-b}$$

$$\psi^1_{\theta,q}(\zeta; f) = \alpha^1_{\theta,q}\phi_{\epsilon_e}^{-1/3}\phi_{\epsilon_{\theta q}}(2\pi\kappa f)^{-2/3} \tag{2.67-c}$$

whereas, for the cospectra with the vertical wind velocity w,

$$\psi^1_{w,u}(\zeta; f) = \alpha^1_{w,u}\phi_\tau\phi_{\epsilon_e}^{1/3}(2\pi\kappa f)^{-4/3} \tag{2.68-a}$$

$$\psi^1_{w,\theta}(\zeta; f) = \alpha^1_{w,\theta}\phi_H\phi_{\epsilon_e}^{1/3}(2\pi\kappa f)^{-4/3} \tag{2.68-b}$$

$$\psi^1_{w,q}(\zeta; f) = \alpha^1_{w,q}\phi_E\phi_{\epsilon_e}^{1/3}(2\pi\kappa f)^{-4/3} \; . \tag{2.68-c}$$

These equations can be compared with relationships obtained from experiments. For instance, Wyngaard and Coté (1972) obtained the following empirical fits for the inertial subrange of cospectra with the vertical velocity under stable conditions:

$$\psi^1_{w,\theta}(\zeta; f) = 0.40(1 + 6.4\zeta)(2\pi\kappa f)^{-4/3} \tag{2.69-a}$$

$$\psi^1_{w,u}(\zeta; f) = 0.56(1 + 7.8\zeta)(2\pi\kappa f)^{-4/3} \; . \tag{2.69-b}$$

To compare these with the predictions of (2.68), we adopt the consensus functions given in Brutsaert (1982 pp. 68–71) for the dimensionless mean gradients in stable conditions,

$$\phi_\tau = 1 + 5\zeta \tag{2.70-a}$$

$$\phi_H = 1 + 5\zeta \tag{2.70-b}$$

$$\phi_E = 1 + 5\zeta \; . \tag{2.70-c}$$

There is, of course, some uncertainty regarding these functions: in a recent review, Högström (1988) found the constants 6.0 and 7.8, instead of 5, for ϕ_τ and ϕ_H; on the other hand Högström's figures for stable conditions show the large scatter typical of stable conditions (Brutsaert, 1982 p. 71) which can easily acommodate the values in (2.70). Also, Parlange and Katul (1992) obtained good results with their proposed modified advection-adridity approach by using (2.70) in stable conditions. As we begin to show now, even though it is not possible to arrive at definitive values for the functions in (2.70) at present, these adopted here render virtually all results in this work very consistent with one another, which makes them at least as good as any other possible choice. Another central theme of this thesis is, of course, the equality between (2.70-b) and (2.70-c) assumed above. That this is also quite reasonable will be extensively shown in the next three chapters, so for the time being we just anticipate the result.

Once the dimensionless gradients are available, (2.29-a), (2.29-e) and (2.29-f) then provide the dissipation functions ϕ_{ϵ_e}, $\phi_{\epsilon_{\theta\theta}}$ and $\phi_{\epsilon_{qq}}$. Linearizing $\phi_H\phi_{\epsilon_e}^{1/3}$ and $\phi_\tau\phi_{\epsilon_e}^{1/3}$ with a Taylor expansion to the first term around $\zeta = 0$, one obtains

$$\phi_\tau\phi_{\epsilon_e}^{1/3} = \phi_H\phi_{\epsilon_e}^{1/3} \approx 1 + \frac{19}{3}\zeta = 1 + 6.33\zeta \; . \tag{2.71}$$

which shows excellent agreement with (2.69). The "Wyngaard-Coté" "constants" for stable conditions would then be

$$\alpha^1_{wu} = 0.56 \tag{2.71-d}$$

$$\alpha^1_{w\theta} = 0.40 \tag{2.71-e}$$

where it should be noted that α^1_{wu} and $\alpha^1_{w\theta}$ are *not* constant under *unstable* conditions (Kaimal *et al.*, 1972; Wyngaard and Coté, 1972).

The dimensionless spectral budgets (2.63) actually predict that similarity holds for *the entire range* of dimensionless wavenumbers η_1, or frequencies f. Empirical relationships covering the low-frequency end and the inertial subrange have been available for a long time, and are still widely used. Probably the best known are Kaimal's (1973) curves,

$$\frac{\psi^1_{aa}}{\phi_{aa}} = \frac{nS_{a,a}}{\sigma^2_a} = \frac{0.164\,(f/f_{0,aa})}{1 + 0.164\,(f/f_{0,aa})^{5/3}} \tag{2.72-a}$$

$$\psi^1_{wa} = \frac{nS_{w,a}}{u_* a_*} = \frac{0.88\,(f/f_{0,wa})}{1 + 1.5\,(f/f_{0,wa})^{2.1}} \tag{2.72-b}$$

where the exponent 2.1 is slightly different from $7/3 = 2.3333...$ predicted in (2.68). Originally, the frequencies $f_{0,aa}$ and $f_{0,wa}$ were related empirically by Kaimal to the Richardson's number; Olesen *et al.* (1984) proposed to relate $f_{0,aa}$ linearly with the dimensionless mean gradients ϕ_F, based on the argument that $f_{0,aa}$ is proportional to the frequency of the peak of $\psi^1_{a,a}$, whereas ϕ_F is related to that and lower frequencies in the production terms of the spectral budgets. Probably the best approach is that of Moraes and Epstein (1987), who obtained $f_{0,aa}$ by equating (2.66) to (2.72-a)'s asymptotic behavior:

$$\alpha^1_{uu}\phi^{2/3}_{\epsilon_e}(2\pi\kappa f)^{-2/3} = \phi_{uu}\left(\frac{f}{f_{0,uu}}\right)^{-2/3} \tag{2.73-a}$$

$$f_{0,uu} = \left(\frac{\alpha^1_{uu}}{\phi_{uu}}\right)^{3/2}\frac{1}{2\pi\kappa}\phi_{\epsilon_e} \tag{2.73-b}$$

and analogously, for the vertical velocity spectra,

$$f_{0,ww} = \left(\frac{4\alpha^1_{uu}}{3\phi_{ww}}\right)^{3/2}\frac{1}{2\pi\kappa}\phi_{\epsilon_e}\ . \tag{2.73-c}$$

This procedure can be extended readily for spectra of scalars and cospectra of vertical velocity with u, θ and q, if it is agreed to use the theoretical prediction 7/3 instead of 2.1 in (2.72-b). We then obtain

$$f_{0,\theta\theta} = \left(\frac{\alpha^1_{\theta,\theta}}{\phi_{\theta,\theta}}\right)^{3/2} \frac{1}{2\pi\kappa}\phi_{\epsilon_e}^{-1/2}\phi_H^{3/2} \tag{2.74-a}$$

$$f_{0,qq} = \left(\frac{\alpha^1_{qq}}{\phi_{qq}}\right)^{3/2} \frac{1}{2\pi\kappa}\phi_{\epsilon_e}^{-1/2}\phi_E^{3/2} \tag{2.74-b}$$

$$f_{0,wa} = 1.4918\,(\alpha^1_{wa})^{3/4}\frac{1}{2\pi\kappa}\phi_F^{3/4}\phi_{\epsilon_e}^{1/4}\ . \tag{2.74-c}$$

In this way, *all* the spectral properties of interest are expressed in terms of the functions ϕ_F and Kaimal's dimensionless curves only. To the author's knowledge, equations (2.74) are explicitly derived here for the first time.

Chapter 3

SIMILARITY OF TEMPERATURE AND HUMIDITY

This chapter deals with some definitions about the meaning of "similarity" between two scalars, and how to assess it. It gives an account of the research efforts to establish whether the behavior of two scalars in the surface layer can be assumed to be identical or not, as regards their turbulent transport properties. Several theoretical and experimental works are described and discussed, with particular attention being devoted to the connection, first established by Warhaft (1976), between the correlation coefficient $r_{\theta q}$ for temperature-humidity and their respective eddy diffusivities K_H and K_E. With the help of the turbulent budgets of $\overline{\theta'\theta'}$, $\overline{q'q'}$ and $\overline{\theta'q'}$ it is then shown that, if the divergence of third moments is negligible or zero, such as in the case of homogeneous turbulence, then $r_{\theta q}$ is ± 1 and *all* the turbulent properties, duly non-dimensionalized, are equal for temperature and humidity. These conclusions were reached by Hill (1989a; 1989b), but they are derived here in a rather different way, which allows to elucidate some points raised by earlier analyses.

3.1 The meaning and importance of similarity

The word "similarity" is used here in a different context from that of "Monin-Obukhov Similarity" theory. There, it means the ability to describe turbulent properties with a set of suitable dimensionless parameters: the MOS functions ϕ and the independent variable ζ. Here, it is used in its perhaps more usual sense of two things being equal or having some properties in common. The "things" are temperature and humidity or, more specifically, temperature and humidity fluctuations, and the common properties are now introduced. We shall say that two scalars are similar in some property if the corresponding MOS dimensionless functions are equal. Thus similarity of mean dimensionless gradients, of mixed triple moments with w, variance and covariance will mean, respectively,

$$\phi_H = \phi_E \tag{3.1-a}$$

$$\phi_{w\theta\theta} = \phi_{wqq} \tag{3.1-b}$$

$$\phi_{ww\theta} = \phi_{wwq} \tag{3.1-c}$$

$$\phi_{\theta\theta} = \phi_{qq} = \phi_{\theta q} \; . \tag{3.1-d}$$

Notice however that (3.1-a) through (3.1-d) *do not* imply one another; in particular the second equality in (3.1-d) is to be considered an independent, stronger statement about similarity. If each MOS function for temperature is equal to its counterpart for humidity, then perfect similarity exists between the two scalars.

From a practical point of view, (3.1-a) is probably the most important. First, notice that it implies that the "eddy diffusivities" of heat and water vapor are equal. Indeed, if a is any scalar, then from the definitions of the scalar kinematic flux (2.14) and of dimensionless mean gradient (2.22) one has:

$$-\frac{\kappa z u_*}{\phi_F}\frac{\partial \overline{a}}{\partial z} \equiv u_* a_* \equiv \overline{w'a'} \equiv -K_F \frac{\partial \overline{a}}{\partial z} \tag{3.2}$$

whence $\phi_H = \phi_E \Leftrightarrow K_H = K_E$.

The equality of the dimensionless mean gradients for temperature and humidity is an essential assumption in the energy budget Bowen-ratio (EBBR) method, which derives the heat and water vapor fluxes from energy measurements plus mean temperature and humidity measurements at two levels. The steady-state energy budget for a uniform surface without advection of heat is (Brutsaert, 1982)

$$R_n = H + LE + G \tag{3.3}$$

where R_n is the net radiation reaching the ground, L is the latent heat of evaporation and G is the ground heat flux. Now if a is a scalar, it follows from the integration of (3.2) that

$$\Delta\overline{a} = \overline{a}_1 - \overline{a}_2 = \frac{a_*}{\kappa}\int_{\zeta_1}^{\zeta_2} \phi_F \frac{d\zeta}{\zeta}\ . \tag{3.4}$$

Let the *flux* Bowen Ratio be defined by (Lang *et al.*, 1983a):

$$Bo_f \equiv \frac{H}{LE}\ . \tag{3.5}$$

Then, using (3.4) above,

$$Bo_f = \frac{\overline{\rho} c_p \overline{w'\theta'}}{\overline{\rho} L \overline{w'q'}} = \frac{c_p}{L}\frac{\theta_*}{q_*} = \frac{c_p}{L}\frac{\Delta\overline{\theta}}{\Delta\overline{q}}\frac{\int_{\zeta_1}^{\zeta_2}\phi_E\, d\zeta/\zeta}{\int_{\zeta_1}^{\zeta_2}\phi_H\, d\zeta/\zeta} \tag{3.6}$$

whence

$$\phi_H = \phi_E \Rightarrow Bo_f = Bo_g \equiv \frac{c_p}{L} \frac{\Delta\overline{\theta}}{\Delta\overline{q}} \tag{3.7}$$

where the *gradient* Bowen Ratio Bo_g (Lang *et al.*, 1983a), defined above, is what is actually measured in the EBBR method . With the measurement of Bo_g, R_n and G, it is then possible to obtain the fluxes H and LE.

Now if (3.1-a) does not hold, the EBBR method cannot be applied any longer; in fact, *all* methods which are based on assuming a value for ϕ_E are then questionable, since most flux-gradient relationships, such as (2.70) have been derived from *temperature* profiles associated with heat flux measurements (Businger *et al.*, 1971; Dyer, 1974; Högstrom, 1988).

As it turns out, the question of equality of ϕ_H and ϕ_E is intimately related to the correlation coefficient between temperature and humidity fluctuations. This is fortunate in the sense that it is much easier to calculate $r_{\theta q}$ in stable conditions than to measure humidity gradients $\Delta\overline{q}$, given the smallness of humidity differences in the air during nighttime and the fact that mean humidity usually requires *two* temperature measurements (dry- and wet-bulb), whereas air temperature requires only one (dry-bulb), making the former more prone to error.

3.2 The controversy on the similarity of θ and q

The first connection between the correlation coefficient $r_{\theta q}$ and the equality (or not) of ϕ_H and ϕ_E seems to have been made by Swinbank and Dyer

(1963). They observed similar profiles of $\overline{\theta}$ and $\overline{q}$ together with a high correlation ($r_{\theta q} = 0.9$). Warhaft (1976) was the first to provide a theoretical framework for this connection. He considered the budgets of heat and humidity fluxes, (2.15-c) and (2.15-d),

$$0 = -\,\overline{w'w'}\,\frac{\partial\,\overline{\theta}}{\partial z} - \frac{\partial\,\overline{w'w'\theta'}}{\partial z} + \frac{g}{\overline{\theta}_v}\,\overline{\theta'\theta'_v} + \overline{\frac{p'}{\overline{\rho}}\frac{\partial\,\theta'}{\partial z}} - 2\epsilon_{w\theta} \tag{3.8-a}$$

$$0 = -\,\overline{w'w'}\,\frac{\partial\,\overline{q}}{\partial z} - \frac{\partial\,\overline{w'w'q'}}{\partial z} + \frac{g}{\overline{\theta}_v}\,\overline{q'\theta'_v} + \overline{\frac{p'}{\overline{\rho}}\frac{\partial\,q'}{\partial z}} - 2\epsilon_{wq} \tag{3.8-b}$$

which were closed as follows. The dissipation terms were shown to be unimportant by Wyngaard *et al.* (1971): the high-wavenumber components of w' and θ' (or q') should become less and less correlated due to local isotropy:

$$\epsilon_{w\theta} = \overline{\frac{\partial\,w'}{\partial x_k}\frac{\partial\,\theta'}{\partial x_k}} = \frac{\nu_w + \nu_\theta}{2}\int_0^\infty k^2 E_{w,\theta}(k)\,dk \approx 0\;, \tag{3.9}$$

since, due to the presence of k^2, it is exactly the high-wavenumber, highly isotropic (and hence very nearly null) part of the cospectrum which contributes most for the dissipation (the same holding for ϵ_{wq}). The divergence terms $\partial\,\overline{w'w'\theta'}\,/\partial z$ and $\partial\,\overline{w'w'q'}\,/\partial z$ were assumed to be neglible too; this will be shown to be a very reasonable approximation in Chapter 4. Finally, the pressure-scalar covariances were closed following Launder (1975):

$$\overline{\frac{p'}{\overline{\rho}}\frac{\partial\,\theta'}{\partial z}} = -\left[3.2\frac{\epsilon_e}{\overline{e'}}\,\overline{w'\theta'} + \frac{1}{2}\frac{g}{\overline{\theta}_v}\,\overline{\theta'\theta'_v}\right] \tag{3.10-a}$$

$$\overline{\frac{p'}{\overline{\rho}}\frac{\partial\,q'}{\partial z}} = -\left[3.2\frac{\epsilon_e}{\overline{e'}}\,\overline{w'q'} + \frac{1}{2}\frac{g}{\overline{\theta}_v}\,\overline{q'\theta'_v}\right] \tag{3.10-b}$$

where the same constants were used in (3.10-a) and (3.10-b). This was justified by noticing that a suitable linear combination of them has to yield the budget of virtual heat flux $\overline{w'\theta_v'}$. Indeed, given the relation (2.3) between θ_v', θ' and q',

$$\theta_v' = (1 + 0.61\overline{q})\theta' + 0.61\overline{\theta}q' \ , \tag{3.11}$$

one obtains

$$(1 + 0.61\overline{q})\overline{\frac{p'}{\overline{\rho}}\frac{\partial \theta'}{\partial z}} + 0.61\overline{\theta}\overline{\frac{p'}{\overline{\rho}}\frac{\partial q'}{\partial z}} \equiv \overline{\frac{p'}{\overline{\rho}}\frac{\partial \theta_v'}{\partial z}} \ , \tag{3.12}$$

the same holding for all the other terms in (3.8). Interestingly, the same kind of argument was used by Hill (1989a) to show that two scalars in the surface layer are perfectly similar.

Pressure-scalar closures were extensively analyzed by Moeng and Wyngaard (1986) with the help of a Large-Eddy Simulation model for the whole atmospheric boundary layer (ABL), which had essentially the same form as that used by Warhaft; their closure was

$$-\frac{1}{\rho_0}\overline{c'\frac{\partial p'}{\partial z}} = -\left[\frac{1}{2}\frac{g}{\overline{\theta}}\overline{\theta'c'} - \frac{\overline{w'c'}}{\mathcal{T}}\right] \tag{3.13-a}$$

$$\widetilde{\tau} = \mathcal{T}\frac{w_*}{z_i} \tag{3.13-b}$$

$$w_* \equiv \left[\frac{g z_i}{\overline{\theta}}\overline{w'\theta'}|_0\right]^{1/3} \tag{3.13-c}$$

where the dimensionless time scale $\widetilde{\tau}$ is between 0 and 2.5; w_* is a convective velocity scale, z_i is the height of the ABL and $\mathcal{T}$ represents a characteristic time for the whole ABL, whereas one can clearly identify, from (2.23) and (2.25),

$$\frac{\epsilon_e}{\overline{e'}} = \frac{u_*^3}{\kappa z}\phi_{\epsilon_e}\frac{1}{\phi_e u_*^2} = \frac{u_*}{\kappa z}\frac{\phi_{\epsilon_e}}{\phi_e} \tag{3.14}$$

in Launder's closure (3.10) as a characteristic time for the *surface* layer. Dakos and Gibson (1987) proposed a considerably more complicated closure based on a solution for the scalar transport equation in Fourier space, but their model seems to remain untested in atmospheric flows.

In any case, both Dakos and Gibson's and Launder's closures turn out to be quite reasonable in the light of MOS theory, since we know from (2.24) that the most general form of the pressure-scalar closure in the surface layer should read

$$\overline{\frac{p'}{\overline{\rho}}\frac{\partial\theta'}{\partial z}} = \frac{u_*^2\theta_*}{\kappa z}\phi_{p\partial\theta}(\zeta)\ . \tag{3.15}$$

It is a simple exercise to show that Launder's closure (3.10) does indeed have the form predicted above.

Now "opening up" the terms $\overline{\theta'\theta_v'}$ and $\overline{q'\theta_v'}$ in the flux budget equations (3.8), we obtain the variances $\overline{\theta'\theta'}$ and $\overline{q'q'}$ and the covariance $\overline{\theta'q'}$ explicitly, and replacing the scalar fluxes $\overline{w'\theta'}$ and $\overline{w'q'}$ by the corresponding product of eddy diffusivity and mean gradient in (3.2), we finally obtain Warhaft's expression for the ratio K_H/K_E,

$$\frac{K_H}{K_E} = \frac{1 - \frac{1}{2}\frac{g}{\overline{w'w'}}\left[\frac{\overline{\theta'\theta'}}{\overline{\theta}} + 0.61\overline{\theta'q'}\right](\frac{\partial\overline{\theta}}{\partial z})^{-1}}{1 - \frac{1}{2}\frac{g}{\overline{w'w'}}\left[\frac{\overline{\theta'q'}}{\overline{\theta}} + 0.61\overline{q'q'}\right](\frac{\partial\overline{q}}{\partial z})^{-1}} \tag{3.16}$$

from which Warhaft was able to show that $K_H = K_E$ only if $r_{\theta q} = \pm 1$. An expression somewhat simpler than (3.16) can be obtained by neglecting the effect of humidity in the density stratification; the terms involving the 0.61 factor, which accounts for virtual temperature, then drop. Substituting the mean gradients with (3.2) and expanding the resulting expression, Warhaft obtained

$$\frac{K_H}{K_E} = 1 + \frac{1}{2}\frac{g}{\overline{w'w'}}\frac{\overline{\theta'\theta'}}{\overline{\theta}}\left(\frac{\partial\,\overline{\theta}}{\partial z}\right)^{-1}\left(r_{\theta q}\frac{r_{w\theta}}{r_{wq}} - 1\right) \tag{3.17}$$

from which he anticipated that when the two fluxes H and E were of opposite sign, it was possible that $|r_{\theta q}| < 1$, with the implication that

$$\textit{Warhaft, 1976 (theoretical):} \qquad -1 < r_{\theta q} < 0 \;\Rightarrow\; \frac{K_H}{K_E} < 1\,. \tag{3.18}$$

Verma *et al.* (1978) measured eddy diffusivities over an alfafa field. To obtain estimates of H and LE independently of measured $\overline{\theta}$ and $\overline{q}$ gradients, they measured E with a lysimeter and inferred H by means of the energy budget equation (3.3). Even though they obtained different eddy diffusivities in stable conditions for heat and water vapor, their result contradicts Warhaft's theory:

$$\textit{Verma et al., 1978 (experimental):} \qquad \frac{K_H}{K_E} \sim 2 > 1 \tag{3.19}$$

where the factor 2 above is only an approximate average obtained from Verma *et al.*'s tables and pictures.

Verma *et al.*'s work generated some discussion; Hicks and Everett (1979) pointed out that different values of the zero-plane displacement height for heat and water vapor, associated with different sources and sinks within the canopy, can explain at least partially Verma *et al.*'s results. Commenting on the same paper, Brost (1979) mentioned an intriguing fact: by incorporating the budgets of temperature variance, humidity variance and temperature-humidity covariance into Warhaft's analysis, it is also possible to *refute* his results, obtaining $K_H =$

K_E *regardless* of $r_{\theta q}$. Since Brost's comments do not include all the calculations involved, it is well worth undertaking them here. Thus, consider the variance and covariance budgets (2.15) in the case of homogeneous turbulence,

$$\overline{w'\theta'}\,\frac{\partial\,\overline{\theta}}{\partial z} = -\epsilon_{\theta\theta} \tag{3.20-a}$$

$$\overline{w'q'}\,\frac{\partial\,\overline{q}}{\partial z} = -\epsilon_{qq} \tag{3.20-b}$$

$$\overline{w'\theta'}\,\frac{\partial\,\overline{q}}{\partial z} + \overline{w'q'}\,\frac{\partial\,\overline{\theta}}{\partial z} = -2\epsilon_{\theta q}\ . \tag{3.20-c}$$

He then parameterized the dissipation terms as

$$\epsilon_{\theta\theta} = \frac{\sigma_w\sigma_\theta^2}{l} \tag{3.21-a}$$

$$\epsilon_{qq} = \frac{\sigma_w\sigma_q^2}{l} \tag{3.21-b}$$

$$\epsilon_{\theta q} = r_{\theta q}\frac{\sigma_w\sigma_\theta\sigma_q}{l}\ . \tag{3.21-c}$$

Notice how the same length scale l is being assumed for all 3 cases, which may be debatable when one is discussing the similarity of θ and q. Substituting (3.21) in (3.20) above, and expressing covariances as products of correlation coefficients and standard deviations, we then obtain:

$$\overline{\theta'\theta'} \equiv \sigma_\theta^2 = -l r_{w\theta}\sigma_\theta\frac{\partial\,\overline{\theta}}{\partial z} \tag{3.22-a}$$

$$\overline{q'q'} \equiv \sigma_q^2 = -l r_{wq}\sigma_q\frac{\partial\,\overline{q}}{\partial z} \tag{3.22-b}$$

$$\overline{\theta'q'} \equiv r_{\theta q}\sigma_\theta\sigma_q = -\frac{l}{2}\left(r_{w\theta}\sigma_\theta\frac{\partial\,\overline{q}}{\partial z} + r_{wq}\sigma_q\frac{\partial\,\overline{\theta}}{\partial z}\right) \tag{3.22-c}$$

and now, substituting (3.22) above into Warhaft's ratio of K_H to K_E (3.16):

$$\frac{K_H}{K_E} = \frac{1 + \frac{1}{2}\frac{gl}{\sigma_w^2}\left[\frac{r_{w\theta}\sigma_\theta}{\overline{\theta}} + \frac{0.61}{2}\left(r_{w\theta}\sigma_\theta(\frac{\partial\,\overline{q}}{\partial z})(\frac{\partial\,\overline{\theta}}{\partial z})^{-1} + r_{wq}\sigma_q\right)\right]}{1 + \frac{1}{2}\frac{gl}{\sigma_w^2}\left[\frac{1}{2\overline{\theta}}\left(r_{w\theta}\sigma_\theta + r_{wq}\sigma_q(\frac{\partial\,\overline{\theta}}{\partial z})(\frac{\partial\,\overline{q}}{\partial z})^{-1}\right) + 0.61 r_{wq}\sigma_q\right]}\ . \tag{3.23}$$

where the correlation $r_{\theta q}$ has been canceled out. This can misleadingly suggest that its value is irrelevant. In order to eliminate the mean gradients, we can use the definition of eddy diffusivities one more time,

$$r_{w\theta}\sigma_w\sigma_\theta \equiv K_H \frac{\partial \overline{\theta}}{\partial z} \tag{3.24-a}$$

$$r_{wq}\sigma_w\sigma_q \equiv K_E \frac{\partial \overline{q}}{\partial z} \tag{3.24-b}$$

whence

$$\frac{K_H}{K_E} = \frac{1 + \frac{1}{2}\frac{gl}{\sigma_w^2}\left[\frac{r_{w\theta}\sigma_\theta}{\overline{\theta}} + \frac{0.61}{2}\left(r_{w\theta}\sigma_\theta \frac{r_{wq}\sigma_w\sigma_q}{K_E}\frac{K_H}{r_{w\theta}\sigma_w\sigma_\theta} + r_{wq}\sigma_q\right)\right]}{1 + \frac{1}{2}\frac{gl}{\sigma_w^2}\left[\frac{1}{2\overline{\theta}}\left(r_{w\theta}\sigma_\theta + r_{wq}\sigma_q \frac{r_{w\theta}\sigma_w\sigma_\theta}{K_H}\frac{K_E}{r_{wq}\sigma_w\sigma_q}\right) + 0.61 r_{wq}\sigma_q\right]}$$

$$\frac{K_H}{K_E} = \frac{1 + \frac{1}{2}\frac{gl}{\sigma_w^2}\left[\frac{r_{w\theta}\sigma_\theta}{\overline{\theta}} + \frac{0.61}{2}\left(\frac{K_H}{K_E} + 1\right) r_{wq}\sigma_q\right]}{1 + \frac{1}{2}\frac{gl}{\sigma_w^2}\left[\frac{1}{2}\left(\frac{K_E}{K_H} + 1\right)\frac{r_{w\theta}\sigma_\theta}{\overline{\theta}} + 0.61 r_{wq}\sigma_q\right]} \tag{3.25}$$

and with simple algebra one can show that (3.25) above implies

Brost, 1979 (theoretical): $$\forall\, r_{\theta q}\,,\ \frac{K_H}{K_E} = 1\ . \tag{3.26}$$

Thus, whereas Warhaft's theory leaves the door open for the equality / inequality of K_H and K_E depending on the correlation coefficient $r_{\theta q}$, Brost's modification, which simply *adds* some budget relations to Warhaft's result, leads to an almost contradictory conclusion, namely that $K_H = K_E$ *regardless* of $r_{\theta q}$ . . . But the story continues.

Lang *et al.* (1983a) calculated eddy diffusivities under stable conditions, this time over a rice field under flood irrigation in Australia; this was a careful experiment where the minimum fetch was approximately 300 m, and where the turbulent fluxes were obtained with state-of-the-art eddy correlation techniques. The main results were as follows. The correlation coefficient $r_{\theta q}$ was -0.70 ± 0.02, from which Warhafts ratio K_H/K_E predicted in (3.16) would have been between -0.9 and -1.0; the actual measured values were

$$\textit{Lang et al., 1979 (experimental):} \qquad \forall\, r_{\theta q} = -0.70;\ 0.6 < \frac{K_H}{K_E} < 1\ , \tag{3.27}$$

which is qualitatively in agreement with Warhaft's (3.18). There certainly is less ground to debate Lang *et al.*'s results than those of Verma *et al.*; two facts, however, deserve careful mention.

First, in the next two chapters we will see that the correlation coefficient of *raw* turbulent temperature and humidity data for FIFE-89 is indeed larger than -1, as in Lang *et al.*. Then, in Chapter 5 it will be shown that the coherence function for θ, q is very close to 1 over frequencies down to 0.1 Hz, falling off to zero from 0.1 to 10 Hz. We believe that there is now convincing evidence that this fall-off is purely due to instrumental separation, as will be discussed carefully in Chapter 5. Thus, it is perfectly possible to attribute less-than-perfect correlations to instrumental separation, which leaves some doubt about the actual value of $r_{\theta q}$ in Lang *et al.*'s experiment had this effect been taken into account.

Secondly, Lang *et al.* did examine properly non-dimensionalized cospectra of w, θ and w, q. Contrary to what one might expect in a case where the two scalars were dissimilar, the two cospectra collapsed perfectly on top of one another.

Hill (1989a) showed that, if MOS theory is valid for two scalars *and* a linear combination thereof, then these scalars are similar in the sense of (3.1). Moreover, all the spectral dimensionless functions will also be equal. As an example, we use Hill's line of argumentation to derive the equality of ϕ_H and ϕ_E in a way slightly different from and faster than his. Although most of Hill's developments are done with the index of refraction whose fluctuating part is a linear combination of θ' and q', the same of course can be done with the virtual temperature, for which we know that the fluctuating part is given by equation (3.11) which, upon multiplication by w' and averaging yields relation (2.18) for the virtual temperature scale,

$$\theta_{v*} = (1 + 0.61\overline{q})\theta_* + 0.61\overline{\theta}q_* \ . \tag{3.28}$$

Now assume that θ, q *and* θ_v follow MOS in the surface layer so that

$$\theta_*\phi_H = \kappa z \frac{\partial \overline{\theta}}{\partial z} \tag{3.29-a}$$

$$q_*\phi_E = \kappa z \frac{\partial \overline{q}}{\partial z} \tag{3.29-b}$$

$$\theta_{v*}\phi_{H_v} = \kappa z \frac{\partial \overline{\theta}_v}{\partial z} \ . \tag{3.29-c}$$

With the use of the definition of virtual temperature, equation (2.1), (3.29-c) becomes

$$\theta_{v*}\phi_{H_v} = \kappa z \left[(1 + 0.61\overline{q}) \frac{\partial \overline{\theta}}{\partial z} + 0.61\overline{\theta} \frac{\partial \overline{q}}{\partial z} \right] \tag{3.30}$$

whereas the corresponding linear combination of (3.29-a) and (3.29-b) above gives

$$(1 + 0.61\overline{q})\theta_*\phi_H + 0.61\overline{\theta}q_*\phi_E = \kappa z \left[(1 + 0.61\overline{q}) \frac{\partial \overline{\theta}}{\partial z} + 0.61\overline{\theta} \frac{\partial \overline{q}}{\partial z} \right] \ . \tag{3.31}$$

Thus, equating the two expressions, one finds

$$\theta_{v*}\phi_{H_v} = (1 + 0.61\overline{q})\theta_*\phi_H + 0.61\overline{\theta}q_*\phi_E \tag{3.32}$$

and now, in order for (3.28) to be always true, we must have

$$\phi_{H_v} = \phi_H = \phi_E \ . \tag{3.33}$$

Notice that the essence of this derivation lies in the assumption

$$a', b' \text{ obey MOS } \ \Rightarrow\ c' = k_A a' + k_B b' \text{ obeys MOS } \ . \tag{3.34}$$

At any rate, the assumption that θ_v itself follows MOS is highly intuitive and very hard to refute. By repeatedly invoking (3.34), Hill was able to show that *all* dimensionless functions ϕ are equal for temperature and humidity. Not only that, using the triangle and Hölder's inequalities (Abramowitz and Stegun, 1972) he showed that

$$r^2_{\theta q} = 1 \ \Rightarrow\ \frac{\theta'}{\theta_*} = \frac{q'}{q_*} \ , \tag{3.35}$$

a very strong result indeed. In short,

$$\textit{Hill, 1988 (theoretical):} \qquad \theta', q' \text{ and } \theta'_v \text{ obey MOS } \Rightarrow \begin{cases} r^2_{\theta q} = 1 \\ \text{and} \\ \phi_H = \phi_E \end{cases} \ . \tag{3.36}$$

Bertela (1989) analyzed the conditions under which the EBBR method may fail. He cites several occasions in an experiment where the solution of the energy budget equation (3.3) with the Bowen ratio calculated by means of (3.7) leads to values of H and LE having the opposite sign to that predicted by the observed mean gradients. His examples include both stable *and* unstable cases. His main conclusion is that such occurrences can be explained by advection of sensible and latent heat, a hypothesis considered in Brost's (1979) comments. It is interesting that Lang *et al.* (1983b) in a second paper concluded that local advection of sensible or latent heat was not important at their main point of measurement (in other words, they considered their fetch adequate). This conclusion, however, was reached indirectly from a set of assumptions which included evaporation tending to the Priestley-Taylor (1972) value asymptotically over distance. This is questionable, insofar as the Priestley-Taylor model assumes $H \geq 0$, a condition not met in Lang *et al.*'s (1983b) case. Notice that LeClerc and Thurtel (1990), using a random-walk Markovian model for the vertical velocity field found out that the typical fetch for an internal boundary layer to adjust to a step change in surface conditions was much larger for stable than unstable conditions, so local advection may be a more serious problem in the former case. They also observed that Bowen ratio measurements are particularly sensitive to surface inhomogeneities because of the different footprints "seen" by the lower and upper sensors.

We now derive essentially the same results as Hill's (3.36), but using a totally different set of assumptions. We shall say nothing about linear combinations of scalars and, indeed, MOS is assumed only insofar as stationarity and surface uniformity are; there will be no explicit references to ϕ_{H_v}. We do however require the transport terms in the $\overline{\theta'\theta'}$, $\overline{q'q'}$ and $\overline{\theta'q'}$ budgets to be negligible, a condition automatically fulfilled under homogeneous turbulence. Then, recall from (2.29) that the *dimensionless* budgets are simply

$$\phi_H = \phi_{\epsilon_{\theta\theta}} \tag{3.37-a}$$

$$\phi_E = \phi_{\epsilon_{qq}} \tag{3.37-b}$$

$$\phi_H + \phi_E = 2\phi_{\epsilon_{\theta q}} \, . \tag{3.37-c}$$

Now consider

$$\frac{\epsilon_{\theta q}^2}{\epsilon_{\theta\theta}\epsilon_{qq}} = \frac{\left(\frac{\nu_\theta+\nu_q}{2}\right)^2 \left(\overline{\frac{\partial\,\theta'}{\partial x_k}\frac{\partial\,q'}{\partial x_k}}\right)^2}{\nu_\theta \nu_q \left(\overline{\frac{\partial\,\theta'}{\partial x_k}\frac{\partial\,\theta'}{\partial x_k}}\right)\left(\overline{\frac{\partial\,q'}{\partial x_k}\frac{\partial\,q'}{\partial x_k}}\right)} \tag{3.38-a}$$

$$\frac{\phi_{\epsilon_{\theta q}}^2}{\phi_{\epsilon_{\theta\theta}}\phi_{\epsilon_{qq}}} = \frac{\nu_\theta^2 + 2\nu_\theta\nu_q + \nu_q^2}{4\nu_\theta\nu_q} r_{\nabla\theta\,\nabla q}^2$$

$$= 1.008 r_{\nabla\theta\,\nabla q}^2 \approx r_{\nabla\theta\,\nabla q}^2 \tag{3.38-b}$$

where the following values for the molecular diffusivities of heat and water vapor in air at 20 °C were substituted (Brutsaert, 1982):

$$\nu_\theta = 2.122 \times 10^{-5}\ \mathrm{m^2\,s^{-1}} \tag{3.39-a}$$

$$\nu_q = 2.536 \times 10^{-5}\ \mathrm{m^2\,s^{-1}}\ , \tag{3.39-b}$$

and the usual non-dimensionalization was done on the left hand side with the turbulence scales u_*, θ_* and q_*;

$$r_{\nabla\theta\,\nabla q}^2 \equiv \frac{\left(\overline{\nabla\theta' \cdot \nabla q'}\right)^2}{\left(\overline{\nabla\theta' \cdot \nabla\theta'}\right)\left(\overline{\nabla q' \cdot \nabla q'}\right)} \tag{3.40}$$

can be interpreted as the correlation coefficient between the fluctuating temperature and humidity *gradients.* From the dimensionless budgets (3.37) and (3.38-b) the following simple algebraic system obtains:

$$z^2 = r^2 xy \tag{3.41-a}$$

$$x + y = 2z \tag{3.41-b}$$

for $z = \phi_{\epsilon_{\theta q}}$, $x = \phi_H = \phi_{\epsilon_{\theta\theta}}$, $y = \phi_E = \phi_{\epsilon_{qq}}$ and $r = r_{\nabla\theta\,\nabla q}$, whose solution for x/z is

$$\frac{x}{z} = \frac{r^2 \pm \sqrt{r^4 - r^2}}{r^2}\ . \tag{3.42}$$

Since $r^2 \leq 1$, (3.42) only has real solutions for $r^2 = 1$, whence $x = y = z$; this shows, at the same time, that the dimensionless gradients ϕ_H and ϕ_E are equal, and that the fluctuating temperature and humidity *gradients* are perfectly correlated, or anti-correlated. Moreover, using Hill's (3.35) for the *gradients* instead of the scalar fluctuations, it is obvious that

$$r^2_{\nabla\theta\,\nabla q} = 1 \;\Rightarrow\; \nabla\theta' = C\nabla q' \;, \tag{3.43}$$

a result which can also be obtained in a simpler way by analogy with the equation for the linear regression of two variables through the origin. Indeed, if the correlation coefficient between a' and b' is ± 1 and their averages are null,

$$r^2_{ab} = 1 \;\Rightarrow\; \frac{\overline{a'b'}^{\,2}}{\overline{a'a'}\;\overline{b'b'}} = 1 \tag{3.44-a}$$

or

$$\left[\frac{\overline{a'b'}}{\overline{a'a'}}\right]^2 = \frac{\overline{b'b'}}{\overline{a'a'}} \;; \tag{3.44-b}$$

set

$$\alpha \equiv \frac{\overline{a'b'}}{\overline{a'a'}} \tag{3.44-c}$$

to obtain

$$\overline{b'b'} = \alpha^2\,\overline{a'a'} \;. \tag{3.44-d}$$

Now, using (3.44-c) and (3.44-d):

$$\begin{aligned}
\overline{(b' - \alpha a')^2} &= \overline{b'b'} - 2\alpha\,\overline{a'b'} + \alpha^2\,\overline{a'a'} \\
&= 2\alpha^2\,\overline{a'a'} - 2\left[\frac{\overline{a'b'}}{\overline{a'a'}}\right]^2\overline{a'a'} \\
&= (2\alpha^2 - 2\alpha^2)\,\overline{a'a'} = 0
\end{aligned} \tag{3.45}$$

whence

$$r_{ab}^2 = 1 \;\Rightarrow\; b' = \alpha a' \;. \tag{3.46}$$

It is now very easy to show that the fluctations of temperature and humidity are themselves proportional; from (3.46) above with $a' = \nabla\theta'$, $b' = \nabla q'$,

$$\begin{aligned} \nabla q' &= C\nabla\theta' \\ \frac{\partial\, q'}{\partial x_k} &= C\frac{\partial\, \theta'}{\partial x_k} \\ \frac{\partial}{\partial x_k}(q' - C\theta') &= 0 \\ q' - C\theta' &= D \end{aligned} \tag{3.47}$$

where D is an integration constant. Taking averages,

$$\overline{q'} = C\overline{\theta'} = 0 = D \tag{3.48}$$

whence:

$$q' = C\theta' \tag{3.49-a}$$

$$r_{\theta q}^2 = 1 \;. \tag{3.49-b}$$

Multiplying (3.49-a) by w' and averaging one can easily find the constant C, which of course is the same as that obtained by Hill:

$$C = \frac{q_*}{\theta_*} \;. \tag{3.50}$$

This proportionality between θ' and q' can now be used to show that all remaining dimensionless statistics and dimensionless spectral functions must be equal; for example, for the dimensionless one-dimensional spectrum,

$$\psi^1_{\theta\theta} = \frac{2n\overline{\widehat{\theta}^*\widehat{\theta}}}{\theta_*^2}\,\delta(0) \tag{3.51-a}$$

$$\psi^1_{qq} = \frac{2n\overline{\widehat{q}^*\widehat{q}}}{q_*^2}\,\delta(0)\ . \tag{3.51-b}$$

From

$$\begin{aligned}
\widehat{\theta} &= \int_{-\infty}^{+\infty} \theta'(t) e^{-2\pi\, i\, nt}\, dt \\
&= \frac{\theta_*}{q_*}\int_{-\infty}^{+\infty} q'(t) e^{-2\pi\, i\, nt}\, dt \\
&= \frac{\theta_*}{q_*}\widehat{q}\ ,
\end{aligned} \tag{3.52}$$

it follows that

$$\psi^1_{\theta,\theta} = \psi^1_{q,q}\ , \tag{3.53}$$

etc.

This derivation also serves to solve the apparent contradiction between Warhaft's (1976) and Brost's (1979) results. For even though Brost's expression (3.25) does not *explicitly* contain $r_{\theta q}$, it is noticeable that the heart of his derivation contains the same variance and covariance budgets for $\overline{\theta'\theta'}$, $\overline{q'q'}$ and $\overline{\theta' q'}$ used above. But we have just seen that the set of equations (3.37) is sufficient to prove $\phi_H = \phi_E$ and $r^2_{\theta q} = 1$ so that, even though Brost doesn't seem to have realized it, his derivation actually implies perfect correlation or anti-correlation, which reconciles his results with Warhaft's.

3.3 Further comments on $r_{\theta q}$

The preceding section firmly establishes, on a theoretical ground, that $r^2_{\theta q} = 1$ is a necessary and sufficient condition for $\phi_H = \phi_E$ *if* the flow is stationary and homogeneous, and the surface is uniform (see equations (3.41) and (3.42)). Actually, it is quite possibly a sufficient condition even when the transport terms involving triple moments are non-zero, because the corresponding dimensionless functions $\phi_{w\theta\theta}$ and ϕ_{wqq} would still be equal: see the dimensionless budgets (2.28)-e and (2.28)-f.

It should also be pointed out that $r^2_{\theta q} = 1$ is an approximation that breaks down, as it should, when one considers the effect of the slight difference (20%) in molecular diffusivities. In fact, if we now assume that the ratio of dimensionless dissipation rates is 1 on the left-hand side of (3.38-b), it will follow that $r^2_{\nabla\theta\nabla q} = 1.008^{-1} = 0.9921$. Clearly, less-than-perfect correlation between θ' and q' in the high-wavenumber range of the cospectrum is necessary for the dimensionless dissipations $\phi_{\epsilon_{\theta\theta}}$ and $\phi_{\epsilon_{qq}}$ to be equal in spite of the aforementioned differences in molecular diffusivities: see equations (2.10) and (2.25).

One can now raise the question of whether *advection* and correlation are connected. As a matter of fact, there is some experimental evidence that the correlation itself can be used as an index of advective effects, judging from the striking example provided in figure 1 of Wesely (1988), and shown in figure (3.1) below. It depicts $r_{\theta q}$ measured at various distances downwind over water from

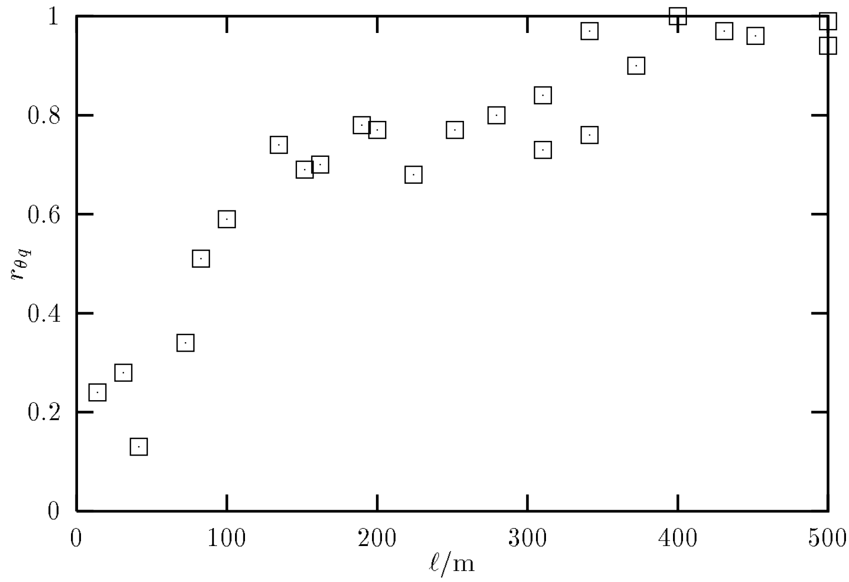

Figure 3.1 – The correlation coefficient $r_{\theta q}$ as a function of distance over water over a warm cooling pond, measured by Wesely and Hicks (1978). Adapted from Wesely (1988).

the edge of a cooling pond whose warm water increases the instability of the advected air. Notice how $r_{\theta q}$ tends asymptotically to $+1$.

Secondly, the widespread and sucessful use of the EBBR method under unstable conditions, plus a few experiments in which ϕ_H and ϕ_E were independently measured (Swinbank and Dyer, 1963; Dyer, 1967) lends credence to

$$\zeta < 0 \;\Rightarrow\; \phi_H = \phi_E \; . \tag{3.54}$$

This in turn, of course, means that one would expect to measure high correlations in unstable conditions. As mentioned before, Swinbank and Dyer obtained $r_{\theta q} = 0.9$. However, in a survey of reported observed values of $r_{\theta q}$, it shows a large variation and there is no more reason to assume $r_{\theta q}^2 = 1$ in unstable conditions than in stable ones. In fact, it seems that the correlation is actually better in stable conditions. These values are listed in table (3.1); when several values were measured, the range of observed $r_{\theta q}$ is indicated by brackets.

It is clear that on the basis of $r_{\theta q}$ alone, there should actually be more concern about the equality of ϕ_H and ϕ_E under unstable conditions than stable ones. Notice also that some of the measurements were probably distorted by the effect of sensor separation, which is not always duly taken into account; notable exceptions are found in Wesely and Hicks's (1978) and Priestley and Hill's (1985) papers. Adjusting for sensor separation increases the value of $r_{\theta q}^2$. This is an important point, which will be taken up again in the next chapters.

3.4 Closure

This chapter defined the meaning of similarity between two scalars. It also reported what have been the main theoretical and experimental efforts to establish or disprove this similarity. The experimental results of Verma *et al.* (1978) and Lang *et al.* (1983) are contradictory between themselves and with theory. It is not the intent of the present work to explain those discrepancies. It should be enough to notice that there are many possible explanations which do not contradict the assumption of similarity of θ and q: different zero-plane displacement heights and local advection of heat and/or water vapor are two main candidates. A third possibility which might be important in nocturnal

Table 3.1 – values of $r_{\theta q}$ found in the literature

Author	Stability	$r_{\theta q}$	Comments
Swinbank and Dyer (1963)	unstable	0.9	wet-bulb psychrometer was used for q'
Phelps and Pond (1971)	unstable	$[0.3, 0.87]$	measured over the sea
Wesely and Hicks (1978)	unstable	1.0	asymptotic value in developed internal boundary layer
McBean and Elliott (1981)	unstable	$[0.6, 0.9]$	0.5 m transversal separation between θ and q sensors
Koshiek (1982)	unstable	0.75	inferred from structure parameters
Lang *et al.*(1983a)	stable	-0.7	measured over an irrigated rice field
Ohtaki (1985)	unstable	-1.0	actually r_{cq}, where $c = CO_2$ concentration
Priestley and Hill (1985)	unstable	$[0.76, 0.89]$	inertial subrange spectral correlation coefficient
Priestley and Hill (1985)	stable	$[-1.0, -0.94]$	same as above
De Bruin *et al.*(1993)	unstable	$[0.0, 1.0]$	low $r_{\theta q}$ attributed to small E and large-scale ABL processes
This work (1994)	stable	$[-0.6, -1.0]$	most frequent value is -1 at $n \leq 0.1 Hz$

conditions is radiative effects, since they are introduced asymmetrically in the $\overline{\theta'\theta'}$, $\overline{q'q'}$ and $\overline{\theta'q'}$ budgets. Since the data used in the next two chapters were measured at night, it is mportant to assess quantitiatively the effects of radiation. This is done in Chapter 6.

Theoretical analysis, on the other hand, consistently indicates that temperature and humidity are indeed very similar, to the point of their instantaneous fluctuations being proportional. This result was first solidly established by Hill (1989a), even though it loomed in the previous analyses of Warhaft (1976) and Brost (1979). We have been able to substantiate it with a different and somewhat more parsimonious derivation which does not require *a priori* the ϕ-functions for linear combinations of scalars to follow MOS theory. Instead, the similarity between θ and q is established directly from the turbulent budgets for their variances and covariances. In so doing, we reconciled the remaining apparent contradictions between the former analyses by Warhaft and Brost.

A review of values of $r_{\theta q}$ found in the literature both in stable and in unstable conditions suggests that less than perfect correlation may actually be more common in the latter case. Therefore, if one considers the correlation coefficient alone, there should be at least as much reason to doubt the equality of dimensionless gradients of temperature and humidity in unstable conditions. It is possible that in many cases instrument separation was the cause of lower correlations: a standard way for correlation calculation, which of course can be highly dependent on instrumental setup, does not exist.

Chapter 4

ANALYSIS OF SIMILARITY OF θ AND q WITH DATA FROM FIFE-89

The objective of this chapter is to assess the validity of the assumptions of similarity of temperature and humidity with field data. The data consist mainly of turbulence measurements of vertical and horizontal velocity, temperature and humidity, but measurements from an energy budget Bowen ratio station and a meteorological station are also used. The validity of the flux-gradient relationship for temperature is verified; humidity gradients however are too noisy to give reliable conclusions. The correlation coefficient between θ' and q' is calculated from the raw measurements and from low-pass filtered data, and if sensor separation is duly taken into account, it is close to the theoretical value of -1. The dimensionless second- and third-order moments are calculated from the raw data for 26-minute and 52-minute runs, with the longer averaging periods yielding more stable statistics. The temperature and humidity data are shown to be statistically indistinguishable (except for one of the nights studied); this, together with the high correlations observed, lends considerable weight to the assumption of perfect similarity between the two. We also show that the third order dimensionless moments are very small and constant with stability, which implies that the corresponding transport terms are negligible in the covariance budget equations. Perhaps the poorest performance of Monin-Obukhov similarity theory is the prediction that the correlation coefficients $r_{w\theta}$ and r_{wq} are functions of stability ζ: the observed scatter is too big so that only their average behavior can be inferred.

4.1 Site and instrument characteristics

The data were measured in a natural prairie in Manhattan, Kansas, during the First International Satellite Land Surface Climatology Project (ISLSCP) International Field Experiment (FIFE-89), in July and August of 1989. For a general account of FIFE, see the special 1992 issue of the *Journal of Geophysical Research* dedicated to it (Volume 97 D No 17), and in particular Sellers et al (1992). The local topography consists of small hills terminating, sometimes abruptly, into gullies, and crisscrossed by small creeks. Vegetation was mainly grass, some of it previously burned, with sparse bushes and trees. The so-called supersite 904 was located on top of a hill. To the south (over the predominant wind direction), west and southwest there was a long mild slope generally clear of obstacles for more than 1,000 m; to the north, however, the hill ended abruptly after about 150 m into gullies. The present description is an account of a personal visit to the FIFE-89 site three years later, in june of 1992. Of course, there was no trace of the field equipment anymore, but the location of site 904 was easily found. A useful source of additional information can be found in Fritschen *et al.*

(1992). Three measuring stations were co-located: one energy budget Bowen ratio (EBBR) station run by Dr. Leo Fritschen from the University of Washington, one Portable Automated Mesonet station (PAM) and one eddy correlation (EC) station run by Dr. Marvin Wesely from Argonne National Laboratories. The energy budget station had sensors located at 1.5 and 2.7 m, whereas the eddy correlation measurements were made at a height of 2.5 m above the ground. Table 4.1 shows the measurements at each station which are relevant for this study.

Vapor pressure measurements e are equivalent to specific humidity measurements q via

$$q = \frac{0.622e}{p} \tag{4.1}$$

where p is atmospheric pressure. The turbulence measurements, in particular, were made as follows. Horizontal velocity u was measured with a fast-cup anemometer; vertical velocity fluctuations w' were measured with a sonic anemometer; temperature with an unspecified temperature sensor and humidity with a Lyman-α hygrometer (Wesely, 1991 — personal communication). All quantities were sampled at 20 Hz and stored on computer tape. The original measurement runs were 25.8133 min. long, corresponding to 30,976 measurements per run. Here, they are called "short runs". We have also analyzed consecutive pairs of short runs, calling them "long runs". Six nights were used: August 03rd, 06th, 07th, 08th, 10th and 11th. By "the night of the 03rd" is meant the period beginning around 6:00 pm (local CDST time) on August 03rd, and going until around 6:00 am (local time) the next morning, August 04th. The precise times for each night depend on data availability. These nights were chosen from the

Table 4.1 – Atmospheric measurements at FIFE supersite 904 used in this study.

Station	Measurement	Symbol
PAM	avg. air temperature at 2.0 m	$\overline{\theta}$
PAM	avg specific humidity at 2.0 m	$\overline{q}$
PAM	avg atmospheric pressure	$\overline{p}$
PAM	avg wind direction	Z
EBBR	avg air temperature at 1.5 m	$\overline{\theta}_1$
EBBR	avg air temperature at 2.7 m	$\overline{\theta}_2$
EBBR	avg vapor pressure at 1.5 m	$\overline{e}_1$
EBBR	avg vapor pressure at 2.7 m	$\overline{e}_2$
EC	avg horizontal wind speed	$\overline{u}$
EC	fluctuating vertical velocity	w'
EC	fluctuating horizontal velocity	u'
EC	fluctuating temperature	θ'
EC	fluctuating specific humidity	q'

available data to provide a reasonably large stability range. Moreover, almost all runs analyzed had sensible and latent heat fluxes such that $H \leq -10.0\ \mathrm{W\,m^{-2}}$ and $LE \geq 3.0\ \mathrm{W\,m^{-2}}$ (the exceptions being very close to these figures). Table 4.2 shows the times corresponding to the center of the short runs analyzed, and table 4.3 does the same for the long runs.

Table 4.2 – List of short runs.

03 Aug	06 Aug	07 Aug	08 Aug	10 Aug	11 Aug
	19:45	19:45			19:45
	20:15	20:15			20:15
20:45	20:45	20:45	20:45		20:45
21:15	21:15	21:45			21:15
21:45	21:45		21:45		21:45
22:15	22:15		22:15		22:15
22:45	22:45		22:45	22:45	22:45
23:15	23:15			23:15	23:15
23:45	23:45			23:45	23:45
00:15	00:15			00:15	00:15
00:45	00:45			00:45	00:45
01:15	01:15			01:15	01:15
01:45	01:45			01:45	01:45
02:15	02:15			02:15	02:15
02:45	02:45			02:45	02:45
03:15	03:15			03:15	03:15
03:45	03:45				03:45
04:15	04:15			04:15	04:15
04:45					04:45
05:15					05:15
05:45					05:45
06:15					06:15
06:45					06:45
07:15					07:15

4.2 Data Processing

The data for this study consisted of the 30-min. means for the PAM and EBBR stations listed on table 4.1 , plus the turbulence data collected at the EC station. The raw turbulence data were stored in one binary data file for each short run. The data file contains 122 records, and each record is 2,560 bytes long, holding (up to) 1,280 16-bit integers. The first five variables of the first record (a

Table 4.3 – List of long runs.

03 Aug	06 Aug	07 Aug	08 Aug	10 Aug	11 Aug
	20:30	20:30			20:30
21:30	21:30				21:30
22:30	22:30		22:00		22:30
23:30	23:30		23:00	23:00	23:30
00:30	00:30			00:00	00:30
01:30	01:30			01:00	01:30
02:30	02:30			02:00	02:30
03:30	03:30			03:00	03:30
04:30					04:30
05:30					05:30
06:30					06:30

header record) are the day, month, year, hour, and minute that the acquisition started for the run (start times are local); the remaining 1,275 values of the record being non-significant. Each of he next 121 records contains 256 simultaneous measurements of vertical wind velocity from the sonic anemometer, horizontal wind speed, water vapor pressure, temperature, and vertical wind velocity from a propeller anemometer (used to obtain the small average vertical velocity), taken at a sampling rate of 20 Hz. The total measuring time for a short run is then $121 \times 256/20 = 30{,}976/20 = 1{,}548\,\mathrm{s} = 25.8133\,\mathrm{min.}$. The integer data values range from 0 to 4095, corresponding to a 12-bit analog-to-digital conversion. For any turbulence quantity a, the recorded 16-bit integer value I_a is converted back to SI units by means of

$$a_i = F_a(I_a - 2{,}048) + G_a \tag{4.2}$$

Table 4.4 – Turbulence instruments time constants and conversion factors.

instrument	T_a/ s	F_a	G_a
sonic anemometer	0.1 m/$\overline{u}$	500/2,048	0.00 m s^{-1}
fast-cup anemometer	0.5 m/$\overline{u}$	2,150/2,048	0.26 m s^{-1}
Lyman-alpha hygrometer	0.001	0.674$\overline{e}$/2,048	0.00 Pa
temperature sensor	0.007	10/2,048	0.00 K
propellor anemometer	2.0 m/$\overline{u}$	502/2,048	0.00 m s^{-1}

where i runs from 0 to 30,975 in each run. The factors F_a and G_a for each variable are listed in table 4.4, together with the time constants T_a of each instrument.

Notice that for the sonic anemometer, temperature and humidity data, a_i *does not* represent an actual vertical velocity, temperature or vapor pressure, but the turbulent time series superimposed on an unknown mean. In the case of the fast cup and propeller anemometers their readings are absolute velocity values after the transformation (4.2). Notice also that the transformation for the Lyman-alpha data involves the mean vapor pressure (from the PAM station), whereas the time constants for the anemometers depend on the mean horizontal wind speed $\overline{u}$.

The turbulent fluctuations a'_i are calculated as follows:

$$\widetilde{a}_i = \begin{cases} \widetilde{a}_0 & i < K \\ \frac{L-1}{L}\widetilde{a}_{i-1} + \frac{1}{L}a_i & i \geq K \end{cases} \tag{4.3-a}$$

$$\widetilde{a}_0 = \frac{1}{K}\sum_{i=0}^{K-1} a_i \tag{4.3-b}$$

$$a'_i = a_i - \widetilde{a}_i \tag{4.3-c}$$

with $K = 2{,}048$ and $L = 4{,}000$. Here, L of course is not to be confused with the latent heat of evaporation nor with the Obukhov length. The "running average" $\widetilde{a}$ evolves with a typical time scale $4{,}000/20\ \mathrm{Hz} = 200\ \mathrm{s}$ which is considerably larger than that of the turbulence itself. It is therefore in principle possible to identify it with the turbulent average $\overline{a}$ in the turbulence equations. It is also shown in appendix A that the low-pass linear filter described in (4.3-a) is a digital approximation to a sensor whose analog input-output relationship is that of a RC-circuit (Lumley and Panofsky, 1964 pp. 48–50; see also Appendix A). Therefore, $\widetilde{a}$ is the time series that would be "seen" by a very slow response instrument measuring the mean flow.

Given the turbulent fluctuations a'_i, it is now possible to calculate statistics such as variances, covariances, etc. Consider the simplest case, that of estimating the standard deviation σ_a. It still can be calculated in many slightly different ways. We present two; the first is

$$s^2_{a,1} = \frac{1}{M}\sum_{i=K}^{N}(a'_i)^2\ , \tag{4.4}$$

where $N = 30,975$ and $M = N - K + 1$, which is true to the identification of $\widetilde{a}$ with a turbulent mean evolving in time. The second is

$$s^2_{a,2} = \frac{1}{M}\sum_{i=K}^{N}(a'_i - m_a)^2 \tag{4.5-a}$$

$$m_a = \frac{1}{M}\sum_{i=K}^{N} a'_i\ . \tag{4.5-b}$$

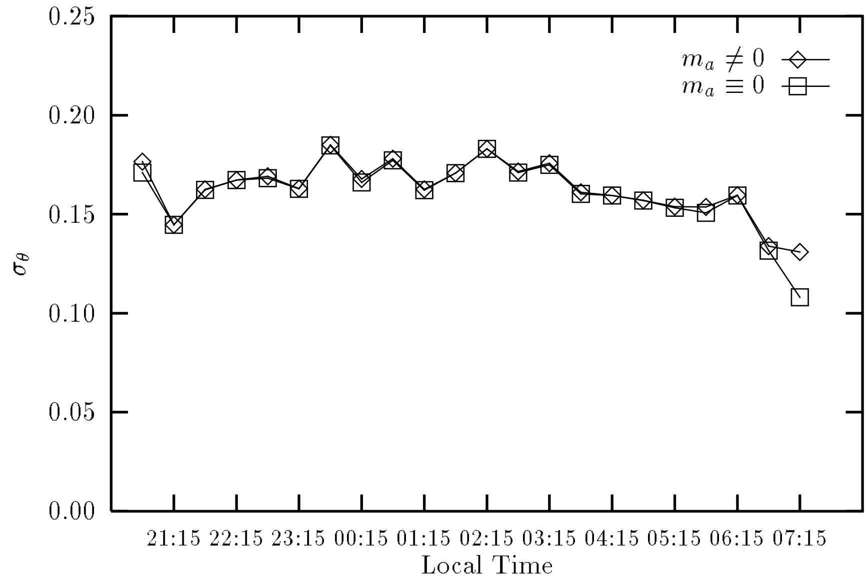

Figure 4.1 – σ_θ calculated with (4.4) (diamonds) and (4.5) (squares) for Aug 03.

Notice how m_a is simply a residual sample average of the turbulent fluctuations. In practice, the difference between the two procedures is usually very small. As an example, figure 4.1 shows the standard deviation of temperature fluctuations calculated by means of (4.4) and (4.5) on the night of Aug 03rd. The statistics presented in these chapters were obtained with the first procedure. In general, for any three quantities a, b and c the covariances are, therefore,

$$\overline{a'b'} = \frac{1}{M}\sum_{i=K}^{N} a'_i b'_i \;, \tag{4.6-a}$$

$$\overline{a'b'c'} = \frac{1}{M}\sum_{i=K}^{N} a'_i b'_i c'_i \;. \tag{4.6-b}$$

Table 4.5 – Meterological means for Aug 03.

Day	Time	$\overline{\theta}/\,^{\circ}\mathrm{C}$	$\overline{q}/\,\mathrm{g\,kg^{-1}}$	$\overline{p}/\,\mathrm{Pa}$	$\overline{u}/\,\mathrm{m\,s^{-1}}$	$Z/\,^{\circ}$	$R_n/\,\mathrm{W\,m^{-2}}$
03	2045	28.24	18.48	95,621	7.20	200.00	−29.00
03	2115	27.99	18.11	95,639	7.99	206.00	−30.70
03	2145	27.73	17.80	95,657	8.09	205.00	−30.37
03	2215	27.75	17.19	95,680	8.79	208.00	−30.96
03	2245	27.68	16.55	95,702	8.86	211.00	−30.96
03	2315	27.41	16.39	95,697	8.96	211.00	−31.61
03	2345	26.83	16.44	95,697	7.95	209.00	−32.55
03	0015	26.07	16.61	95,704	6.68	205.00	−33.17
03	0045	25.78	16.23	95,691	7.67	206.00	−33.83
03	0115	25.63	15.82	95,677	8.00	208.00	−35.35
03	0145	25.33	15.63	95,665	7.61	207.00	−36.30
03	0215	25.17	15.46	95,659	7.98	207.00	−36.55
03	0245	24.93	15.45	95,648	8.17	209.00	−36.37
03	0315	24.67	15.54	95,632	8.30	209.00	−36.80
03	0345	24.64	15.58	95,631	8.50	210.00	−38.01
03	0415	24.45	15.57	95,618	8.45	209.00	−39.17
03	0445	24.20	15.55	95,615	8.19	209.00	−39.79
03	0515	23.96	15.53	95,619	7.57	208.00	−39.24
03	0545	23.79	15.48	95,640	7.46	212.00	−38.15
03	0615	23.69	15.38	95,638	7.37	210.00	−37.35
03	0645	23.58	15.34	95,652	7.01	209.00	−30.88
03	0715	23.71	15.39	95,673	6.80	208.00	−15.41

In tables 4.5, 4.6 and 4.7, the average values of temperature, specific humidity, atmospheric pressure, wind direction and net radiation recorded at the PAM station are listed, together with the mean wind speed at 2.5 m from the fast cup anemometer at the EC station for the nights of (03), (06, 07 & 08), and (10 & 11), respectively. The values are for (26-min.) short runs. The times listed are local, and correspond to the center of each run.

Table 4.6 – Meterological means for Aug 06, 07 and 08.

Day	Time	$\overline{\theta}/\,^\circ$C	$\overline{q}/$ g kg^{-1}	$\overline{p}/$ Pa	$\overline{u}/$ m s^{-1}	$Z/^\circ$	$R_n/$ W m^{-2}
06	1945	22.06	10.05	96,699	3.99	21.00	-19.77
06	2015	20.92	9.93	96,730	4.90	21.00	-36.22
06	2045	19.48	9.72	96,777	4.86	10.00	-41.71
06	2115	18.55	9.70	96,808	4.35	18.00	-40.98
06	2145	17.68	9.48	96,862	4.34	20.00	-44.54
06	2215	17.08	9.22	96,922	4.52	23.00	-46.58
06	2245	16.41	9.05	96,945	3.96	22.00	-47.45
06	2315	15.88	8.84	96,968	4.14	19.00	-46.83
06	2345	15.34	8.70	96,983	3.54	18.00	-44.62
06	0015	14.96	8.62	97,017	3.12	27.00	-45.60
06	0045	14.54	8.57	97,040	3.21	35.00	-45.56
06	0115	13.95	8.52	97,056	2.58	43.00	-46.36
06	0145	13.66	8.44	97,043	3.01	32.00	-46.80
06	0215	13.64	8.37	97,020	3.72	24.00	-49.27
06	0245	13.17	8.26	97,041	3.23	24.00	-49.70
06	0315	12.65	8.15	97,054	2.96	23.00	-50.54
06	0345	12.24	8.07	97,061	2.86	19.00	-52.54
06	0415	11.88	7.98	97,088	2.41	20.00	-53.96
07	1945	20.86	6.37	96,815	2.83	57.00	-34.00
07	2015	19.54	6.48	96,815	2.18	66.00	-49.63
07	2045	19.21	6.36	96,822	1.82	67.00	-49.92
07	2145	19.51	6.11	96,863	1.67	45.00	-46.18
08	2045	20.05	8.30	96,619	2.54	151.00	-47.20
08	2145	19.27	7.99	96,649	2.47	149.00	-45.31
08	2215	19.30	7.87	96,671	3.05	169.00	-48.18
08	2245	19.19	7.82	96,686	3.25	180.00	-48.32
08	2315	19.32	7.70	96,688	3.44	190.00	-48.98

The fluxes adopted for the short runs in this study are available in the FIS (FIFE INFORMATION SYSTEM) database, which is resident at the laboratory for Terrestrial Physics (LTP) at NASA/Goddard Space Flight Center in Greenbelt, MD. They are not simply the covariances $\overline{w'u'}$, $\overline{w'\theta'}$ and $\overline{w'q'}$, because corrections for the slow response of the fast-cup anemometer (Hicks, 1972;

Table 4.7 – Meterological means for Aug 10 and 11.

Day	Time	$\overline{\theta}/\,^{\circ}\mathrm{C}$	$\overline{q}/\,\mathrm{g\,kg^{-1}}$	$\overline{p}/\,\mathrm{Pa}$	$\overline{u}/\,\mathrm{m\,s^{-1}}$	$Z/\,^{\circ}$	$R_n/\,\mathrm{W\,m^{-2}}$
10	2245	19.38	9.34	96,929	3.38	187.00	−38.84
10	2315	18.88	9.41	96,928	3.41	189.00	−38.44
10	2345	18.66	9.50	96,937	3.41	189.00	−36.26
10	0015	18.38	9.45	96,954	3.39	192.00	−39.02
10	0045	18.18	9.34	96,952	3.30	192.00	−38.62
10	0115	18.13	9.29	96,937	3.44	196.00	−38.91
10	0145	17.79	9.29	96,930	3.23	197.00	−38.33
10	0215	17.62	9.27	96,916	3.25	198.00	−37.93
10	0245	17.67	9.30	96,931	2.68	202.00	−29.14
10	0315	17.62	9.32	96,932	2.80	202.00	−30.63
10	0415	17.40	9.52	96,947	2.34	211.00	−17.69
11	1945	24.15	9.84	96,727	3.04	168.00	−22.00
11	2015	22.67	9.79	96,744	2.70	168.00	−39.60
11	2045	22.24	9.71	96,748	3.25	166.00	−44.55
11	2115	21.86	9.74	96,796	3.28	167.00	−43.78
11	2145	21.71	9.83	96,849	3.38	165.00	−42.22
11	2215	21.44	9.91	96,885	3.60	167.00	−42.33
11	2245	21.33	9.92	96,886	3.90	166.00	−42.29
11	2315	20.86	9.94	96,894	3.67	168.00	−37.31
11	2345	21.31	9.92	96,911	3.81	172.00	−19.07
11	0015	21.04	9.90	96,914	3.45	173.00	−34.70
11	0045	20.63	9.76	96,904	3.71	171.00	−41.64
11	0115	20.48	9.66	96,892	3.83	174.00	−40.22
11	0145	19.21	9.73	96,877	3.30	180.00	−37.53
11	0215	18.69	9.78	96,881	3.41	177.00	−38.22
11	0245	18.48	9.75	96,869	3.64	182.00	−39.31
11	0315	18.34	9.70	96,875	3.52	180.00	−38.91
11	0345	18.27	9.65	96,882	3.54	178.00	−38.69
11	0415	18.24	9.55	96,891	3.35	181.00	−38.48
11	0445	18.24	9.51	96,881	3.65	187.00	−38.48
11	0515	17.95	9.42	96,864	3.56	186.00	−38.70
11	0545	17.82	9.21	96,858	3.47	182.00	−37.86
11	0615	17.68	9.09	96,866	3.35	183.00	−35.17
11	0645	17.84	9.02	96,883	3.40	186.00	−26.49
11	0715	18.60	9.18	96,911	3.28	182.00	−0.58

Moore, 1986), density effects due to water vapor (Webb et al, 1980) plus a rotation of coordinates to take into account non-zero values of $\overline{w}$ measured by the vertical propeller anemometer have been applied (Wesely, 1991 — personal communication). Of those, only the corrections for the u'-sensor slow time response are usually significant for the data set analyzed. For statistics such as $\overline{\theta'\theta'}$ and $\overline{w'w'}$, however, the above-mentioned corrections are insignificant and were not applied. For the nights of (03), (06, 07 & 08) and (10 & 11) of August, 1989, Tables 4.8, 4.9 and 4.10 list the corresponding values of flux-related values: sensible and latent heat fluxes, friction velocity, and the "friction" temperature and humidity (or turbulent temperature and humidity scales) θ_* and q_* introduced in Chapter 2.

For the long runs listed in Table 4.3, mean values are simply the arithmetic mean of the corresponding two consecutive short runs, and are listed in table 4.11. A "new" set of fluxes was calculated for the long runs, by integrating the cospectra for w,u, w,θ and w,q whose calculation is detailed is Chapter 5. This allowed corrections to the limited time response of the fast-cup anemometer to be applied in a straightforward way (Hicks, 1972; Moore, 1986) for the obtention of u_*; H and LE were calculated in the same way to keep the procedure for calculating fluxes for the long runs uniform.

The flux and stability values obtained are listed in table 4.12.

It is also useful to analyze the data as they would have been measured by idealized slower instruments with a time constant of 0.5 s. This is done using the same linear recursive low-pass filter introduced in (4.3) to obtain turbulent

Table 4.8 – Flux variables for Aug 03.

Day	Time	H/ W m^{-2}	LE/ W m^{-2}	u_*/ m s^{-1}	θ_*/ K	q_*/ g kg^{-1}	ζ
03	20:45	−36.85	46.42	0.4884	−0.0676	0.0357	0.008
03	21:15	−29.07	38.94	0.4826	−0.0539	0.0303	0.006
03	21:45	−30.45	40.61	0.4871	−0.0559	0.0312	0.007
03	22:15	−29.97	40.75	0.4876	−0.0550	0.0313	0.006
03	22:45	−34.81	43.02	0.4934	−0.0631	0.0326	0.007
03	23:15	−32.00	38.90	0.4775	−0.0599	0.0304	0.007
03	23:45	−30.81	34.19	0.4582	−0.0600	0.0278	0.008
03	00:15	−28.98	31.31	0.4215	−0.0612	0.0276	0.010
03	00:45	−30.62	36.79	0.4673	−0.0582	0.0292	0.008
03	01:15	−31.58	36.98	0.4863	−0.0577	0.0282	0.007
03	01:45	−29.29	32.04	0.4545	−0.0572	0.0261	0.008
03	02:15	−26.41	29.49	0.4583	−0.0511	0.0238	0.007
03	02:45	−25.12	29.21	0.4632	−0.0481	0.0233	0.006
03	03:15	−30.20	29.73	0.4859	−0.0551	0.0226	0.007
03	03:45	−29.78	31.10	0.4990	−0.0529	0.0230	0.006
03	04:15	−27.85	29.15	0.5004	−0.0493	0.0215	0.006
03	04:45	−21.48	24.17	0.4454	−0.0427	0.0200	0.006
03	05:15	−25.29	25.30	0.4530	−0.0494	0.0206	0.007
03	05:45	−21.50	22.58	0.4298	−0.0442	0.0193	0.007
03	06:15	−23.60	24.27	0.4254	−0.0490	0.0210	0.008
03	06:45	−19.13	24.19	0.4184	−0.0404	0.0213	0.007
03	07:15	−10.92	28.42	0.4011	−0.0240	0.0260	0.004

Table 4.9 – Flux variables for Aug 06, 07 and 08.

Day	Time	$H/\,\mathrm{W\,m^{-2}}$	$LE/\,\mathrm{W\,m^{-2}}$	$u_*/\,\mathrm{m\,s^{-1}}$	$\theta_*/\,\mathrm{K}$	$q_*/\,\mathrm{g\,kg^{-1}}$	ζ
06	19:45	−25.62	34.54	0.2444	−0.0912	0.0509	0.045
06	20:15	−34.26	28.42	0.3233	−0.0918	0.0315	0.027
06	20:45	−33.55	26.82	0.3405	−0.0849	0.0280	0.023
06	21:15	−27.29	20.66	0.2834	−0.0827	0.0258	0.032
06	21:45	−27.65	18.89	0.2901	−0.0815	0.0229	0.031
06	22:15	−30.23	19.30	0.3048	−0.0846	0.0222	0.029
06	22:45	−30.66	17.00	0.2773	−0.0941	0.0215	0.040
06	23:15	−30.58	17.30	0.2790	−0.0931	0.0217	0.039
06	23:45	−27.67	14.82	0.2416	−0.0971	0.0214	0.055
06	00:15	−18.95	9.45	0.1933	−0.0830	0.0170	0.073
06	00:45	−15.73	8.06	0.1728	−0.0769	0.0162	0.085
06	01:15	−9.93	4.20	0.1149	−0.0729	0.0126	0.184
06	01:45	−12.25	5.87	0.1502	−0.0687	0.0135	0.102
06	02:15	−19.94	9.09	0.2039	−0.0824	0.0154	0.066
06	02:45	−23.18	8.89	0.2124	−0.0918	0.0144	0.069
06	03:15	−21.09	7.80	0.1943	−0.0911	0.0138	0.082
06	03:45	−15.16	4.25	0.1791	−0.0709	0.0081	0.076
06	04:15	−11.26	1.79	0.1293	−0.0729	0.0047	0.151
07	19:45	−27.72	27.21	0.1226	−0.1958	0.0792	0.396
07	20:15	−16.48	12.90	0.0740	−0.1920	0.0619	1.093
07	20:45	−9.21	4.03	0.0252	−0.3147	0.0566	15.880
07	21:45	−14.91	6.61	0.0431	−0.2981	0.0544	5.133
08	20:45	−15.46	4.89	0.0745	−0.1795	0.0234	1.039
08	21:45	−27.73	7.48	0.1064	−0.2248	0.0250	0.643
08	22:15	−26.42	4.87	0.1342	−0.1698	0.0129	0.307
08	22:45	−30.67	9.65	0.1540	−0.1716	0.0222	0.234
08	23:15	−28.32	8.81	0.1693	−0.1442	0.0185	0.163

Table 4.10 – Flux variables for Aug 10 and 11.

Day	Time	$H/\ \mathrm{W\,m^{-2}}$	$LE/\ \mathrm{W\,m^{-2}}$	$u_*/\ \mathrm{m\,s^{-1}}$	$\theta_*/\ \mathrm{K}$	$q_*/\ \mathrm{g\,kg^{-1}}$	ζ
10	22:45	−25.08	4.88	0.1821	−0.1184	0.0095	0.117
10	23:15	−21.79	3.98	0.1755	−0.1066	0.0080	0.114
10	23:45	−22.00	3.97	0.1877	−0.1005	0.0075	0.094
10	00:15	−24.42	5.22	0.1885	−0.1110	0.0098	0.103
10	00:45	−23.80	4.78	0.1818	−0.1121	0.0093	0.112
10	01:15	−24.93	4.63	0.1952	−0.1094	0.0084	0.095
10	01:45	−21.53	3.75	0.1792	−0.1028	0.0074	0.106
10	02:15	−21.85	3.67	0.1877	−0.0995	0.0069	0.094
10	02:45	−19.79	4.51	0.1784	−0.0948	0.0089	0.098
10	03:15	−16.37	3.57	0.1840	−0.0760	0.0068	0.074
10	04:15	−11.10	3.64	0.1587	−0.0597	0.0081	0.078
11	19:45	−19.14	12.18	0.1859	−0.0902	0.0238	0.080
11	20:15	−20.43	4.78	0.1084	−0.1642	0.0159	0.444
11	20:45	−34.62	5.74	0.1826	−0.1649	0.0113	0.159
11	21:15	−41.56	6.89	0.1983	−0.1820	0.0125	0.149
11	21:45	−43.15	6.96	0.2130	−0.1757	0.0117	0.125
11	22:15	−40.29	6.63	0.2251	−0.1551	0.0106	0.099
11	22:45	−52.65	9.32	0.2793	−0.1632	0.0120	0.068
11	23:15	−34.75	6.94	0.2278	−0.1319	0.0109	0.082
11	23:45	−24.56	10.20	0.2261	−0.0940	0.0162	0.058
11	00:15	−30.93	8.07	0.2159	−0.1239	0.0134	0.085
11	00:45	−43.84	8.61	0.2561	−0.1479	0.0120	0.073
11	01:15	−44.44	9.85	0.2607	−0.1472	0.0135	0.070
11	01:45	−21.93	3.81	0.1717	−0.1098	0.0079	0.122
11	02:15	−27.45	4.70	0.2003	−0.1176	0.0083	0.096
11	02:45	−26.23	4.38	0.2011	−0.1119	0.0077	0.091
11	03:15	−25.35	4.23	0.1845	−0.1178	0.0081	0.114
11	03:45	−29.57	5.01	0.1952	−0.1298	0.0091	0.112
11	04:15	−27.40	4.70	0.1839	−0.1277	0.0090	0.124
11	04:45	−26.41	4.61	0.1965	−0.1152	0.0083	0.098
11	05:15	−24.74	5.47	0.1810	−0.1170	0.0107	0.118
11	05:45	−25.75	5.67	0.1810	−0.1218	0.0110	0.122
11	06:15	−24.74	4.93	0.1722	−0.1229	0.0101	0.137
11	06:45	−18.75	5.62	0.1583	−0.1014	0.0125	0.132
11	07:15	−13.32	12.41	0.1931	−0.0592	0.0227	0.049

Table 4.11 – Meteorological means for long runs.

Day	Time	$\overline{\theta}$/ °C	$\overline{q}$/ g kg^{-1}	$\overline{p}$/ Pa	$\overline{u}$/ m s^{-1}
03	21:30	27.86	18.15	95,648	8.04
03	22:30	27.72	17.04	95,691	8.82
03	23:30	27.12	16.58	95,697	8.45
03	00:29	25.92	16.58	95,698	7.18
03	01:30	25.48	15.87	95,671	7.81
03	02:30	25.05	15.60	95,653	8.08
03	03:30	24.65	15.71	95,632	8.40
03	04:30	24.32	15.71	95,616	8.32
03	05:30	23.87	15.65	95,629	7.51
03	06:30	23.63	15.50	95,645	7.19
06	20:30	20.20	9.88	96,753	4.88
06	21:30	18.11	9.65	96,835	4.34
06	22:30	16.74	9.18	96,933	4.24
06	23:30	15.61	8.82	96,975	3.84
06	00:29	14.75	8.64	97,028	3.16
06	01:30	13.80	8.52	97,049	2.79
06	02:30	13.40	8.36	97,030	3.47
06	03:30	12.44	8.15	97,058	2.91
07	20:30	19.37	6.44	96,818	2.00
08	22:00	19.28	7.96	96,660	2.76
08	23:00	19.25	7.80	96,687	3.34
10	23:00	19.13	9.43	96,929	3.34
10	24:00	18.52	9.53	96,945	3.40
10	01:00	18.15	9.37	96,944	3.40
10	02:00	17.71	9.33	96,923	3.37
10	03:00	17.64	9.37	96,932	3.24
11	20:30	22.46	9.81	96,746	2.98
11	21:30	21.78	9.84	96,823	3.33
11	22:30	21.38	9.97	96,886	3.75
11	23:30	21.09	9.99	96,902	3.74
11	00:30	20.84	9.89	96,909	3.58
11	01:30	19.85	9.75	96,884	3.57
11	02:30	18.59	9.82	96,875	3.52
11	03:30	18.30	9.73	96,878	3.53
11	04:30	18.24	9.59	96,886	3.50
11	05:30	17.88	9.37	96,861	3.51
11	06:30	17.76	9.10	96,874	3.38

Table 4.12 – Flux variables for long runs.

Day	Time	$H/\,\mathrm{W\,m^{-2}}$	$LE/\,\mathrm{W\,m^{-2}}$	$u_*/\,\mathrm{m\,s^{-1}}$	$\theta_*/\,\mathrm{K}$	$q_*/\,\mathrm{g\,kg^{-1}}$	ζ
03	21:30	−22.98	35.64	0.4247	−0.0484	0.0315	0.008
03	22:30	−25.68	38.98	0.4537	−0.0506	0.0322	0.007
03	23:30	−24.84	35.62	0.4260	−0.0521	0.0312	0.008
03	00:30	−23.50	32.11	0.4172	−0.0501	0.0286	0.009
03	01:30	−24.22	33.24	0.4262	−0.0505	0.0289	0.008
03	02:30	−20.95	28.94	0.4230	−0.0439	0.0253	0.007
03	03:30	−23.41	29.72	0.4634	−0.0448	0.0237	0.006
03	04:30	−19.31	24.85	0.4348	−0.0393	0.0211	0.006
03	05:30	−17.97	22.93	0.4223	−0.0376	0.0200	0.006
03	06:30	−16.89	24.08	0.3965	−0.0376	0.0223	0.007
06	20:30	−31.82	27.65	0.3102	−0.0886	0.0318	0.029
06	21:30	−23.94	20.11	0.2937	−0.0699	0.0242	0.026
06	22:30	−28.26	19.89	0.2816	−0.0855	0.0248	0.035
06	23:30	−25.32	15.37	0.2522	−0.0852	0.0213	0.044
06	00:30	−15.56	8.45	0.1731	−0.0760	0.0170	0.084
06	01:30	−9.90	4.97	0.1304	−0.0640	0.0132	0.125
06	02:30	−17.13	8.20	0.1844	−0.0782	0.0153	0.077
06	03:30	−15.33	6.07	0.1777	−0.0724	0.0117	0.077
07	20:30	−12.62	6.21	0.0573	−0.1898	0.0384	1.882
08	22:00	−29.00	9.18	0.1229	−0.2036	0.0265	0.445
08	23:00	−27.12	9.65	0.1476	−0.1584	0.0232	0.239
10	23:00	−19.91	5.46	0.1724	−0.0992	0.0112	0.111
10	24:00	−19.18	5.30	0.1769	−0.0930	0.0106	0.099
10	01:00	−22.00	5.99	0.1777	−0.1061	0.0119	0.112
10	02:00	−18.66	4.45	0.1730	−0.0922	0.0091	0.103
10	03:00	−15.47	4.77	0.1731	−0.0764	0.0097	0.085
11	20:30	−25.74	6.98	0.1483	−0.1510	0.0170	0.225
11	21:30	−37.20	8.95	0.1937	−0.1667	0.0166	0.146
11	22:30	−41.17	10.38	0.2364	−0.1509	0.0157	0.089
11	23:30	−26.90	10.10	0.2142	−0.1087	0.0169	0.077
11	00:30	−31.54	9.78	0.2263	−0.1205	0.0154	0.077
11	01:30	−30.33	8.60	0.2130	−0.1227	0.0144	0.089
11	02:30	−24.43	6.23	0.1920	−0.1092	0.0115	0.098
11	03:30	−22.25	5.66	0.1732	−0.1101	0.0115	0.122
11	04:30	−21.62	5.55	0.1731	−0.1070	0.0113	0.119
11	05:30	−22.31	6.23	0.1729	−0.1105	0.0127	0.123
11	06:30	−19.88	6.29	0.1592	−0.1069	0.0139	0.140

fluctuations at the 20 Hz time scale; a window of width $W = 10$ is used to low-pass filter the raw series; this generates a filtered series $a^{\triangleleft}$ which corresponds to the oversampled raw output of a slow instrument. The series is resampled every W points and the resampled, smaller series is called $\breve{a}$. Finally, time trends are removed from $\breve{a}$ with a second filtering operation with the same time constant (200 s) used in (4.3):

$$a_i^{\triangleleft} = \begin{cases} a_0^{\triangleleft} & i < W \\ \frac{W-1}{W} a_{i-1}^{\triangleleft} + \frac{1}{W} a_i & i \geq W \end{cases} \tag{4.7-a}$$

$$a_0^{\triangleleft} = \frac{1}{W} = \sum_{i=0}^{W-1} a_i \tag{4.7-b}$$

$$\breve{a}_j = a_{jW}^{\triangleleft} \tag{4.7-c}$$

$$\widetilde{\breve{a}}_j = \begin{cases} \widetilde{\breve{a}}_0 & j < X \\ \frac{Y-1}{Y} \widetilde{\breve{a}}_j + \frac{1}{Y} \breve{a}_j & j \geq X \end{cases} \tag{4.7-d}$$

$$\widetilde{\breve{a}}_0 = \frac{1}{Y} \sum_{j=0}^{Y-1} \breve{a}_j \tag{4.7-e}$$

$$\breve{a}_j' = \breve{a}_j - \widetilde{\breve{a}} \tag{4.7-f}$$

where $X = 204$ and $Y = 400$, as opposed to $K = 2,048$, $L = 4,000$, since the sampling is ten times slower. The $\breve{a}'$ series sampled at 2 Hz (every 0.5 s) has a Nyquist frequency of 1 Hz, and will be useful for the computation of the low-frequency part of spectra for the long runs. It has only $30,976/10 = 3,097$ points, which considerably speeds up the calculation of statistics and spectral characteristics (by means of numerical Fast Fourier Transforms). It is important to notice that this is a simple and straighforward way to “filter out” the high frequencies which are associated to the smallest turbulent scales, or eddies. This in turn means that we will be analyzing only those eddies with a typical size larger than $\overline{u}T_W$, where $T_W = 0.5\,\mathrm{s}$. Since the smallest values of $\overline{u}$ are of the order of 2.0 $\mathrm{m\,s^{-1}}$ (see tables 4.5, 4.6 and 4.7) this in general means eddies larger than 1 m. Therefore, the "low-frequency" data series $\breve{a}$ will tend to be less influenced by sensor separation effects.

4.3 Dimensionless temperature and humidity gradients

In principle, the best way to assess the eqality of ϕ_H and ϕ_E is to measure them independently. Two facts that compound the problem of measuring scalar gradients in stable conditions are the intrinsic larger scatter that is typically observed, discussed in section 2.6, and the lesser precision of humidity measurements, which usually (until now at least) involve measurement of wet- and dry-bulb temperatures. The present data set is not an exception. We tried to assess the validity of equations (2.70) for ϕ_H and ϕ_E by substituting them in (3.4) for the mean temperature and humidity differences, and comparing them with observed values. Brutsaert (1982 p. 71) suggests that there may be an upper limit of validity of the linear relationships (2.70) at around $\zeta = 1$, beyond which ϕ_H (and supposedly ϕ_E) become constant. Therefore, we actually used

$$\phi_F = \begin{cases} 1 + 5\zeta & \zeta \le \zeta_{\mathrm{LIM}} \\ \phi_{\mathrm{LIM}} = 1 + 5\zeta_{\mathrm{LIM}} & \zeta > \zeta_{\mathrm{LIM}} \end{cases} . \tag{4.8}$$

The theoretical value of the scalar difference between two levels z_1 and z_2 is given by

$$\Delta\overline{a} = \overline{a}_1 - \overline{a}_2 = \frac{a_*}{\kappa}\int_{\zeta_1}^{\zeta_2} \phi_F \frac{d\zeta}{\zeta} \tag{4.9-a}$$

$$\equiv \frac{a_*}{\kappa}\Phi_{F12}(\zeta_1, \zeta_2) \tag{4.9-b}$$

where the following 3 cases can happen:

$$\Phi_{F12} = \begin{cases} \ln\left(\frac{\zeta_2}{\zeta_1}\right) + 5(\zeta_2 - \zeta_1) & \zeta_1 \leq \zeta_{\mathrm{LIM}} \text{ and } \zeta_2 \leq \zeta_{\mathrm{LIM}} \\ \ln\left(\frac{\zeta_{\mathrm{LIM}}}{\zeta_1}\right) + 5(\zeta_{\mathrm{LIM}} - \zeta_1) + \phi_{\mathrm{LIM}} \ln\left(\frac{\zeta_2}{\zeta_{\mathrm{LIM}}}\right) & \zeta_1 \leq \zeta_{\mathrm{LIM}} \text{ and } \zeta_2 > \zeta_{\mathrm{LIM}} \\ \phi_{\mathrm{LIM}} \ln\left(\frac{\zeta_2}{\zeta_1}\right) & \zeta_1 > \zeta_{\mathrm{LIM}} \text{ and } \zeta_2 > \zeta_{\mathrm{LIM}} \end{cases} . \tag{4.10}$$

A "best" value (fit by eye) $\zeta_{\mathrm{LIM}} = 0.4$ was obtained by trial and error with successive plots of the theoretical against the observed temperature differences. The result is shown in figure 4.2. Humidity differences are in vapor pressure units, because this is how they were reported (Fritschen, 1991 — personal communication) at the EBBR station. Notice how the humidity differences are too noisy for any conclusion to be drawn. In fact, there is a large number of points with the "wrong" sign, suggesting an unphysical situation of countergradient fluxes. These points correspond in their majority to the night of August 03rd, which will be seen to exhibit dissimilarity between temperature and humidity for all properties investigated. Even if the points from that night are deleted, the remaining plot is still too scattered for any firm conclusion to be reached, so the subject has to be left at that.

It should be emphasized that the behavior displayed in figure 4.2 should not be interpreted as indicating some malfunctioning of the EBBR station. On the contrary, it seems to be usual under nocturnal stable conditions. For a comparison, see for instance figure 5 of Fritschen and Simpson (1989).

Notice also that the *temperature* difference is remarkably well predicted by (4.9), which lends confidence in the adopted ϕ_H. It is also worthwhile noticing the unusually low value obtained for ζ_{LIM} compared to Hicks's (1976) figure (see

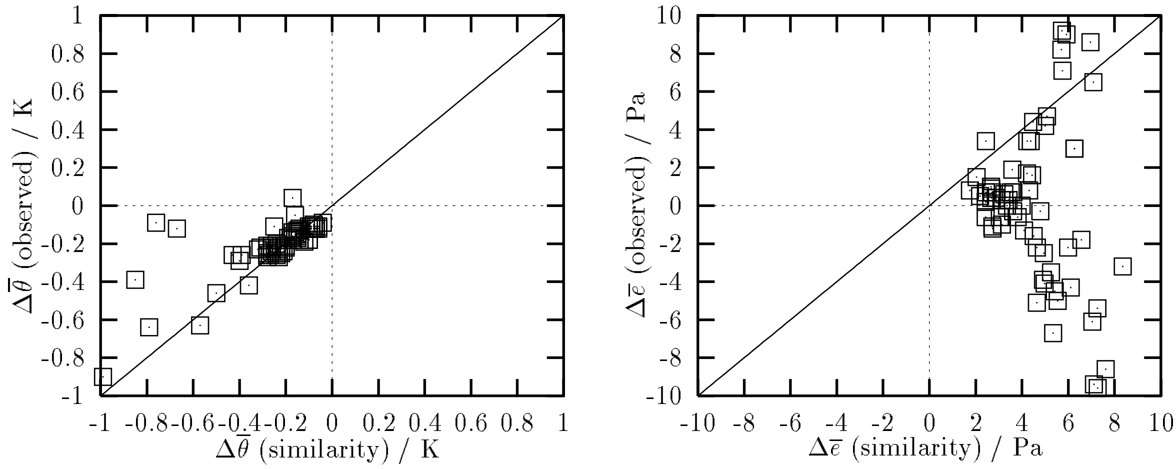

Figure 4.2 – Calculated (by means of (4.9) and (4.10)) and observed temperature and humidity differences

also Brutsaert, 1982, figure 4.6). Given the relatively few cases of strong (say, larger than 0.5) stability ζ in the record analyzed, however, this observation too will require further experimental investigation.

4.4 Temperature-humidity correlation

The correlation coefficient $r_{\theta q}$ was calculated for all short runs for the raw turbulent fluctuations θ', q' and the low-pass filtered series $\check{\theta}'$ and $\check{q}'$. In each case, the calculations are straightforward and follow (2.26). The plot of $r_{\theta q}$ versus stability is shown in figure 4.3, with diamonds indicating the high-frequency 20 Hz series, and squares the low-frequency 2 Hz series. Notice that the low-frequency correlation coefficient is most of the time closer to -1, i.e., filtering out the small-scale turbulence *increases* the correlation between the two scalars. With some exceptions, the correlation coefficient for the "raw" data is around -0.8, and for the filtered data -0.9. When the coherence function for the long runs is plotted, it will be seen that there is a wide frequency range for which the *"spectral"* correlation approaches -1, as predicted by theory in Chapter 3.

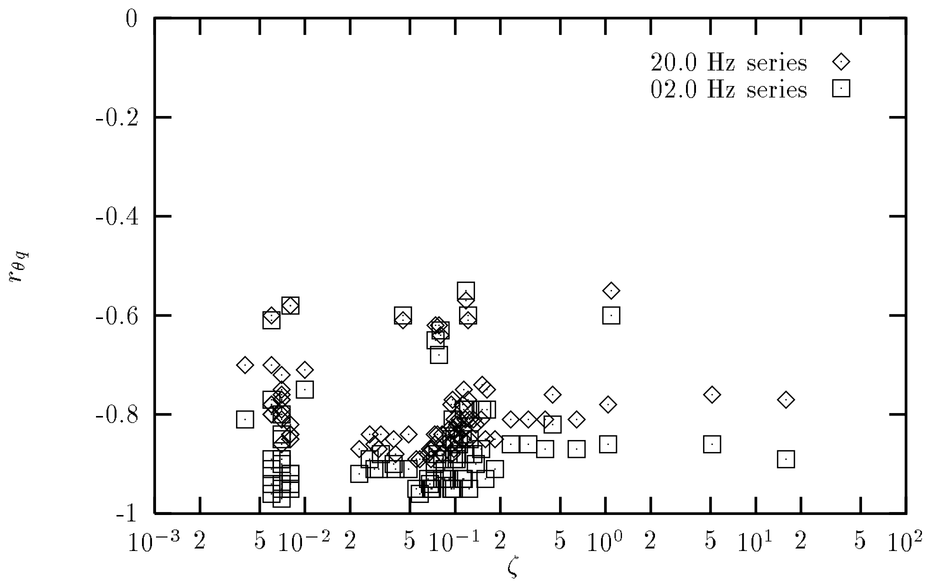

Figure 4.3 – Correlation coefficient between θ' and q', $\check{\theta}'$ and $\check{q}'$.

4.5 Dimensionless statistics for temperature and humidity

Following the definitions in Chapter 3, an alternative way to asses similarity is to look at the dimensionless ϕ functions for both scalars. The simplest form for the non-dimensionalized standard deviation of turbulent quantities in the stable surface layer is (Tillman, 1972; Ariel and Nadezhina, 1976; Hicks, 1981; Wesely, 1988; De Bruin et al, 1992)

$$\frac{\sigma_w}{u_*} = \sqrt{\phi_{ww}} = A_w \tag{4.11-a}$$

$$\frac{\sigma_u}{u_*} = \sqrt{\phi_{uu}} = A_u \tag{4.11-b}$$

$$\frac{\sigma_\theta}{\theta_*} = \sqrt{\phi_{\theta\theta}} = A_\theta \tag{4.11-c}$$

$$\frac{\sigma_q}{q_*} = \sqrt{\phi_{qq}} = A_q \tag{4.11-d}$$

where A_u, A_w, A_θ and A_q are constants. There is no deeper reason to assume the functions ϕ_{aa}, and hence A_a, to be constant in the stable range of ζ; in the face of the wide scatter that many of them present, however, this is probably the best assumption that can be made for the time being. In Chapter 6, however, we will be able to derive a "theoretical" $\phi_{\theta\theta}$ function from a simple spectral model. That function will be seen to vary extremely slowly with stability (on the stable range), being virtually indistinguishable from a constant when statistical variability is considered.

We begin by surveying some values from the literature with which to compare the present study, in table 4.13. It should be noted that some of the values were inferred from pictures or are averages from tables, and that they do not always appear explicitly in the papers referred. It is clear that there is still considerable uncertainty regarding the values of the constants, of which A_w is probably the one best known.

With the simple forms of (4.11), it is not only possible to estimate the values of A_a by linear regression with the FIFE-89 data set, but also to test the

Table 4.13 – Values of A_a in the literature.

Author	A_w	A_u	A_θ	A_q	Comments
Tillman (1972)	–	–	1.77	–	From Wyngaard et al's (1971) Kansas data.
Tillman (1972)	–	–	2.50	–	As $\zeta \uparrow 0$.
Ariel and Nadezhina (1977)	1.30	2.50	–	–	
Caughey *et al.* (1979)	1.43	–	2.24	–	Average of all runs at 4.0 m (in their table 2)
Wesely (1988)	1.30	–	1.85	1.85	A_q assumed equal to A_θ.
Smedmann (1988)	1.28	2.30	–	–	
Högström (1990)	1.32	–	2.50	–	Values deduced from Högström's figures.
Weaver (1990)	–	–	2.57	2.17	Average values of Weaver's regressions.
Wang and Mitsuta (1991)	1.14	–	3.00	–	Measured in the Gobi desert.
De Bruin *et al.* (1993)	1.50	2.50	2.90	–	

hypothesis $A_\theta = A_q$. Notice that, by forcing the regression through the origin, there are *two* estimators for A_a, depending on the choice of σ_a or a_* as the independent variable. We have performed the calculations both for short and long runs. For the short runs, the standard deviations were calculated with the procedure outlined in section 4.2. In the case of long runs, the standard deviations are obtained from the integral of the respective spectra, which are presented in Chapter 5, whereas the fluxes, and therefore u_*, θ_* and q_* were calculated from the integral of the respective cospectra, as mentioned earlier.

The regression parameters thus obtained, and their standard errors, are shown in tables 4.14 , 4.15 , 4.16 and 4.17 for each of the possible cases. The results are always presented with and without the data points from the night of August 03rd, since we believe that this night showed a strong (and unexplained) dissimilarity between temperature and humidity. Evidence for this has already been seen in the plots of humidity differences, and will continue to show up in this and the next chapter. The corresponding plots, with the regression lines as calculated in tables 4.16 and 4.17 are shown in figures 4.4, 4.5, 4.6 and 4.7. In those tables, a indicates the variable being regressed, r is the correlation coefficient of the regression, RMSE is the root mean square error of the linear estimate, in the same units as a; $\hat{A}$ or $\hat{A}^{-1}$ is the estimate for the constant A, and $\hat{\sigma}_A$ is (the estimate of) the standard deviation of $\hat{A}$. For example, in table 4.14 , the regression for σ_w without the night of Aug 03rd has a correlation coefficient of 0.91; the average of the square root of the square of the devations of σ_w from the regression line is $0.033\ \mathrm{m\,s^{-1}}$ and the estimate for the regression is $\hat{A} = (1.399 \pm 0.163)$.

Due to statistical variation alone, one would expect A_θ and A_q to be different in the linear regressions. Moreover, some bias should also be expected due to the fact that the temperature and humidity sensors were about 30 cm apart. Therefore, in order to assess how similar temperature and humidity are in this respect, we applied a statistical test whose null hypothesis is $A_\theta = A_q$ or $A_\theta^{-1} = A_q^{-1}$. For short and long runs, with and without the night of Aug 03, we

Table 4.14 – Regression parameters of $\sigma_a = A_a a_*$ for short runs.

	without Aug 03				**with Aug 03**			
a	r	RMSE	$\hat{A}$	$\hat{\sigma}_A$	r	RMSE	$\hat{A}$	$\hat{\sigma}_A$
w	0.91	0.033	1.399	0.163	0.97	0.038	1.326	0.131
u	0.85	0.106	2.680	0.406	0.97	0.107	2.902	0.351
θ	0.70	0.056	1.833	0.175	0.65	0.058	1.892	0.143
q	0.76	0.017	2.000	0.199	0.74	0.018	2.231	0.203

Table 4.15 – Regression parameters of $\sigma_a = A_a a_*$ for long runs.

	without Aug 03				**with Aug 03**			
a	r	RMSE	$\hat{A}$	$\hat{\sigma}_A$	r	RMSE	$\hat{A}$	$\hat{\sigma}_A$
w	0.96	0.020	1.468	0.266	0.99	0.021	1.452	0.228
u	0.89	0.086	2.829	0.651	0.97	0.104	3.148	0.595
θ	0.84	0.032	1.999	0.289	0.68	0.045	2.071	0.220
q	0.95	0.005	2.216	0.409	0.95	0.006	2.326	0.393

Table 4.16 – Regression parameters of $a_* = A_a^{-1}\sigma_a$ for short runs.

	without Aug 03				**with Aug 03**			
a	r	RMSE	$\hat{A}^{-1}$	$\hat{\sigma}_{A^{-1}}$	r	RMSE	$\hat{A}^{-1}$	$\hat{\sigma}_{A^{-1}}$
w	0.92	0.024	0.705	0.094	0.98	0.028	0.747	0.088
u	0.77	0.039	0.359	0.038	0.96	0.037	0.339	0.033
θ	0.85	0.030	0.520	0.088	0.85	0.030	0.496	0.080
q	0.87	0.008	0.447	0.077	0.84	0.008	0.405	0.057

Table 4.17 – Regression parameters of $a_* = A_a^{-1}\sigma_a$ for long runs.

	without Aug 03				**with Aug 03**			
a	r	RMSE	$\hat{A}^{-1}$	$\hat{\sigma}_{A^{-1}}$	r	RMSE	$\hat{A}^{-1}$	$\hat{\sigma}_{A^{-1}}$
w	0.97	0.014	0.678	0.130	0.99	0.015	0.687	0.112
u	0.83	0.030	0.345	0.053	0.96	0.033	0.313	0.043
θ	0.91	0.016	0.491	0.119	0.88	0.021	0.463	0.117
q	0.95	0.002	0.444	0.084	0.95	0.002	0.424	0.065

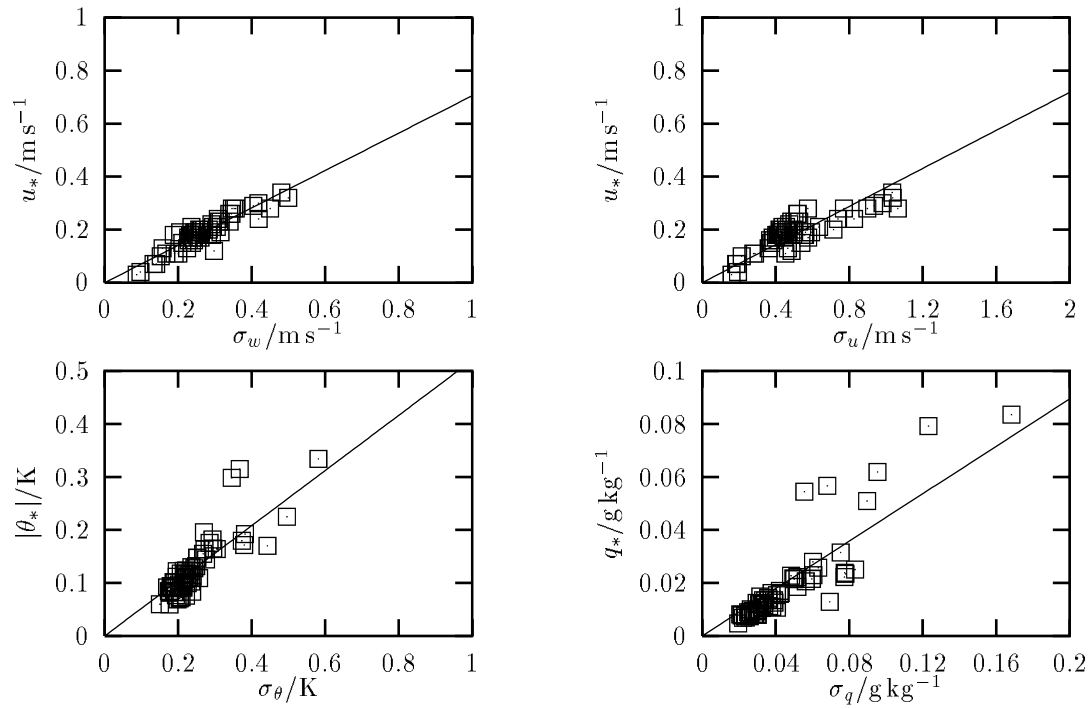

Figure 4.4 – Regressions between σ_a and a_* for short runs without Aug 03.

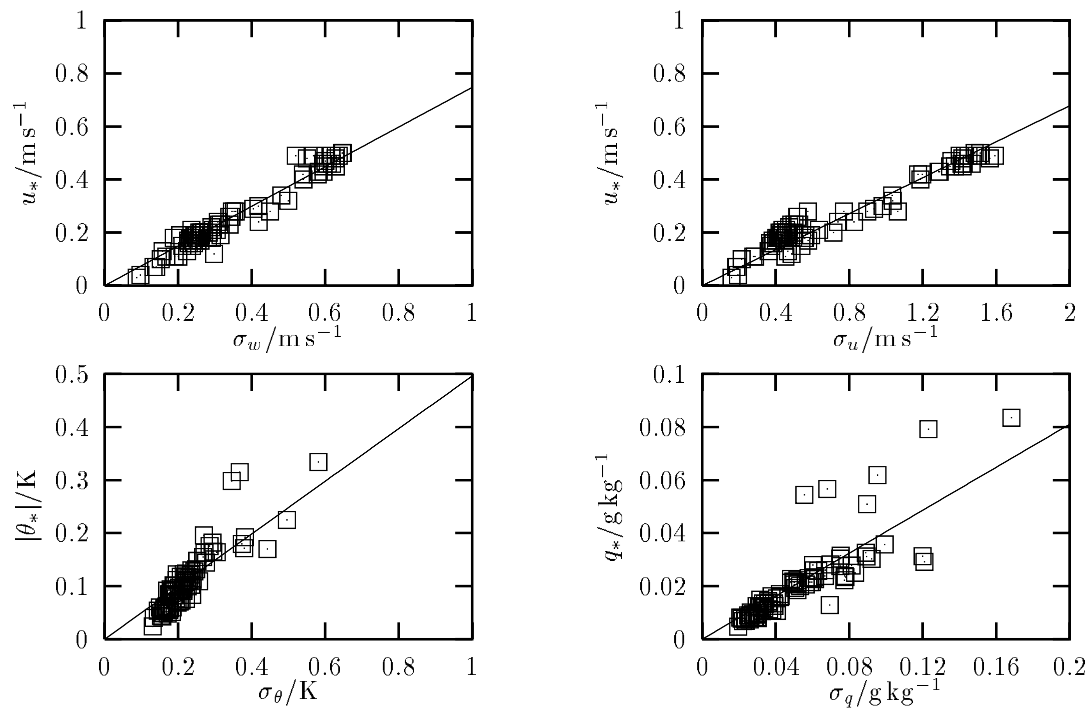

Figure 4.5 – Regressions between σ_a and a_* for short runs with Aug 03.

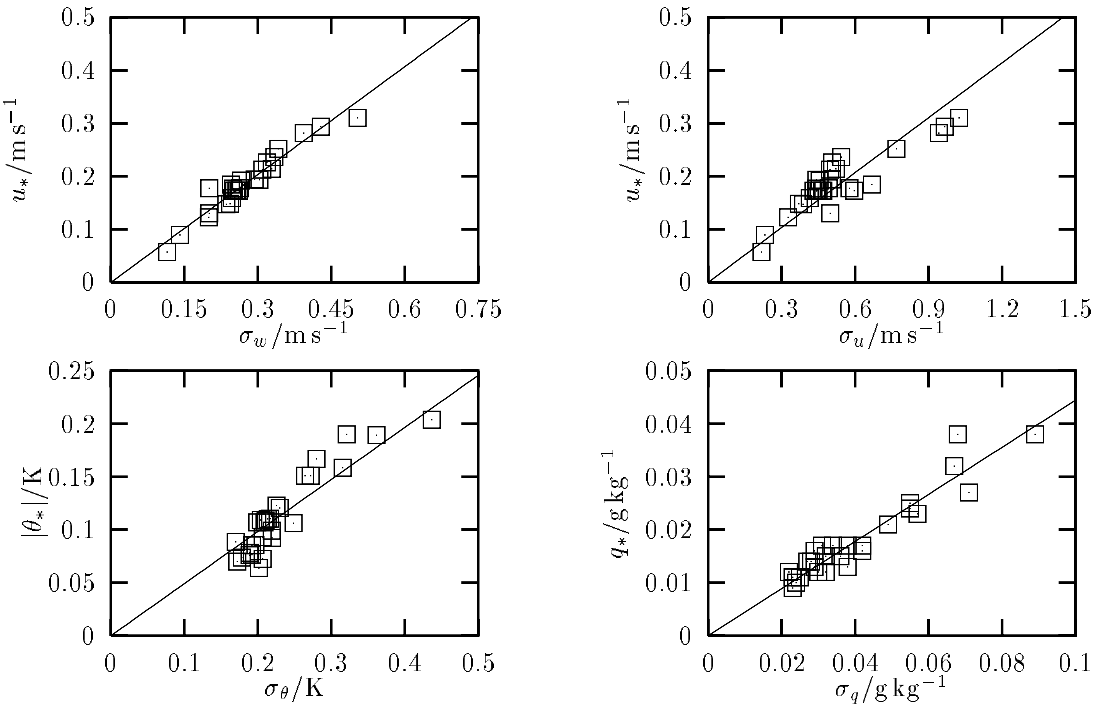

Figure 4.6 – Regressions between σ_a and a_* for long runs without Aug 03.

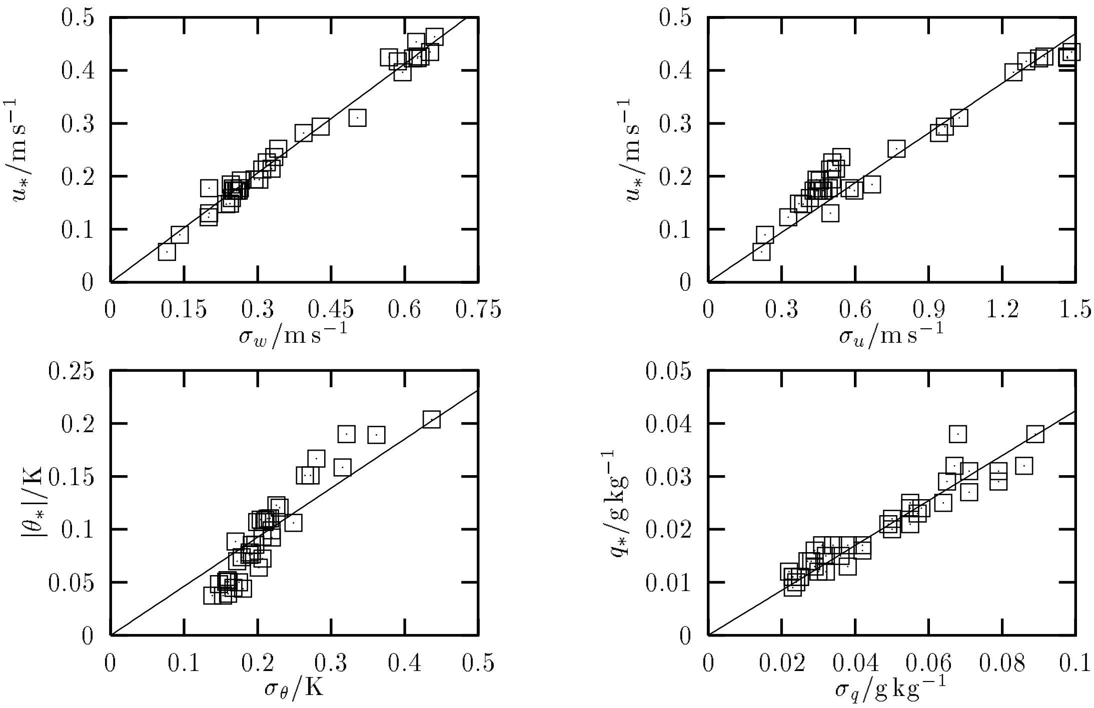

Figure 4.7 – Regressions between σ_a and a_* for long runs with Aug 03.

calculate

$$u = \frac{|\hat{A}_\theta - \hat{A}_q|}{\min(\hat{\sigma}_{A_\theta}, \hat{\sigma}_{A_q})} \ , \tag{4.12-a}$$

$$p = P[U \geq u] \tag{4.12-b}$$

and accept the null hypothesis if $p > 0.05$, which sets the significance level at 10%. The symbols u and p are used here following common statistical practice, and hopefully will not cause confusion with horizontal velocity or pressure; also, $P[U \geq u]$ is the standard notation for the probablity that the random variable U exceeds the quantile u, and will depend on the underlying probability distribution of U. The u-statistic has Student's t-distribuition, but assuming it to be normally distributed to evaluate p makes the test more conservative (Benjamin and Cornell, 1970 pp. 432–439). The results are presented in tables 4.18 and 4.19. Notice that we can only reject the null hypothesis when data from the night of Aug 03rd are included, and even then only for the short runs.

Another way to analyze turbulence statistics is to plot the dimensionless functions ϕ_{ab} and ϕ_{abc} defined in Chapter 2 against the stability ζ. We therefore calculated the four functions ϕ_{aa}, ϕ_{aaa}, ϕ_{waa} and ϕ_{wwa}, for $a = \theta$ and $a = q$, both for short and long runs. The statistics for the long runs can be obtained by simply merging the series of a'_i for two consecutive short runs. An alternative way is to integrate the higher-order cospectra presented in the next chapter; results for both procedures are presented.

We begin by presenting the statistics for the short runs in figures 4.8 and 4.9; the corresponding statistics for the long runs, calculated in a conventional

Table 4.18 – Test for equality of the slopes A_θ and A_q.

	without Aug 03		**with Aug 03**	
data series	u	p	u	p
short runs	0.954	0.170	2.371	0.009
long runs	0.751	0.226	1.159	0.123

Table 4.19 – Test for equality of the slopes A_θ^{-1} and A_q^{-1}.

	without Aug 03		**with Aug 03**	
data series	u	p	u	p
short runs	0.948	0.172	1.596	0.055
long runs	0.560	0.288	0.600	0.274

way by means of simply merging two adjacent short runs and their θ_i' and q_i' series are shown next on figures 4.10 and 4.11. Finally, third moments calculated by integration of higher-order cospectra are shown in figures 4.12 and 4.13.

There is a considerable improvement in the overall appearance of the dimensionless statistics when long runs are used, regardless of whether conventional (figures 4.10 and 4.11) or spectral (figures 4.12 and 4.13) estimates are made. Moreover, the long run statistics lead us to important conclusions. The overall behavior of ϕ_{aa} and ϕ_{aaa} seems to be constant with stability, in spite of the considerable scatter which also appears, however, in other works (Högström, 1990; Wang and Mitsuta, 1991). Temperature skewness is postive (since $\theta_* < 0$)

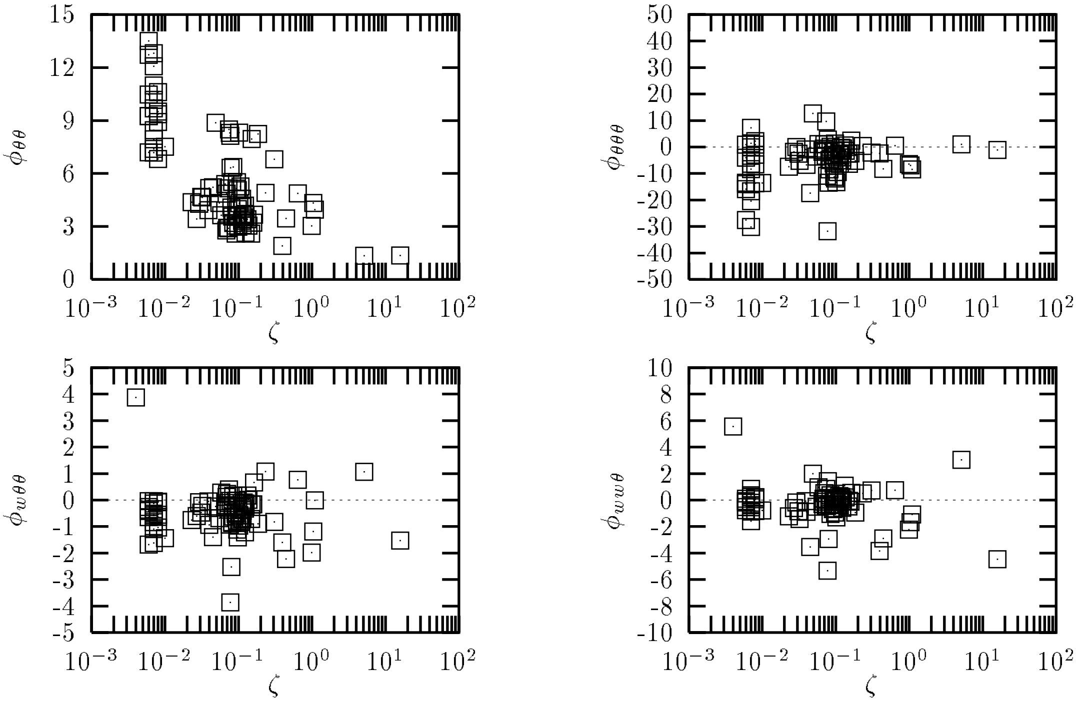

Figure 4.8 – Dimensionless temperature statistics for short runs.

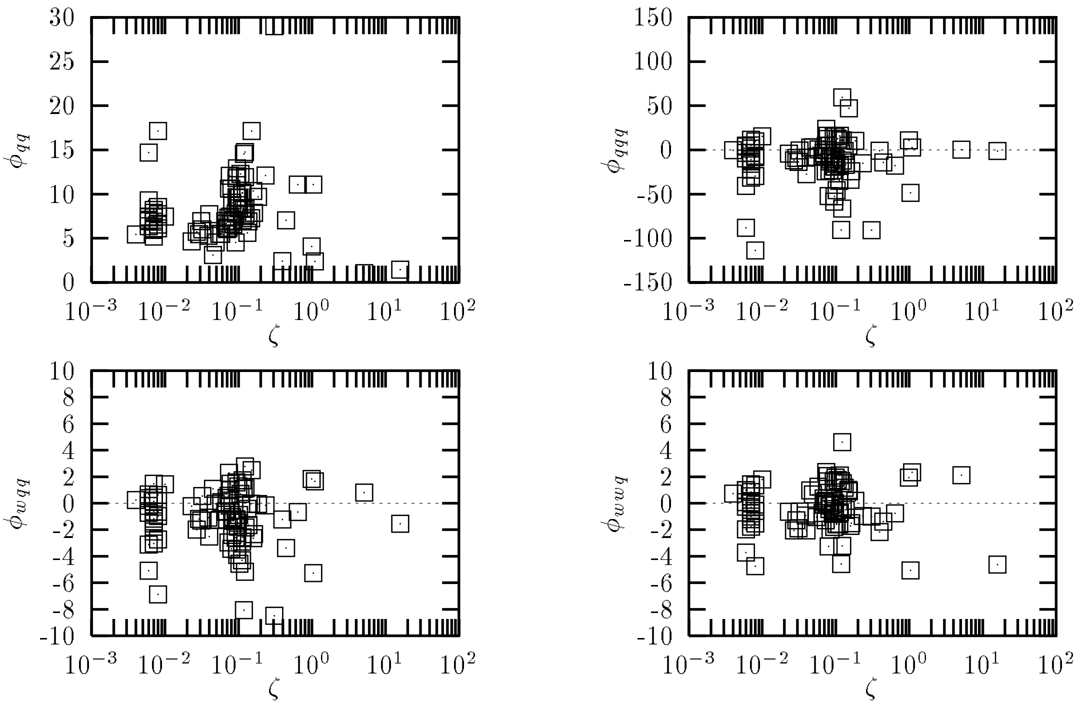

Figure 4.9 – Dimensionless humidity statistics for short runs.

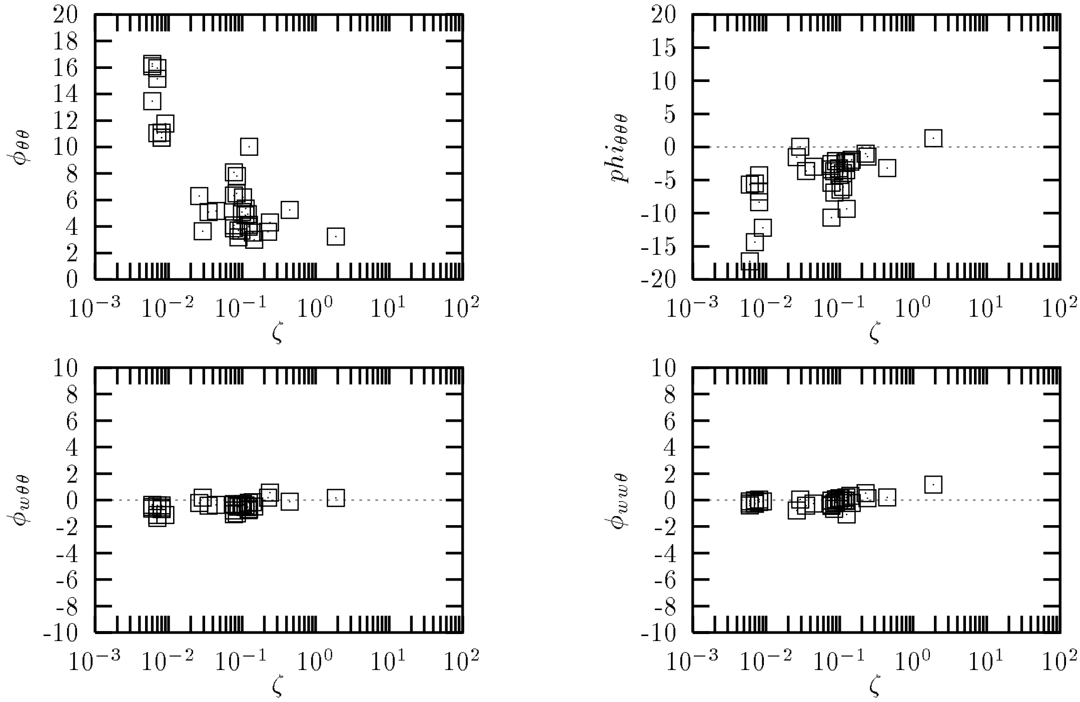

Figure 4.10 – Dimensionless temperature statistics for long runs from time series.

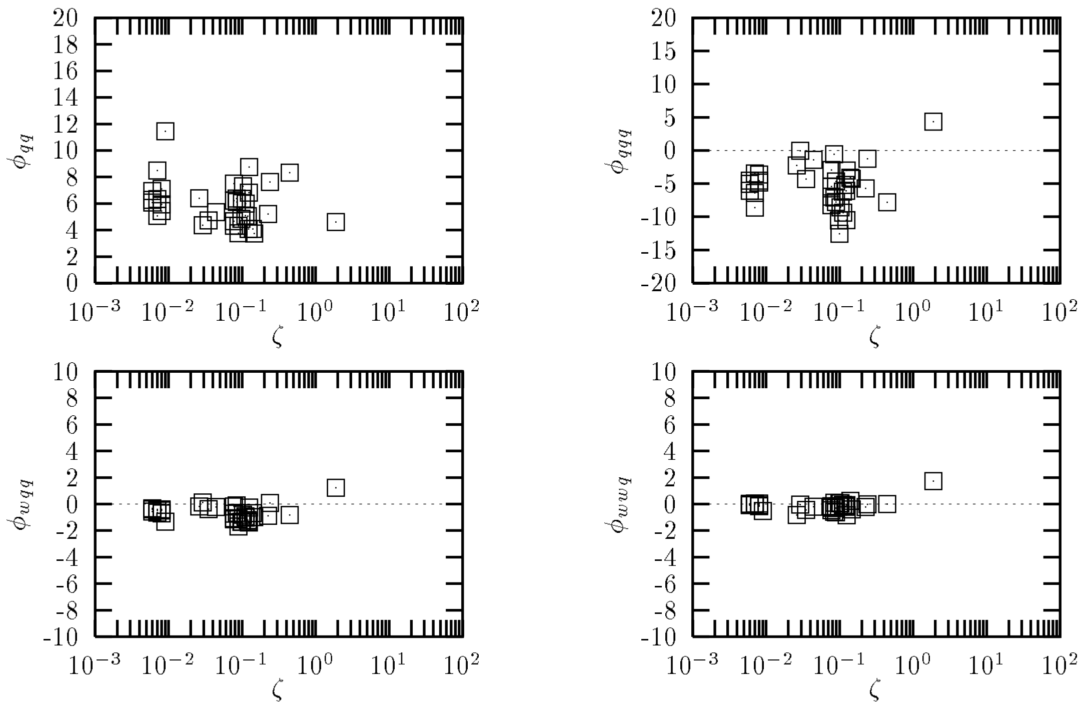

Figure 4.11 – Dimensionless humidity statistics for long runs from time series.

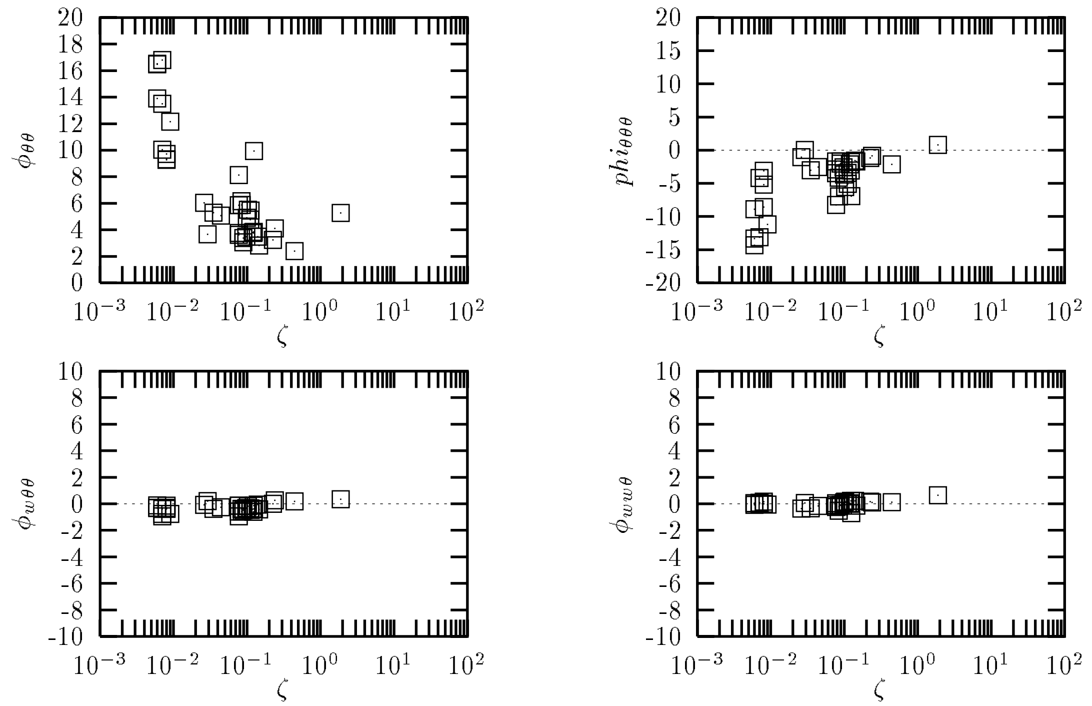

Figure 4.12 – Dimensionless temperature statistics for long runs from spectra.

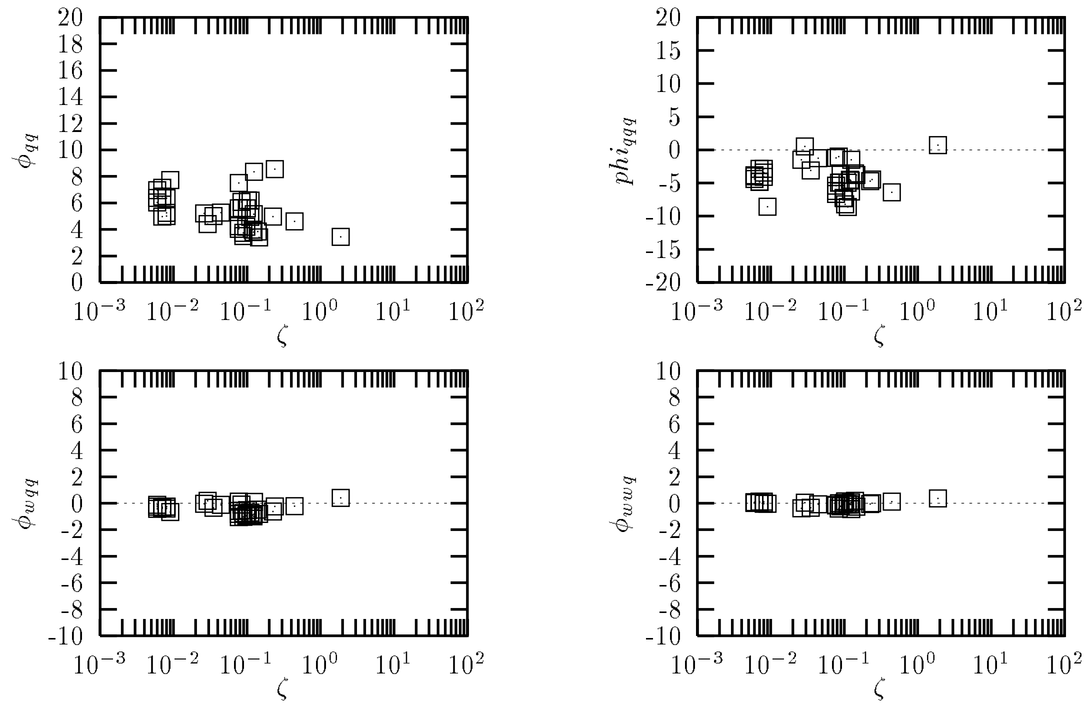

Figure 4.13 – Dimensionless humidity statistics for long runs from spectra.

indicating the downward heat flux, whereas humidity skewness is negative (since $q_* > 0$) indicating the upward water vapor flux.

More interesting is the behavior of ϕ_{waa} and ϕ_{wwa} ($a = \theta$ or q) for the long runs. It is clear that the assumptions

$$\frac{\partial \phi_{waa}}{\partial \zeta} = 0 \qquad (4.13\text{-a})$$

$$\frac{\partial \phi_{wwa}}{\partial \zeta} = 0 \qquad (4.13\text{-b})$$

in stable conditions are very reasonable. Remember that these assumptions simplify the dimensionless budgets of variances and covariances in the set of equations (2.28), implying the simpler form (3.37) for the dimensionless scalar variance and covariance budgets, which was used in Chapter 3 to derive $r^2_{\theta q} = 1$ and $\phi_H = \phi_E$. This technique of plotting ϕ_{waa} and ϕ_{wwa} against $zeta$ in order to infer their behavior from one-level measurements seems to have been first used by Wyngaard et al (1978) in unstable conditions.

With hindsight, the results presented here are not surprising. In fact, Wyngaard (1973) shows how the main features of turbulence can be predicted by an asymptotic analysis of very stable conditions. Then, the turbulence should become independent of z (that is to say, homogenenous in the vertical direction), with the result that the dimensionless functions ϕ_{aa}, ϕ_{aaa}, ϕ_{waa} and ϕ_{wwa} are constant with ζ, whereas the dimensionless gradients ϕ_F are asymptotically linear with ζ. The constancy of the dimensionless statistics with stability is essentially confirmed in the figures above, both for temperature and humidity, providing further evidence of their similar behavior.

Wyngaard also showed that the averaging time required for calculating 2nd-order moments in the surface layer could be of the order of 1 hour, for accuracies of about 10 to 20%. It is only natural to expect 3rd-order statistics to require even longer averaging times, so the improvement noticed in the 3rd-order statistics for the long runs should not be surprising.

It is also harder to estimate the uncertainties involved in the 3rd-order statistics. A possible approach is the following: consider ϕ_{wwa}, and assume (as a rough approximation) that w and a are jointly normally distributed with $|r_{wa}| = 0.3$, which is an average value often obtained for stable conditions (Hicks, 1981; see also page 100); then, we know that the population value of $\overline{w'w'a'}$ is zero (Bendat and Piersol, 1986, section 3.3). The standard deviation of the (sample) value of $\overline{w'w'a'}$ in this case is given by (Lumley and Panofsky, 1964, p. 36)

$$\sigma^2_{\overline{w'w'a'}} \approx \frac{2\tau_i}{\mathcal{T}} \overline{w'^4 a'^2} \tag{4.14}$$

where $\mathcal{T}$ is the averaging time, and τ_i is the integral time scale of the process $w'w'a'$. Because the population value of $\overline{w'w'a'}$ is zero, we may set an accuracy ϵ with respect to u_* and a_*,

$$\epsilon^2 \equiv \frac{\sigma^2_{\overline{w'w'a'}}}{u_*^4 a_*^2} \ , \tag{4.15}$$

so that

$$\mathcal{T} = \frac{2\tau_i}{\epsilon^2} \frac{\overline{w'^4 a'^2}}{u_*^4 a_*^2} \tag{4.16-a}$$

$$= \frac{2\tau_i}{\epsilon^2} \overline{\left(\frac{w'}{\sigma_w}\right)^4 \left(\frac{a'}{\sigma_a}\right)^2} \left(\frac{\sigma_w}{u_*}\right)^4 \left(\frac{\sigma_a}{a_*}\right)^2 \ . \tag{4.16-b}$$

The 6th-order moment above can be calculated using the moment-generating function of a joint normal distribution with unit variances and $|r_{wa}| = 0.3$ (Bendat and Piersol, 1986, pp. 57–67); it is

$$\overline{\left(\frac{w'}{\sigma_w}\right)^4 \left(\frac{a'}{\sigma_a}\right)^2} = 3 + 12r_{wa}^2 = 4.08 \tag{4.17}$$

so that (4.16) becomes

$$\mathcal{T} = \frac{2\tau_i}{\epsilon^2}\, 4.08\, A_w^4 A_a^2 \,, \tag{4.18}$$

and for $A_w = 1.3$, $A_a = 2.0$ and $\epsilon = 0.2$, this gives

$$\mathcal{T} = 2330\tau_i \,, \tag{4.19}$$

but τ_i still needs to be properly estimated. Because spectral characteristics of higher-order moments are not well known, we may roughly approximate τ_i with the peak value of the w, a cospectrum. Using the expression (2.74-c) introduced in Chapter 2 for $f_{0,wa}$ we obtain for near-neutral conditions ($\zeta = 0$), $f_{0,wa} \approx 0.30$. The corresponding peak frequency of the cospectrum is found by setting the derivative of (2.72-b) equal to zero; it is $0.7430 f_{0,wa} = 0.22$. At a height of 2.5 m and an average horizontal wind speed of 8 $\mathrm{m\,s^{-1}}$, typical of the near-neutral conditions in this study, the peak frequency will be 0.70 Hz, whence $\tau_i = 1.42$ s and $\mathcal{T} = 3{,}309$ s $= 55.16$ min..

Even though this result is undoubtedly pleasant to the author, it has to be regarded as the mere exercise it is; it is quite likely that w' and a' are *not* jointly normal: it is known that scalars exhibit “ramp” structures associated with skewness values different from zero (Antonia and Atkinson, 1976; Antonia and

Van Atta, 1978; Kikuchi and Chiba, 1985). Still, Thorodsen and Van Atta (1992) observed nearly gaussian probability distributions of w' and θ' in a wind tunnel experiment; they were also able to obtain a fair representation of the random variable $w'\theta'$ by assuming w' and θ' to be jointly gaussian, as we are doing here. Notice also that using the w, a instead of the w, wa cospectrum introduces yet another layer of approximation.

Finally, the correlation coefficients $r_{w\theta}$ and r_{wq} were calculated for the short runs, and are presented in figure 4.14 plotted against stability. Hicks (1981) and Wesely (1988) give a value of about -0.3 for $r_{w\theta}$ under stable conditions. Notice that the plots do not contradict that value *on the average*, and that they are very similar to each other. On the other hand, the scatter is too large, making it very hard to estimate the correlation coefficients as a function of ζ. Of course, this phenomenon was already present in the large scatter of the functions $\phi_{\theta\theta}$ and ϕ_{qq} shown above, since, from equation (2.26) in Chapter 2,

$$r_{w\theta} = \frac{\phi_{w\theta}}{\sqrt{\phi_{ww}\phi_{\theta\theta}}} = \frac{1}{A_w A_\theta} \, , \tag{4.20}$$

so that the scatter in $r_{w\theta}$ can only be as good (or bad), as that in figures 4.4-4.7 and 4.8-4.13. An analogous observation applies, of course, for r_{wq}.

4.6 Closure

In this chapter, we analyzed the behavior of temperature and humidity from the point of view of statistics in the time domain. Turbulent statistics are relatively insensitive to the particular way to calculate them if the mean

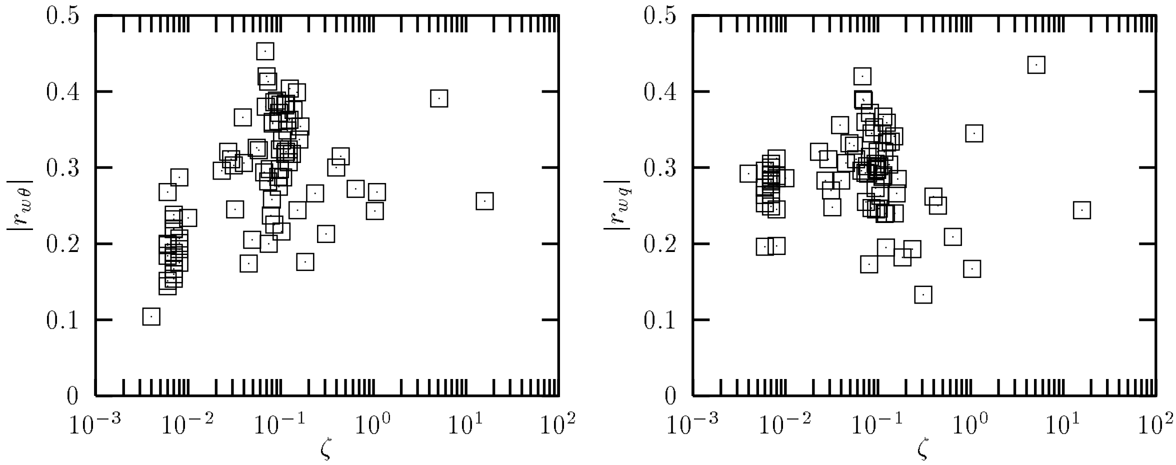

Figure 4.14 – Correlation coefficients $r_{w\theta}$ and r_{wq} for short runs.

tendency in time is first extracted by a high-pass filter operation with a time constant of 200 s. The time-honored log-linear expression for ϕ_H fits the observed temperature differences in the EBBR station well, but may have a limit of validity as low as $\zeta = 0.4$, beyond which its behavior is uncertain; this is compatible with Högström's (1990) re-evaluation of ϕ_H, which was done for $\zeta \leq 0.5$. The temperature-humidity correlation coefficient $r_{\theta q}$ is about -0.8; using low-pass, low-frequency (2 Hz) data instead of the original high-frequency (20 Hz) data *increases* it to -0.9 on the average. This is a first indication that the spatial separation of the temprature and humidity sensors may be an important cause of understimation of $|r_{\theta q}|$, more of which will be presented in the next chapter. Thus, the correlation coefficient in stable conditions for FIFE-89 can safely be assumed to be close to the "theoretical" value of -1 derived in Chapter 3, and predicted by Hill (1989a). We used a hypothesis test to show that $\phi_{\theta\theta}$ and ϕ_{qq}

are statistically indistinguishable; moreover, the overall quality of the regressions to obtain their (constant) values improves considerably when 52-min. long runs are used, instead of the 26-min short runs. The same applies to the functions ϕ_{aa}, ϕ_{aaa}, ϕ_{waa} and ϕ_{wwa} plotted against stability ζ: the long runs show much less scatter, and can be used to infer the constancy of the last two with ζ. The superiority of the longer averaging times is confirmed by a rough estimate of the errors involved using the (admittedly poor) hypothesis of joint normality of w' and a'. The correlation coefficients $r_{w\theta}$ and r_{wq} were analyzed for the short runs, as an alternative to $\phi_{\theta\theta}$ and ϕ_{qq}, but (as expected) the same large scatter only allows the average behavior to be inferred.

Chapter 5

A GALLERY OF (CO)SPECTRA

This chapter shows the analysis of the FIFE-89 long runs in the frequency domain. We calculated and compared temperature and humidity spectra ($S_{\theta,\theta}$ and $S_{q,q}$) and cospectra with vertical velocity ($S_{w,\theta}$ and $S_{w,q}$), coherence and phase functions between θ' and q' and finally the higher-order cospectra $S^c_{\theta,\theta\theta}$ and $S^c_{q,qq}$. The spectral analysis discloses the strong similarity between θ' and q' except during the night of Aug 03rd, confirming the pattern already apparent in the statistical analysis of last chapter. Besides the evaluation of spectral similarity between the 2 scalars, the asymptotic behavior in the low frequencies is analyzed. Kader and Yaglom's (1991) and Kader's (1993) prediction of a -1 slope holds for near-neutral conditions, but in the more stable cases the 0 slope of Kaimal's (1973) curves seems more likely. It is hypothesized that this change of behavior is connected with the z-less nature of stable turbulence, indicating that the lower frequencies scale with z under near-neutral (and probably unstable) , but not stable, conditions. Finally, ample evidence is given for the validity of a -2 slope for the higher-order cospectra in the inertial subrange, exactly as predicted in Chapter 2.

5.1 Data processing

Consider the time series a'_i and $\breve{a}'_j$ (equations 4.3-a and 4.7-e) introduced in Chapter 4, from a long run. They are regrouped in blocks of length L_B and relabeled as follows

$$a'_i \;\Rightarrow\; a'_{k,l} \text{ where } i = L_B k + l \tag{5.1-a}$$

$$\breve{a}'_i \;\Rightarrow\; \breve{a}'_{k,l} \text{ where } i = L_B k + l \tag{5.1-b}$$

where k will run from 0 to the number of blocks N_B, and l from 0 to L_B. Averaging over blocks will provide an estimate of the population (ensemble) averages. The time t *from the beginning of a block* k is counted as

$$t = l\Delta t \tag{5.2-a}$$

$$t = l\Delta\breve{t} \tag{5.2-b}$$

where $\Delta t = 0.05$ s, $\Delta\breve{t} = 0.5$ s. The series $a'_{k,l}$ and $\breve{a}'_{k,l}$ were analyzed separately. Each long run yielded 60 blocks of length $L_B = 1{,}024$ of a', and 6 blocks of the same length of $\breve{a}'$. Thus, $k = 1, \ldots, 60$ for the high-frequency data, and $k = 1, \ldots, 6$ for the low-frequency data. (Remember that a long run consists of 61,952 a' data points measured at 20 Hz, and 6,195 $\breve{a}'$ data points generated from the former by a low-pass filter with a cutoff frequency of 2 Hz. Of these, $1{,}024 \times 60 = 61{,}440$ points were actually used for the analysis of the a' data, and $1{,}024 \times 6 = 6{,}144$ data points for the analysis of $\breve{a}'$. The $30{,}976 - 1{,}024 \times 30 = 256$ points remaining at the end of each *short* run composing the long run were discarded.)

The numerical Fourier transform of a block k of $a'(t)$ is (Jenkins and Watts, 1986 pp. 16–56; Bendat and Piersol, 1986 p. 371)

$$\begin{aligned}\widehat{a}_m^k &\equiv \Delta t \sum_{l=0}^{L_B-1} a'_{k,l} \exp\left[-2\pi\, i\, nt\right] \\ &= \Delta t \sum_{l=0}^{L_B-1} a'_{k,l} \exp\left[-2\pi\, i\, \frac{m}{L_B \Delta t} l \Delta t\right] \\ &= \Delta t \sum_{l=0}^{L_B-1} a'_{k,l} \exp\left[-2\pi\, i\, \frac{ml}{L_B}\right] \ .\end{aligned} \tag{5.3}$$

If $a'_{k,l}$ is renormalized so that its sample mean is zero (which is convenient in the present context), then $\widehat{a}_0^k$ is also zero. Solving (5.3) above then yields $L_B/2$ complex Fourier coefficients $\widehat{a}_m^k$, $m = 1, \ldots, L_B/2$. Similarly, one can calculate $\widehat{\check{a}}_m^k$ from the low-frequency series. Notice that in each case the frequencies corresponding to the given Fourier coefficients are $n = m/(L_B \Delta t)$ and $n = m/(L_B \Delta \check{t})$. Thus, the minimum and maximum frequencies (in Hz) obtained for each series are

$$a' \ \Rightarrow\ 0.019531 \le n \le 10.0 \tag{5.4-a}$$

$$\check{a}' \ \Rightarrow\ 0.001953 \le n \le 1.0 \ , \tag{5.4-b}$$

where the upper limits are the Nyquist frequencies for each series (Bendat and Piersol, 1986, section 10.3). The cross-spectral density between two series a', b' at frequency $m/(L_B \Delta t)$ is then given by the average over all blocks,

$$S_{a,b}\left(\frac{m}{L_B \Delta t}\right) = S_{a,b;\,m} = \frac{2}{N_B L_B \Delta t} \sum_{k=1}^{N_B} \widehat{a}_m^{k\,*}\, \widehat{b}_m^k \ . \tag{5.5}$$

Here, the average over N_B blocks mimicks the ensemble average, whereas dividing by $L_B \Delta t$ (the total record length) plays the role (numerically) of multiplication by $\delta(0)$ in the definition of $S_{i,j}$ given in Chapter 2.

The Fourier coefficients $\widehat{a}_m^k$ and $\widehat{b}_m^k$ can be calculated very efficiently by means of the Fast Fourier Transform (FFT) (Press *et al.*, 1993, pp. 496–536; Bendat and Piersol, 1986, pp. 370–383). An algorithm similar to the one given by Press *et al.* (1986, p. 507) was used for the FFT, except that all floating-point operations were coded with complex arithmetic to make the code clearer, and that recursion was used (i.e., the ability of a procedure to "call" itself). The calculation of the cross-spectral densities, on the other hand, followed the procedures of Chapter 11 of Bendat and Piersol. A Hanning window was applied to the data series to reduce aliasing (Kaimal *et al.*, 1989; Kaimal and Kristensen, 1991).

For each long run, 3 estimates of $S_{a,b}$ were obtained; the first with $\Delta\check{t} = 0.5$ s, $N_B = 6$, $L_B = 1{,}024$ from the low-frequency data, and the other two with $\Delta t = 0.05$ s, $N_B = 30$, $L_B = 1{,}024$ by analyzing the first and second 26-min. periods within a long run separately. The analysis of low- and high-frequency data separately is in essence the same technique used by Kaimal *et al.* (1972) and Kaimal (1973).

Let $\mathbf{n}$, $\mathbf{S}_{a,b}$ be the matrices of frequencies $n_{r,m}$ and cross-spectral densities $S_{a,b;\,r,m}$ thus obtained; $r = 0$ represents the estimates from the $\check{a}$, $\check{b}$ series, whereas $r = 1, 2$ represents the estimates from the first and second short runs of a', b'. There is a total of 1,536 points spanning 4 decades, roughly from 10^{-3}

to 10^1 Hz. This number of points is too large to be plotted comfortably, so a final smoothing is applied by grouping the data points into 128 frequency bins arranged logarithmically:

$$n_{min} = 0.001953 \text{ Hz} \equiv n_0 \tag{5.6-a}$$

$$n_{max} = 10.0 \text{ Hz} \equiv n_{128} \tag{5.6-b}$$

$$\Delta = \frac{\ln n_{max} - \ln n_{min}}{128} \tag{5.6-c}$$

$$n_p \equiv \exp\left(\ln n_0 + p\Delta\right) \ . \tag{5.6-d}$$

We now form the index sets

$$I_p^+ \equiv \left\{ (r,m) \mid n_{p-1} < n_{r,m} \le n_p \wedge \frac{S^c_{a,b;\,r,m}}{a_* b_*} \ge 0 \right\} \tag{5.7-a}$$

$$I_p^- \equiv \left\{ (r,m) \mid n_{p-1} < n_{r,m} \le n_p \wedge \frac{S^c_{a,b;\,r,m}}{a_* b_*} < 0 \right\} \ . \tag{5.7-b}$$

Notice that the population (ensemble) cospectra $S^c_{a,b}$ normalized by $a_* b_*$ are always positive; (5.7-b) is defined in order to cope with the relatively infrequent case when the *sample* cospectral density has the "wrong" sign due to statistical variability. Now if $N_p^\pm$ is the number of points in each index set, we form the bin averages

$$\overline{n}_p^{\pm} \equiv \left[\prod_{(r,m)\in I_p^\pm} n_{r,m} \right]^{1/N_p^\pm} \tag{5.8-a}$$

$$\overline{S}^{c\,\pm}_{a,b;\,p} \equiv \left[\prod_{(r,m)\in I_p^\pm} S^c_{a,b;\,r,m} \right]^{1/N_p^\pm} \tag{5.8-b}$$

$$\overline{S}^{q\,\pm}_{a,b;\,p} \equiv \left[\prod_{(r,m)\in I_p^\pm} S^q_{a,b;\,r,m} \right]^{1/N_p^\pm} \tag{5.8-c}$$

and finally

$$\overline{n}_p = N_p^+ \overline{n}_p^+ + N_p^- \overline{n}_p^- \tag{5.9-a}$$

$$\overline{S}_{a,b;\,p} = N_p^+ \overline{S}_{a,b;\,p}^+ + N_p^- \overline{S}_{a,b;\,p}^- \,. \tag{5.9-b}$$

It is a simple exercise to show that the geometric means defined in (5.8) preserve a power law density. Thus, assume for simplicity the most usual case, $I_p^- = \{\}$ (i.e., all sample normalized cospectral densities are positive, and the set containing the negative ones is empty); then, if each point in I_p^+ follows a power law

$$S^c_{a,b;\,r,m} = \alpha (n_{r,m})^\beta \,, \tag{5.10}$$

it follows from (5.8) above that

$$\overline{S}^c_{a,b;\,p} = \alpha (\overline{n}_p)^\beta \,. \tag{5.11}$$

Coherences and phases can be calculated from the smoothed $S_{a,b}$ densities following the definitions in Chapter 2, (2.42) and (2.43):

$$\overline{\Gamma}_{a,b;\,p} \equiv \frac{|\overline{S}_{a,b;\,p}|^2}{|\overline{S}_{a,a;\,p}|\,|\overline{S}_{b,b;\,p}|} \tag{5.12-a}$$

$$\vartheta_p^+ \equiv \arctan \left| \frac{\overline{S}^q_{a,b;\,p}}{\overline{S}^c_{a,b;\,p}} \right| \tag{5.12-b}$$

$$\overline{\vartheta}_p = \begin{cases} \vartheta_p^+ & \text{if } S^c_{a,b;\,p} \geq 0 \wedge S^q_{a,b;\,p} \geq 0 \\ -\vartheta_p^+ & \text{if } S^c_{a,b;\,p} \geq 0 \wedge S^q_{a,b;\,p} < 0 \\ \pi - \vartheta_p^+ & \text{if } S^c_{a,b;\,p} < 0 \wedge S^q_{a,b;\,p} \geq 0 \\ \vartheta_p^+ - \pi & \text{if } S^c_{a,b;\,p} < 0 \wedge S^q_{a,b;\,p} < 0 \end{cases} \,. \tag{5.12-c}$$

For the higher-order cospectra, say, $S_{a,bc}$, some care has to be taken. In particular, densities involving specific humidity squared or cubed proved hard to evaluate due to the very small numerical values of q'. This was circumvented by multiplying the humidity data by 1,000 throughout which effectively corresponds to doing the calculations in units of grams (of water vapor) per kilogram, and by subtracting the mean of each block from products of fluctuations before the numerical FFT's:

$$(b'c')_{k,l} \leftarrow (b'c')_{k,l} - \overline{b'c'}_k \,, \tag{5.13}$$

where $\leftarrow$ indicates the assignment operator in the computer program. The corresponding third-order moments are unaffected and can still be estimated by the integral of the cospectrum $S^c_{a,bc}$, because

$$\overline{a'(b'c' - \overline{b'c'})} = \overline{a'b'c'} - \overline{a'\overline{b'c'}} = \overline{a'b'c'} \,. \tag{5.14}$$

With these provisions, the calculation of the densities $S_{a,bc}$ were done exactly in the same way as those for $S_{a,b}$, with the normalized $b'c'$ series substituted for b'.

5.2 Temperature and humidity spectra

In Chapters 2 and 3, we saw that the dimensionless quantities $nS_{\theta,\theta}/\theta_*^2$ and $nS_{q,q}/q_*^2$ should be equal in case of perfect similarity. Thus, in principle the spectra provide a way to analyze similarity at different scales. Figures 5.1-5.6 show six spectra each, beginning with the night of Aug 03rd, and proceeding until Aug 11th. Each spectrum corresponds to one of the long runs in table 4.12, except for the 37th in the early morning of Aug 11th, which was left out in order to fit all figures in six pages. It is important to note that Kaimal's curve (2.72) together with Moraes and Epstein's (1987) model for $f_{0,\theta\theta}$ and $f_{0,qq}$ imply that

$$\frac{S_{\theta,\theta}}{\theta_*^2} = \frac{S_{q,q}}{q_*^2} \Rightarrow \phi_H = \phi_E \tag{5.15}$$

Clearly, this does not happen on Aug 03rd. A check of field conditions (Fritschen *et al.*, 1993; Brutsaert, 1993, personnal communication) shows that it rained about 6 mm during the day on Aug 03rd, and that the sky was overcast throughout this day. Indeed, nighttime evaporation was very strong, as can be seen in table 4.12. The atmosphere was probably disturbed by the passage of a front which caused the rain, and advection of humidity cannot be overruled. For the remaining nights, however, the normalized temperature and humidity spectra are remarkably similar.

The plots show two straight lines, with slopes $-5/3$ and -1. The -1 slope is predicted in Kader and Yaglom (1991) and Kader (1993) for the low-frequency range of the spectrum by means of dimensional analysis, and this is in fact observed for all spectra during Aug 03rd, during which near-neutral conditions prevailed. The more stable runs, however, seem to follow closer the 0 slope which is predicted in Kaimal's (1973) curve (2.72-a). This is probably due to the different behavior of turbulence under stable and unstable conditions. Thus, under near-neutral and unstable conditions, z (or a multiple thereof) is a natural length scale in the production range (low frequencies, or wavenumbers), so that Kader argued that spectra should scale according to $S_{a,a} \sim (kz)^{-1}$. Kader's analysis, however, probably does not hold under stable conditions where z ceases to be a valid length scale due to the damping of turbulence by negative buoancy; in this last case we would then have $S_{a,a} \sim$ const as predicted (without justification) by Kaimal's curves (the low-frequency behavior of Kaimal's curves seems to have been proposed on the purely empirical basis that it fit the data at hand).

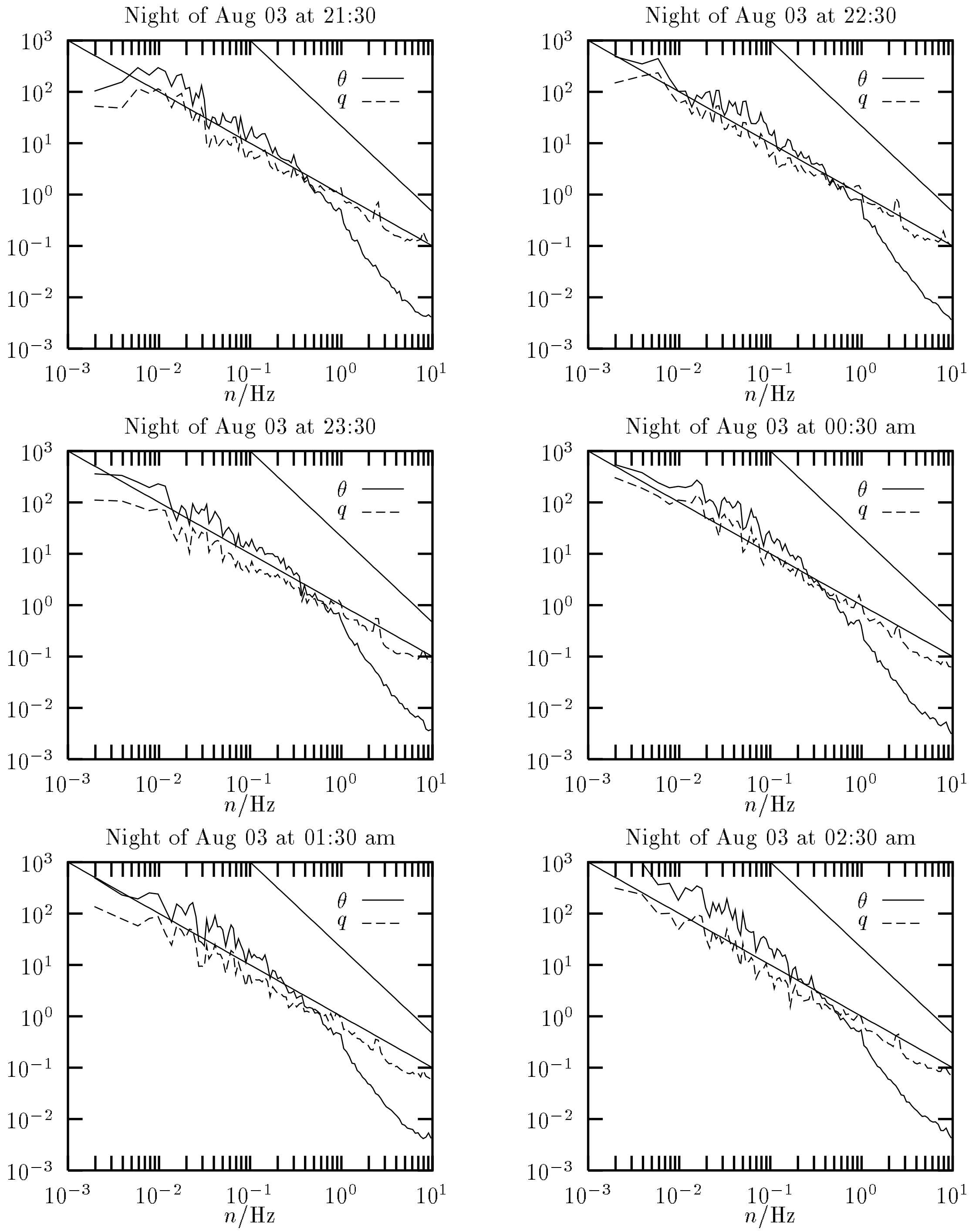

Figure 5.1 – Reduced spectral densities $S_{a,a}/a_*^2$, $a = \theta, q$ on Aug 03.

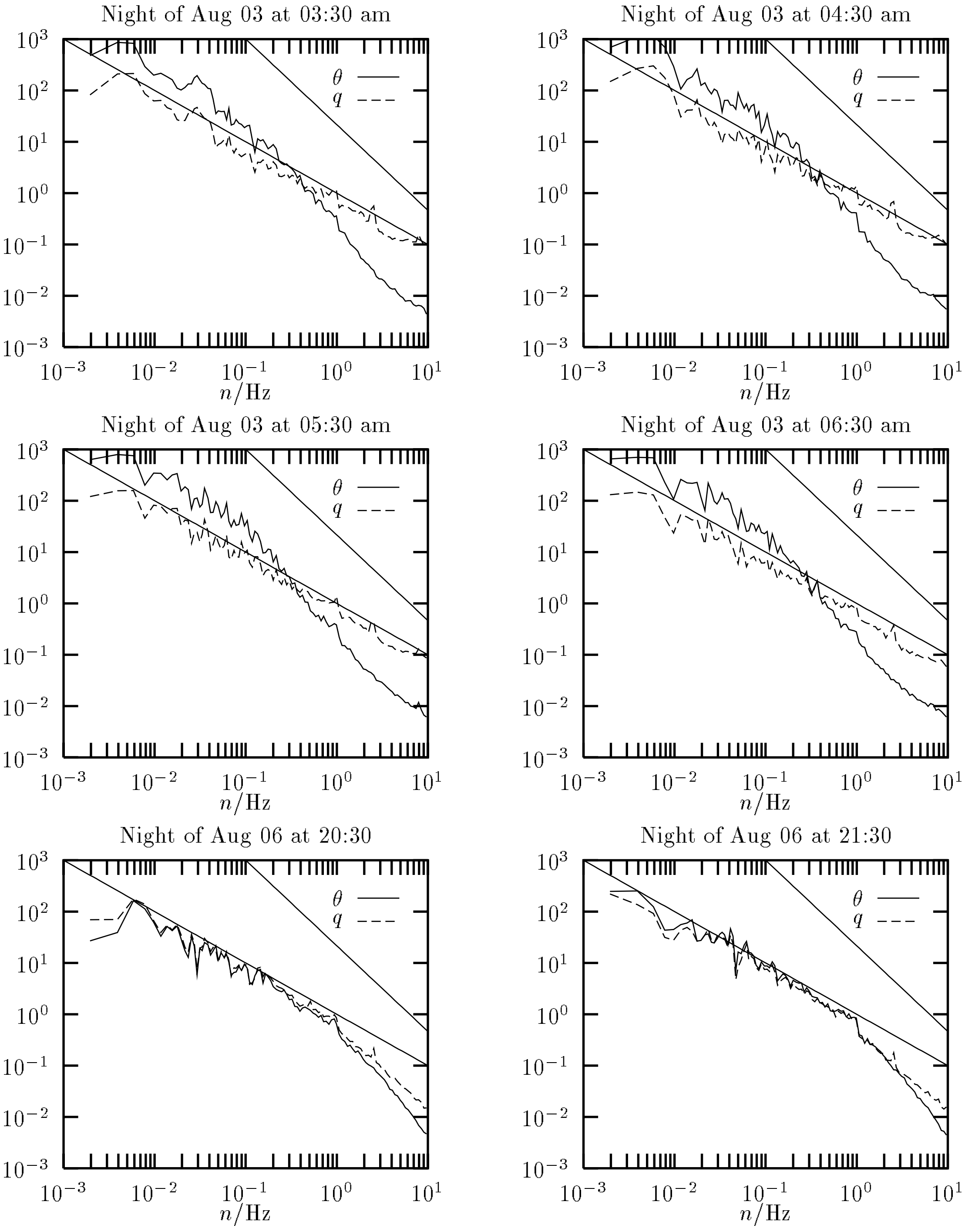

Figure 5.2 – Reduced spectral densities $S_{a,a}/a_*^2$, $a = \theta, q$ on Aug 03 and 06.

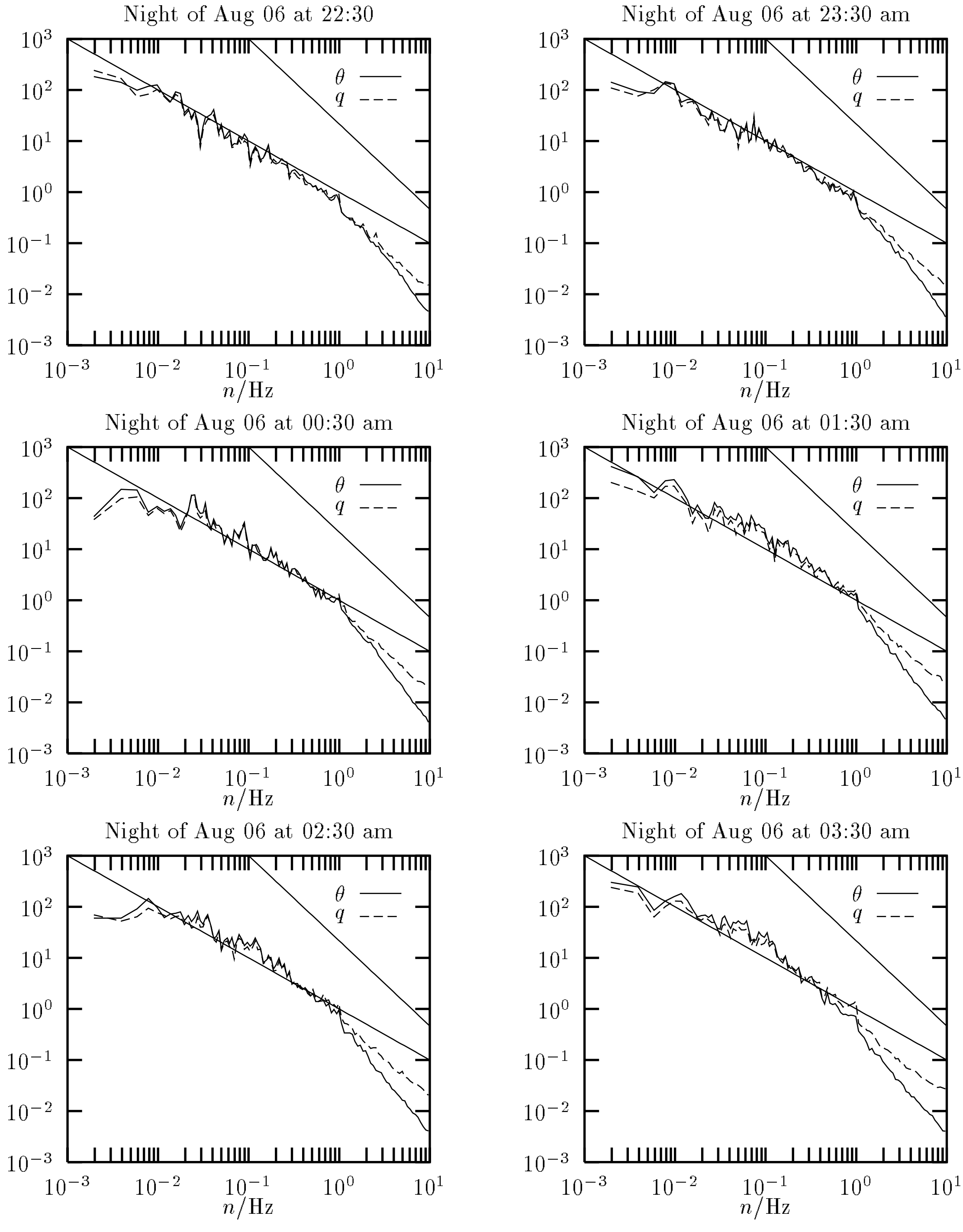

Figure 5.3 – Reduced spectral densities $S_{a,a}/a_*^2$, $a = \theta, q$ on Aug 06 (cont.).

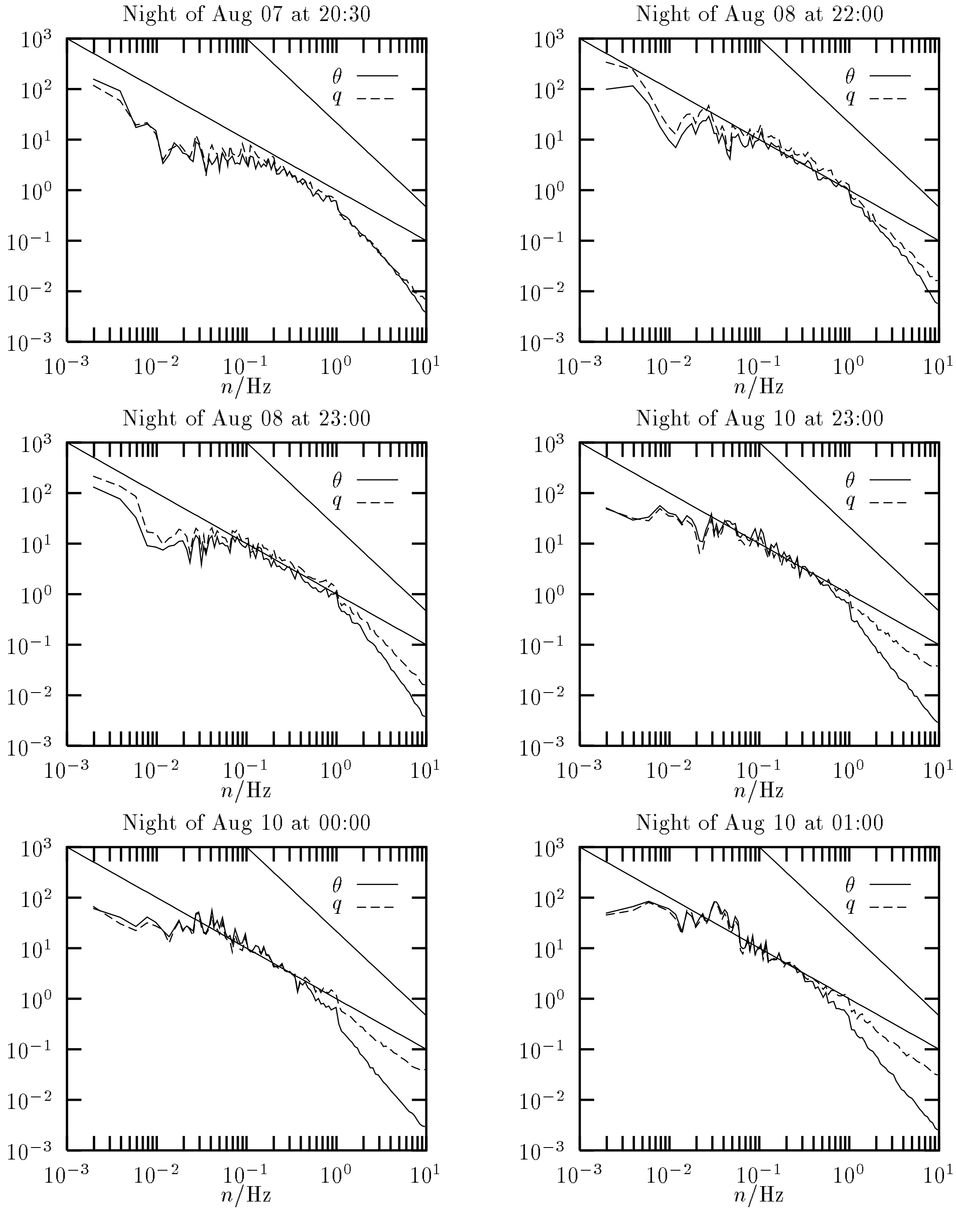

Figure 5.4 – Reduced spectral densities $S_{a,a}/a_*^2$, $a = \theta, q$ on Aug 07, 08 and 10.

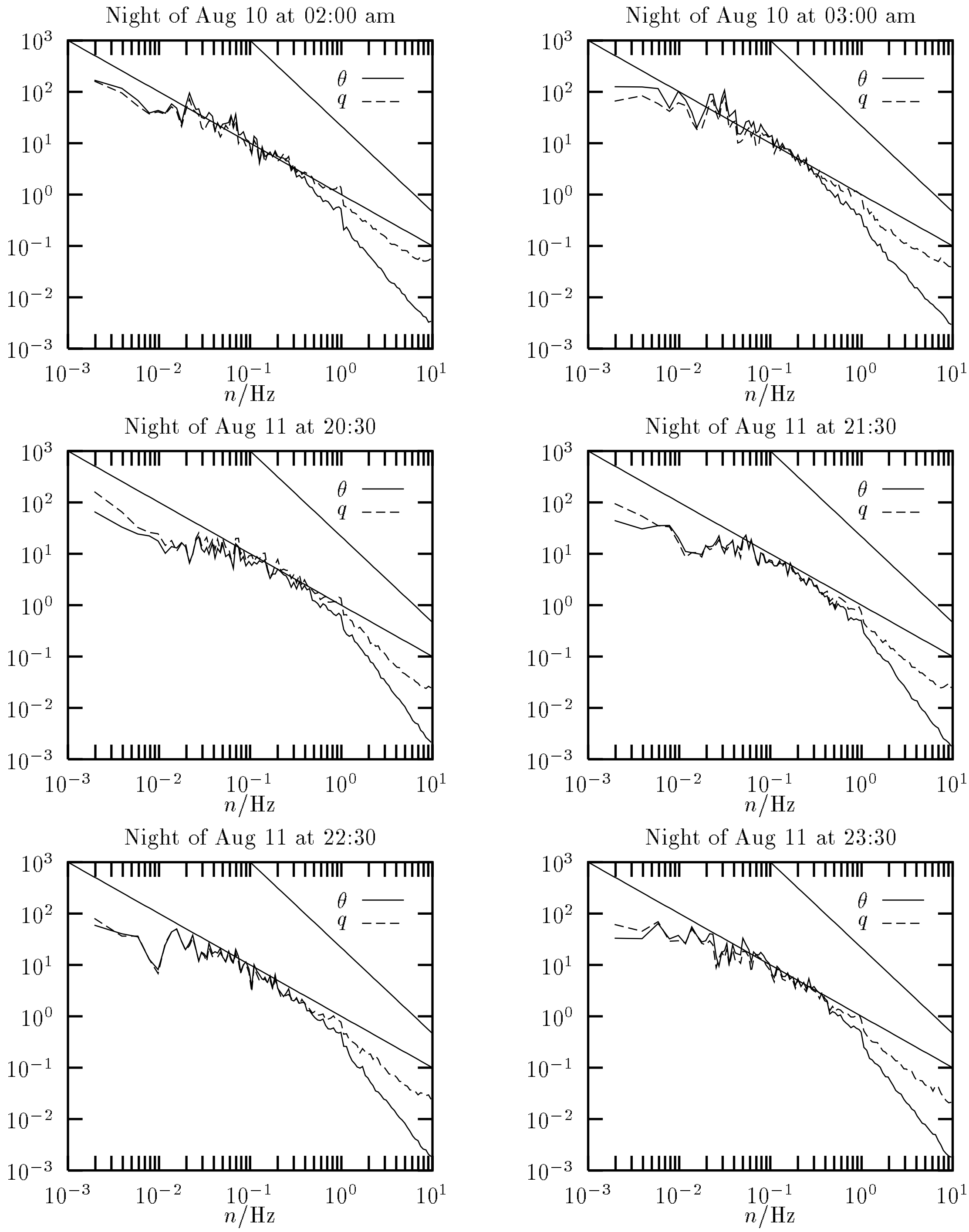

Figure 5.5 – Reduced spectral densities $S_{a,a}/a_*^2$, $a = \theta, q$ on Aug 10 (cont.) and 11.

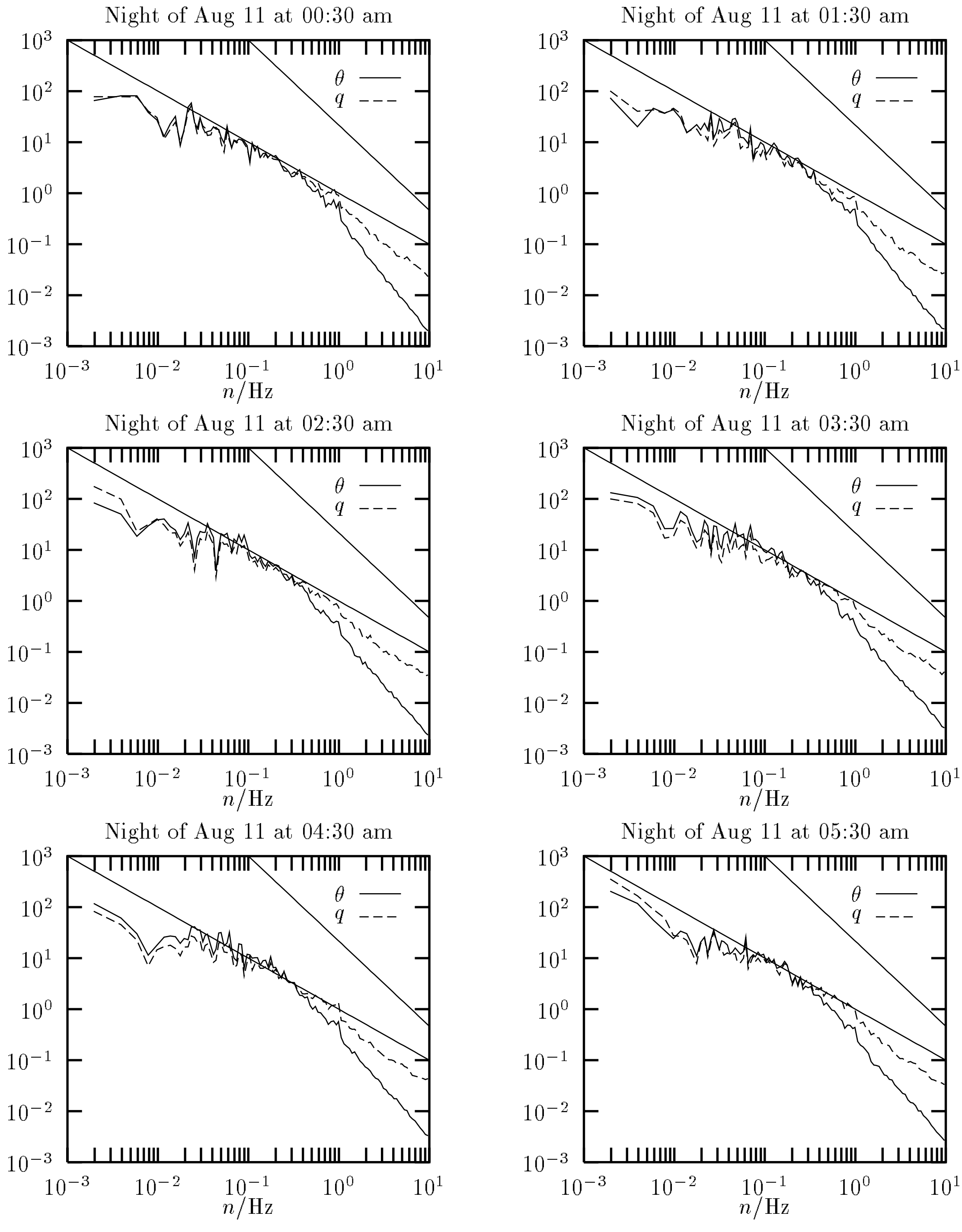

Figure 5.6 – Reduced spectral densities $S_{a,a}/a_*^2$, $a = \theta, q$ on Aug 11 (cont.).

5.3 Cospectra with vertical velocity

The cospectra $S^c_{w,\theta}$ and $S^c_{w,q}$ normalized by $u_*\theta_*$ and $u_*q_*$are shown next, on figures 5.7-5.12, in the same order as that of spectra. Again, we can use Kaimal's curve (2.72-b) (this time for the dimensionless cospectra) together with the extension of Moraes and Epstein's (1987) model to $f_{0,w\theta}$ and $f_{0,wq}$ developed in Chapter 2, to show that

$$\frac{S_{w,\theta}}{u_*\theta_*} = \frac{S_{w,q}}{u_*q_*} \Rightarrow \phi_H = \phi_E \tag{5.16}$$

under the validity of MOS theory. Cospectra with vertical velocity have been used by Lang *et al.* (1983a) and Ohtaki (1985) to assess the similarity between different scalars (water vapor and temperature, in the first case; CO_2 and temperature, in the second), without the connection made above, however, between them and the similarity functions ϕ_F. Not surprisingly, the same pattern repeats itself, with the night of Aug 03rd showing strong dissimilarity between the cospectra with w, but none of the others. The plots also contain a straight line with a slope of $-7/3$, which is the well-known Wyngaard and Coté's (1972) prediction for the inertial-subrange behavior of cospectra with w, discussed in Chapter 2.

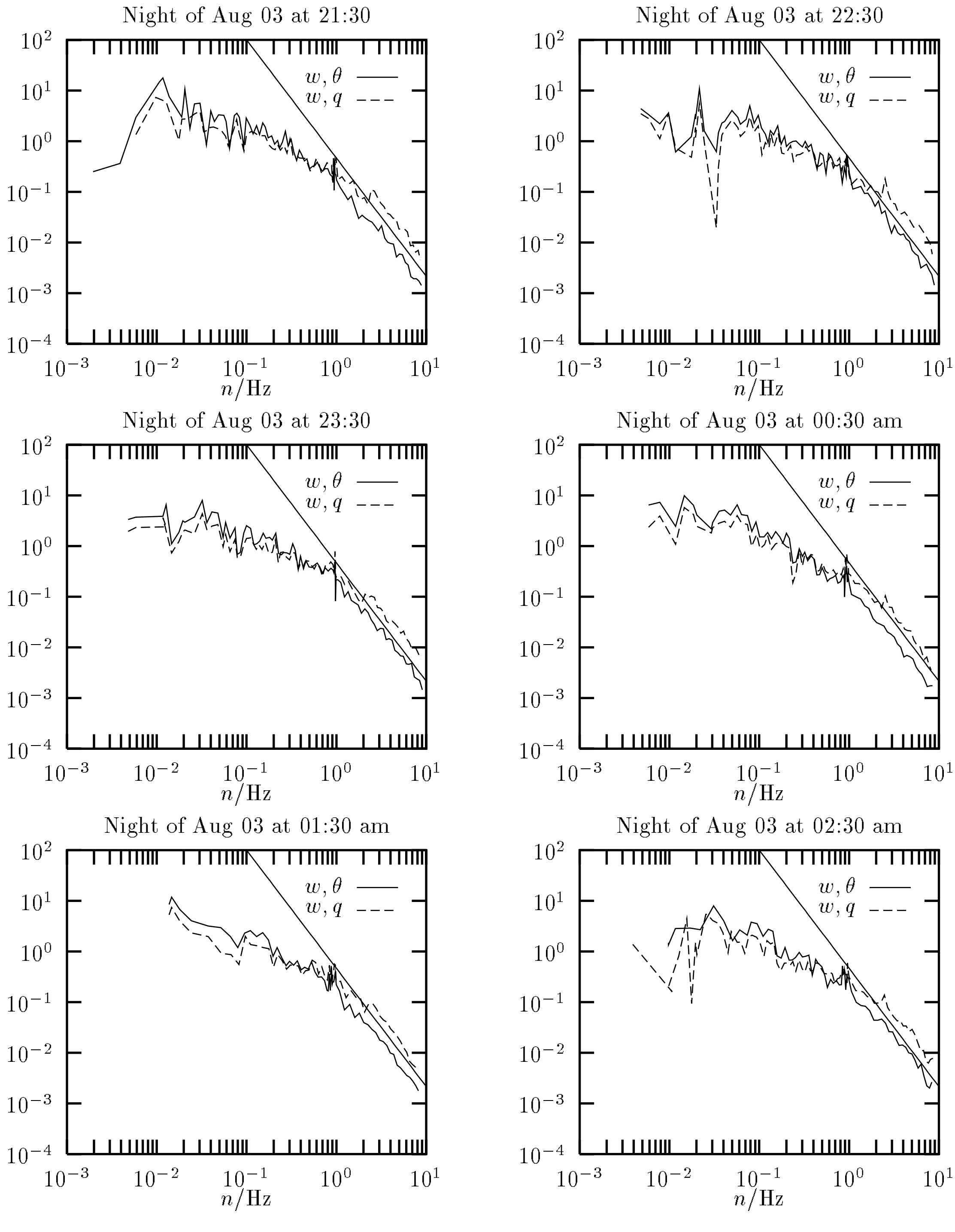

Figure 5.7 – Reduced cospectral densities $S_{w,a}/(u_* a_*)$, $a = \theta, q$ on Aug 03.

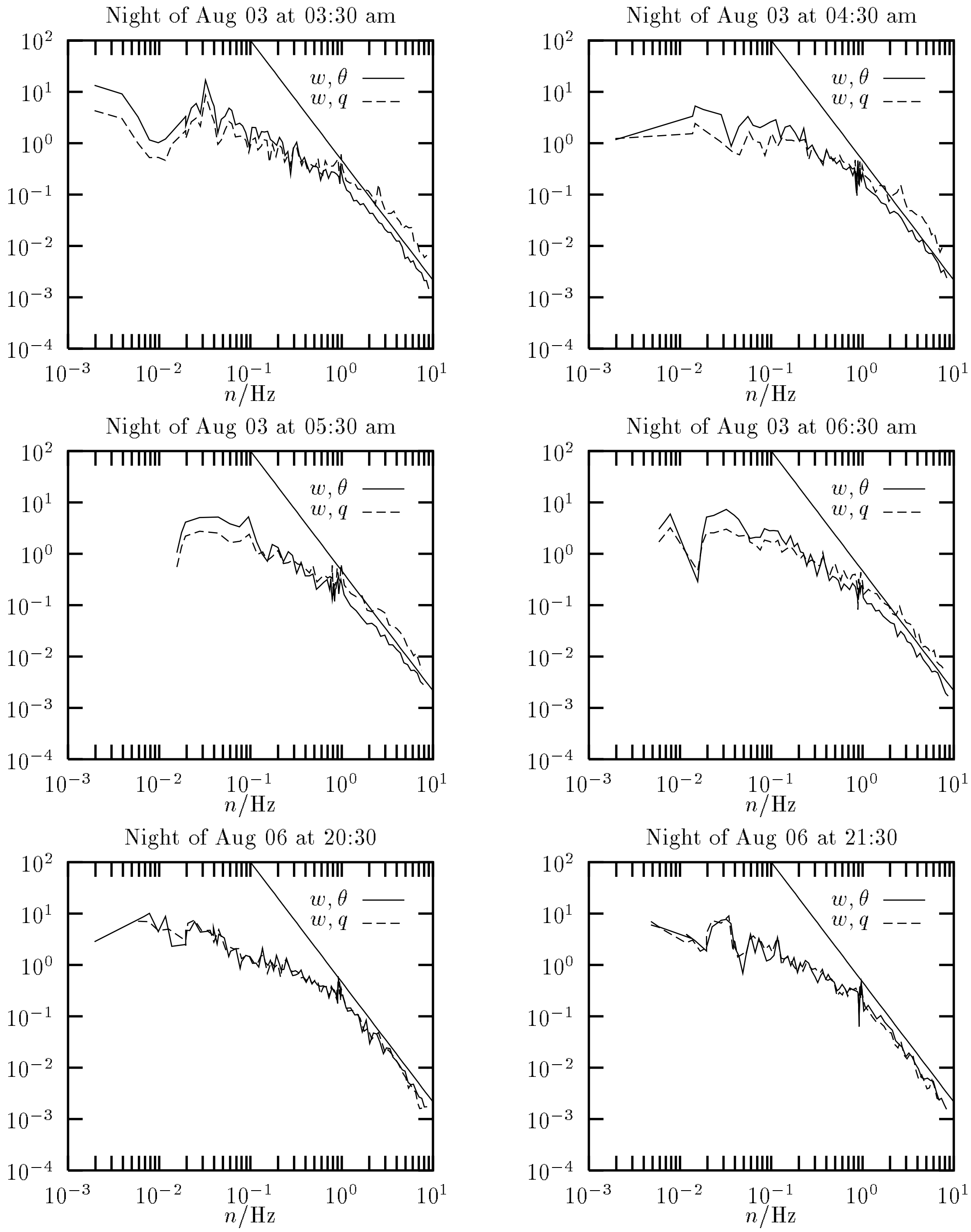

Figure 5.8 – Reduced cospectral densities $S_{w,a}/(u_* a_*)$, $a = \theta, q$ on Aug 03 and 06.

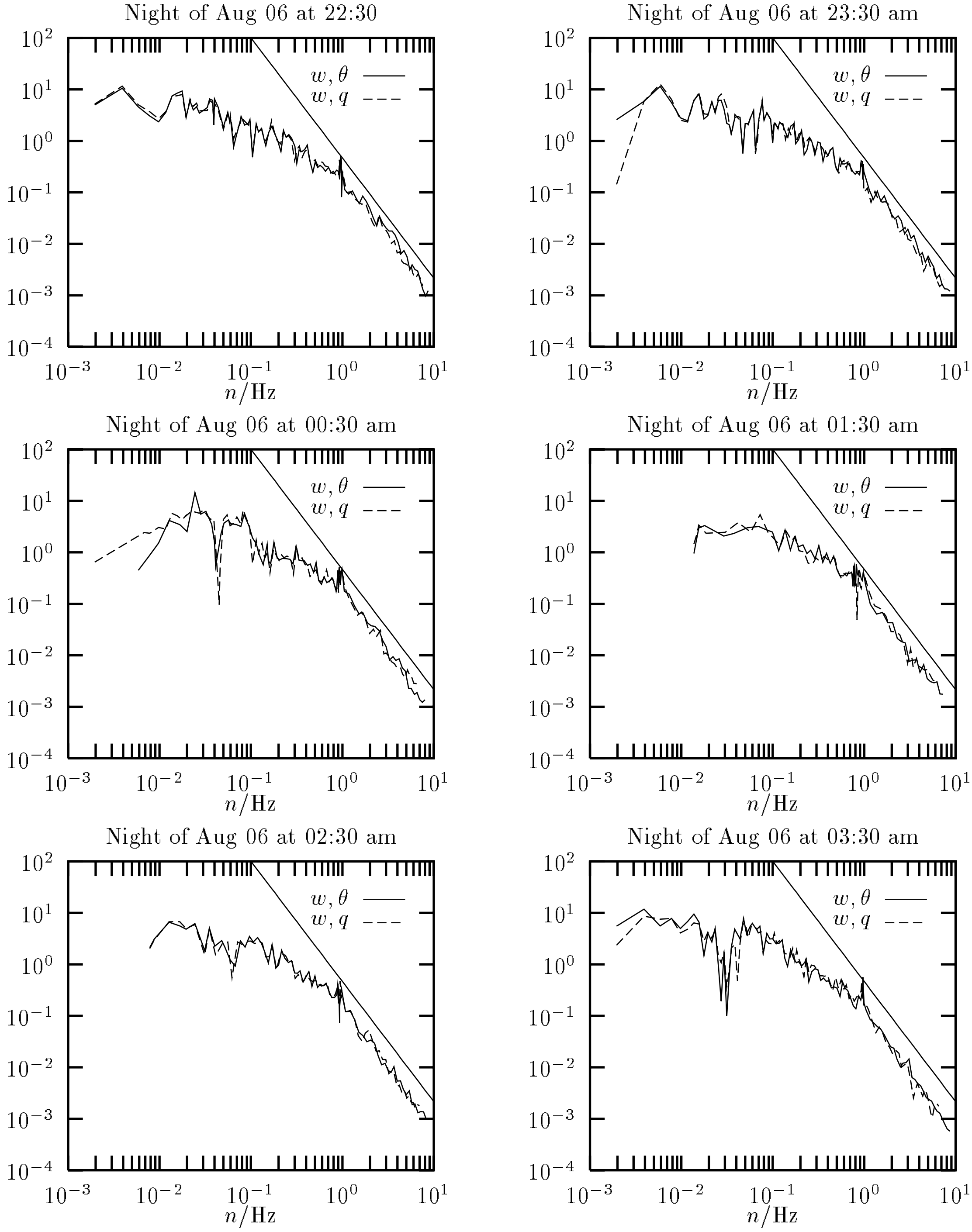

Figure 5.9 – Reduced cospectral densities $S_{w,a}/(u_* a_*)$, $a = \theta, q$ on Aug 06 (cont.).

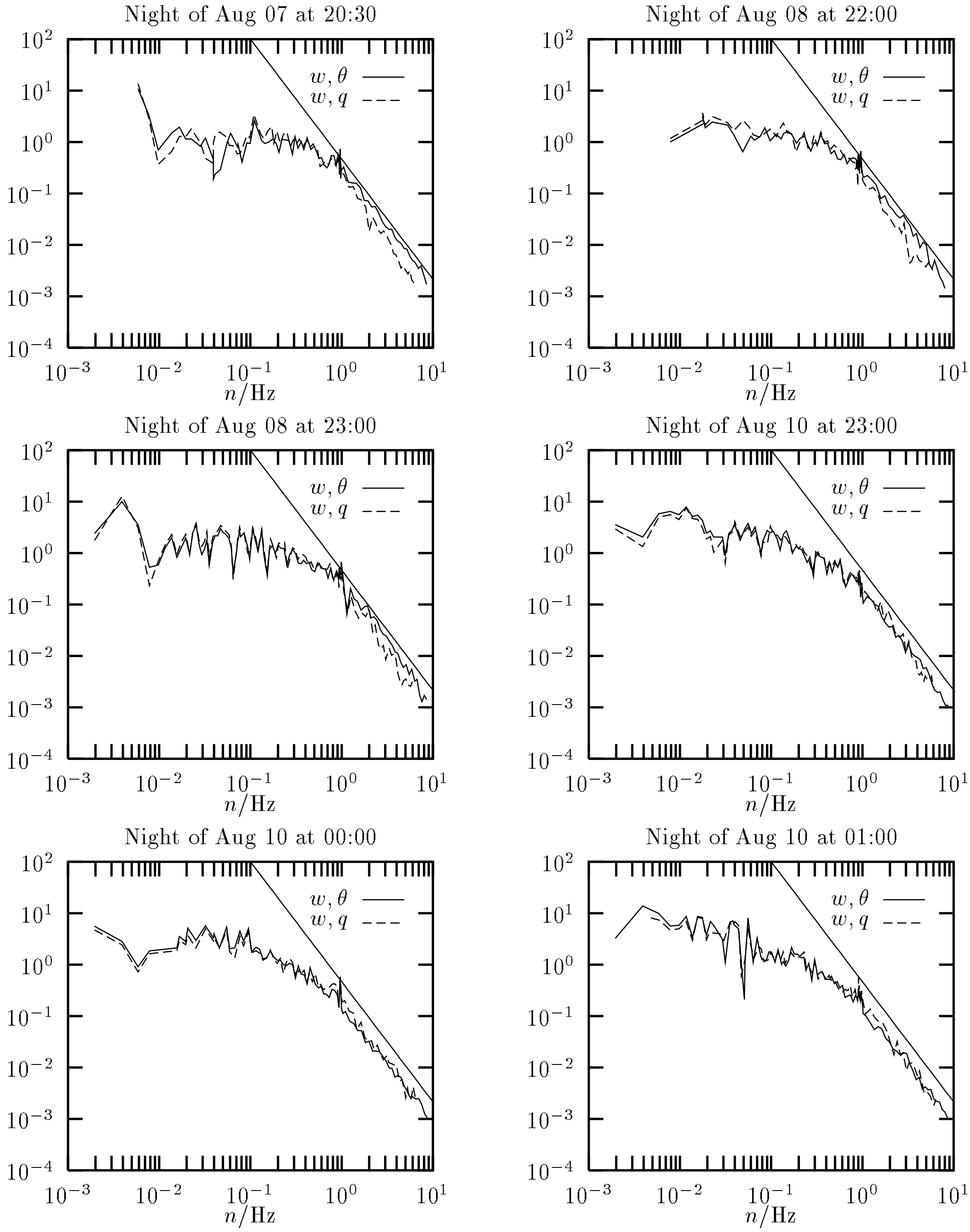

Figure 5.10 – Reduced cospectral densities $S_{w,a}/(u_* a_*)$, $a = \theta, q$ on Aug 07, 08 and 10.

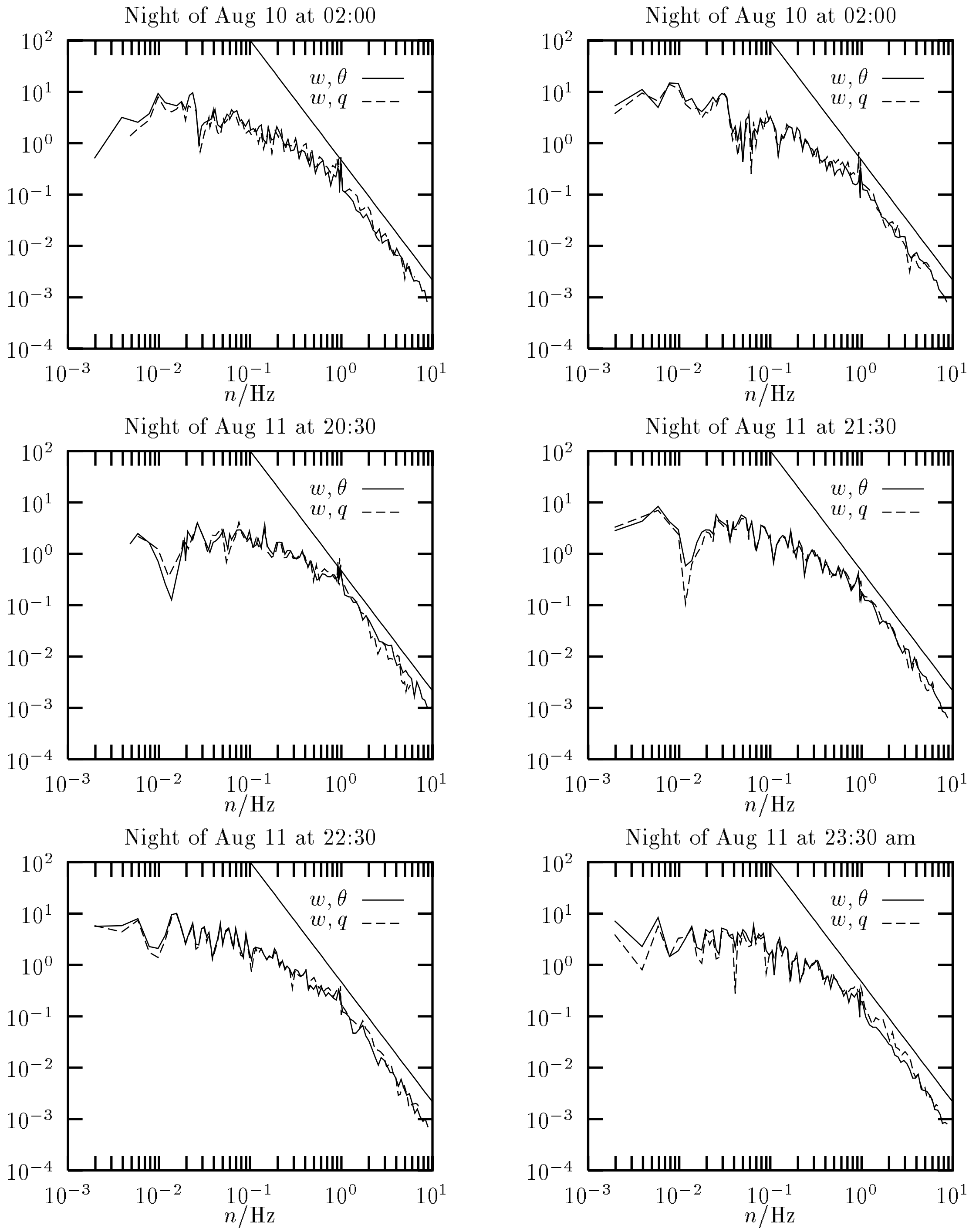

Figure 5.11 – Reduced cospectral densities $S_{w,a}/(u_* a_*)$, $a = \theta, q$ on Aug 10 (cont.) and 11.

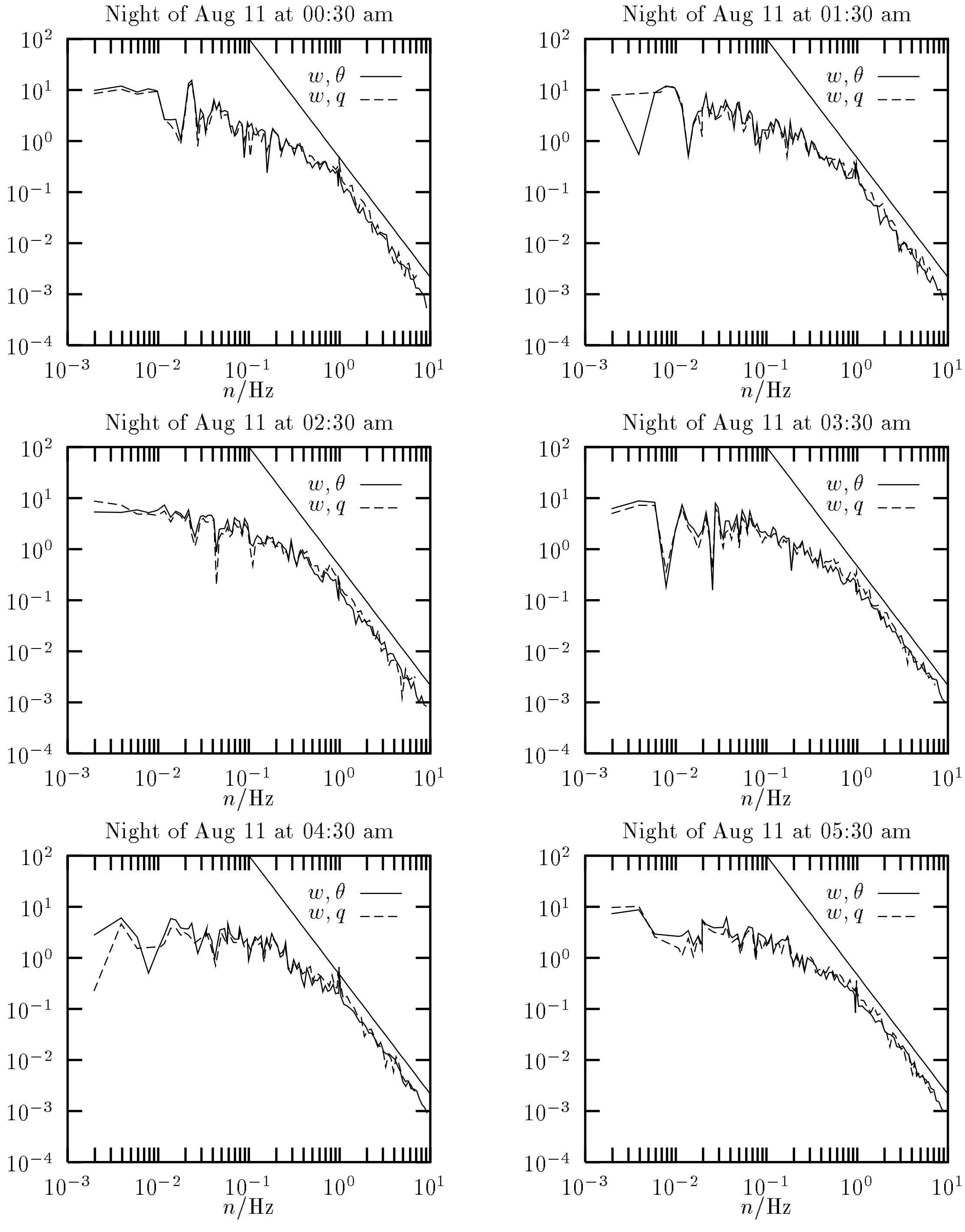

Figure 5.12 – Reduced cospectral densities $S_{w,a}/(u_* a_*)$, $a = \theta, q$ on Aug 11 (cont.).

5.4 Coherence and Phase between temperature and humidity

It should be possible to obtain a strong indication of the similarity between θ' and q' by looking at their cross-spectral properties alone. If θ' and q' are perfectly anti-correlated in stable conditions, then $S^q_{\theta,q} \equiv 0$, $\vartheta_{\theta,q} \equiv -180\,^\circ$ and $\Gamma_{\theta,q} \equiv 1$ according to the predictions of Wyngaard *et al.* (1978) (equation (2.59-c)), Hill (1988b) and Chapter 3.

We show coherence and phase functions side by side for each long run on figures 5.13-5.24, in the usual order, except that now there are only three long runs per page. The computed coherence falls off after $n = 0.1$ Hz in all cases, whereas the theoretical prediction of Wyngaard *et al.* (1978) is for a "flat" coherence in the inertial subrange. Such a fall-off in the temperature-humidity coherence has also been observed by Priestley and Hill (1985); they attributed it to spatial sensor separation. Of course, in order to establish this fact, it would be best to calculate the coherence between a scalar and *itself* at a certain distance. This is exactly the case reported by Moncrieff *et al.* (1993), in an intercomparison of eddy correlation measurements of CO_2 flux by different instruments. They plotted the coherence between the CO_2 traces measured by 2 instruments (open-path, fast response analyzers, sampled at 20 Hz) placed approximately 40 cm apart in the cross-wind direction. The result is *exactly* as any of the 36 plots of $\Gamma_{\theta,q}$ shown here, and leaves little doubt about the fact that the observed fall-off is indeed due to spatial separation. If it had been possible to measure θ' and q' at the same *point* in space, we would have obtained $\Gamma_{\theta,q} \approx 1$ throughout the frequency range, except possibly for the night of Aug 03rd.

This observed fall-off seems to hinder the ability of the coherence function to spot the similarity between θ' and q. The phase function fares better: it shows a "bump" in the higher frequencies during the night of Aug 03rd which is different from the behavior in the remaining cases, where $\vartheta_{\theta,q}$ "falls" to $\pm 90^\circ$ (no correlation) in a random way. It is not clear, however, how to explain this behavior.

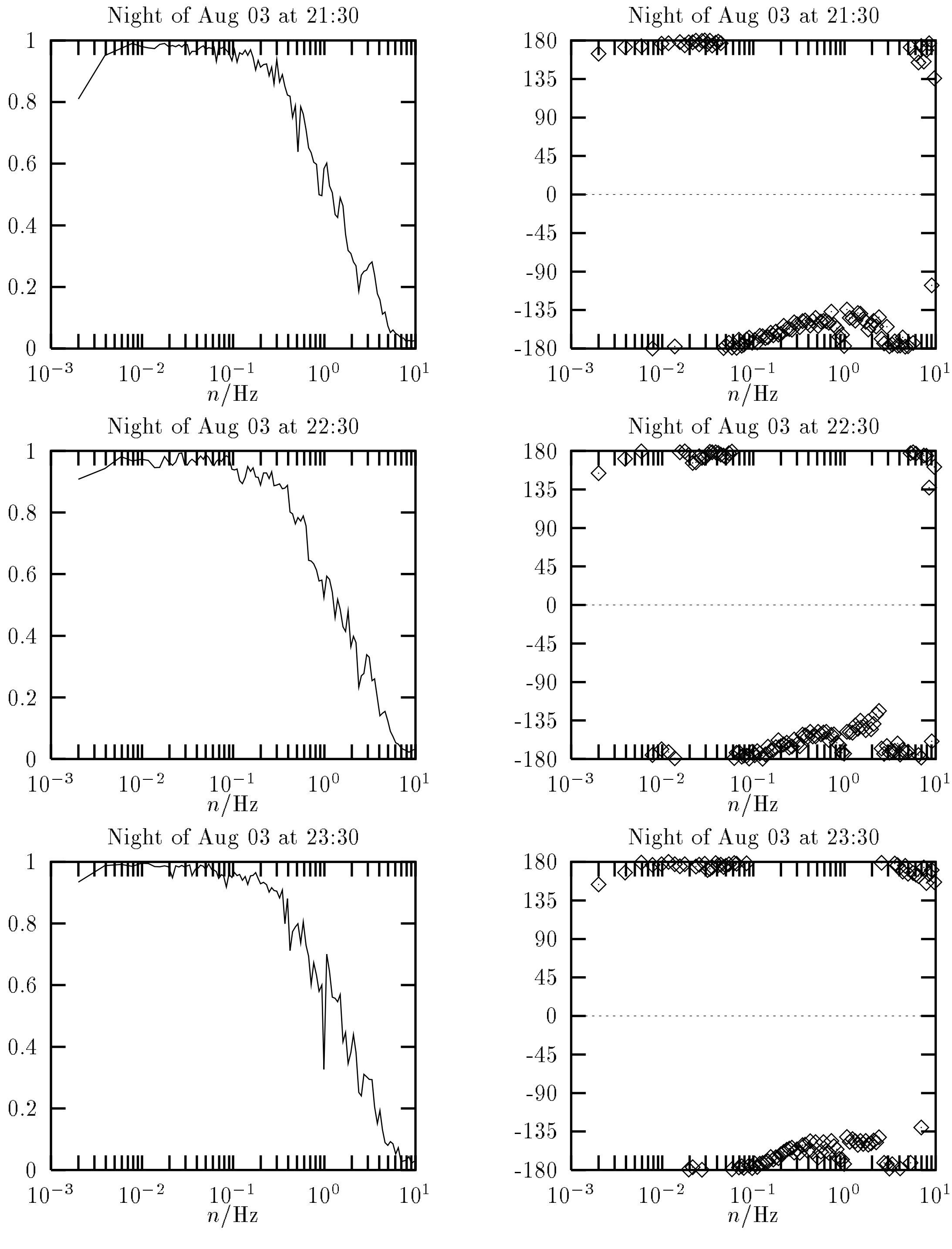

Figure 5.13 – Coherence $\Gamma_{\theta,q}$ and Phase $\vartheta_{\theta,q}$ on Aug 03.

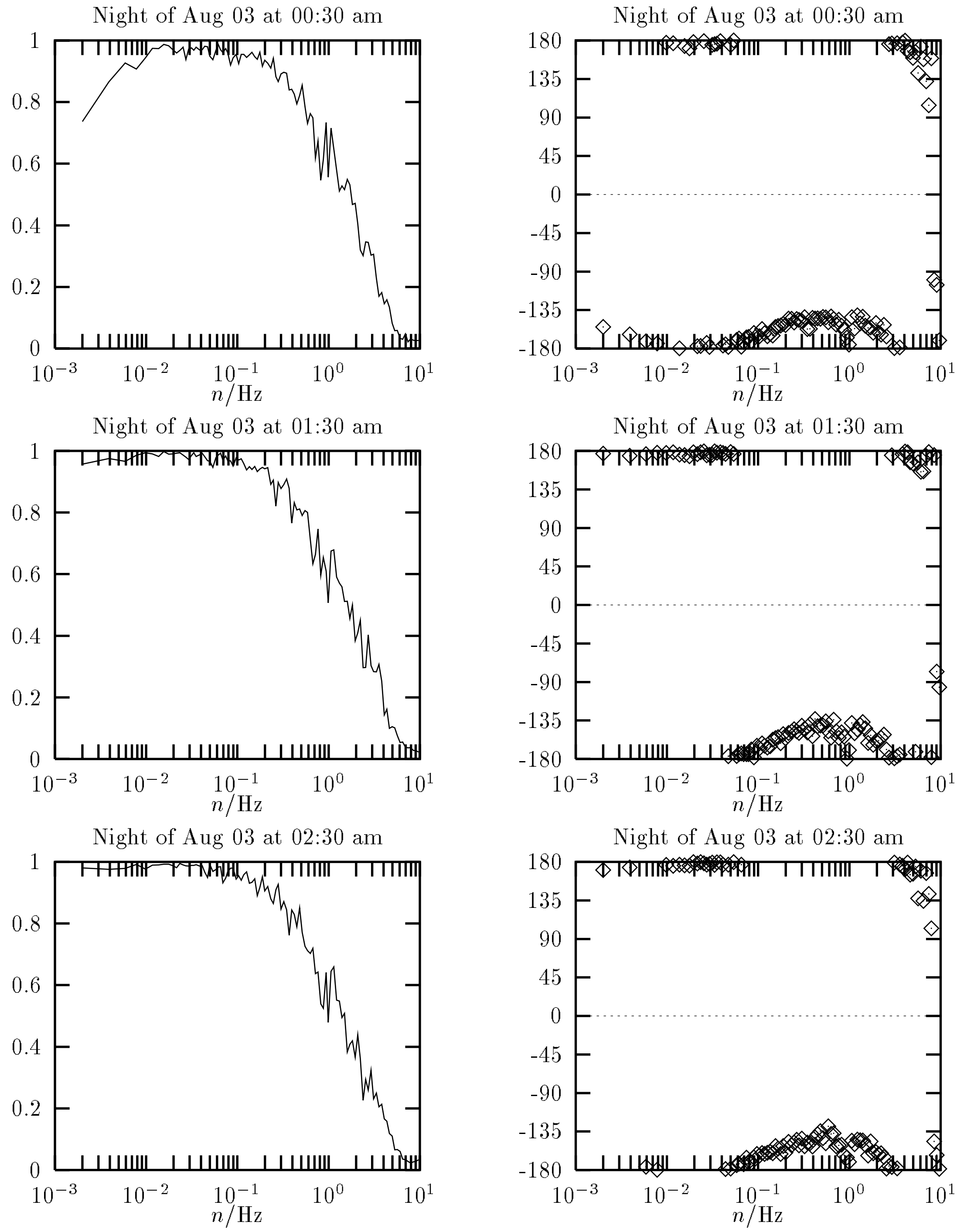

Figure 5.14 – Coherence $\Gamma_{\theta,q}$ and Phase $\vartheta_{\theta,q}$ on Aug 03 (cont.).

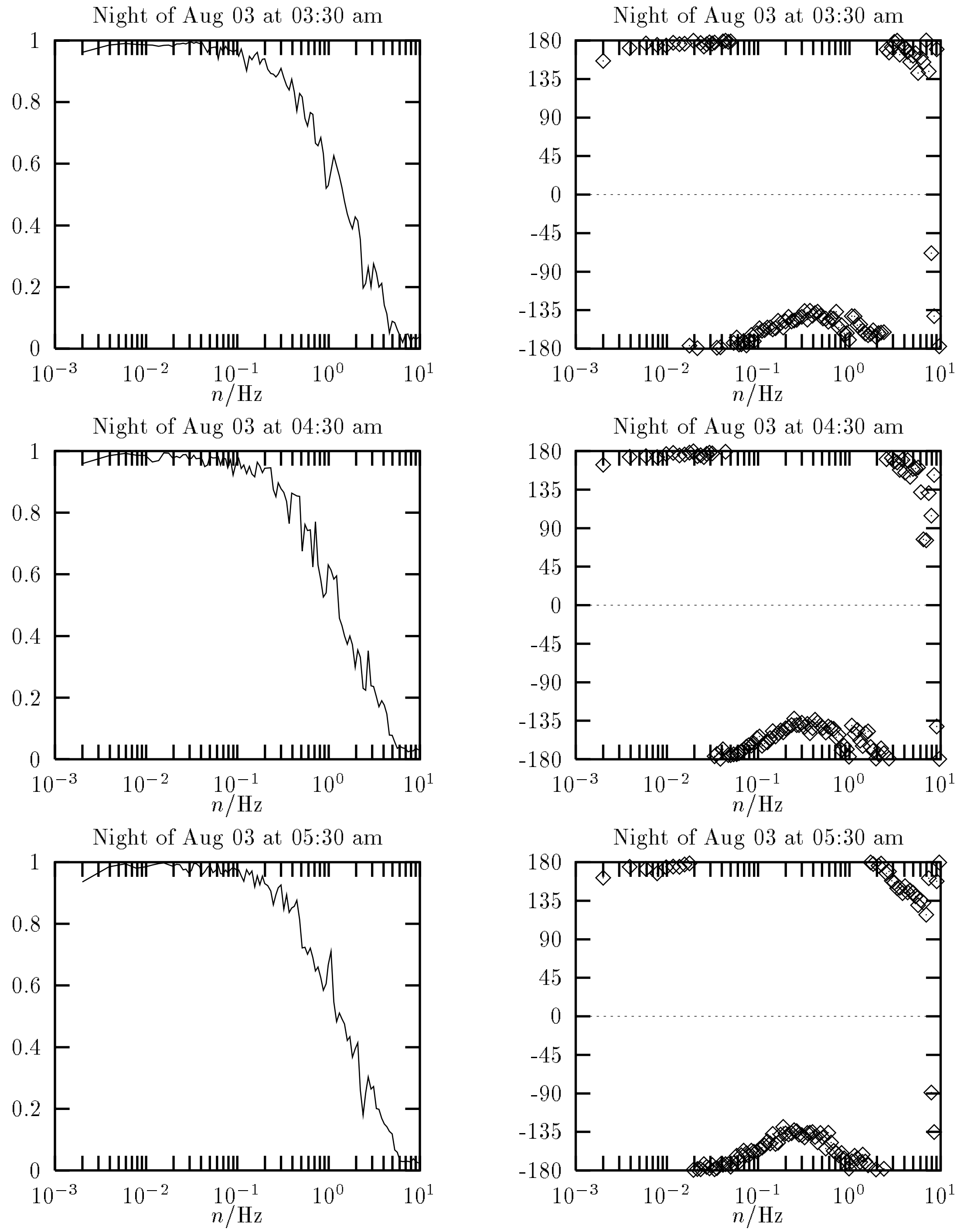

Figure 5.15 – Coherence $\Gamma_{\theta,q}$ and Phase $\vartheta_{\theta,q}$ on Aug 03 (cont.).

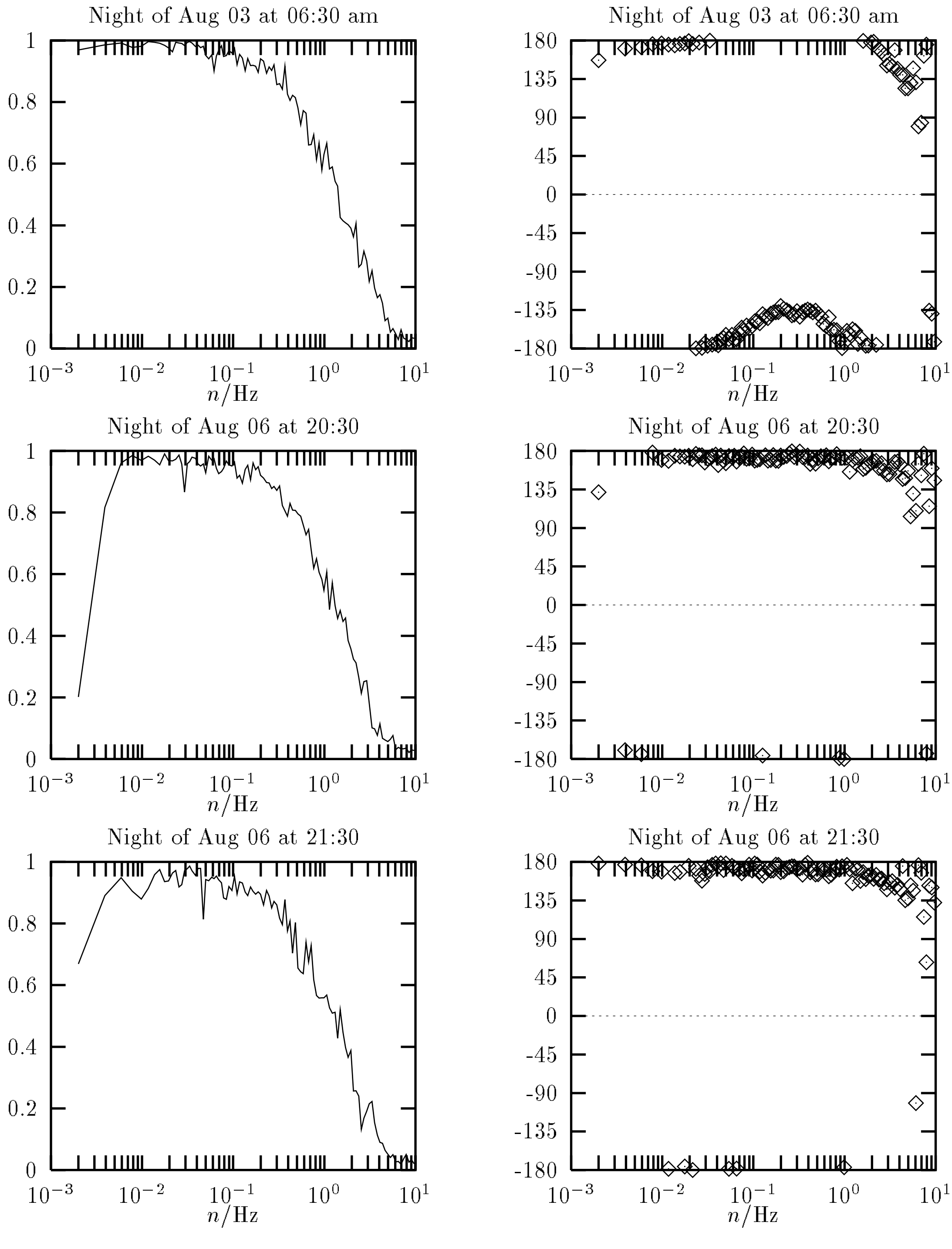

Figure 5.16 – Coherence $\Gamma_{\theta,q}$ and Phase $\vartheta_{\theta,q}$ on Aug 03 (cont.) and Aug 06.

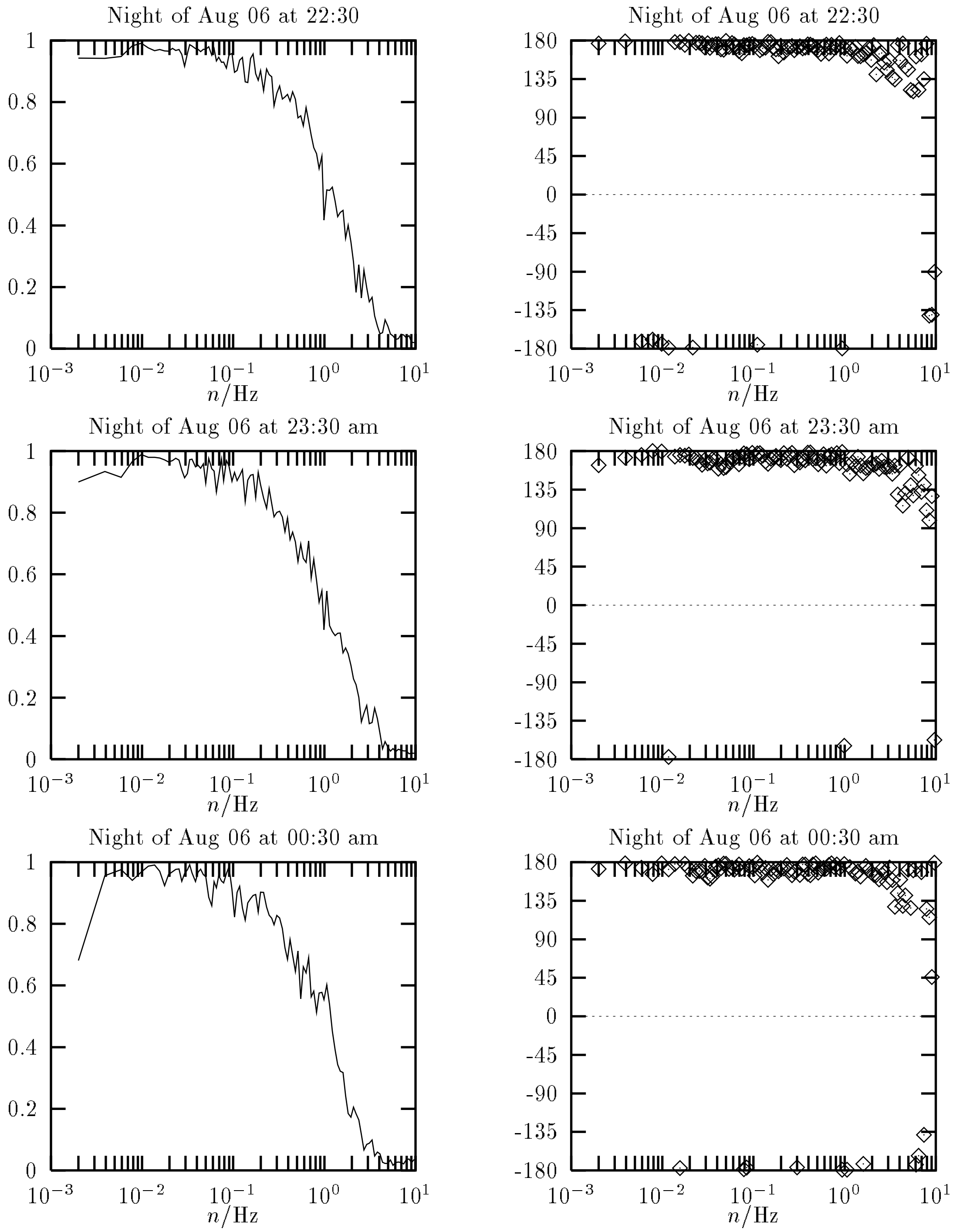

Figure 5.17 – Coherence $\Gamma_{\theta,q}$ and Phase $\vartheta_{\theta,q}$ on Aug 06 (cont.).

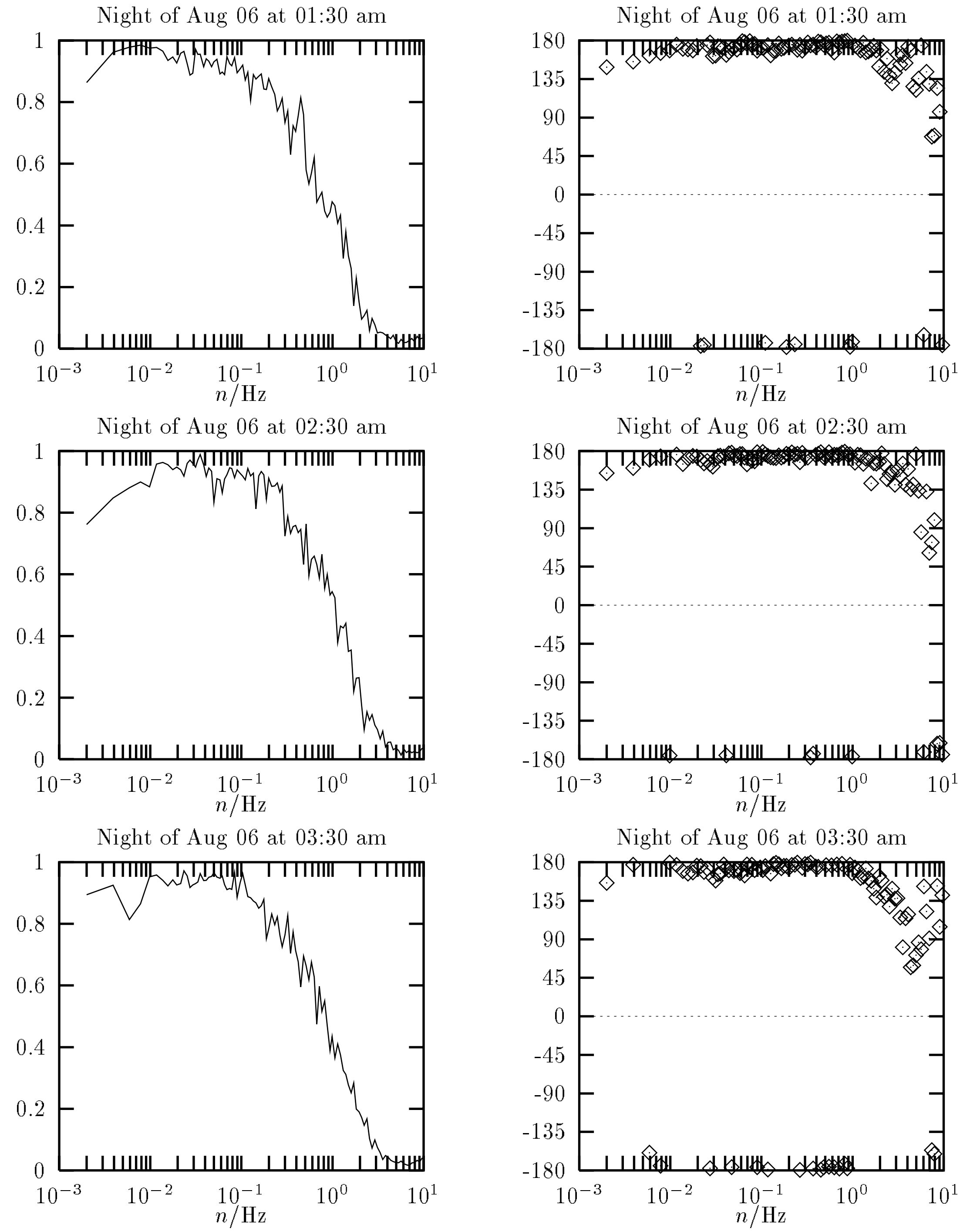

Figure 5.18 – Coherence $\Gamma_{\theta,q}$ and Phase $\vartheta_{\theta,q}$ on Aug 06 (cont.).

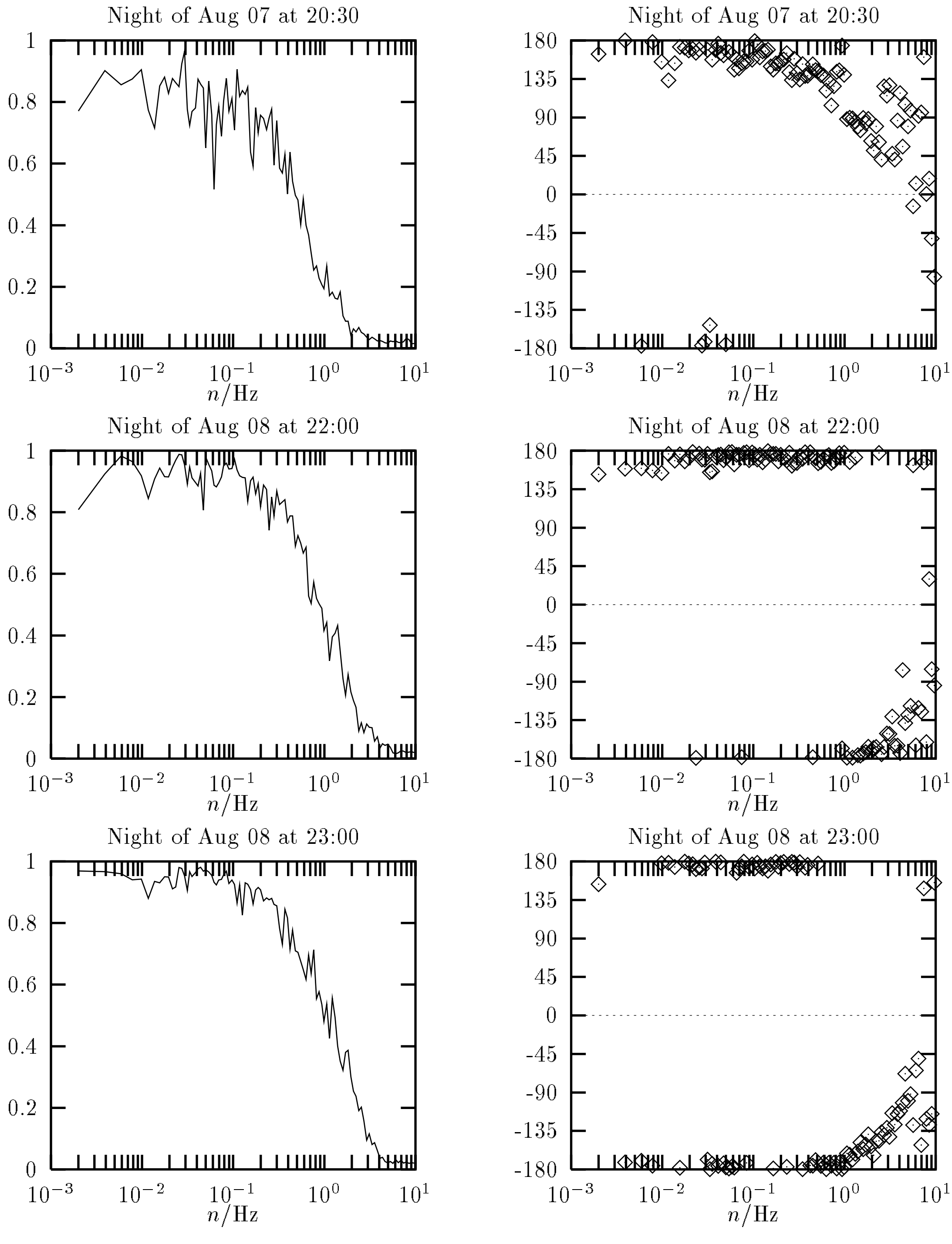

Figure 5.19 – Coherence $\Gamma_{\theta,q}$ and Phase $\vartheta_{\theta,q}$ on Aug 07 and Aug 08.

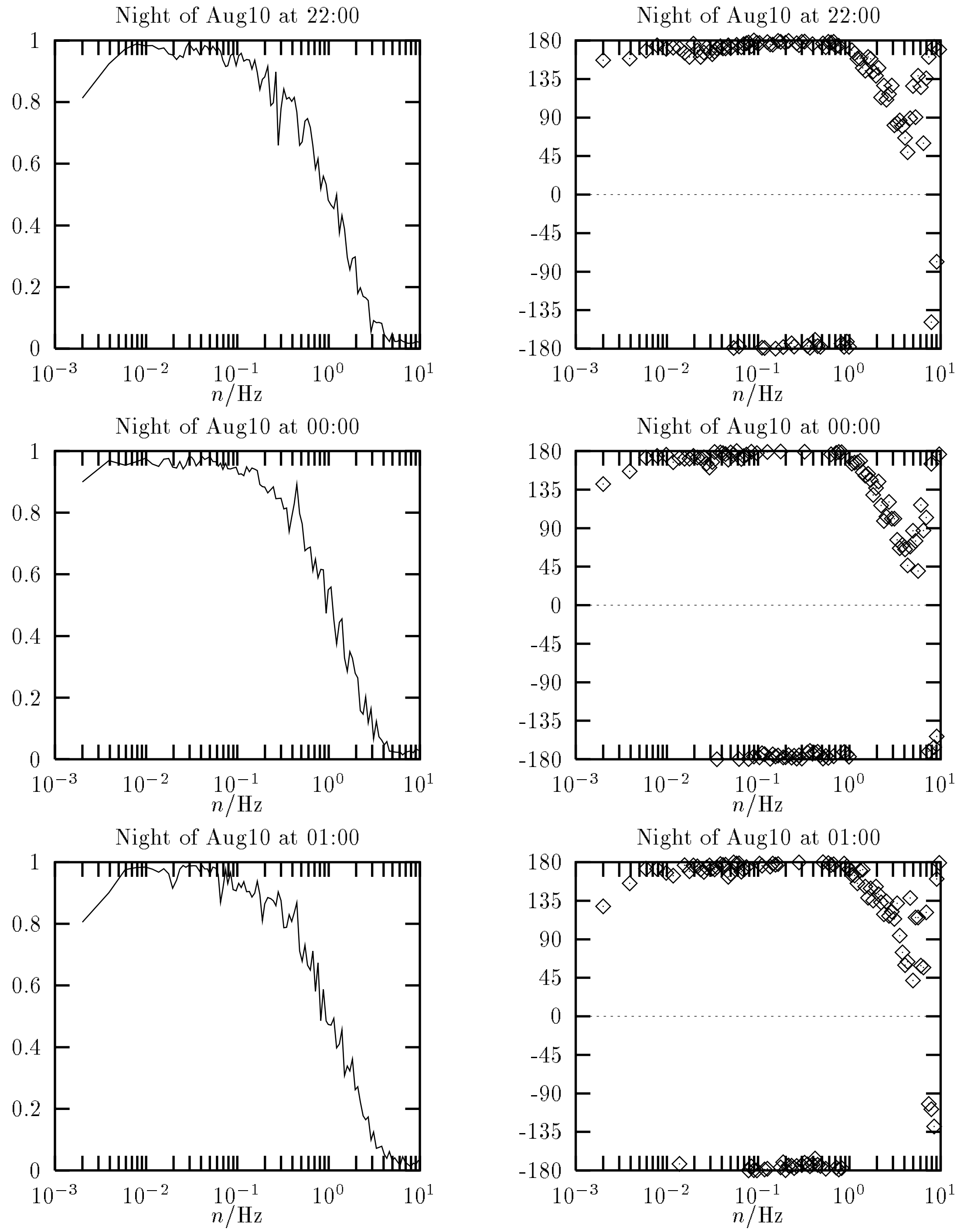

Figure 5.20 – Coherence $\Gamma_{\theta,q}$ and Phase $\vartheta_{\theta,q}$ on Aug 10.

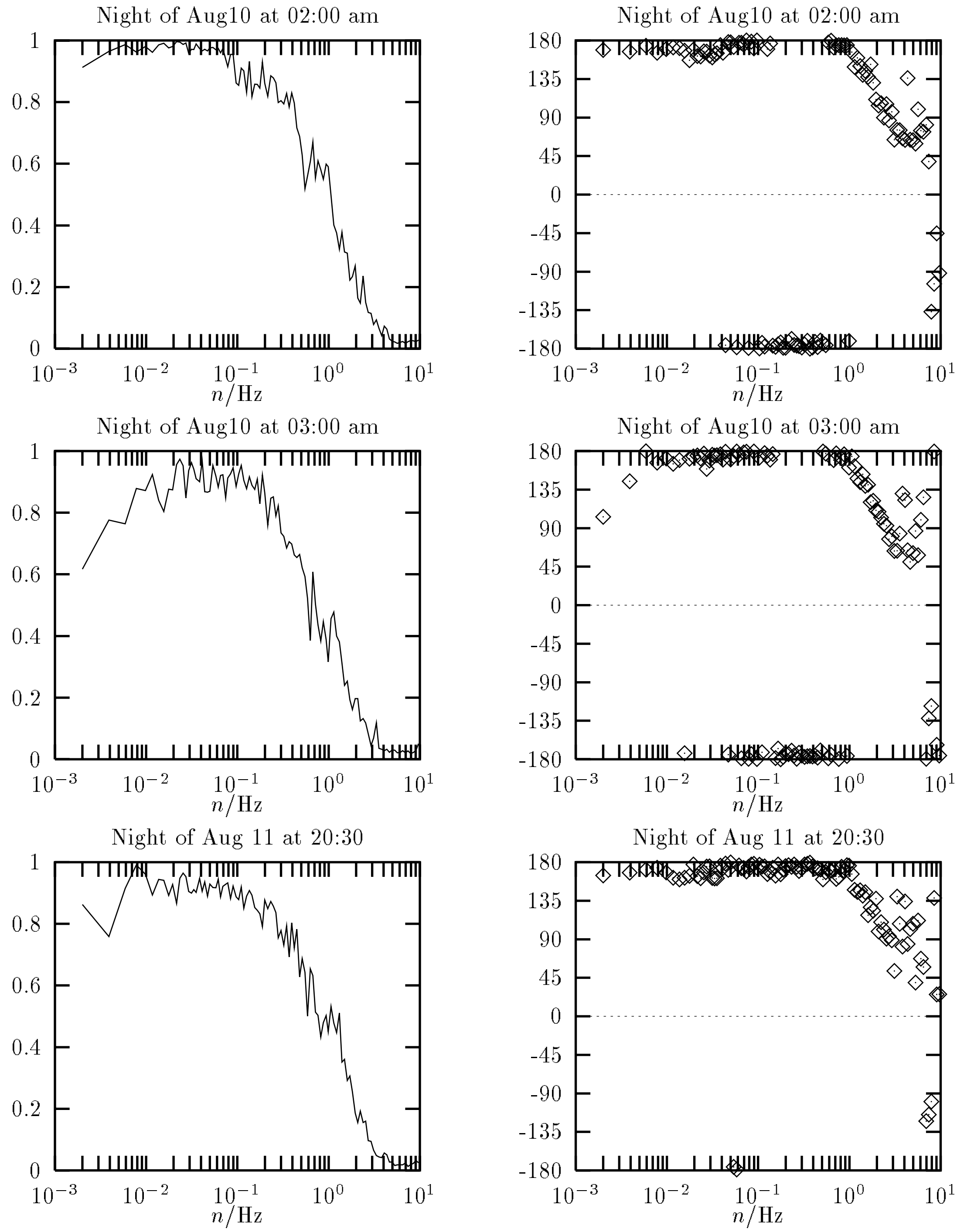

Figure 5.21 – Coherence $\Gamma_{\theta,q}$ and Phase $\vartheta_{\theta,q}$ on Aug 10 (cont.) and Aug 11.

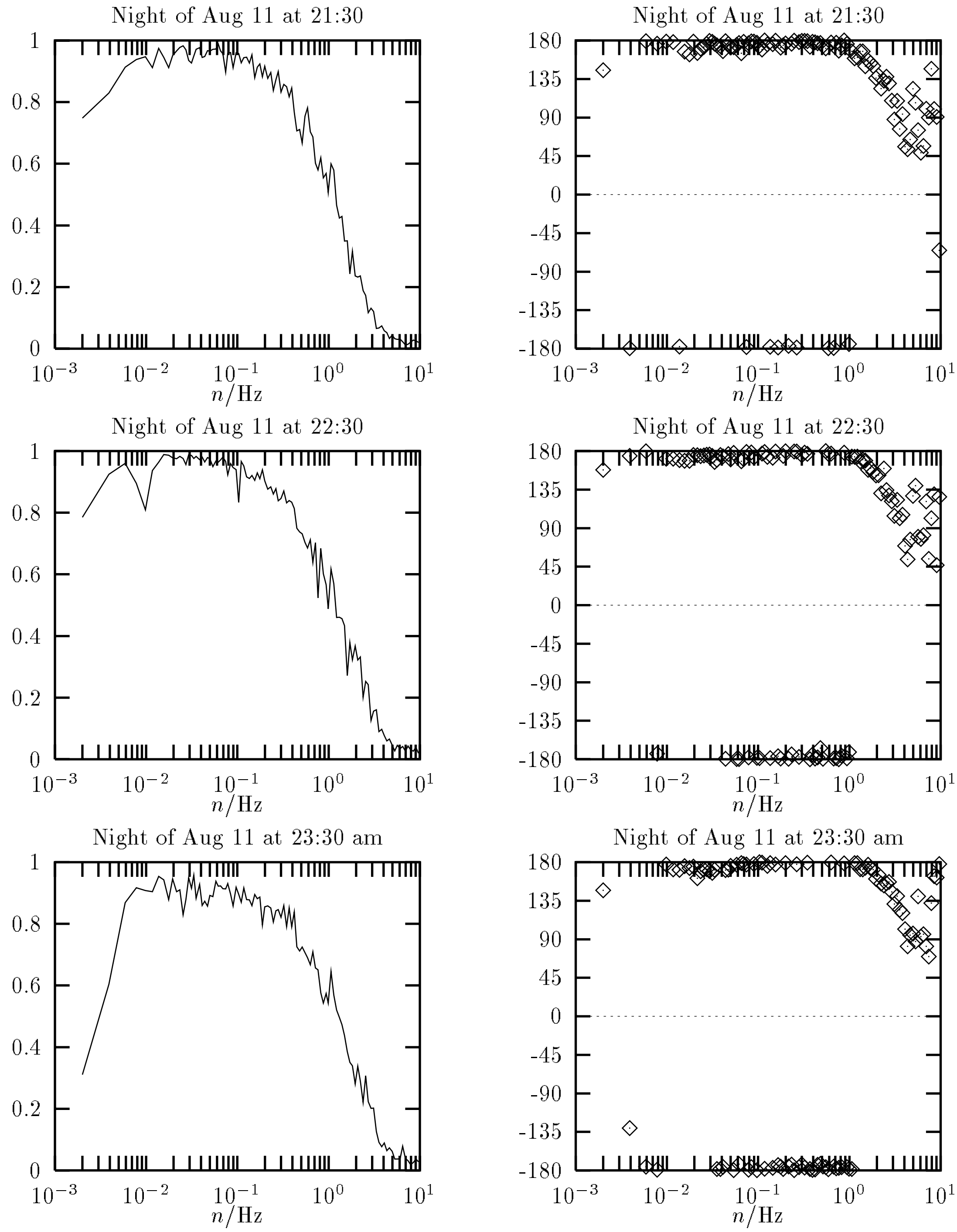

Figure 5.22 – Coherence $\Gamma_{\theta,q}$ and Phase $\vartheta_{\theta,q}$ on Aug 11 (cont.).

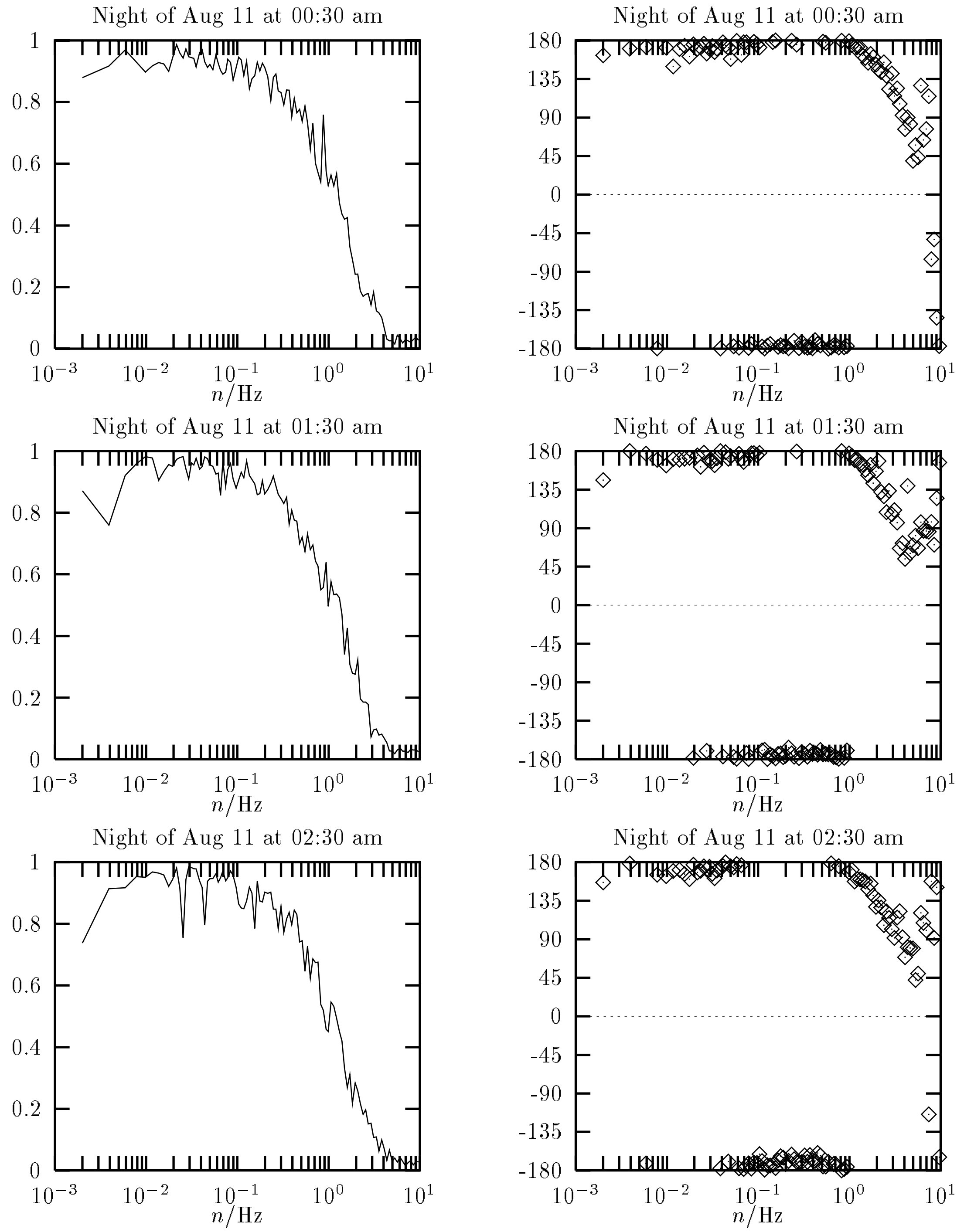

Figure 5.23 – Coherence $\Gamma_{\theta,q}$ and Phase $\vartheta_{\theta,q}$ on Aug 11 (cont.).

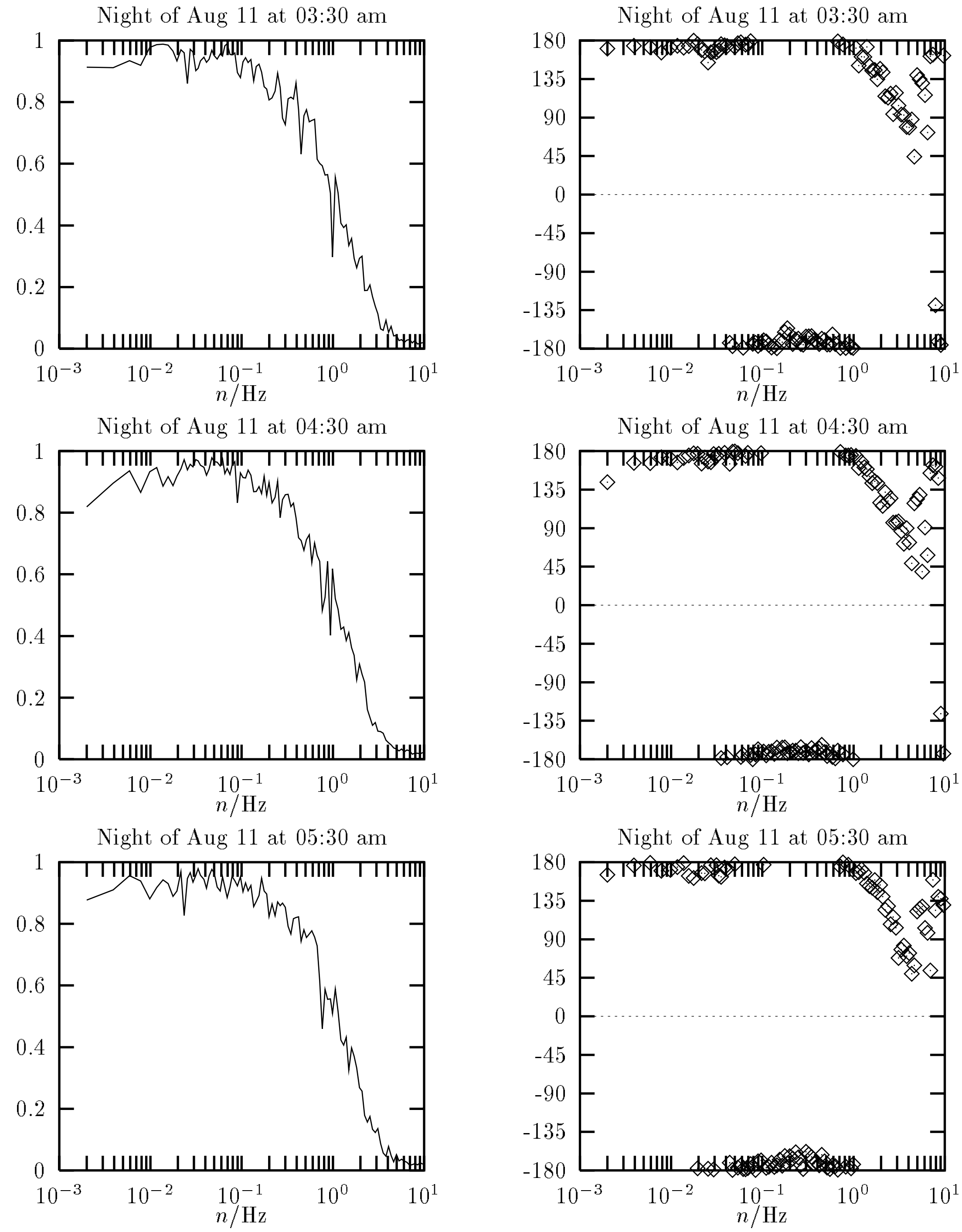

Figure 5.24 – Coherence $\Gamma_{\theta,q}$ and Phase $\vartheta_{\theta,q}$ on Aug 11 (cont.).

5.5 Higher-order cospectra

Remember that in Chapter 2 the Kolmogorov-Corrsin behavior of scalars in the inertial subrange was extended to the cospectrum $S_{a,aa}$, with the prediction that $S_{a,aa} \sim k^{-2}$. This prediction is confirmed in Figures 5.25-5.30, where $S_{\theta,\theta\theta}$ and $S_{q,qq}$ are plotted in the range of 0.1 to 10 Hz. The humidity data seem to perform poorer in the estimation of higher-order statistics, as was already hinted with the plots of spectra; there are extensive regions of "missing" data, i.e.: regions with the "wrong" cospectral density sign. The straight lines in the figures have a slope of -2.

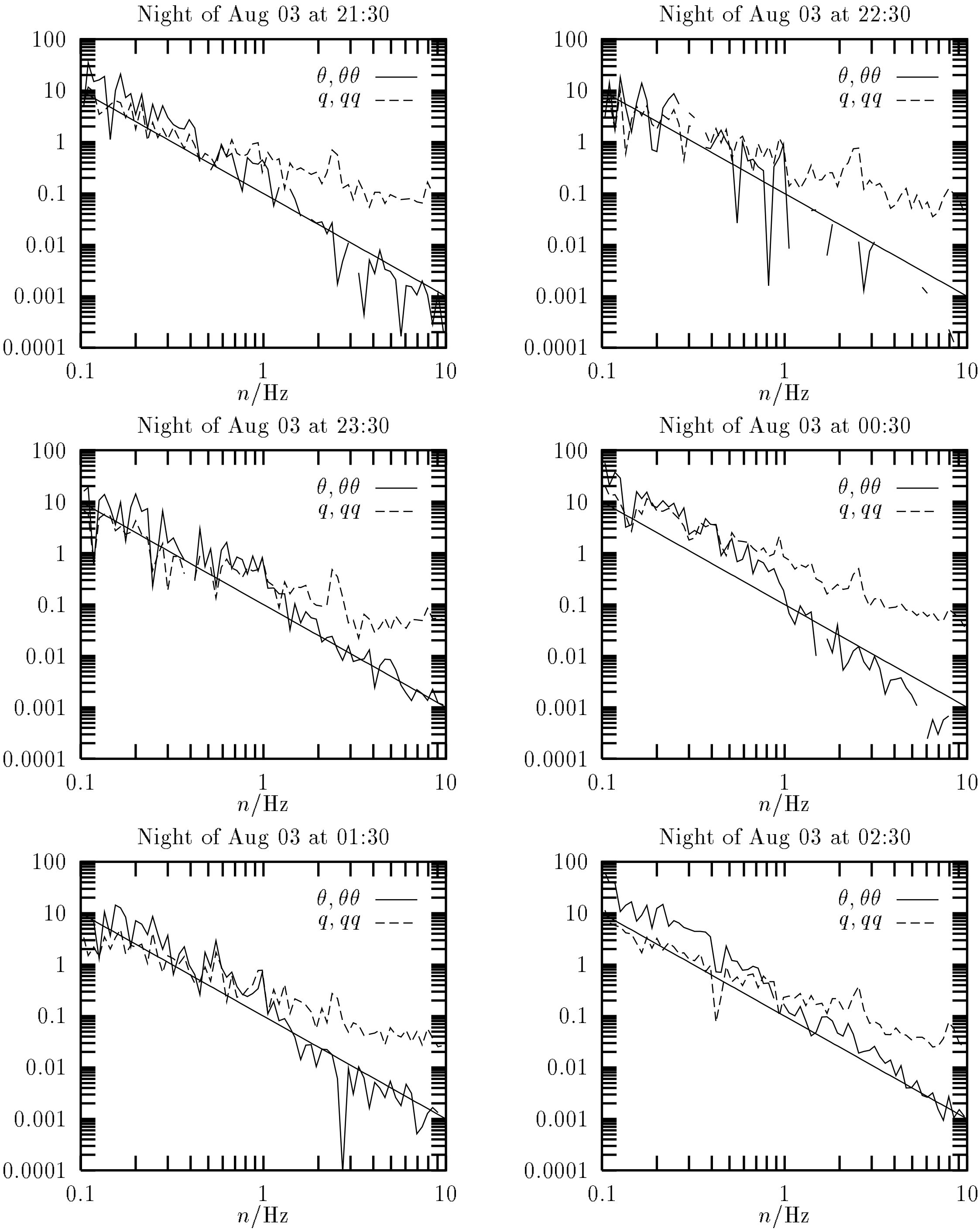

Figure 5.25 – Cospectra $S_{a,aa}/a_*^3$, $a = \theta, q$ on Aug 03rd.

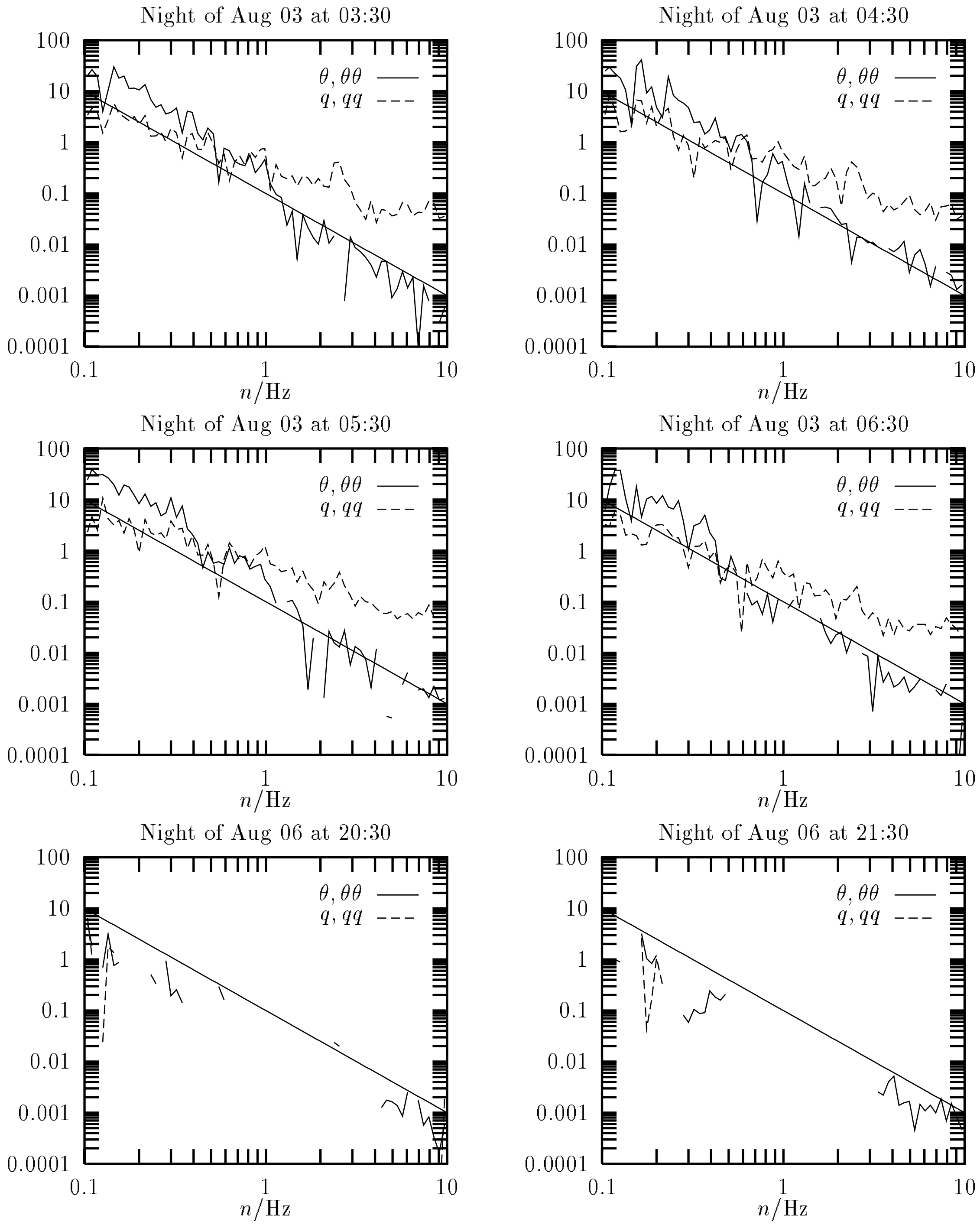

Figure 5.26 – Cospectra $S_{a,aa}/a_*^3$, $a = \theta, q$ on Aug 03rd (cont.) and Aug 06

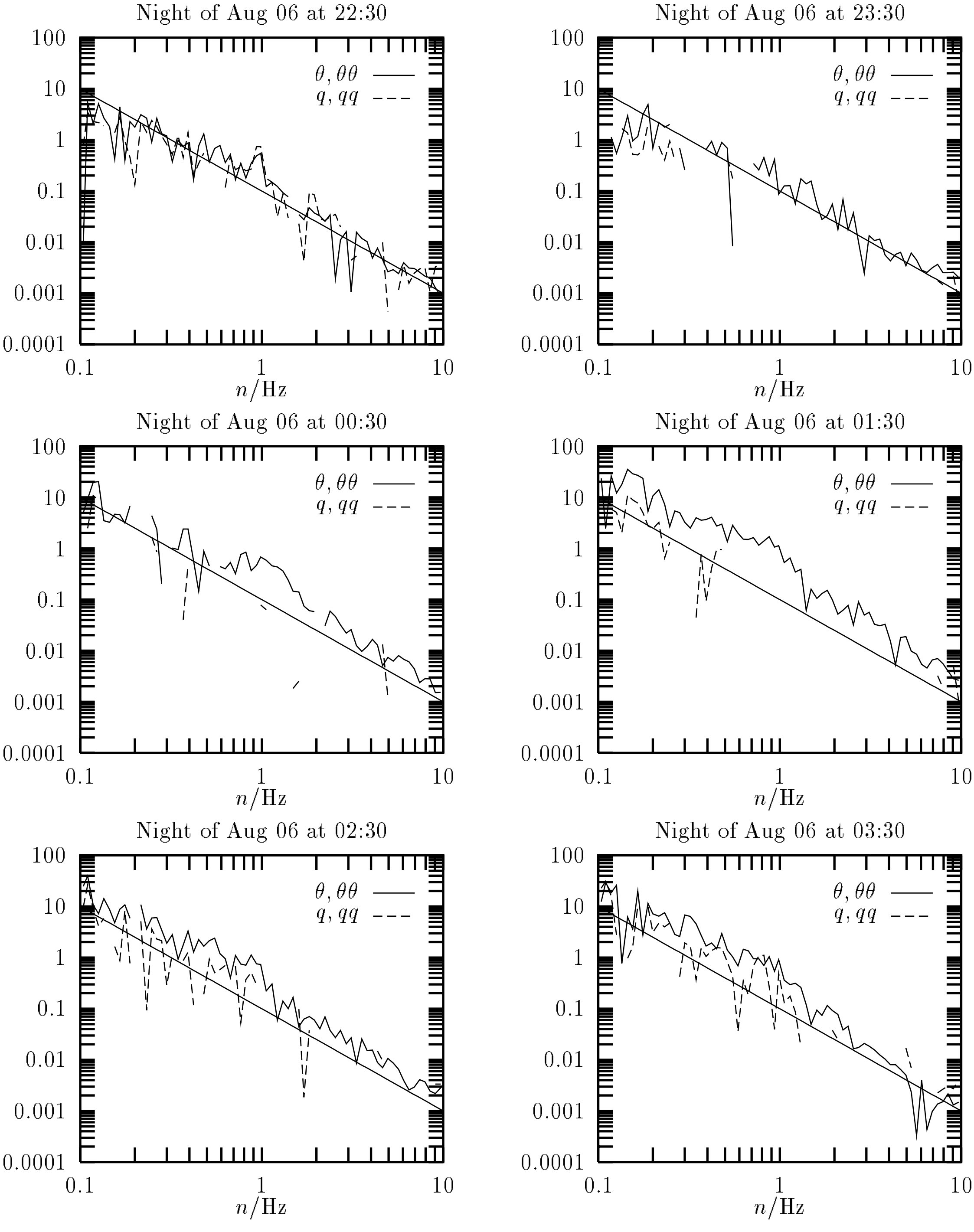

Figure 5.27 – Cospectra $S_{a,aa}/a_*^3$, $a = \theta, q$ on Aug 06 (cont.).

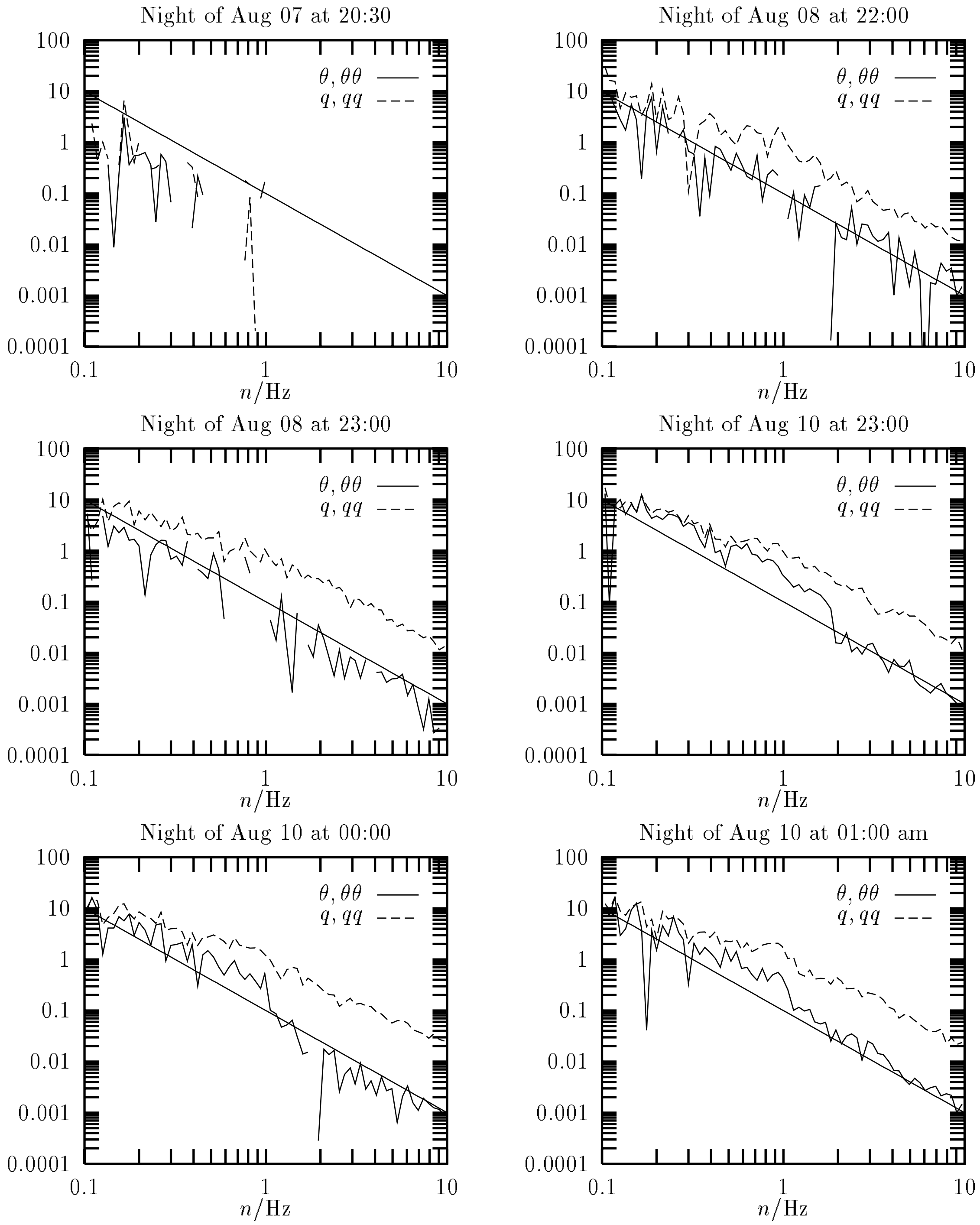

Figure 5.28 – Cospectra $S_{a,aa}/a_*^3$, $a = \theta, q$ on Aug 07, 08 and 10.

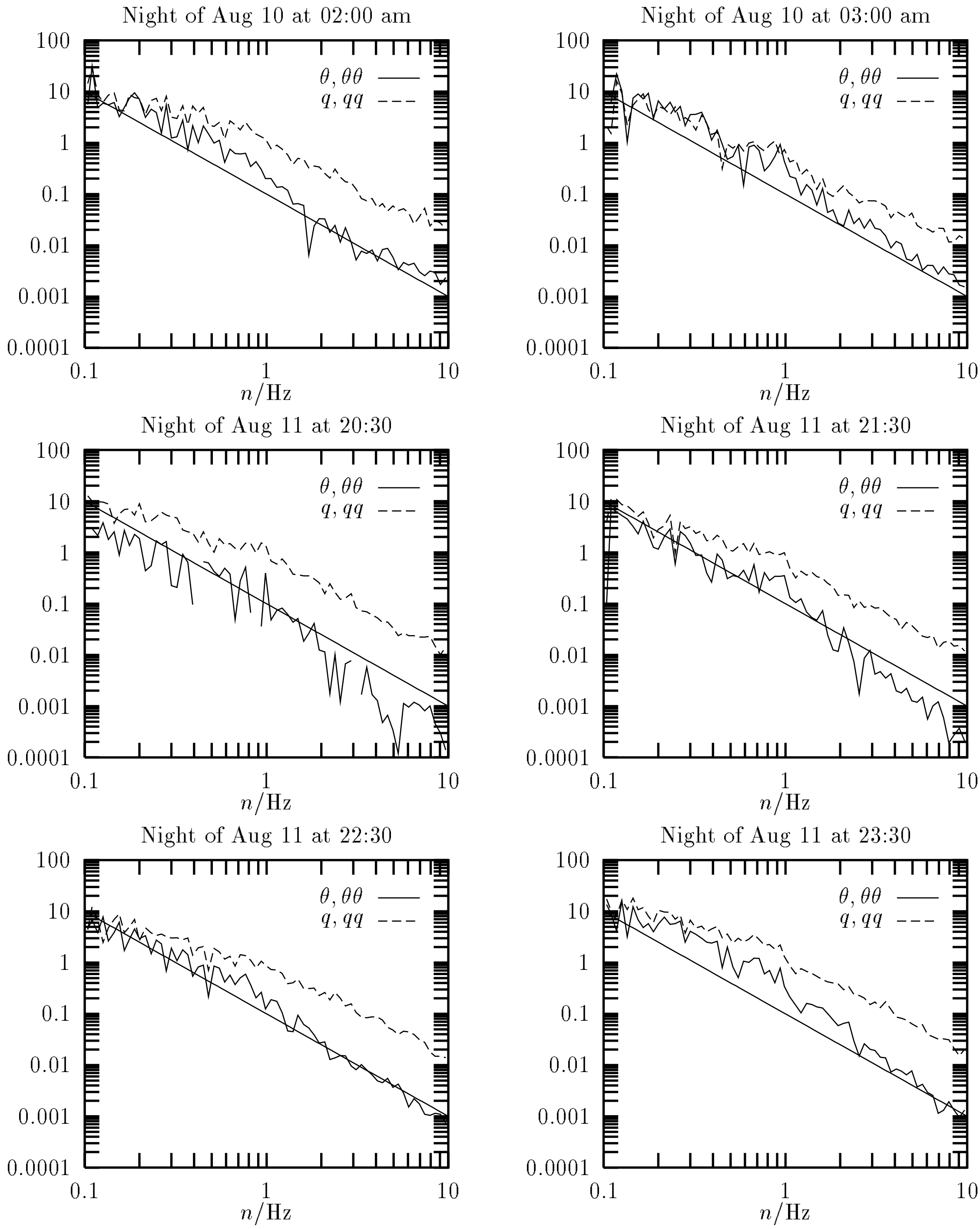

Figure 5.29 – Cospectra $S_{a,aa}/a_*^3$, $a = \theta, q$ on Aug 10 (cont.) and 11.

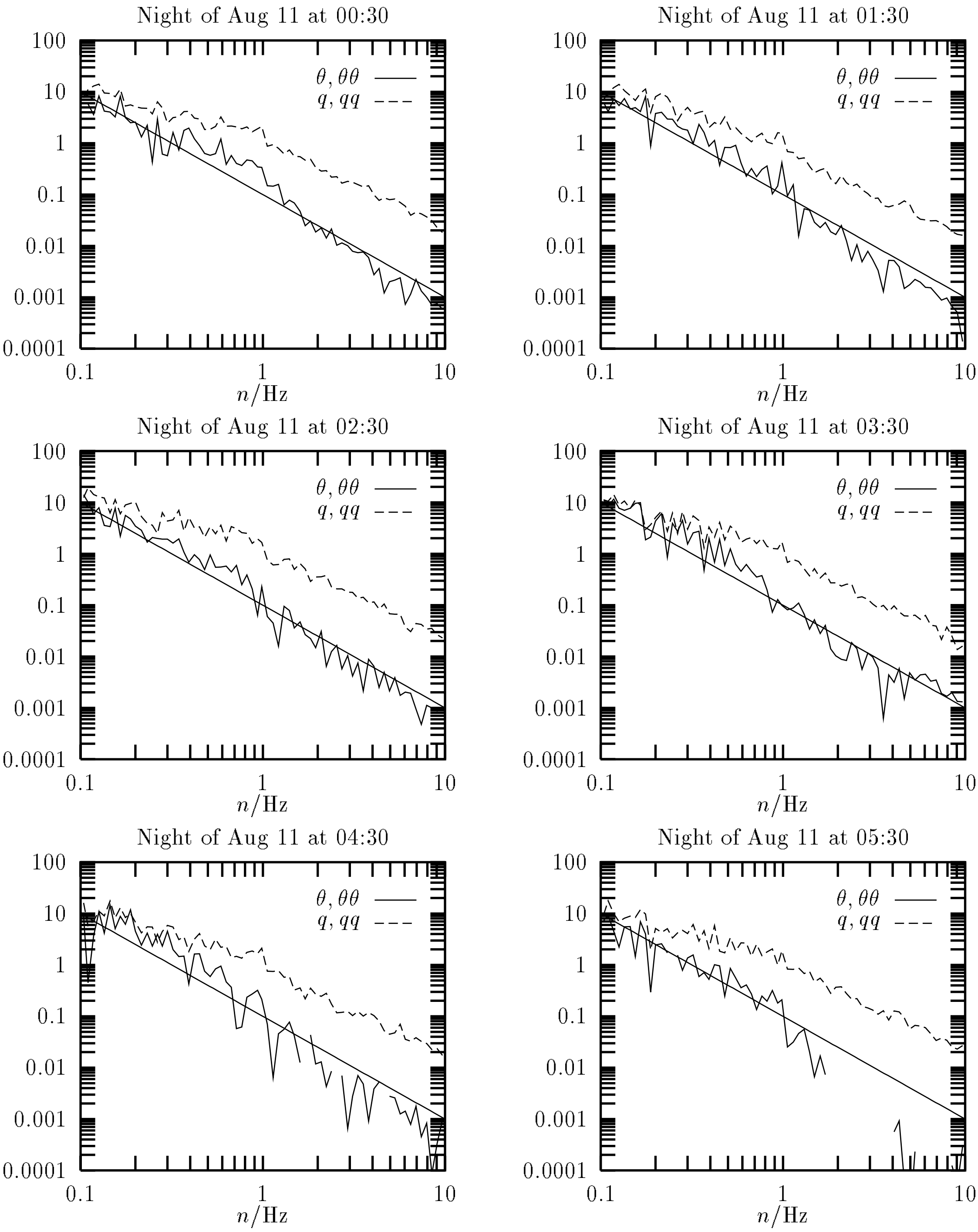

Figure 5.30 – Cospectra $S_{a,aa}/a_*^3$, $a = \theta, q$ on Aug 11 (cont.).

5.6 Closure

An extensive spectral analysis of quantities involving temperature and humidity was performed. In all analyses, the first night (Aug 03rd) shows unequivocal signs of dissimilarity between temperature and humidity. Because it had rained during the same day, and the atmosphere was disturbed with the passage of a frontal system causing the rain, it is possible that MOS conditions did hot hold for this night. After that, no more rain fell and a progressive drying of the soil took place. During this period, temperature and humidity show a remarkable degree of similarity.

We investigated the low-frequency behavior of the scalar spectra; they seem to follow Kader's (1993) -1 law only for near-neutral conditions. It is hypothesized that under more stable conditions the lower-frequency regions no longer scale with z (because of z-less stratification), but rather tend to show the behavior predicted empirically by Kaimal's (1973) curves (slope 0).

Coherence between θ' and q' is also admirably close to the theoretical value of $+1$ up to 0.1 Hz, decaying at higher frequencies due to sensor separation. This fact has not been emphasized enough in the literature (only Wesely and Hicks (1975) and Priestley and Hill (1985) seem to have given it its due importance), and can elicit some questioning. For instance, it is usually the temperature sensor which is placed closest to the vertical temperature sensor, with the humidity sensor some distance (a few decimeters, typically) apart in the cross-wind direction. Arguably, this arrangement may lead to underestimation of the water vapor flux in the high-frequency end of the w, q cospectrum. Curiously, there is no indication in the cospectra with w of any differences between θ and q in the high-frequency range: both show the expected $-7/3$ slope. Possibly, this is caused by the inherently higher frequency of the vertical velocity fluctuations. At any rate, this separation effect precludes the use of the coherence function itself to spot possible dissimilarities such as those observed on the night of Aug 03rd; they can be disclosed, however, by the phase function.

We concluded by showing how higher-order spectra, in this case the $S_{a,aa}$ cospectra, also have a power-law behavior in the inertial subrange: the predicted -2 slope is indeed observed over two decades, particularly well with the temperature data.

Chapter 6

RADIATION AND TURBULENCE IN THE STABLE BOUNDARY LAYER

In the previous chapters, it was shown that under conditions of near-stationarity and no advection, radiative effects are the only physical source of dissimilarity between water vapor and temperature, insofar as phase changes (i.e., condensation of water vapor) do not take place. Given the near-perfect anti-correlation between θ' and q' observed in the data sets analyzed in Chapters 4 and 5, in agreement with the analysis of the temperature and humidity variance and covariance budgets (3.37) performed in Chapter 3, which neglects radiation altogether, one is led to expect radiative effects to be relatively unimportant close to the surface even in nighttime conditions. This is in essence the conclusion to be reached in this chapter. We will also show, however, that it is possible to estimate how some surface-layer similarity functions change in the presence of radiation, and by how much. In fact, dimensionless spectral equations can be formulated which contain two new independent dimensionless variables in addition to Monin-Obukhov's parameter ζ. These new parameters govern the relative importance of the radiative effects on the temperature spectrum.

6.1 Modeling the interaction of radiation and turbulence in the atmosphere

The inclusion of radiative terms in the turbulent budgets (2.9) affects the temperature variance ($i = j = \theta$), and the temperature-humidity covariance ($i = \theta$, $j = q$) budgets, but not the budget of humidity variance ($i = j = q$). Thus, if radiation plays an important role in stable turbulence, it is bound to create dissimilarity between temperature and humidity.

The importance of radiative effects on the mean temperature field has long been recognized, and is usually included in models of the nocturnal boundary layer. More sophisticated, second-order closure models however must also include the temperature variance budget, and there the effect of radiation in the dissipation of temperature fluctuations is often missing (Wyngaard, 1975; Brost and Wyngaard, 1978; Garratt and Brost, 1982; Nieuwstadt, 1984). Two-point spectral models can significantly help to understand the mechanisms of inertial transfer and dissipation of velocity and temperature variance in the atmospheric boundary layer, as has been shown by Straka and Fiedler (1977) and Claussen (1985a) without the inclusion of radiative effects, and Coantic and Simonin (1984) with radiation included. It has also been suggested that such models could be useful for the parameterization of sub-grid scale processes in large-eddy simulations (Chollet and Lesieur, 1981); thus it is very likely that spectral models can contribute to improved closures which better describe the physical processes involved.

Townsend (1958) seems to have been the first to analyze explicitly the interaction of radiation and turbulence in the atmosphere. He was basically interested in phenomena ocurring at considerable heights, $70 - 100\,\mathrm{Km}$ above sea-level. Townsend modeled the radiative dissipation term in the temperature budget as a "first-order" reaction, i.e., he took it to be proportional to $\overline{\theta'\theta'}$, and obtained an expression for the limiting flux Richardson number under which turbulence can be maintained. This modeling is strictly valid only at length scales small compared to the distance over which radiation of a given wavelength is effectively absorbed by the atmosphere (Townsend, 1958; Coantic and Simonin, 1984).

Brutsaert (1972) used Townsend's theoretical framework to analyze, for the first time, the interaction of radiation and turbulence in the atmospheric boundary layer. He too studied the critical values of the flux Richardson number for the maintenance of turbulence and its dependence on radiation, but did the whole analysis with turbulence and radiative models appropriate to the atmospheric boundary layer, instead of the much higher regions studied by Townsend.

Spiegel (1957) had adopted a different approach to that of Townsend or Brutsaert to study the decay of temperature fluctuations in a stellar atmosphere. He studied solutions to the equation for the fluctuating temperature in the form of complex exponentials $\exp(i\,\mathbf{k}\cdot\mathbf{x})$, and introduced a "spectral radiative dissipation function" (the term appeared much later, with Coantic and Simonin (1984)) which gave the intensity of the damping of the temperature fluctuations at each radiative wavelength λ and wavenumber k. Although the works of Spiegel and Townsend could have been related (Townsend works with the temperature covariance $\overline{\theta'\theta''}(\mathbf{x}'' - \mathbf{x}')$ between two points in space, which can be related to the temperature spectrum), Townsend seems to have been unaware of Spiegel's work.

Goody (1964, Chapter 9) took up the subject of intereaction between radiation and a fluid in motion; he generalized the definition of the spectral radiative dissipation function to account for the effect of the whole wavelength spectrum, showing that it could be split into three main regions (weak-line, strong-line and the continuum) where it behaves as k^0, k^1 and k^2 respectively.

Simonin, Coantic and Shertzer (1981) rederived the temperature spectral budgets and the spectral dissipation function by Fourier-transforming the equations for homogenenous and isotropic turbulence, analyzing the quantitative effect of radiation on the temperature spectrum. Schertzer and Simonin (1981), still in the framework of isotropic turbulence, observed the appearance of an "inertial-radiative" range with a slope steeper than -3; the appearance of this range however was predicted for values of a dimensionless radiative parameter ζ_R less than 1. They pointed out that such a behavior was unlikely in the case of the Earth's atmosphere. They also proposed a dimensionless form (but not a *formula*) for the spectral radiative dissipation function.

Coantic and Simonin (1984), in a landmark paper, applied those earlier results to the Earth's planetary boundary layer; both isotropic and non-isotropic spectral temperature budgets were used, and a very thorough analysis of radiative effects was performed, with the inclusion of the continuum absorption, CO_2

effects, and scattering by water vapor droplets. Some of their conclusions include the fact that the absolute water vapor density ρ_v is relatively unimportant; the turbulence kinetic energy $\overline{e'}/2$, on the other hand, plays an important role, with radiative effects becoming important for sufficiently small ($< 2 \times 10^{-2}\mathrm{m}^2\,\mathrm{s}^{-2}$) values of it. In their analysis of non-isotropic turbulence, they used Kaimal's (1973) curve for near-neutral conditions as an initial value in the calculation of the temperature spectrum, and production was calculated with a near-neutral dimensionless temperature gradient $\phi_H(0)$.

Clearly, it is highly desirable that the statements about the *relative* importance of radiation be framed in terms of dimensionless quantities. It is also important to extend the analysis into a larger range of stable stratification conditions, farther from neutral. In this chapter, we introduce the relevant physics, and its relation to the spectral budgets. By making the equations dimensionless, the similarity parameters which include the radiative effects are found. They are then applied in a dimensionless formulation for the spectral radiative function which is considerably simpler than the extensive numerical integration over the absorption bands of H_2O (the main absorber) that has been used ever since Goody's (1964) work. This allows a simple spectral model (Claussen, 1985a) to be used and solved analytically for stability and radiative dimensionless parameters. Finally, this solution can be used to assess the relative importance of radiation in terms of its effect on the dimensionless temperature spectra and the dimensionless statistic $\phi_{\theta\theta}$.

6.2 Physical background

Given radiation of a certain wavelength λ, the *radiative wavenumber* μ is λ^{-1}. Consider a certain direction in space defined by the unit vector $\mathbf{s}$. Let $dA_\perp$ be an element of area perpendicular to $\mathbf{s}$, $d\omega$ an element of solid angle around $\mathbf{s}$ and dt an element of time during which the amount of electromagnetic energy crossing $dA_\perp$ is dE_μ. The intensity of radiation at radiative wavenumber μ is (Goody and Yung, 1989 pp. 16–17)

$$I_\mu(\mathbf{s}) \equiv \frac{dE_\mu}{dA_\perp dt d\omega} . \tag{6.1}$$

Schwarzschild's equation for absorption is

$$\frac{dI_\mu}{ds} = -\rho_a \beta_\mu (I_\mu - J_\mu) \tag{6.2}$$

where d/ds is the total derivative in the direction of $\mathbf{s}$, ρ_a is the density of the absorbing material, β_μ is the absorption coefficient at wavenumber μ, and J_μ is the thermal emission. We will assume that water vapor is the main absorbant, i.e.: $\rho_a = \rho_v$ (CO_2 effects, which are much smaller, will not be included) and that the atmosphere is in local thermodynamic equilibrium, such that

$$J_\mu = B_\mu = \frac{2hc^2\mu^3}{\exp(\frac{hc\mu}{kT}) - 1} \tag{6.3}$$

where B_μ is Planck's Blackbody Function, $h = 6.6262 \times 10^{-34}$ J s is Planck's constant, $c = 2.998 \times 10^8$ m s^{-1} is the velocity of light in the vacuum and $k = 1.381 \times 10^{-23}$ J K^{-1} is Boltzmann's constant. Then (6.2) becomes

$$\frac{dI_\mu}{ds} = -\rho_v \beta_\mu (I_\mu - B_\mu) . \tag{6.4}$$

The transmission of electromagnetic radiation over a distance r through an absorbing medium of (water vapor) density ρ_v is

$$T_\mu \equiv \exp(-\beta_\mu \rho_v r) \tag{6.5}$$

and the *mean* transmission over wavenumber range ("band") $\Delta\mu$ is

$$\overline{T}_\mu \equiv \frac{1}{\Delta\mu} \int_{\Delta\mu} \exp(-\beta_\mu \rho_v r)\, d\mu\ . \tag{6.6}$$

The main reason for introducing a mean transmission is that β_μ varies rapidly with frequency. Thus, the radiative wavenumber range is usually divided into absorption bands with a typical width of $\Delta\mu = 2{,}500\ \mathrm{m}^{-1}$, each containing thousands of individual lines. Each line in turn gives rise to a β_μ distribution around its center μ. (Houghton, 1986 p. 41; Goody and Yung, 1989 p. 125).

Houghton (1986) gives tables of the transmission function for water vapor for 105 bands, in terms of Goody's band model using the Malkmus expression (Tjemkes and Duynkerke, 1988):

$$\overline{T}_{\Delta\mu_j} = \exp\left\{ -\frac{2b_j^2}{a_j \Delta\mu_j} \left[\left(1 + \frac{a_j^2 \rho_v r}{b_j^2}\right)^{1/2} - 1 \right] \right\} \tag{6.7}$$

where for each band j, $\Delta\mu_j$ is the width of the band, and a_j and b_j are constants. The bands are unevenly distributed in the $0 - 1{,}110{,}000\ \mathrm{m}^{-1}$ range.

In addition to the H_2O absorption bands, there is a region of continuous absorption, i.e.: a region where β_μ is a smooth function of wavenumber μ, in the $\lambda = 8 - 12\,\mu\mathrm{m}$ range, which can be modeled by (Roberts, Selby and Biberman, 1976)

$$\beta_\mu = [a + be^{c\mu}] \exp\left[1800 \left(\frac{1\mathrm{K}}{T} - \frac{1}{296}\right)\right] \frac{N_A \rho_v R_v T}{M_v} \tag{6.8}$$

where $a = 1.2337 \times 10^{-31}\,\mathrm{kg}^{-1}\mathrm{m}^{-1}\mathrm{s}^2$, $b = 1.6482 \times 10^{-28}\,\mathrm{kg}^{-1}\mathrm{m}^{-1}\mathrm{s}^2$, $c = -7.87 \times 10^{-5}\,\mathrm{m}$, T is absolute temperature, $N_A = 6.02 \times 10^{23}$ is Avogadro's number, $R_v = 461.51\,\mathrm{J\,kg}^{-1}\mathrm{K}^{-1}$ is the gas constant for water vapor and $M_v = 18.015 \times 10^{-3}\mathrm{kg}^{-1}\mathrm{mol}^{-1}$ is the molecular mass of water vapor.

Given the small values of β_μ, absorption in the continuum range can only become significant for extremely long distances (see (6.5)), of the order of 1 km or more. On the other hand, the turbulence integral scale close to the surface is of the order of the distance to the surface, or 2.5 m in our case. Due to this fact, the continuum absorption will not be included in the simplified approach presented in this chapter.

6.3 Radiative Divergence

Radiation acts like a source or sink in the temperature equation; if $\mathbf{R}$ $[\mathrm{W} \cdot \mathrm{m}^{-2}]$ is the (long-wave) radiative flux density vector, the radiative heating or cooling will then depend on its divergence

$$\nabla \cdot \mathbf{R} = \frac{\partial R_k}{\partial x_k} = \int_{\mu=0}^{\infty} \int_{\omega=0}^{4\pi} \frac{dI_\mu}{ds}\, d\omega\, d\mu\ . \tag{6.9}$$

Using (6.4) and assuming that ρ_v, I_μ and B_μ can be decomposed into a mean and a fluctuating part,

$$\begin{aligned}
\frac{\partial R_k}{\partial x_k} &= \frac{\partial \overline{R}_k}{\partial x_k} + \frac{\partial R'_k}{\partial x_k} \\
&= \int_{\mu=0}^{\infty} \int_{\omega=0}^{4\pi} -\beta_\mu(\overline{\rho}_v + \rho'_v)(\overline{I}_\mu + I'_\mu - \overline{B}_\mu - B'_\mu)\, d\omega\, d\mu \\
&= \int_{\mu=0}^{\infty} \int_{\omega=0}^{4\pi} -\beta_\mu\overline{\rho}_v(\overline{I}_\mu - \overline{B}_\mu)\, d\omega\, d\mu
\end{aligned}$$

$$+\int_{\mu=0}^{\infty}\int_{\omega=0}^{4\pi} -\beta_\mu \left[\overline{\rho}_v(I'_\mu - B'_\mu) + \rho'_v(\overline{I}_\mu - \overline{B}_\mu)\right] \, d\omega \, d\mu \tag{6.10}$$

where we *define* $\partial\overline{R}_k/\partial x_k$ to be given by the first integral in the right-hand side of (6.10), and products of fluctuations are neglected. We are also assuming that, to first order, turbulent fluctuations of temperature, humidity and pressure do not affect the value of β_μ. Coantic and Simonin (1984) have shown that the water vapor density fluctuations ρ'_v play a relatively unimportant part in $\partial R'_k/\partial x_k$; therefore, considering the effects of temperature fluctuations only, and using

$$B'_\mu \approx \frac{dB_\mu}{dT}\theta' \tag{6.11}$$

we finally get

$$\frac{\partial R'_k}{\partial x_k} \approx \int_{\mu=0}^{\infty}\int_{\omega=0}^{4\pi} -\beta_\mu \overline{\rho}_v (I'_\mu - \frac{dB_\mu}{dT}\theta') \, d\omega \, d\mu \; . \tag{6.12}$$

6.4 Spectral budgets and the effect of radiation

In Chapter 2, the spectral budgets for homogeneous turbulence and steady state were obtained. Here, as opposed to previous chapters, we do not include the water vapor spectral behavior directly. Instead, we make the (reasonable) assumption that buoancy effects are due to temperature fluctuations alone. In fact, since the only difference between the humidity and the temperature variance budget equations is in the radiative terms appearing in the latter, it will be possible to assess those differences by comparing the results obtained with the case where radiation is absent, which is assumed to be representative of humidity.

We will use the budgets (2.56) for twice the turbulence kinetic energy spectrum E_e and for the temperature spectrum $E_{\theta,\theta}$ (Lumley and Panofsky, 1964; Hinze, 1975; Coantic and Simonin, 1984; Claussen, 1985a):

$$2\frac{\partial \overline{u}}{\partial z}E_{w,u} - \frac{\partial \overline{u}}{\partial z}U_e + T_e - \frac{2g}{\overline{\theta}}E_{w,\theta} + 2\nu_u k^2 E_e = 0 \qquad (6.13\text{-a})$$

$$2\frac{\partial \overline{\theta}}{\partial z}E_{w,\theta} - \frac{\partial \overline{u}}{\partial z}U_{\theta,\theta} + T_{\theta,\theta} + 2\nu_\theta k^2 E_{\theta,\theta} + 2N(k)E_{\theta,\theta} = 0 \qquad (6.13\text{-b})$$

where

$$\begin{aligned} N(k) &= \frac{1}{\overline{\rho} c_p}\mathcal{F}\left\{\frac{\partial R'_k}{\partial x_k}\right\}\frac{1}{\widehat{\theta}} \\ &= \frac{4\pi}{\overline{\rho} c_p}\int_{\mu=0}^{\infty} \overline{\rho}_v \beta_\mu \frac{dB_\mu}{dT}\left[1 - \frac{\beta_\mu \overline{\rho}_v}{k}\arctan\frac{k}{\beta_\mu \overline{\rho}_v}\right] d\mu \\ &\approx \frac{4\pi}{\overline{\rho} c_p}\sum_{j=1}^{N_B}\frac{dB_{\mu_j}}{dT}\Delta\mu_j \left[\overline{T}'_\mu(0) + \int_0^\infty \frac{\overline{T}''(r)}{k}\frac{\sin kr}{r}\, dr\right] \end{aligned} \qquad (6.14)$$

is the spectral radiative dissipation function derived in Appendix B, and N_B is the number of water vapor bands.

In order to study the joint effects of stability *and* radiation on the temperature spectrum, equations (6.13-a) and (6.13-b) must be solved together. We will adopt a Claussen (1985a)-like type of closure for the fluctuating rate-of-strain transfer terms T_e and $T_{\theta,\theta}$ and the cospectra $E_{w,u}$ and $E_{w,\theta}$. This will allow E_e and $E_{\theta,\theta}$ to be calculated directly as a function of both radiation and stability parameters. This approach is different from Coantic and Simonin's (1984), who solved for $E_{\theta,\theta}$ assuming an initial spectral shape based on Kaimal's (1973) spectral curves, and a *neutral* temperature gradient, and did not utilize the equation for E_e. The adopted closure for (6.13) is

$$T_e = \frac{1}{\alpha_e}\frac{d}{dk}\left[\epsilon_e^{1/3}k^{2/3}E_e\right] \tag{6.15-a}$$

$$T_{\theta,\theta} = \frac{1}{\alpha_{\theta\theta}}\frac{d}{dk}\left[\epsilon_e^{1/3}k^{2/3}E_{\theta,\theta}\right] \tag{6.15-b}$$

$$2E_{w,u} = -\frac{\partial \overline{u}}{\partial z}c_I\epsilon_e^{-1/3}k^{-2/3}E_e \tag{6.15-c}$$

$$2E_{w,\theta} = -\frac{\partial \overline{\theta}}{\partial z}c_{II}\epsilon_e^{-1/3}k^{-2/3}E_e \tag{6.15-d}$$

$$U_e = U_{\theta,\theta} = 0\ , \tag{6.15-e}$$

together with the integral constraints for the rates of dissipation of turbulence kinetic energy ϵ_e and temperature variance $\epsilon_{T\theta}$

$$\epsilon_e = \int_0^\infty \nu_u k^2 E_e\, dk \tag{6.16-a}$$

$$\epsilon_{T\theta} = \epsilon_{\theta\theta} + \epsilon R\theta = \int_0^\infty \nu_u k^2 E_{\theta,\theta}\, dk + \int_0^\infty N(k)E_{\theta,\theta}\, dk \tag{6.16-b}$$

where $\epsilon_{T\theta}$ indicates total (molecular (ν) plus radiative) dissipation. Even though the end result is equivalent, notice that the closure represented by the above equations is somewhat different from Claussen's, in that it is being explicitly assumed here that the mean rate-of-strain transfer terms U_e and $U_{\theta,\theta}$ are zero, whereas Claussen "lumps" them with $E_{w,u}$ and $E_{w,\theta}$. In this case, the closures (6.15-c) and (6.15-d) for the cospectra have the same *form* as that proposed by Wyngaard and Coté (1972) for one-dimensional cospectra in the inertial subrange, which makes the set of equations (6.15) physically consistent. Indeed, Hinze (1975 p. 341) shows that U_e is small at high wavenumbers compared to the other terms, whereas Coantic and Simonin (1984) assumed the same for $U_{\theta,\theta}$, neglecting it. Also notice that this term is identically zero in the case of isotropic turbulence. Although atmospheric turbulence is not isotropic (given the existence of vertical fluxes) it is often necessary to assume the validity of isotropic relations between one- and three-dimensional spectra when comparisons with one-dimensional measured spectra are made.

Equations (6.15) represent one of the simplest ways to close the spectral budgets, known as a Corrsin-Pao closure (Corrsin, 1964; Pao, 1965) They are an example of a "local" closure in which the spectral transfer terms are modeled as derivatives of a spectral flux (Hinze, 1975 p. 249). Although more sophisticated schemes have been available for a long time (e.g. the Eddy-Damped Quasi-Normal Markovian (EDQNM) approximation and the Test Field Model (TFM) compared by Herring *et al.* (1982)), their use in atmospheric modelling has been rare. One reason is that in the surface layer the scales of turbulent motion (the eddy sizes) are limited by the distance to the surface, which is often only a few meters when micrometerological towers are utilized for measurements, and then local closures perform satisfactorily, as for that matter does MOS Theory. Thus, Claussen (1985a) was able to reproduce qualitatively the main features of spectral dependence on stability (the well-known shift towards higher wavenumbers with increasing stability) using a closure effectively equivalent to (6.15); Claussen (1985b) used the same model to estimate the MOS ϕ_F functions and Moraes and Goedert (1988), using the same approach plus the isotropic relations between one- and three-dimensional spectra were able to obtain a fair reproduction of Kaimal's (1973) curves. Coantic and Simonin (1984) also obtained essentially equivalent results when comparing a closure very similar to (6.15-b), due to Hill (1978), and an EDQNM modeling, for isotropic turbulence. Equation (6.15) may yield a somewhat simplified shape of the scalar spectrum since it is unable to reproduce a "bump" that has been observed experimentally at high wavenumbers in the end of the inertial subrange (Champagne *et al.*, 1977), with a tendency towards a viscous-convective subrange, and which has been the object of Hill's (1978) attention. Yet Claussen's work has shown that the model's overall performance in the context of near-surface atmospheric flows is quite reasonable, and we retain it here for its analytical simplicity.

The next steps in solving for the temperature spectrum involve obtaining a convenient dimensionless formulation for the radiative spectral dissipation function, and rewriting the spectral budgets in dimensionless form as well. In the next two sections, these issues are tackled.

6.5 An analytical approximation for the spectral radiative dissipation function

Calculation of the function $N(k)$ in (6.14) involves the evaluation of N_B improper integrals numerically for *each* k, so that a considerable numerical effort is involved. It is highly desirable to obtain an analytical approximation to the function $N(k)$ depending on just a few parameters instead of the $3N_B$ constants a_j, b_j and $\Delta\mu_j$ present in (6.14), so that the solution of (6.13) may also be analytical.

The main features of $N(k)$ were established by Goody (1964 figure 9.3 p. 351). In the region where the continuum absorption is dominant (very small k), $N(k) \sim k^2$; this behavior will not be sought, given the small importance of continuum absorption in the scales of interest for turbulence. In the *strong-line* region, which is valid over a wide range of k – including the smallest scales of interest in turbulence – $N(k) \sim k$; finally, in the *weak-line* region, $N(k) \uparrow N_\infty$ as $k \uparrow \infty$, with

$$N_\infty = \frac{4\pi}{\overline{\rho} c_p} \int_{\mu=0}^{\infty} \frac{dB_\mu}{dT} \overline{\rho}_v \beta_\mu \, d\mu \, . \tag{6.17}$$

This can also be written as

$$N_\infty = \frac{4\pi}{\overline{\rho} c_p} \frac{4\sigma\overline{\theta}^3}{\pi} \overline{\rho}_v \beta_P \tag{6.18}$$

where

$$\beta_P \equiv \frac{\int_{\mu=0}^{\infty} \frac{dB_\mu}{dT} \beta_\mu \, d\mu}{\int_{\mu=0}^{\infty} \frac{dB_\mu}{dT} \, d\mu} = \frac{\int_{\mu=0}^{\infty} \frac{dB_\mu}{dT} \beta_\mu \, d\mu}{4\sigma\overline{\theta}^3/\pi} \tag{6.19}$$

is Planck's coefficient and $\sigma = 5.67 \times 10^{-8} \mathrm{W\,m^{-2}\,K^{-4}}$ is the Stefan-Boltzmann constant. Planck's coefficient can be calculated much more easily than $N(k)$ itself. Since the derivative dB_μ/dT is approximately constant over each absorption band $\Delta\mu_j$ (see Appendix B), it is possible to write

$$\beta_P \approx \frac{\sum_{j=1}^{N_B} \frac{dB_{\mu_j}}{dT} \int_{\Delta\mu_j} \beta_\mu \, d\mu}{4\sigma\overline{\theta}^3/\pi} \tag{6.20}$$

and the integral above turns out to be obtainable in terms of average transmissions. In fact, equating (6.6) and (6.7) and considering a Taylor expansion on

$x = \overline{\rho}_v r$ of both sides up to the first term only, one gets

$$\frac{1}{\Delta\mu_j}\int_{\Delta\mu_j}\left(1-\overline{\rho}_v\beta_\mu r\right)\,d\mu = 1-\frac{a_j}{\Delta_{\mu_j}}\overline{\rho}_v r$$

so that

$$\int_{\Delta\mu_j}\beta_\mu\,d\mu = a_j\ , \tag{6.21}$$

whence

$$\beta_P \approx \frac{\sum_{j=1}^{N_B}\frac{dB_{\mu_j}}{dT}a_j}{4\sigma\overline{\theta}^3/\pi}\ . \tag{6.22}$$

Thus, Planck's coefficient becomes just a weighted sum of the $a_j's$ in Houghton's (1986) tables. As defined here (independently of the absorbing gas density $\overline{\rho}_v$), it is a very mild function of temperature only. Typical values for different temperatures in the range of those expected in the Earth's atmosphere, calculated with (6.22), are shown in Table 6.1 .

We seek an approximation for $N(k)$ such that $N(k)\sim k$ as $k\downarrow 0$ and $N(k)\uparrow N_\infty$ as $k\uparrow\infty$, in dimensionless form. Let

$$\frac{N(k)}{N_\infty} = F\left(\frac{k}{\beta_P\overline{\rho}_v}\right) = F\left(\frac{\kappa z k}{\kappa z\beta_P\overline{\rho}_v}\right) = F\left(\frac{\eta}{\eta_P}\right) \tag{6.23}$$

(Schertzer and Simonin, 1981), where $\eta = \kappa z k$ is a dimensionless wavenumber that will appear naturally in the spectral budget equations in dimensionless form, $\kappa = 0.4$ is von Karman's constant, z is height above ground and $\eta_P = \kappa z\beta_P\overline{\rho}_v$ is a dimensionless Planck (wave) number which effectively defines the order of magnitude of scales at which radiative dissipative effects begin to be important.

Table 6.1 – Plancks' coefficient as a function of temperature

$T\,/\,\mathrm{K}$	$\beta_P\,/\,\mathrm{kg^{-1}\,m^2}$
270.0	4.3141×10^1
275.0	4.2564×10^1
280.0	4.2038×10^1
285.0	4.1558×10^1
290.0	4.1118×10^1
295.0	4.0715×10^1
300.0	4.0344×10^1
305.0	4.0000×10^1
310.0	3.9682×10^1

A good approximation to $N(k)$ with the correct behavior in the strong- and weak-line regions is

$$F(x) = \frac{x + x^{5/4}}{[1 + x^{5/12}]^3} \tag{6.24-a}$$

$$x = \frac{\eta}{20\eta_P}\ . \tag{6.24-b}$$

Figure 6.1 shows the function $N(k)$ computed at $\overline{\theta} = 290\,\mathrm{K}$ and $\overline{\rho}_v = 1.43 \times 10^{-2}$, $\overline{\rho}_v = 0.71 \times 10^{-2}$, $\overline{\rho}_v = 1.43 \times 10^{-3}\ \mathrm{kg\,m^{-3}}$ by means of (6.14) with numerical integration and use of Houghton's tables, and by the approximations (6.23) and (6.24), in a log-linear plot. Figure 6.2 is the same in a log-log plot, so that both

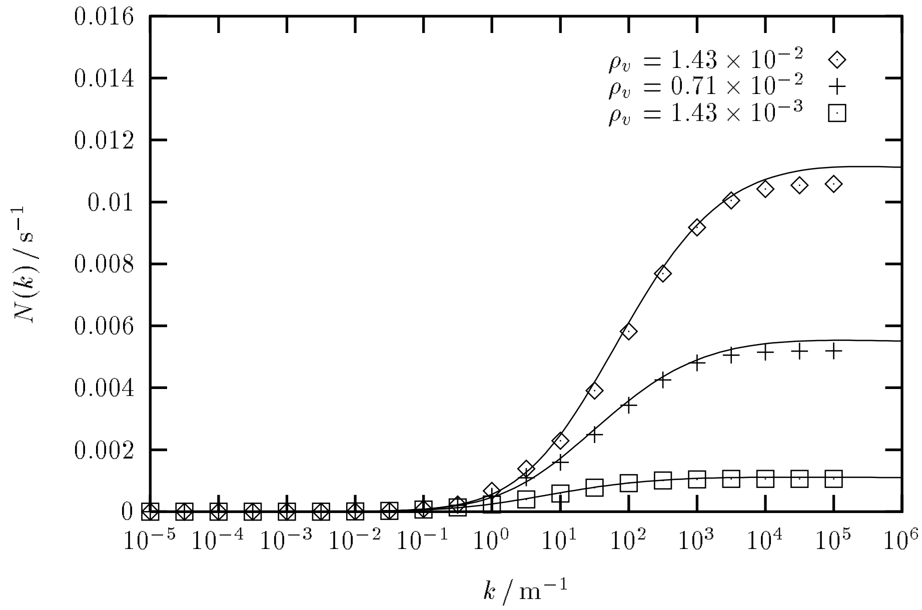

Figure 6.1 – $N(k)$ computed with equations (6.14) for $\overline{\theta} = 290\,\mathrm{K}$ and $\overline{\rho}_v = 1.43 \times 10^{-2}$ (diamonds), $\overline{\rho}_v = 0.71 \times 10^{-2}$ (crosses) and $\overline{\rho}_v = 1.43 \times 10^{-3}$ (squares) kgm^{-3} and by equation (6.24) (continuous lines)

the overall asymptotic behavior and the goodness of fit of the approximation can be observed.

6.6 Dimensionless spectral budget equations

The turbulent spectral budgets (6.13) can be made dimensionless in a straightforward manner by properly multiplying and dividing by turbulent scales. For (6.13-a), we multiply by $\kappa z k$ and divide by u_*^3; for (6.13-b), we multiply by

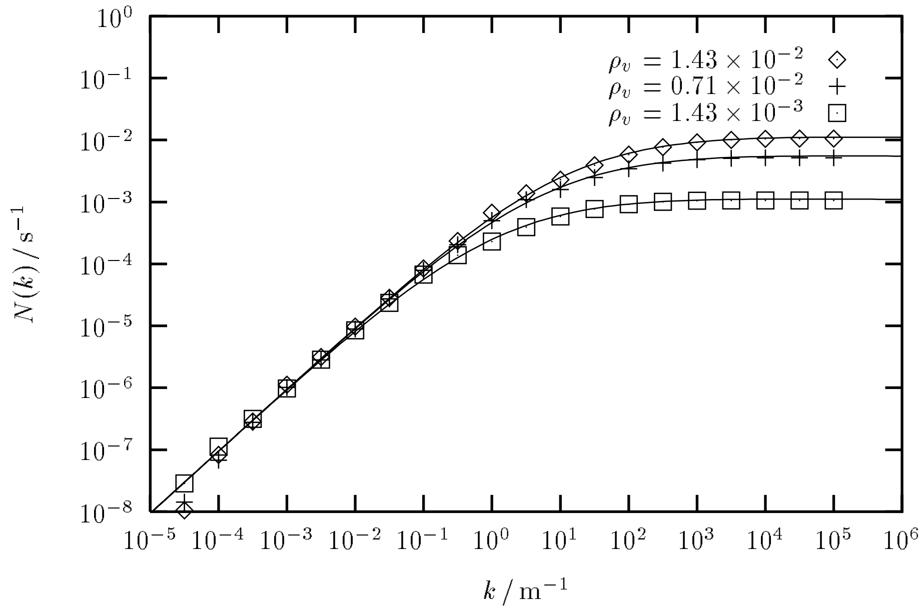

Figure 6.2 – Same as figure 6.24, with a log-log scale

$\kappa z k$ and divide by $u_* \theta_*^2$. The result is then

$$2\frac{\kappa z}{u_*}\frac{\partial \overline{u}}{\partial z}\frac{kE_{w,u}}{u_*^2} + \frac{\kappa z k T_e}{u_*^3} - 2\frac{\kappa g z \theta_*}{\overline{\theta} u_*^2}\frac{kE_{w,\theta}}{u_* \theta_*} + 2\frac{\nu_u}{\kappa z u_*}(\kappa z k)^2 \frac{kE_e}{u_*^2} = 0 \tag{6.25-a}$$

$$2\frac{\kappa z}{\theta_*}\frac{\partial \overline{\theta}}{\partial z}\frac{kE_{w,\theta}}{u_*\theta_*} + \frac{\kappa z k T_{\theta,\theta}}{u_*\theta_*^2} + 2\frac{\nu_\theta}{\kappa z u_*}(\kappa z k)^2 \frac{kE_{\theta,\theta}}{\theta_*^2} + 2\frac{\kappa z N(k)}{u_*}\frac{kE_{\theta,\theta}}{\theta_*^2} = 0 \tag{6.25-b}$$

or

$$-2\phi_\tau \psi_{w,u} + \tau_e + 2\zeta\psi_{w,\theta} + \frac{2}{\mathrm{Re}_*}\eta^2\psi_e = 0 \tag{6.26-a}$$

$$-2\phi_H \psi_{w,\theta} + \tau_{\theta,\theta} + \frac{2}{\mathrm{Pe}_*^\theta}\eta^2\psi_{\theta,\theta} + N_*\eta_P F(\eta/\eta_P)\psi_{\theta,\theta} = 0 \tag{6.26-b}$$

where Re_* and Pe_*^θ are turbulent Reynolds and Péclet numbers; ϕ_τ and ϕ_H are the dimensionless velocity and temperature gradients; ψ_e and $\psi_{\theta,\theta}$ are dimensionless energy and temperature spectra; $\psi_{w,u}$ and $\psi_{w,\theta}$ are dimensionless cospectra, τ_e and $\tau_{\theta,\theta}$ are dimensionless transfer terms due to fluctuating rates of strain, N_* and η_P are dimensionless radiative parameters. These parameters, most of which were already introduced in Chapter 2, are listed in equation (6.27) below, with their definitions on the left indicated by an identity sign ($\equiv$) and the non-dimensional closures appearing on the right indicated by an equal sign, when appropriate.

$$\frac{\kappa z u_*}{\nu_u} \equiv \mathrm{Re}_* \tag{6.27-a}$$

$$\frac{\kappa z u_*}{\nu_t} \equiv \mathrm{Pe}_*^{\theta} \tag{6.27-b}$$

$$\frac{\kappa z}{u_*}\frac{\partial \overline{u}}{\partial z} \equiv \phi_\tau \tag{6.27-c}$$

$$\frac{\kappa z}{\theta_*}\frac{\partial \overline{\theta}}{\partial z} \equiv \phi_H \tag{6.27-d}$$

$$\frac{kE_e}{u_*^2} \equiv \psi_e \tag{6.27-e}$$

$$\frac{kE_{\theta,\theta}}{\theta_*^2} \equiv \psi_{\theta,\theta} \tag{6.27-f}$$

$$-\frac{kE_{w,u}}{u_*^2} \equiv \psi_{w,u} = \frac{1}{2}\phi_\tau c_I \phi_{\epsilon_e}^{-1/3}\eta^{-2/3}\psi_e \tag{6.27-g}$$

$$-\frac{kE_{\theta,u}}{u_*\theta_*} \equiv \psi_{w,\theta} = \frac{1}{2}\phi_H c_{II} \phi_{\epsilon_e}^{-1/3}\eta^{-2/3}\psi_e \tag{6.27-h}$$

$$\frac{\kappa z k T_e}{u_*^3} \equiv \tau_e = \frac{\eta}{\alpha_e}\frac{d}{d\eta}\left[\phi_{\epsilon_e}^{1/3}\eta^{2/3}\psi_e\right] \tag{6.27-i}$$

$$\frac{\kappa z k T_{\theta,\theta}}{u_*\theta_*^2} \equiv \tau_{\theta,\theta} = \frac{\eta}{\alpha_e}\frac{d}{d\eta}\left[\phi_{\epsilon_e}^{1/3}\eta^{2/3}\psi_{\theta,\theta}\right] \tag{6.27-j}$$

$$N_* \equiv \frac{4\pi}{\overline{\rho}c_p}\frac{4\sigma\overline{\theta}^3}{\pi u_*} \tag{6.27-k}$$

$$\eta_P \equiv \kappa z \beta_P \overline{\rho}_v \ . \tag{6.27-l}$$

From the point of view of the influence of radiation on the temperature spectrum, notice the appearance of the dimensionless parameters η_P and N_*. A quantity equivalent to η_P appears in Coantic and Simonin (1984) whose solutions, however, are not presented in dimensionless terms, whereas a dimensionless parameter related to N_* and η_P was introduced by Schertzer and Simonin (1981) in the context of the inertial transfer of turbulence kinetic energy, which they called ζ_R. The relationship is

$$\zeta_R = \left[0.04 N_\infty (\beta_P \overline{\rho}_v)^{-2/3} \epsilon_e^{-1/3}\right]^{-1} = \left[0.04 N_* \eta_P^{1/3} \phi_{\epsilon_e}^{-1/3}\right]^{-1} \tag{6.28}$$

where the first equality is Schertzer and Simonin's definition, and the second translates it to the dimensionless parameters used in this work. Schertzer and Simonin observed the appearance of an inertial-radiative subrange with a slope steeper than -3, when $\zeta_R < 1.0$, which is equivalent, for neutral conditions and typical humidities in the atmosphere ($\phi_{\epsilon_e} = 1$; $\eta_P = 0.5$), to $N_* > 4.4$, approximately. We shall see that this is an extraordinarily high value of N_* for the conditions prevailing in the Earth's atmosphere, so that one is unlikely to observe such a behavior in terrestrial temperature spectra. This is important because the solution of (6.26) will *assume* the existence of a classical inertial subrange with a slope of $-5/3$, as will be shown presently. It should also be pointed out that the parameters η_P and N_* are a more natural choice than ζ_R to represent the effects of radiation; whereas η_P indicates the relative scales of turbulence at which radiative effects begin to be important in the spectrum (see equation (6.24)), N_* physically represents a ratio of convective to radiative flux changes with temperature. This is easily seen by assuming a hypothetical surface with temperature $\overline{\theta}$ which is exchanging heat convectively at the rate

$$H = \overline{\rho} c_p C_H u_* (\overline{\theta} - \overline{\theta}_a) \tag{6.29}$$

where C_H is a heat transfer coefficient and $\overline{\theta}_a$ the air temperature far from the surface, and radiatively at

$$R = \sigma \overline{\theta}^4 \tag{6.30}$$

The ratio of the unit changes of H and R with $\overline{\theta}$ will then be

$$\frac{\partial R / \partial \overline{\theta}}{\partial H / \partial \overline{\theta}} = \frac{4\sigma \overline{\theta}^3}{\overline{\rho} c_p C_H u_*} \tag{6.31}$$

which is equal to N_* times a numerical constant. On the other hand, the combination $N_* \eta_P^{1/3} \phi_{\epsilon_e}^{-1/3}$ *will* appear naturally in the solution for the temperature spectrum (see equation (6.44) below), so that it can be regarded as a single parameter controlling the shape of the spectrum.

The solution of (6.26) must obey the integral constraints that production by mean gradients and buoancy is equal to dissipation by molecular and radiative effects:

$$\int_0^\infty \left(\phi_\tau \psi_{w,u} - \zeta \psi_{w,\theta}\right) \frac{d\eta}{\eta} = \int_0^\infty \frac{\psi_e}{\mathrm{Re}_*} \eta \, d\eta = \phi_{\epsilon_e} \tag{6.32-a}$$

$$\begin{aligned} \int_0^\infty \phi_H \psi_{w,\theta} \frac{d\eta}{\eta} &= \int_0^\infty \frac{\psi_{\theta,\theta}}{\mathrm{Pe}_*^\theta} \eta \, d\eta + \int_0^\infty N_* \eta_P F(\frac{\eta}{20\eta_P}) \psi_{\theta,\theta} \frac{d\eta}{\eta} \\ &= \phi_{\epsilon_{\theta\theta}} + \phi_{\epsilon_{R\theta}} = \phi_{\epsilon_{T\theta}} \end{aligned} \tag{6.32-b}$$

We first solve for the spectrum of twice the turbulence kinetic energy, assuming the solution to have the classical inertial subrange behavior times low- and high-wavenumber "perturbations" $f_e(\eta)$ and $g_u(\eta)$ (Claussen, 1985a),

$$\psi_e = 2\alpha_e \phi_{\epsilon_e}^{2/3} \eta^{-2/3} f_e(\eta) g_u(\eta) \tag{6.33}$$

such that

$$\lim_{\eta \downarrow 0} f_e(\eta) = 0 \tag{6.34-a}$$

$$\lim_{\eta \uparrow \infty} f_e(\eta) = 1 \tag{6.34-b}$$

$$\lim_{\eta \downarrow 0} g_u(\eta) = 1 \tag{6.34-c}$$

$$\lim_{\eta \uparrow \infty} g_u(\eta) = 0 \ , \tag{6.34-d}$$

i.e., f_e and g_u will represent the falling of the spectrum in the lower and higher wavenumbers, respectively. Using (6.33) and the closure equations in (6.27-g) and (6.27-i), we get

$$\left(-c_I \phi_\tau^2 + c_{II} \phi_H \zeta\right) \alpha_e \phi_{\epsilon_e}^{1/3} \eta^{-7/3} f_e g_u + \frac{d}{d\eta}\left[\phi_{\epsilon_e} f_e g_u\right] + \frac{2\eta^{1/3}}{\mathrm{Re}_*} \alpha_e \phi_{\epsilon_e}^{2/3} f_e g_u = 0 \ . \tag{6.35}$$

Let

$$\beta \equiv c_I \phi_\tau^2 - c_{II} \phi_H \zeta \tag{6.36}$$

then (6.35) becomes

$$\begin{gathered}
-\alpha_e \beta \phi_{\epsilon_e}^{-2/3} \eta^{-7/3} f_e g_u + f_e \frac{dg_u}{d\eta} + g_u \frac{df_e}{d\eta} + 2\alpha_e \mathrm{Re}_*^{-1} \phi_{\epsilon_e}^{-1/3} \eta^{1/3} f_e g_u = 0 \\
g_u(\eta) \left[\frac{df_e}{d\eta} - \alpha_e \beta \phi_{\epsilon_e}^{-2/3} \eta^{-7/3} f_e\right] + f_e(\eta) \left[\frac{dg_u}{d\eta} + 2\alpha_e \mathrm{Re}_*^{-1} \phi_{\epsilon_e}^{-1/3} \eta^{1/3} g_u\right] = 0
\end{gathered} \tag{6.37}$$

where the two brackets represent the asymptotic behavior of (6.37) respectively as $\eta \downarrow 0$ and $\eta \uparrow \infty$. Letting η approach each limit and using (6.34) we are then left with two independent differential equations for f_e and g_u, whose solutions are

$$f_e(\eta) = \exp\left[-\frac{3}{4} \beta \alpha_e \phi_{\epsilon_e}^{-2/3} \eta^{-4/3}\right] \tag{6.38-a}$$

$$g_u(\eta) = \exp\left[-\frac{3}{2} \alpha_e \mathrm{Re}_*^{-1} \phi_{\epsilon_e}^{-1/3} \eta^{4/3}\right] \ . \tag{6.38-b}$$

It is straighforward to check that (6.33) with (6.38) obey the constraint (6.32-a). For the temperature spectrum, we again assume the form of the solution to be

$$\psi_{\theta,\theta} = 2\alpha_{\theta\theta}\phi_{\epsilon_e}^{-1/3}\phi_{\epsilon_{T\theta}}\eta^{-2/3}f_e(\eta)g_\theta(\eta)\ , \tag{6.39}$$

which has the classical inertial subrange behavior for a scalar plus a "low-wavenumber" component f_e and a "high-wavenumber" component g_θ. Notice the asymptotic behavior of g_θ, which is the same as that of g_u:

$$\lim_{\eta\downarrow 0} g_\theta(\eta) = 1 \tag{6.40-a}$$

$$\lim_{\eta\uparrow\infty} g_\theta(\eta) = 0\ . \tag{6.40-b}$$

Notice also that we are assuming the same f_e for both ψ_e and $\psi_{\theta,\theta}$, so that the production term in (6.26-b) which is modeled to depend on ψ_e in (6.27-h), has a common factor with the others. Using (6.39), (6.26-b) and (6.27-h) and (6.27-j), we obtain

$$\begin{aligned}&-(\alpha_e c_{II})\phi_H^2\phi_{\epsilon_e}^{1/3}\phi_{\epsilon_{T\theta}}^{-1}\eta^{-7/3}f_e g_u + \frac{df_e}{d\eta}g_\theta + f_e\frac{dg_\theta}{d\eta}\\ &+2\alpha_{\theta\theta}\phi_{\epsilon_e}^{-1/3}\mathrm{Pe}_*^{\theta-1}\eta^{1/3}f_e g_\theta + 2\alpha_{\theta\theta}\phi_{\epsilon_e}^{-1/3}N_*\eta_P\eta^{-5/3}F\left(\frac{\eta}{20\eta_P}\right)f_e g_\theta = 0\end{aligned} \tag{6.41}$$

From (6.38),

$$\frac{df_e}{d\eta} = \alpha_e\beta\phi_{\epsilon_e}^{-2/3}\eta^{-7/3}f_e \tag{6.42}$$

so that the equation for the temperature spectrum becomes

$$\begin{aligned}&\left[\alpha_e\beta\phi_{\epsilon_e}^{-2/3}g_u - \alpha_e c_{II}\phi_H^2\phi_{\epsilon_e}^{1/3}\phi_{\epsilon_{T\theta}}^{-1}g_\theta\right]\eta^{-7/3}+\\ &\frac{dg_\theta}{d\eta} + 2\left[\alpha_{\theta\theta}\phi_{\epsilon_e}^{-1/3}\left(\mathrm{Pe}_*^{\theta-1}\eta^{1/3} + N_*\eta_P\eta^{-5/3}F\left(\frac{\eta}{20\eta_P}\right)\right)\right]g_\theta = 0\end{aligned} \tag{6.43}$$

For small values of η, $g_\theta \approx g_u \approx 0$, whereas for large η, $\eta^{-7/3} \approx 0$. We shall also show that, except for the fact that g_u is slightly different from g_θ, the term in brackets in the first line of (6.43) above is essentially zero, given the relationship (to be established presently) between β, ϕ_{ϵ_e}, ϕ_τ, ϕ_H and $\phi_{\epsilon_{T\theta}}$. Thus, (6.43) simplifies to

$$\frac{dg_\theta}{d\eta} + 2\left[\alpha_{\theta\theta}\phi_{\epsilon_e}^{-1/3}\left(\mathrm{Pe}_*^{\theta-1}\eta^{1/3} + N_*\eta_P\eta^{-5/3}F\left(\frac{\eta}{20\eta_P}\right)\right)\right]g_\theta = 0 \qquad (6.44)$$

whose solution subject to (6.40) is

$$g_\theta = \exp\left[-\alpha_{\theta\theta}\phi_{\epsilon_e}^{-1/3}\left(\frac{3}{2}\mathrm{Pe}_*^{\theta-1}\eta^{-4/3} + 2N_*\eta_P^{1/3}(20)^{-2/3}\int_0^{\eta/20\eta_P} u^{-5/3}F(u)\,du\right)\right] \qquad (6.45)$$

which now completes the solution for the energy and temperature spectra. Notice that the combination $N_*\eta_P^{1/3}\phi_{\epsilon_e}^{-1/3}$ appears naturally in (6.45). The temperature spectrum in particular is given by (6.39) with f_e given by (6.38-a) and g_θ given by (6.45).

To obtain a solution in terms of stability ζ, Planck Number η_P and N_*, one must first discuss the dependence of ϕ_τ, ϕ_H, ϕ_{ϵ_e} and $\phi_{\epsilon_{T\theta}}$ on these parameters; moreover, it would be convenient from the computational point of view, to approximate the integral $\int_0^x u^{-5/3}F(u)\,du$ in closed form, in the same way that was done with $F(x)$ itself.

We shall assume, as did Coantic and Simonin (1984), that the terms responsible for the *production* of turbulence are not themselves a function of radiative parameters. Thus, $\phi_\tau = \phi_\tau(\zeta)$ and $\phi_H = \phi_H(\zeta)$ only. Then, notice that the dimensionless budgets of $\overline{e'}$ and $\overline{\theta'\theta'}$ for homogeneous turbulence read

$$\phi_\tau = \zeta + \phi_{\epsilon_e} \tag{6.46-a}$$

$$\phi_H = \phi_{\epsilon_{T\theta}} = \left(\phi_{\epsilon_{\theta\theta}} + \phi_{\epsilon_{R\theta}}\right) \ . \tag{6.46-b}$$

Under the approximation that production terms are a function of stability ζ only, the viscous dissipation of turbulence kinetic energy is also a function only of ζ, whereas the molecular dissipation of temperature variance $\phi_{\epsilon_{\theta\theta}}$ is supposed to adjust to the radiative dimensionless dissipation $\phi_{\epsilon_{R\theta}}$ in order to match $\phi_H(\zeta)$.

An important result obtained by Claussen (1985a) is the relation between ϕ_H and ϕ_τ that comes out of his model, and which is preserved when radiative terms are included. Here, it is obtained from the dimensionless equations themselves as follows. Using (6.27), the integral constraint (6.32) and (6.33) we can write

$$\int_0^\infty \phi_H \psi_{w,\theta} \frac{d\eta}{\eta} = \phi_{\epsilon_{T\theta}} \tag{6.47-a}$$

$$\int_0^\infty \phi_H^2 \frac{c_{II}}{2} \phi_{\epsilon_e}^{-1/3} \eta^{-2/3} 2\alpha_e {\phi\epsilon_e}^{2/3} \eta^{-2/3} f_e(\eta) g_u(\eta) \frac{d\eta}{\eta} = \phi_{\epsilon_{T\theta}} \tag{6.47-b}$$

$$\frac{\phi\epsilon_e c_{II} \phi_H^2}{\beta} \int_0^\infty \alpha_e \beta {\phi\epsilon_e}^{-2/3} \eta^{-7/3} f_e(\eta)\, d\eta = \phi_{\epsilon_{T\theta}} \tag{6.47-c}$$

where in (6.47-c) we are making the approximation that $g_u(\eta) \approx 1$ in the η-range close to 0 where the $-7/3$ exponent “concentrates” most of the integrand. The integral in (6.47-c) is 1, whence

$$\phi_{\epsilon_e} c_{II} \phi_H^2 = \beta \phi_{\epsilon_{T\theta}}$$

using (6.36) and (6.46):

$$\phi_{\epsilon_e} c_{II} \phi_H^2 = \left(c_I \phi_\tau^2 - c_{II}\phi_H \zeta\right)\phi_H$$

$$\left(\phi_\tau - \zeta\right) c_{II}\phi_H = c_I \phi_\tau^2 - c_{II}\phi_H\zeta$$

$$c_{II}\phi_H = c_I \phi_\tau \tag{6.48}$$

If there are differences between ϕ_τ and ϕ_H in stable conditions, they are certainly small (Högström, 1988), so we set (Brutsaert, 1982)

$$\phi_\tau = \phi_H = 1 + 5\zeta \tag{6.49}$$

In section 6.8, we will show how $c_I = c_{II}$ can be realistically estimated, by means of one-dimensional temperature spectra observed in the Stable Boundary Layer.

6.7 An analytical approximation for g_θ

Finally, to obtain an analytical expression for g_θ, one must evaluate the integral

$$H(x) \equiv \int_0^x u^{-5/3} F(u)\,du \equiv \int_0^x G(u)\,du = \int_0^x \frac{u^{-2/3} + u^{-5/12}}{\left(1+u^{5/12}\right)^3}\,du \tag{6.50}$$

We begin by noticing that (Gradshteyn and Ryzhik, 1980 p. 292)

$$\int_0^\infty \frac{x^{\mu-1}}{\left(1+x^\nu\right)^{n+1}}\,dx = \frac{1}{\nu}\frac{\Gamma\left(\frac{\mu}{\nu}\right)\Gamma\left(n+1-\frac{\mu}{\nu}\right)}{\Gamma(n+1)} \tag{6.51}$$

where $\Gamma(\cdot)$ is the gamma function and μ, ν and n above *do not* bear any physical meaning; then,

$$\begin{aligned} H_\infty &\equiv \int_0^\infty G(u)\,du \\ &= \frac{12}{5\Gamma(3)}\left[\Gamma\left(\frac{12}{15}\right)\Gamma\left(3-\frac{12}{15}\right) + \Gamma\left(\frac{7}{5}\right)\Gamma\left(3-\frac{7}{5}\right)\right] \\ &= 2.4906 \approx \frac{5}{2} \end{aligned} \tag{6.52}$$

We now look at the asymptotic behavior of $H(x)$. When $u \downarrow 0$, $G(u) \sim u^{-2/3}$, whence

$$x \downarrow 0 \qquad \Rightarrow \qquad H(x) \sim 3x^{1/3} \tag{6.53}$$

whereas, as $u \uparrow \infty$, $G(u) \sim u^{-5/3}$; then,

$$\begin{aligned} x \uparrow \infty \qquad \Rightarrow \qquad \int_0^x G(u)\,du &= \int_0^\infty G(u)\,du - \int_x^\infty G(u)\,du \\ &\approx H_\infty - \int_x^\infty u^{-5/3}\,du \\ &= H_\infty - \frac{3}{2}x^{-2/3} \\ &\approx H_\infty \left(1 - \frac{3}{5}x^{-2/3}\right) \end{aligned} \tag{6.54}$$

where in the last line, (6.52) was used. We will seek to approximate $H(x)$ in the form

$$H(x) \approx H_\infty \frac{\frac{6}{5}x^{1/3} + (cx)^m}{[1 + (cx)^n]^p} \tag{6.55}$$

such that $np = m$. Equation (6.55) has the correct asymptotic behavior as $x \downarrow 0$, given, again, the approximation (6.52-c). For $x \uparrow \infty$, m, n, p and c still need to be related in order to ensure the correct behavior predicted in (6.54). Then, we must have

$$x \uparrow \infty \Rightarrow \frac{(cx)^m}{[1 + (cx)^n]^p} \sim 1 - \frac{3}{5}x^{-2/3} \tag{6.56}$$

Let $t = x^{-2/3}$; we can then study the behavior of the function

$$t \downarrow 0 \Rightarrow \tilde{H}(t) \equiv \frac{c^m}{\left[c^n + t^{\frac{3n}{2}}\right]^p} \sim 1 - \frac{3}{5}t \tag{6.57}$$

where the tilde indicates the asymptotic approximation. Equation (6.57) above looks like a Taylor expression to the first term; the derivative of $\tilde{H}$ is

$$\tilde{H}'(t) = -\frac{c^m p \left[c^n + t^{\frac{3n}{2}}\right]^{p-1} \frac{3}{2} t^{\frac{3n}{2}-1}}{\left[c^n + t^{\frac{3n}{2}}\right]^{2p}} \tag{6.58}$$

In order to have $\tilde{H}'(0) \neq 0$ and $\tilde{H}'(0) \neq -\infty$, set

$$n = 2/3\ ; \tag{6.59-a}$$

then,

$$\tilde{H}'(0) = -\frac{p}{c^{2/3}} \quad \Rightarrow \quad c = \left(\frac{5p}{3}\right)^{3/2} \tag{6.59-b}$$

which, together with

$$np = m \tag{6.59-c}$$

reduces the number of degrees of freedom for parameter choice in (6.55) to one, i.e., there is only one free parameter to adjust this approximation to $H(x)$. It turns out that $m = 11/10$ is an excellent choice; figure 6.3 shows the comparison between the numerical integration of (6.50) with the approximation provided by (6.55) with the aforementioned value for m.

6.8 Model calibration and results

In order to calibrate $c_I = c_{II}$, we will assume the simplest case, that of a neutral atmosphere ($\zeta = 0$) with no radiative effects, ($N_* = 0$); then, Kaimal's semi-empirical curves for the dimensionless temperature spectrum can be written

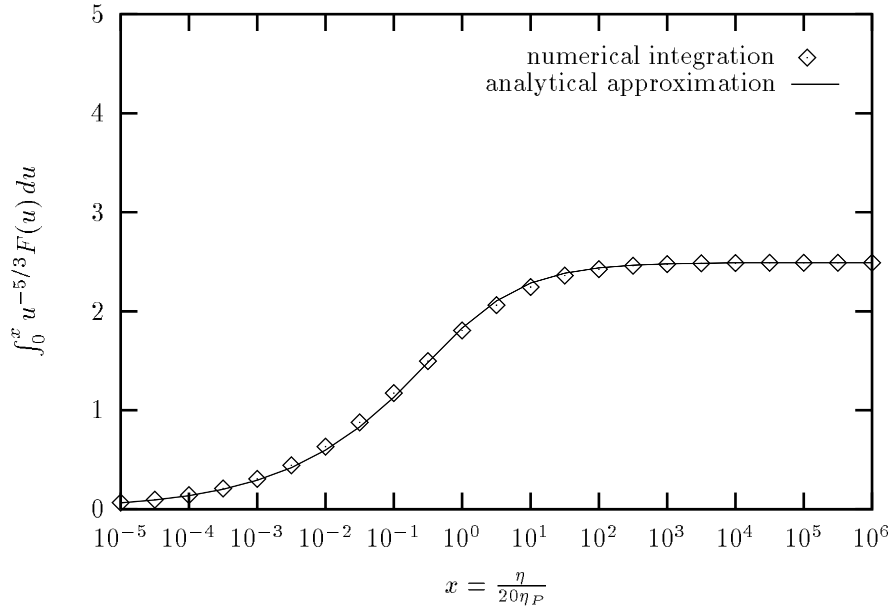

Figure 6.3 – Analytical approximation of $H(x)$ with equation (6.55) (continuous line) compared to numerical integration of equation (6.50-a) (diamonds)

in the form (Kaimal, 1973; Moraes and Epstein, 1987)

$$\psi^1_{\theta,\theta} = \frac{0.164f}{f_{0,\theta\theta}^{5/3} + 0.164 f^{5/3}} f_{0,\theta\theta}^{2/3} \phi_{\theta\theta} \tag{6.60}$$

with

$$f_{0,\theta\theta} = \left(\frac{\alpha^1_{\theta\theta}}{\phi_{\theta\theta}}\right)^{3/2} \frac{1}{2\pi\kappa} \phi_{\epsilon_e}^{-1/2} \phi_H^{3/2} \tag{6.61-a}$$

$$f = \frac{n_1 z}{\overline{u}} = \frac{k_1 z}{2\pi} \tag{6.61-b}$$

where $\alpha^1_{\theta\theta} = 0.80$ is the *one-dimensional* Corrsin-Kolmogorov constant for the temperature spectrum and Taylor's frozen turbulence hypothesis is used to convert from (again, one-dimensional) wavenumber k_1 to frequency n in (6.61-b).

The three-dimensional constant $\alpha_{\theta\theta}$ is related to $\alpha^1_{\theta\theta}$ in isotropic turbulence by (Hinze, 1975 p. 299)

$$\alpha_{\theta\theta} = \frac{5}{3}\alpha^1_{\theta\theta} \tag{6.62}$$

We will assume *a priori* that, under near-neutral conditions, the dimensionless function $\phi_{\theta\theta}$ is

$$\frac{\overline{\theta'\theta'}}{\theta_*^2} \equiv \phi_{\theta\theta} \approx 2.0 \ , \tag{6.63}$$

which is in agreement with table 4.13, and the values obtained in Chapter 4. Later on, an "actual" $\phi_{\theta\theta}$ will be computed from the model as a function both of stability and radiation. The temperature spectrum (6.39) is evaluated with a guessed value of c_I in (6.36) and (6.38-a) and then the one-dimensional dimensionless spectrum $\psi^1_{\theta,\theta}$ is calculated by means of the isotropic relationship (Hinze, 1975, section 3.7)

$$\psi^1_{\theta,\theta}(\eta_1) = \eta_1 \int_{\eta_1}^{\infty} \psi_{\theta,\theta}(\eta)\frac{d\eta}{\eta^2} \tag{6.64}$$

which is then compared to $\psi^1_{\theta,\theta}$ given by (6.60).

Figure 6.4 shows the results obtained for $c_I = c_{II} = 0.15$, with the three-dimensional spectrum $\psi_{\theta,\theta}(\eta)$ drawn with a continuous line, and the one-dimensional spectra $\psi^1_{\theta,\theta}$ drawn with dashed lines. The overall agreement is extremely good, except for the small differences in the behavior around the peak, and the fact that (6.60) does not predict a viscous subrange; in other words, the inertial subrange "goes on" forever . . .

It is desirable to study the behavior of the spectral model for realistic values of η_P and N_*. For temperatures and humidities normally found on the

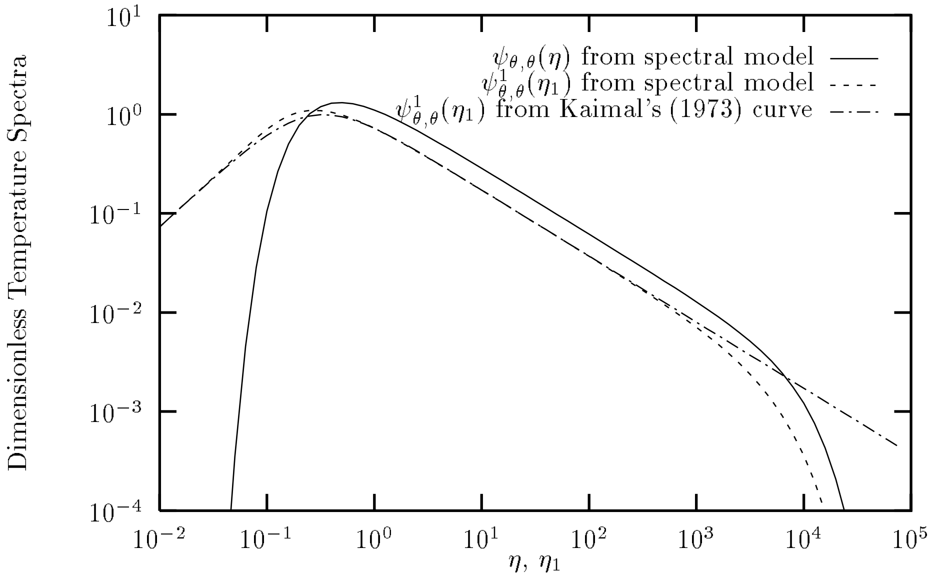

Figure 6.4 – One- and three-dimensional spectra from model compared to Kaimal's (1973) empirical curve

Earth's surface, η_P (equation (6.27-l)) will usually be in the range $0.0 - 1.0$, whereas N_* (equation (6.27-k)), for the same range of temperatures, will depend strongly on the value of the friction velocity u_*. Typical values of the latter during the nights of the FIFE-89 campaign are between 0.1 and 0.5 $\mathrm{m\,s^{-1}}$, which yields N_* values no bigger than 0.2 close to the surface (at a height of 2.5 m). The observed influence on the spectra of such values of N_* will be shown to be small, so that unless very low values of u_* prevail, radiative effects cannot be important. While it is still unclear how frequent this situation is during nighttime at the aforementioned heights, there are several reported cases of intermittent turbulence in a stable boundary Layer both in the atmosphere (Kondo *et al.*, 1978; Nappo, 1991; Mahrt, 1989) and in the laboratory (Warhaft and Bolgiano, 1984), which must be an indication of small friction velocities. On the other hand, we have been unable to detect intermittency in temperature records of the most stable short runs observed during FIFE-89. At any rate, stability increases with height, so that higher up (say at 10 m to 50 m above the ground) there may be regions where radiative effects become very important. Over the lowest few meters of the atmosphere, however, this situation seems unlikely if the FIFE records can be considered representative. We begin by analizing the effect of *both* stability and radiation on temperature spectra. This is done by assuming $\eta_P = 0.5$, which is fairly representative of late summer nights, $\mathrm{Pe}_*^\theta = 250{,}000$, and two stabilities, $\zeta = 0$ and $\zeta = 0.5$, which again cover most of the observed range during FIFE-89. For each of these two stabilities, we take $N_* = 0.0$, 0.1 and 1.0, where this last value can be considered already quite unlikely. Table 6.2 shows these six cases, and they are plotted in Figure 6.5. In order to analyze the behavior of the spectra in the inertial subrange and in the beginning of the viscous subrange, it is also convenient to plot "compensated spectra" (i.e.; spectra multiplied by $\eta^{2/3}$) (Coantic and Simonin, 1984), which is done in figure (6.5). Notice that there is no "bump" showing a tendency for a viscous-convective subrange, which is a shortcoming that might easily be circumvented by a spectral closure of the kind proposed by Hill (1978).

To summarize this part, the effect of radiation can only be felt when the dimensionless parameter N_* becomes of the order of 1, which is maybe too high a value to be expected close to the surface, where shear is always important, even

Table 6.2 - Values of dimensionless parameters used for calculating temperature spectra

η_P	N_*	Pe_*^θ	ζ
0.5	0.0	250,000	0.0
0.5	0.1	250,000	0.0
0.5	1.0	250,000	0.0
0.5	0.0	250,000	0.5
0.5	0.1	250,000	0.5
0.5	1.0	250,000	0.5

in very stable (i.e.; $\zeta = 0.5$) conditions. The interplay of stability and radiation seems to be quite weak: higher values of ζ simply shift the spectra to higher wavenumbers (as well as increasing their ordinates, see (6.39)), whereas higher values of N_* lower their ordinates.

We finish by obtaining the dimensionless function $\phi_{\theta\theta}$, as promised, by means of Claussen's spectral model, and including the effects of radiation in it. We will use it in the case $N_* = 0$ to represent any scalar in the stable surface layer; for non-null N_*'s, however, the results are valid for temperature only. By doing this, we actually will be evaluating to what extent there exists similarity between temperature and humidity in stable conditions. For as long as changes in $\phi_{\theta\theta}$ are small, this means that the radiative terms can be neglected in the

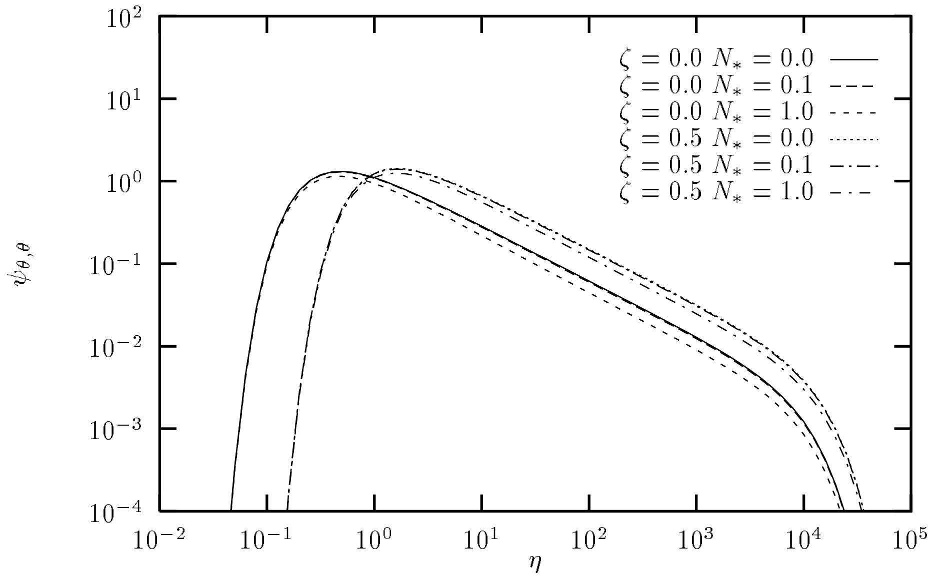

Figure 6.5 – Temperature spectra as a function of ζ and N_*, for $\eta_P = 0.5$, $\mathrm{Pe}_*^\theta = 250{,}000$.

budgets of temperature variance and temperature-humidity covariances, (2.15-e) and (2.15-g).

The relationship between $\phi_{\theta\theta}$ and $\psi_{\theta,\theta}$ is quite simple; since the integral of the spectrum is equal to the variance,

$$\phi_{\theta\theta}(\zeta, \eta_P, N_*) = \int_0^\infty \psi_{\theta,\theta} \frac{d\eta}{\eta} \tag{6.65}$$

where the integral now must be performed numerically; even though there is some variability with η_P, it is minor; this can be seen in equation (6.45), where η_P is raised to 1/3, and confirms in dimensionless form the fact that the absolute water vapor concentration plays a relatively minor role in radiative effects, first realized by Coantic and Simonin (1984). How sensitive the function $\phi_{\theta\theta}$ is to

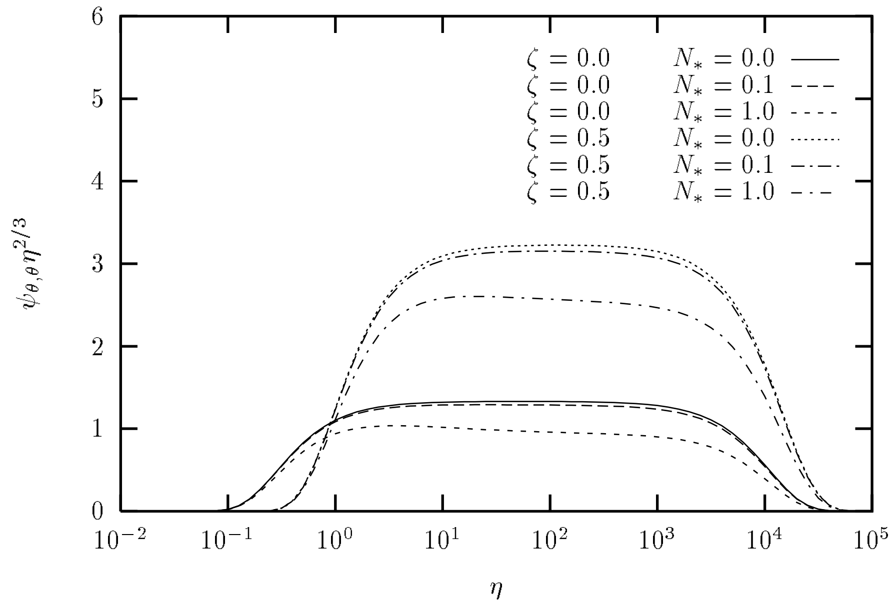

Figure 6.6 – "Compensated" (multiplied by $\eta^{2/3}$) Radiative Spectra as a function of ζ and N_*, for $\eta_P = 0.5$, $\mathrm{Pe}_*^\theta = 250{,}000$

η_P can be seen in Figures 6.7 through 6.10, for $\eta_P = 0.25, 0.50, 0.75$ and 1.00. In these figures, $\phi_{\theta\theta}$ is computed from (6.65) by means of numerical integration for a wide variety of N_*'s, as a function of stability ζ. It is quite interesting that it shows a mild increase with stability. Most researchers have chosen to assume this function to be a constant in stable conditions, but the increase shown in Figures 6.7–6.10 is so gentle that in practical situations it is certainly statistically indistinguishable from a horizontal straight line . . . At the same time it is seen, one more time, that radiative effects are quite inconsequential for $N_* \leq 0.1$; this in a sense explains why, in previous chapters, the results of virtually all statistical tests between temperature and humidity point to their being perfectly similar: radiative effects are just too small to play any important role. On the other hand, it must never be out of sight that the representativeness of field experiments in the atmosphere should be taken with caution until when enough of them under the same conditions have been performed. In the case of stable conditions, luckily for those who study them, this day is yet to come.

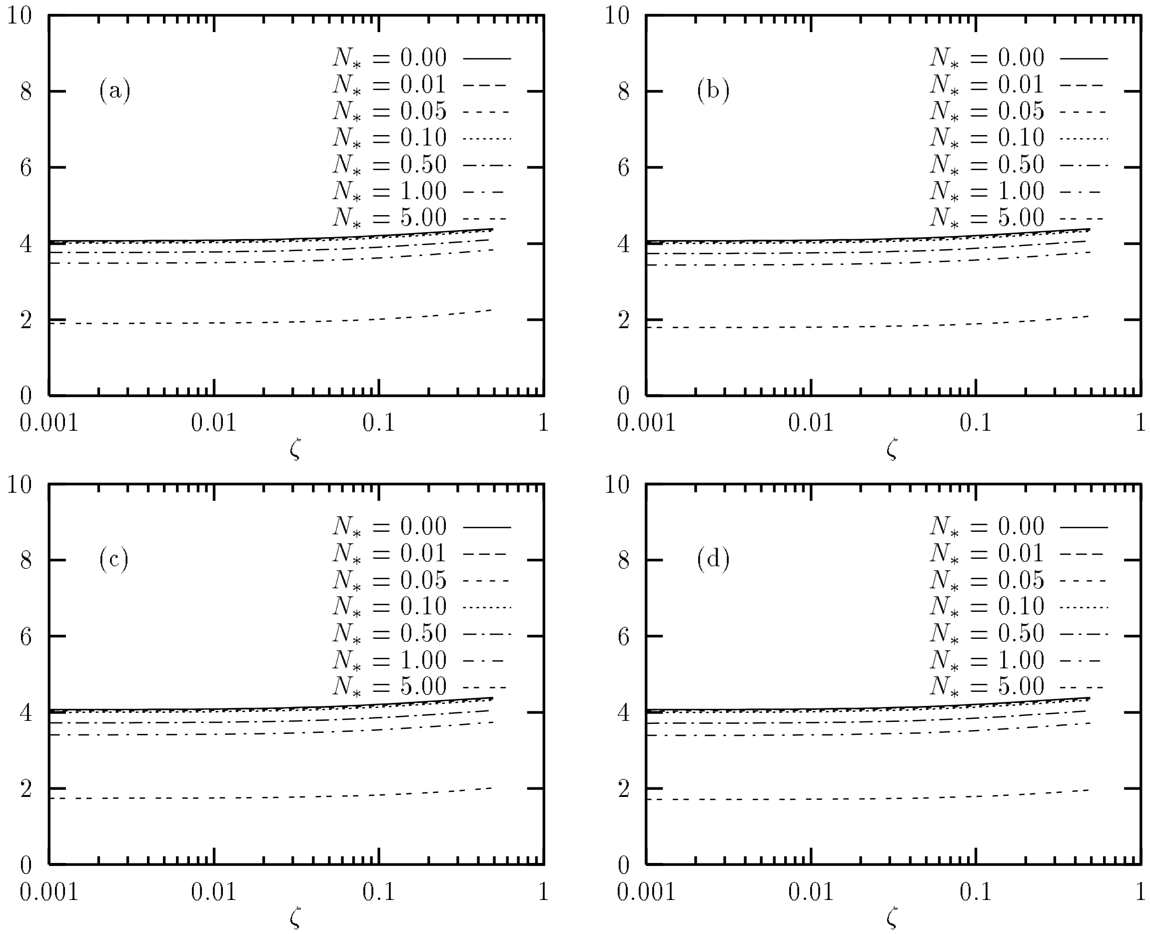

Figure 6.7 – The Dimensionless Function $\phi_{\theta\theta}$ computed for several values of the parameter N_*, for η_P = 0.25 (a), 0.50 (b) 0.75 (c) and 1.00 (d), with $\mathrm{Pe}_*^\theta = 250,000$

6.9 Closure

We have attempted to quantify the relative importance of radiative effects in the stable surface layer, which during nocturnal periods may be just a few meters thick (Stull, 1988). There, it is safe to assume that turbulent fluctuations are homogeneous and stationary. This hypothesis (homogeneity) renders the budgets of turbulence kinetic energy and temperature, and their spectral counterparts, particularly simple. Moreover, the small distance from the surface limits the scales of turbulent motion and facilitates the use of local closures.

With the help of one such simple spectral closure used by Claussen (1985a) in the same context, it is possible to incorporate the radiative effects extensively studied by Coantic and Simonin (1984). Adopting some analytical approximations for the radiative spectral dissipation terms and a related integral, the spectral model yields analytical expressions for the temperature spectra which are a function not only of stability ζ, but also of the dimensionless parameters η_P and N_*. In this way, it is possible to study both stability and radiative effects jointly. We have not only studied the spectral behavior under radiation, but also assessed how the similarity function $\phi_{\theta\theta}$ for the temperature variance is affected. We have used dimensionless functions and variables throughout, so that the relative importance of radiation is easily assessed.

It seems now apparent that a very simple criterion for radiative processes to be unimportant exists, namely that $N_* \leq 0.1$ approximately, where N_*, given by (6.27-k), is very easy to estimate. The results obtained here suggest that radiative effects may not be very important in the surface layer. On the other hand, u_* decreases with height in the Atmospheric Boundary Layer, and under stable conditions turbulence may even become intermittent, so that it is quite reasonable to expect a different situation at higher levels above the surface layer. It is not clear, however, if the same simple-minded approach adopted here would still be valid at these higher levels, where turbulence may not be homogeneous and where the local closures that we used are less likely to be valid.

Chapter 7

CONCLUSIONS AND RECOMMENDATIONS

Briefly, the main questions regarding the possible dissimilarities between temperature and humidity are recapitulated. Then, the main findings of chapters 2, 3, 4, 5 and 6 are reviewed as a whole. There are theoretical and experimental avenues to be pursued ahead; these are then commented upon in the section of recommendations.

7.1 A summary of questions

Once it is realized that molecular diffusivity plays such a small *direct* role in turbulent diffusion and transport, it is tempting to assume that turbulence transports "everything" in the same way, where "everything" includes momentum in a given direction, heat, mass of a certain scalar, derived quantities such as vorticity, etc.. This has been known for a long time as "Reynolds's Analogy" and was first applied to the eddy diffusivities of momentum and heat. In the surface layer of the atmosphere, it is now known that the analogy (as far as eddy diffusivities are concerned) does not hold under unstable conditions (Brutsaert, 1982 p. 68); they are, however, very much the same under neutral conditions(Högström, 1989). Thus, that kind of generalization is less and less acceptable *a priori*, as we try to deepen our understanding of turbulent transport processes.

The two most important scalar atmospheric fluxes are sensible heat H and latent heat LE. Humidity is considerably harder to measure than temperature, however, both in terms of means and of turbulent fluctuations. This is one reason why it has been usually assumed that what has been measured and found for temperature also holds for humidity. During the 70's and 80's, some disquieting signs of a more complicated picture surfaced both in theoretical analyses and in experiments (Warhaft, 1976; Verma *et al.*, 1978; Lang *et al.*, 1983a), particularly in connection with the energy-budget Bowen ratio method. Difficulties with it under stable conditions continue to be reported in the literature to this day as in Assouline and Mahrer's (1993) report on eddy-correlation and Bowen ratio measurements of evaporation on lake Kineret, Israel. It is important to establish where the differences found can be coming from. This thesis did not exhaust the study of possible causes; it concentrated on a subset of questions:

1 – Can the dissimilarities happen under the validity of MOS theory ?

2 – Can radiation significantly change the temperature transport and dissipation *vis-à-vis* humidity ?

7.2 A summary of results

In chapter 2, a full set of equations governing the turbulent flow in the surface layer was written down, both in the time-space domain, where they take the form of the equations for the means $\overline{u_i}$ and the budgets for the covariances $\overline{u_i'u_j'}$, and in the time-wavenumber domain, where they were called spectral budgets. The main simplifications which were assumed were those of stationarity of the turbulence, and of homogeneity in the horizontal; they are usually associated with the Monin-Obukhov Similarity (MOS) theory, which is the accepted standard for analysis of atmospheric flows. Moreover, it is assumed that no phase changes take place. This excludes the analysis of periods of fog formation. With the equations written down, it is possible to analyze the differences between those containing temperature and humidity terms. Formally, the only differences then are in the radiative terms which appear in the w, θ, θ, θ and θ, q equations, and the different molecular diffusivities for heat ν_θ and water vapor ν_q. Several important conclusions were drawn from the theoretical analysis of spectra and cospectra. There, the energy-containing and inertial ranges are not influenced by molecular effects (Tennekes and Lumley, 1972; Hinze, 1975): the prediction is then that, properly non-dimensionalized, the spectral and cospectral densities involving temperature should be equal to those involving humidity, which provides a strong theoretical basis for the spectral analysis of field data and its use to draw conclusions about the similarity of two scalars, such as done (heuristically) by Lang *et al.* (1983a) and Ohtaki (1985). Finally, higher-order cospectra (e.g., $S_{\theta,\theta\theta}$) were predicted to show a -2 slope in the inertial subrange.

Chapter 3 contains a review of theories and experiments regarding the similarity of temperature and humidity in the last 20 years. The theoretical approaches of Warhaft (1976), Brost (1978) and Hill (1989a) relied either on second-order closures, in the first two cases, or on dimensional analysis, in the last, and showed some contradictory points regarding the equality/inequality of eddy diffusivities and the value of the correlation coefficient between temperature and humidity. We then used the dimensionless budgets of temperature variance, humidity variance and temperature-humidity covariance to show that, in the case of homogeneous (in the vertical direction) turbulence, all the former analyses can be reconciled and collapse in the case of *nea*r-perfect similarity and (anti-) correlation between temperature and humidity, plus the equality of their eddy diffusivities. The theory actually predicts a slight dissimilarity (a correlation coefficient squared slightly less than 1, *even* if the eddy diffusivities/dimensionless gradients are equal) due to the different values of the molecular diffusivities, going a step beyond what can be achieved by dimensional analysis alone.

In Chapter 4, actual field turbulence data of temperature, humidity and vertical velocity are analyzed. This is done from the point of view of statistical analysis in the time domain. Some indication of dissimilar behavior during the night of Aug 03rd was found; the rest of the time, however, the dimensionless Monin-Obukhov functions ϕ for temperature and humidity were shown to be statistically indistinguishable. Moreover, it proved extremely fruitful to analyze the turbulent data in runs of 52 min., instead of the original 26 min.-runs as they were measured: this yielded much more stable 3-rd order moments, and disclosed their constancy with stability ζ, showing further experimental evidence of near-homogeneity in the vertical direction. An analysis of errors using the theoretical framework of Lumley and Panofsky (1964) and Wyngaard (1973), plus a rough approximation of vertical velocity and temperature (or humidity) as jointly normally distributed with a correlation coefficient of ± 0.3 yielded an averaging period of equivalent length.

Chapter 5 contains a gallery of spectral and cospectral densities of temperature and humidity plotted together: properly scaled with products of u_*, θ_* and q_*, they confirm the theoretical predictions that the (reduced) densities are equal. Coherence between temperature and humidity displays a large range of values extremely close to $+1$; it gently falls to zero after $n = 0.1$ Hz, but this is very likely due to the spatial separation of the sensors. Finally, the predicted -2 slope for higher-order scalar cospectra was confirmed with the use of the temperature and (to a lesser degree) humidity data.

Finally, in Chapter 6 we investigated the extent to which radiation can alter this picture of similarity: this was done with the help of a simple spectral model originally proposed by Claussen (1985a); the model was re-written in dimensionless form, and radiative effects were incorporated by fitting an empirical function to the spectral radiative dissipation function of Spiegel (1957), Goody (1964) and Coantic and Simonin (1984). This "dimensionless" approach leads to the identification of 2 (dimensionless) parameters which account for the effect of radiation on the temperature spectrum; sensitivity analysis then showed that, in the surface layer, radiation probably plays a minor role, which confirms, after-the-fact, the experimental results of the two former chapters. It was conjectured that it may become important higher up, above the surface layer, as $\overline{w'u'}$ diminishes with height (the controlling parameter, N_*, can always be easily calculated with the values of temperature and friction velocity to check how important radiation is). We also showed how the model is able to predict a function $\phi_{\theta,\theta}$ which agrees extremely well with the average observations.

The answers to the question in the end of last section are then, 1) No, except for extremely small effects due to different molecular diffusivities; and 2)No, except for very large (greater than 1) values of N_*.

7.3 Recommendations

On to the questions which were *not* addressed: in chapter 3, it was conjectured that advection may strongly affect the correlation coefficient between two scalars, as the data from Wesely and Hicks (1978) seem to suggest; yet, there are very few studies relating local advection to the (dis-)similarity of two scalars (an exception is Bertela, 1989). In particular, it may be possible (it was not tried!) to re-do the analysis of chapter 3 including advective terms, and try to assess how this inclusion changes the results. Because advection may be more serious under stable than unstable conditions, and because it is also extremely hard to quantify – so that it cannot be completely dismissed in most studies – it has become the author's favorite villain to blame observed dissimilarities on.

The spectral theories at our disposal are painfully inadequate to deal with cospectra with vertical velocity, because they are mostly about isotropic turbulence, where the fluxes in any direction are null. Yet the ultimate importance of boundary-layer atmospheric turbulence research is in relation to the correct assessment of the surface fluxes of momentum, heat and water vapor, as well (as environmental concerns grow) of other trace gases. It is not possible to relate the one-dimensional cospectra measured to the three-dimensional shell averages in wavenumber space which appear in the theory: this would be a worthy contribution, as well as a way to start to examine the effects of spatial sensor separation on the calculation of scalar fluxes.

On the experimental side of the picture, it seems important that in the future more attention be given to placing temperature and humidity (or any two scalars) sensors as close as possible, when their separation may influence the relevant measurements; it also seems desirable to average over periods longer than 30-min (which has become quite a common period for averages: all of the FIFE fluxes are reported as 30-min averages); during the night, at least, better and more stable statistics can be obtained with averages over one hour.

Appendix A
DIGITAL FILTERING
AND ANALOG MEASUREMENTS

The digital filter

$$\widetilde{a}(t+\Delta t) = \left(1 - \frac{\Delta t}{T}\right)\widetilde{a}(t) + \frac{\Delta t}{T}a(t) \tag{A.1}$$

where $\widetilde{a}$ is the low-pass filtered series with cutoff frequency $1/T$ and a is the "original" signal, is equivalent to an analog measurement with a sensor having a time constant T.

A sensor is often idealistically modeled as an R–C circuit. An applied electromotive forcel $\varepsilon(t)$ results in a potential difference $V(t)$ across the capacitor. We associate $\varepsilon(t)$ with the actual signal, and $V(t)$ with the sensor response. The equation for the R–C circuit is

$$\frac{dV}{dt} + \frac{1}{T}V = \frac{1}{T}\varepsilon(t) \tag{A.2}$$

where $T = C/R$ is the circuit's (sensor's) time constant, C is the capacitance and R the resistance. The solution is

$$V(t) = \int_0^t \frac{1}{T}e^{-\frac{t-\tau}{T}}\varepsilon(\tau)\,d\tau\ . \tag{A.3}$$

Now back to (A.1), put

$$\widetilde{a}(t+\Delta t) = \widetilde{a}(t) - \frac{\Delta t}{T}\widetilde{a}(t) + \frac{\Delta t}{T}a(t)$$

$$\frac{\widetilde{a}(t+\Delta t)-\widetilde{a}(t)}{\Delta t}=-\frac{1}{T}\widetilde{a}(t)+\frac{1}{T}a(t)\ . \tag{A.4}$$

In the limit as $\Delta t \to 0$,

$$\frac{d\widetilde{a}}{dt}+\frac{1}{T}\widetilde{a}(t)=\frac{1}{T}a(t)\ , \tag{A.5}$$

which is the same as (A.2).

Appendix B
THE SPECTRAL RADIATIVE DISSIPATION FUNCTION

In this appendix, standard results concerning the radiative dissipation function are derived. In section B.1, the equation for the spectral radiative dissipation function $N(k)$ defined and used in chapter 6 is derived. This result was originally obtained by Spiegel (1961). Then, in section B.2, we derive an equation that allows the calculation of $N(k)$ by means of average transmissions over frequency bands. That equation appears (but is not derived) in Coantic and Simonin (1984).

B.1 Derivation of the spectral radiative dissipation function

Consider Schwarzschild's equation for the radiative fluctuations,

$$\frac{dI'_\mu}{ds} = s_k \frac{\partial I'_\mu}{\partial x_k} = -\beta_\mu \overline{\rho}_v \left(I'_\mu - \frac{dB_\mu}{dT}\theta' \right) \tag{B.1}$$

Taking the Fourier Transform of both sides of the second equality,

$$i\,(s_k k_k)\widehat{I}_\mu = -\beta_\mu \overline{\rho}_v (\widehat{I}_\mu - \frac{dB_\mu}{dT}\widehat{\theta})$$

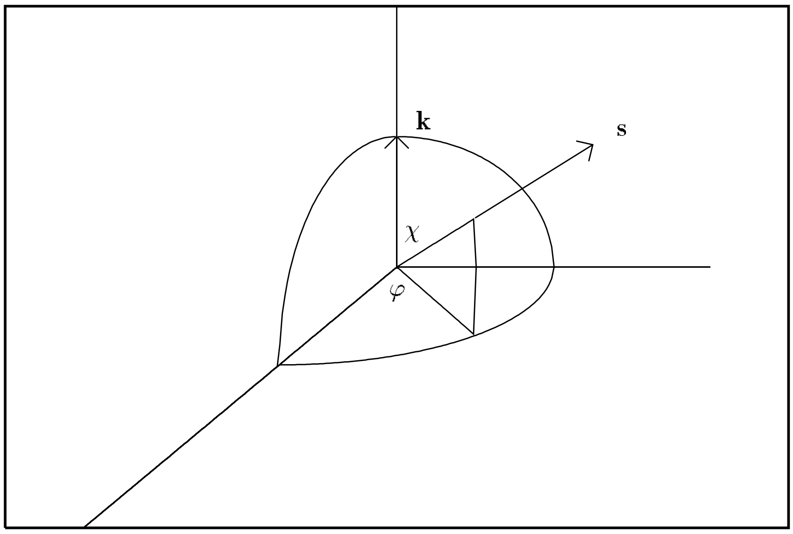

Figure B.1 – Spectral Integration Frame

$$\widehat{I}_\mu = \frac{\beta_\mu \overline{\rho}_v \frac{dB_\mu}{dT}}{i\,(\mathbf{s}\cdot\mathbf{k}) + \beta_\mu \overline{\rho}_v} \widehat{\theta} \tag{B.2}$$

The fluctuating radiative divergence is

$$\frac{\partial\, R'_k}{\partial x_k} = -\int_{\mu=0}^{\infty}\int_{\omega=0}^{4\pi} \beta_\mu \overline{\rho}_v (I'_\mu - \frac{dB_\mu}{dT}\theta')\, d\omega\, d\mu \tag{B.3}$$

and its Fourier transform is

$$\begin{aligned} \mathcal{F}\left\{\frac{\partial\, R'_k}{\partial x_k}\right\} &= -\int_{\mu=0}^{\infty}\int_{\omega=0}^{4\pi} \beta_\mu \overline{\rho}_v (\widehat{I}_\mu - \frac{dB_\mu}{dT}\widehat{\theta})\, d\omega\, d\mu \\ &= -\int_{\mu=0}^{\infty} \beta_\mu \overline{\rho}_v \left\{\int_{\omega=0}^{4\pi} \left[\frac{i\,(\mathbf{s}\cdot\mathbf{k})}{i\,(\mathbf{s}\cdot\mathbf{k}) + \beta_\mu \overline{\rho}_v}\right] d\omega \right\} \frac{dB_\mu}{dT}\widehat{\theta}\, d\mu \end{aligned} \tag{B.4}$$

Where (B.2) was used to obtain the last equality. To calculate the inner integral in (B.4), choose a reference frame such that $\mathbf{k} = (0, 0, k)$ (see Figure B.1) and

$$dA = k^2 \sin\chi \, d\varphi \, d\chi \tag{B.5-a}$$

$$d\omega = \frac{dA}{k^2} = \sin\chi \, d\varphi \, d\chi \tag{B.5-b}$$

$$(\mathbf{s}\cdot\mathbf{k}) = k\cos\chi \tag{B.5-c}$$

Using $\beta = \overline{\rho}_v \beta_\mu$ for simplicity, we now have

$$\begin{aligned}
\int_{\omega=0}^{4\pi} \left[\frac{i\,(\mathbf{s}\cdot\mathbf{k})}{i\,(\mathbf{s}\cdot\mathbf{k}) + \beta_\mu \overline{\rho}_v} \right] d\omega &= \int_{\varphi=0}^{2\pi} \int_{\chi=0}^{\pi} \left[\frac{i\,k\cos\chi}{\beta + \,i\,k\cos\chi} \right] \sin\chi \, d\chi \, d\varphi \\
&= 2\pi \int_{\chi=0}^{\pi} \frac{i\,k\sin\chi\cos\chi}{\beta + \,i\,k\cos\chi} \, d\chi \\
&= 2\pi \int_{\chi=0}^{\pi} \frac{(\beta - \,i\,k\cos\chi)(\,i\,k\sin\chi\cos\chi)}{(\beta - \,i\,k\cos\chi)(\beta + \,i\,k\cos\chi)} \, d\chi \\
&= 2\pi \int_{\chi=0}^{\pi} \frac{\beta\,i\,k\sin\chi\cos\chi}{\beta^2 + k^2\cos^2\chi} \, d\chi \\
&+ 2\pi \int_{\chi=0}^{\pi} \frac{k^2\cos^2\chi\sin\chi}{\beta^2 + k^2\cos^2\chi} \, d\chi
\end{aligned} \tag{B.6}$$

The first integral above is zero: set

$$\alpha = \chi - \pi/2 \tag{B.7}$$

and get

$$\int_{\alpha=-\pi/2}^{\pi/2} \frac{\beta\,i\,k\sin\alpha\cos\alpha}{\beta^2 + k^2\sin^2\alpha} \, d\alpha = 0, \tag{B.8}$$

because the integrand is odd. The second integral can be calculated with $u = \sin\alpha$ and $v = ku$:

$$\begin{aligned}
2\pi \int_{\alpha=-\pi/2}^{\pi/2} \frac{k^2\sin^2\alpha\cos\alpha}{\beta^2 + k^2\sin^2\alpha} \, d\alpha &= \frac{4\pi}{k} \int_0^1 \frac{(ku)^2}{\beta^2 + (ku)^2} k\,du \\
&= \frac{4\pi}{k} \int_0^k \frac{v^2}{\beta^2 + v^2} \, dv
\end{aligned}$$

$$= \frac{4\pi}{k}\int_0^k \left[1 - \frac{\beta^2}{\beta^2 + v^2}\right] dv$$
$$= 4\pi\left[1 - \frac{\beta}{k}\arctan\frac{k}{\beta}\right] \tag{B.9}$$

The spectral radiative dissipation function $N(k)$ is then

$$N(k) \equiv \frac{1}{\overline{\rho}c_p}\mathcal{F}\left\{\frac{\partial R'_k}{\partial x_k}\right\}\frac{1}{\widehat{\theta}}$$
$$= \frac{4\pi}{\overline{\rho}c_p}\int_{\mu=0}^{\infty}\overline{\rho}_v\beta_\mu\frac{dB_\mu}{dT}\left[1 - \frac{\beta_\mu\overline{\rho}_v}{k}\arctan\frac{k}{\beta_\mu\overline{\rho}_v}\right] d\mu \tag{B.10}$$

B.2 Determination of $N(k)$ with mean transmissions

To calculate $N(k)$ by means of a table of mean transmissions of the absorbing gas and their derivatives with respect to distance r, consider

$$T_\mu = e^{-\beta_\mu\overline{\rho}_v r} \tag{B.11-a}$$

$$T'_\mu = -\beta_\mu\overline{\rho}_v e^{-\beta_\mu\overline{\rho}_v r} \tag{B.11-b}$$

$$T''_\mu = (\beta_\mu\overline{\rho}_v)^2 e^{-\beta_\mu\overline{\rho}_v r} \tag{B.11-c}$$

and make use of the fact (Spiegel, 1992 p. 98)

$$\int_0^\infty e^{-ar}\frac{\sin br}{r}\, dr = \arctan\frac{b}{a} \tag{B.12}$$

Taking $(B.11 - b)$ and $(B.11 - c)$ into (B.10),

$$N(k) = \frac{4\pi}{\overline{\rho}c_p}\int_{\mu=0}^{\infty}\frac{dB_\mu}{dT}\left[T'_\mu(0) + \int_0^\infty\frac{T''(r)}{k}\frac{\sin kr}{r}\, dr\right] d\mu$$
$$= \frac{4\pi}{\overline{\rho}c_p}\sum_{j=1}^{N_B}\int_{\Delta\mu_j}\frac{dB_\mu}{dT}\left[T'_\mu(0) + \int_0^\infty\frac{T''(r)}{k}\frac{\sin kr}{r}\, dr\right] d\mu \tag{B.13}$$

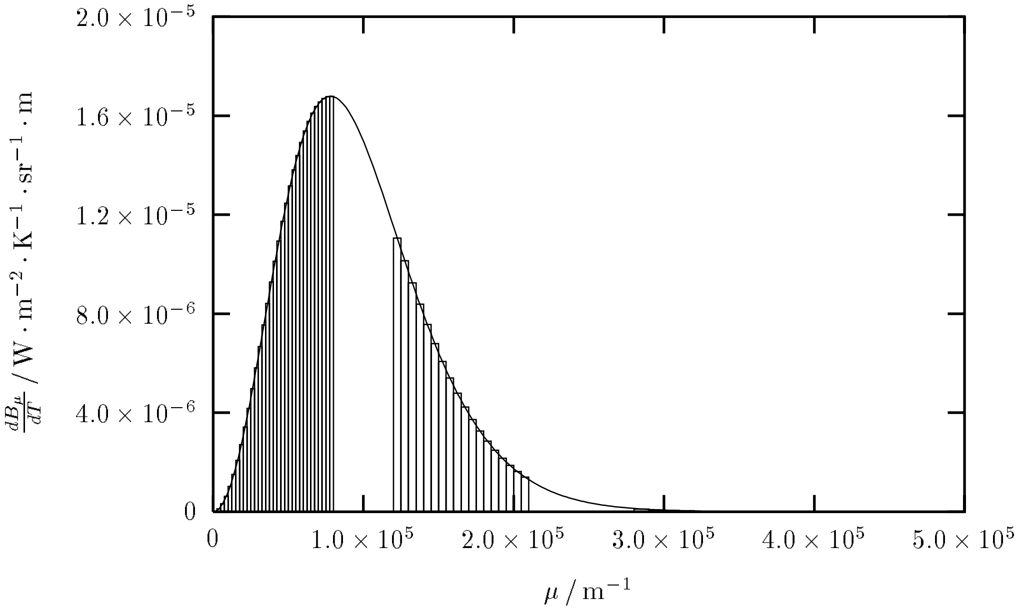

Figure B.2 – Planck's Function dB_μ/dT

where N_B is the number of absorption bands, each having width $\Delta\mu_j$, such that the whole spectrum is covered.

Figure B.2 shows the derivative dB_μ/dT of Planck's function for $T = 293.15\,\mathrm{K}$ together with the absorption bands in Houghton's (1986) tables (some of which cannot be seen in that scale). dB_μ/dT is approximately constant over the wavenumber ranges of the absorption bands, a typical value being $\Delta\mu = 2500\mathrm{m}^{-1}$. Therefore, (B.13) can be rewritten as

$$\begin{aligned} N(k) &\approx \frac{4\pi}{\overline{\rho}c_p} \sum_{j=1}^{N_B} \left[\frac{dB_{\mu_j}}{dT} \Delta\mu_j \right] \frac{1}{\Delta\mu_j} \int_{\Delta\mu_j} \left[T'_\mu(0) + \int_0^\infty \frac{T''(r)}{k} \frac{\sin kr}{r}\, dr \right] d\mu \\ &\approx \frac{4\pi}{\overline{\rho}c_p} \sum_{j=1}^{N_B} \frac{dB_{\mu_j}}{dT} \Delta\mu_j \left[\overline{T}'_\mu(0) + \int_0^\infty \frac{\overline{T}''(r)}{k} \frac{\sin kr}{r}\, dr \right] \end{aligned} \tag{B.14}$$

which should be compared with Coantic and Simonin's (1984) equation (34).

Appendix C

DERIVATION OF TWO-POINT EQUATIONS

Here we derive the equations for the covariance of two quantities a, b at two distinct points of space. Although the analysis is only spatial, extension to two different moments in time should be straightforward. Consider the points

$$\mathbf{x} \equiv (x_1, x_2, x_3) \tag{C.1-a}$$

$$\xi \equiv (\xi_1, \xi_2, \xi_3) = \mathbf{x} + \mathbf{r} \ . \tag{C.1-b}$$

We indicate the average and fluctuating parts of turbulent quantities at $\mathbf{x}$ and ξ as

$$a(\mathbf{x}, t) \equiv \overline{a} + a' \tag{C.2-a}$$

$$b(\xi, t) \equiv \overline{\overline{b}} + b'' \ . \tag{C.2-b}$$

We assume a homogeneous turbulence field, which means that the joint probability functions of the turbulence quantities are invariant under translation. This in turn implies that the covariances of two quantities at two distinct points are a function of the separation vector $\mathbf{r}$ alone:

$$\overline{a'b''} = f(\mathbf{r}) \tag{C.3-a}$$

$$\overline{b'a''} = g(\mathbf{r}) \ . \tag{C.3-b}$$

We now derive the Two-point covariance equations. Consider the fluctuations of any quantity a', b'' at two points. The equation for $a' = u_i'$ reads

$$\frac{\partial u_i'}{\partial t} + \overline{u}_k \frac{\partial u_i'}{\partial x_k} + u_k' \frac{\partial \overline{u}_i}{\partial x_k} + \frac{\partial u_i' u_k'}{\partial x_k} = \frac{g_i}{\overline{\theta}_v}\theta_v' - \frac{1}{\overline{\rho}}\frac{\partial p'}{\partial x_i} + \nu_{u_i}\frac{\partial^2 u_i'}{\partial x_k \partial x_k} + \frac{\partial \overline{u_i' u_k'}}{\partial x_k} \ . \quad \text{(C.4)}$$

Multiplying (C.4) by u_j'' and averaging:

$$\overline{\frac{\partial u_i'}{\partial t}u_j''} + \overline{u}_k \frac{\partial \overline{u_i' u_j''}}{\partial x_k} + \overline{u_k' u_j''}\frac{\partial \overline{u}_i}{\partial x_k} + \frac{\partial \overline{u_i' u_k' u_j''}}{\partial x_k} = \frac{g_i}{\overline{\theta}_v}\overline{\theta_v' u_j''} - \frac{1}{\overline{\rho}}\frac{\partial \overline{p' u_j''}}{\partial x_i} + \nu_{u_i}\frac{\partial^2 \overline{u_i' u_j''}}{\partial x_k \partial x_k} \ . \tag{C.5}$$

By symmetry,

$$\overline{u_i'\frac{\partial u_j''}{\partial t}} + \overline{\overline{u}}_k \frac{\partial \overline{u_i' u_j''}}{\partial \xi_k} + \overline{u_i' u_k''}\frac{\partial \overline{\overline{u}}_j}{\partial \xi_k} + \frac{\partial \overline{u_i' u_j'' u_k''}}{\partial \xi_k} = \frac{g_j}{\overline{\overline{\theta}}_v}\overline{u_i'\theta_v''} - \frac{1}{\overline{\overline{\rho}}}\frac{\partial \overline{u_i' p''}}{\partial \xi_j} + \nu_{u_j}\frac{\partial^2 \overline{u_i' u_j''}}{\partial \xi_k \partial \xi_k} \ . \tag{C.6}$$

Now with f (and g) as in (C.3), we relate derivatives of covariances with respect to x_i, ξ_i and r_i by

$$r_i = \xi_i - x_i \tag{C.7-a}$$

$$\frac{\partial f(x_j)}{\partial r_i} = \frac{\partial f}{\partial x_j}\frac{\partial x_j}{\partial r_i} = -\frac{\partial f}{\partial x_i} \tag{C.7-b}$$

$$\frac{\partial f(\xi_j)}{\partial r_i} = \frac{\partial f}{\partial \xi_j}\frac{\partial \xi_j}{\partial r_i} = \frac{\partial f}{\partial \xi_i} \ . \tag{C.7-c}$$

We shall also assume that

$$\frac{\partial \overline{\overline{a}}}{\partial \xi_k} \approx \frac{\partial \overline{a}}{\partial x_k} \tag{C.8-a}$$

$$\delta a \equiv \overline{\overline{a}} - \overline{a} \tag{C.8-b}$$

$$\delta a / \overline{a}^2 \ll 1 \ , \tag{C.8-c}$$

so that

$$\left(\frac{g}{\overline{\overline{a}}} - \frac{f}{\overline{a}}\right) = \frac{\overline{a}g - \overline{\overline{a}}f}{\overline{\overline{a}}\,\overline{a}} = \frac{\overline{\overline{a}}\,(g-f) - g\,\delta a}{\overline{\overline{a}}\,\overline{a}} \approx \frac{1}{\overline{a}}(g-f) \ . \tag{C.9}$$

Summing (C.5) and (C.6), and using (C.7), (C.8) and (C.9) , we get

$$\frac{\partial \overline{u_i'u_j''}}{\partial t} + (\overline{\overline{u}}_k - \overline{u}_k)\frac{\partial \overline{u_i'u_j''}}{\partial r_k} + \frac{\partial \overline{u}_i}{\partial x_k}\overline{u_k'u_j''} + \frac{\partial \overline{u}_j}{\partial x_k}\overline{u_i'u_k''} + \frac{\partial \left(\overline{u_i'u_j''u_k''} - \overline{u_i'u_k'u_j''}\right)}{\partial r_k} =$$
$$\frac{1}{\overline{\overline{\theta}}_v}(g_i\overline{\theta_v'u_j''} + g_j\overline{u_i'\theta_v''}) - \frac{1}{\overline{\overline{\rho}}}\left(\frac{\partial \overline{u_i'p''}}{\partial r_j} - \frac{\partial \overline{p'u_j''}}{\partial r_i}\right) + (\nu_{u_i} + \nu_{u_j})\frac{\partial^2 \overline{u_i'u_j''}}{\partial r_k \partial r_k} \ . \tag{C.10}$$

Finally, we express the difference in mean velocities between the two points by a Taylor expansion,

$$(\overline{\overline{u}}_k - \overline{u}_k) \approx \frac{\partial \overline{u}_k}{\partial x_l} r_l \ , \tag{C.11}$$

obtaining

$$\frac{\partial \overline{u_i'u_j''}}{\partial t} + \frac{\partial \overline{u}_k}{\partial x_l} r_l \frac{\partial \overline{u_i'u_j''}}{\partial r_k} + \frac{\partial \overline{u}_i}{\partial x_k}\overline{u_k'u_j''} + \frac{\partial \overline{u}_j}{\partial x_k}\overline{u_i'u_k''} + \frac{\partial \left(\overline{u_i'u_j''u_k''} - \overline{u_i'u_k'u_j''}\right)}{\partial r_k} =$$
$$\frac{1}{\overline{\overline{\theta}}_v}(g_i\overline{\theta_v'u_j''} + g_j\overline{u_i'\theta_v''}) - \frac{1}{\overline{\overline{\rho}}}\left(\frac{\partial \overline{u_i'p''}}{\partial r_j} - \frac{\partial \overline{p'u_j''}}{\partial r_i}\right) + (\nu_{u_i} + \nu_{u_j})\frac{\partial^2 \overline{u_i'u_j''}}{\partial r_k \partial r_k} \ . \tag{C.12}$$

Notice that (C.12) cannot be further simplified, because in general $\overline{a'b''} \neq \overline{b'a''}$. This also means that when $a \neq b$, there are *two* covariance equations, which almost doubles their number compared to the one-point equations of Chapter 2.

REFERENCES

1 Abramowitz, M. and Stegun, I.A. (1972), *Handbook of Mathematical Functions*, Dover.

2 Adachi, T. (1980), "Spectra of vertical wind component and temperature fluctuations of katabatic winds observed at Syowa station in case of great snow smokes on the antartic coastal slope", *Journal of The Meteorological Society of Japan* **58**, 436–442.

3 Adkins, C.J. (1986), *An Introduction to Thermal Physics*, Cambridge University Press.

4 Andreas, E.L. (1987), "On the Kolmogorov constants for the temperature-humidity cospectrum and the refractive index spectrum", *Journal of The Atmospheric Sciences* **44**, 2399–2406.

5 Angus, D.E. and Watts, P.J. (1984), "Evapotranspiration – How good is the Bowen ratio method?", *Agricultural Water Management* **8**, 133–150.

6 Antonia, R.A. and Atkinson, J.D. (1976), "A ramp model for turbulent temperature fluctuations", *The Physics of Fluids* **19**, 1273-1278.

7 Antonia, R.A., Chambers, A.J. and Bradley, E.F. (1981), "Temperature structure in the atmospheric surface layer II – The budget of mean cube fluctuations", *Boundary Layer Meteorology* **20**, 293–307.

8 Antonia, R.A. and Van Atta, C.W. (1975), "On the correlation between temperature and velocity dissipation in a heated turbulent jet", *Journal of Fluid Mechanics* **67**, 273–288.

9 Antonia, R.A. and Van Atta, C.W. (1978), "Structure functions of temperature fluctuations in turbulent shear flows", *Journal of Fluid Mechanics* **84**, 561–580.

10 Ariel, N.Z. and Nadezhina, Y.D. (1976), "Dimensionless turbulence characteristics under various stratification conditions", *Izv., Atmospheric and Oceanic Physics* **12**, 802–809.

11 Arya, S.P.S. (1973), "Comments on 'Radiation, evaporation and the maintenance of turbulence under stable conditions in the lower atmosphere' ", *Boundary Layer Meteorology* **3**, 392–393.

12 Arya, S.P.S. (1981), "Parameterizing the height of the stable atmospheric boundary layer", *Journal of Applied Meteorology* **20**, 1192–1202.

13 Assouline, S. and Mahrer, Y. (1993), "Evaporation from lake Kineret 1. Eddy correlation system measurements and energy budget estimates", *Water Resources Research* **29**, 4.

14 Batchelor, G.K. (1967), *An Introduction to Fluid Dynamics*, Cambridge University Press.

15 Bendat, J.S. and Piersol, A.G. (1986), *Random Data: Analysis and Measurement Procedures*, 2nd ed., John Wiley.

16 Benjamin, J.R. and Cornell, C.A. (1970), *Probability, Statistics and Decision for Civil Engineers*, McGraw-Hill.

17 Bertela, M. (1989), "Inconsistent flux partitioning by the Bowen ratio method." *Boundary Layer Meteorology* **49**, 149–167.

18 Bertoglio, J. (1981), "A model of three-dimensional homogeneous turbulence", *Turbulent Shear Flows III*, 253–261, Springer-Verlag.

19 Bertoglio, J. and Jeandel, D. (1987), "A simplified spectral closure for inhomogeneous turbulence: application to the boundary layer", *Turbulent Shear Flows V*, 19–30, Springer-Verlag.

20 Bignell, K.J. (1970), "The water-vapour infra-red continuum", *Quarterly Journal of the Royal Meteorological Society* **96**, 390–403.

21 Bolgiano, R. Jr. (1959), "Turbulent spectra in a stably stratified atmosphere", *Journal of Geophysical Research* **64**, 2226–2229.

22 Bradley, E.F., Antonia, R.A. and Chambers, A.J. (1981a), "Temperature structure in the atmospheric surface layer. I – The budget of temperature variance", *Boundary Layer Meteorology* **20**, 275–292.

23 Bradley E.F., Antonia, R.A. and Chambers, A.J. (1981b), "Turbulence Reynolds number and the turbulent kinetic energy balance in the atmospheric surface layer", *Boundary Layer Meteorology* **21**, 183–197.

24 Brost, R.A. (1979), "Some comments on the 'Turbulent exchange coefficients for sensible heat and water vapor under advective conditions", *Journal of Applied Meteorology* **18**, 378–380.

25 Brost, R.A. and Wyngaard, J.C. (1978), "A model study of the stably stratified planetary boundary layer", *Journal of The Atmospheric Sciences* **35**, 1427–1439.

26 Brutsaert, W. (1972), "Radiation, evaporation and the maintenance of turbulence under stable conditions in the lower atmosphere", *Boundary Layer Meteorology* **2**, 309–325.

27 Brutsaert, W. (1982), *Evaporation Into the Atmosphere*, D. Reidel.

28 Brutsaert, W. and Yeh, G.T. (1970), "Implications of a type of empirical evaporation formula for lakes and pans", *Water Resources Research* **6**, 1202–1208.

29 Businger, J.A. (1982), "Equations and Concepts", in *Atmospheric Turbulence and Air Pollution Modelling*, Nieuwstadt, F.T.M. and Van Dop, H. (ed.), D. Reidel.

30 Businger, J.A., Wyngaard, J.C., Izumi, Y. and Bradley, E.F. (1971), "Flux-Profile Relationships in the Atmospheric Surface Layer", *Journal of The Atmospheric Sciences* **28**, 181–189.

31 Businger, J.A. and Yaglom, A.M. (1971), "Introduction to Obukhov's Paper on 'Turbulence in An Atmosphere with A Non-Uniform Temperature' ", *Boundary Layer Meteorology* **2**, 3–6.

32 Caughey, S.J. (1982), "Observed Characteristics of The Atmospheric Boundary Layer" in *Atmospheric Turbulence and Air Pollution Modelling* (ed. Nieuwstadt F.T.M. and van Dop H.), D. Reidel.

33 Caughey, S.J., Wyngaard, J.C. and Kaimal, J.C. (1979), "Turbulence in the evolving stable boundary layer", *Journal of The Atmospheric Sciences* **36**, 1041–1052.

34 Champagne, F.H., Friehe, C.A., LaRue, J.C. and Wyngaard, J.C. (1977), "Flux measurements, flux estimation techniques, and fine-scale turbulence measurements in the unstable surface layer over land", *Journal of The Atmospheric Sciences* **34**, 515–530.

35 Chiba, O. (1989), "Buoyant subrange observed in the stably stratified atmospheric surface layer", *Journal of Applied Meteorology* **28**, 1236–1243.

36 Chimonas, G. (1985), "Apparent counter-gradient heat fluxes generated by atmospheric waves", *Boundary Layer Meteorology* **31**, 1–12.

37 Chollet, J.P. and Lesieur, M. (1981), "Parameterization of small scales of three-dimensional isotropic turbulence utilizing spectral closures", *Journal of The Atmospheric Sciences* **38**, 2747–2757.

38 Claussen, M. (1985a), "A model of turbulence spectra in the atmospheric surface layer", *Boundary Layer Meteorology* **33**, 151–172.

39 Claussen, M. (1985b), "Estimation of the Monin-Obukhov similarity functions from a spectral model", *Boundary Layer Meteorology* **33**, 233–243.

40 Coantic, M. and Simonin, O. (1984), "Radiative effects on turbulent temperature spectra and budgets in the planetary boundary layer", *Journal of The Atmospheric Sciences* **41**, 2629–2651.

41 Corrsin, S. (1951), "On the spectrum of isotropic temperature fluctuations in isotropic turbulence", *Journal of Applied Physics*, **22**, 469.

42 Corrsin, S. (1959), "Outline of some topics in homogeneous turbulent flow", *Journal of Geophysical Research* **64**, 2134–2150.

43 Corrsin, S. (1964), "Further generalization of Onsager's cascade model for turbulent spectra", *The Physics of Fluids* **8**, 1156–1159.

44 Crow, S.C. (1968), "Viscoelastic properties of fine-grained incompressible turbulence", *Journal of Fluid Mechanics* **33**, 1–20.

45 Dakos, T. and Gibson, M.M. (1987), "On modelling the pressure terms of the scalar flux equations", *Turbulent Shear Flows V*, 7–18, Springer-Verlag.

46 De Bruin, H.A.R., Koshiek, W. and Van der Hurk, B.J.J.M. (1993), "A verification of some methods to determine the fluxes of momentum, sensible heat and water vapor using standard deviation and structure parameter of scalar meteorological quantities", *Boundary Layer Meteorology* **63**, 231–257.

47 Deacon, E.L. (1988), "The streamwise Kolmogoroff constant", *Boundary Layer Meteorology* **42**, 9–17.

48 Deardorff, J.W. (1974), "Three-Dimensional numerical study of turbulence in an entraining mixing layer", *Boundary Layer Meteorology* **7**, 199–226.

49 Deissler, R.G. (1961), "Effects of inhomogeneity and of shear flow in weak turbulent fields", *The Physics of Fluids* **4**, 1187–1198.

50 Deissler, R.G. (1962), "Turbulence in the presence of a vertical body force and temperature gradient", *Journal of Geophysical Research* **67**, 3049–3062.

51 Domaradzki, J.A. and Mellor, G.L. (1984), "A simple turbulence closure hypothesis for the triple-velocity correlation functions in homogeneous isotropic turbulence", *Journal of Fluid Mechanics* **140**, 45–61.

52 Dyer, A.J. (1967), "The turbulent transport of heat and water vapor in an unstable atmosphere", *Quarterly Journal of the Royal Meteorological Society* **102**, 501–508.

53 Dyer, A.J. (1974), "A review of flux-profile relationships", *Boundary Layer Meteorology* **7**, 363–372.

54 Driedonks, A.G.M. and Tenekees, H. (1984), "Entrainment effects in the well-mixed atmospheric boundary layer", *Boundary Layer Meteorology* **30**, 75–105.

55 Eichinger, W. E., Cooper, D. I., Holtkamp, D. B., Karl Jr, R. R., Quick, C. R. and Tiee, J. J. (1993), "Derivation of water vapor fluxes from lidar measurements", *Boundary Layer Meteorology* **63**, 39–64.

56 EstourneL, C. and Guedalia, D. (1985), "Influence of geostrophic wind on atmospheric nocturnal cooling", *Journal of The Atmospheric Sciences* **42**, 2695–2698.

57 Estournel, C. and Guedalia, D. (1987), "A new parameterization of eddy diffusivities for nocturnal boundary-layer modeling", *Boundary Layer Meteorology* **39**, 191–203.

58 Fairall, C.W. and Larsen, S.E. (1986), "Inertial-dissipation methods and turbulent fluxes at the air-ocean interface", *Boundary Layer Meteorology* **34**, 287–301.

59 Fleagle, R.G. and Businger, J.A. (1980), "An Introduction to Atmospheric Physics", Academic Press.

60 Fox, J. (1964), "Velocity correlations in weak turbulent shear flow", *The Physics of Fluids* **7**, 562–564.

61 Frenzen, P. (1977), "A generalization of the Kolmogorov-von Karman relation and further implications on the values of the constants", *Boundary Layer Meteorology* **11**, 375–380.

62 Frenzen, P. and Voguel, C.A. (1992), "The turbulent kinetic energy budget in the atmospheric surface layer: a review and an experimental reexamination in the field", *Boundary Layer Meteorology* **60**, 49–76.

63 Fritschen, L.J. and Simpson, J.R. (1989), "Surface energy and radiation balance systems: general description and improvements", *Journal of Applied Meteorology* **28**, 680–689.

64 Fritschen, L. J., Qian, P., Kanemasu, E. T., Nie, D., Smith, E. A., Stewart, J. B., Verma, S. B. and Wesely, M. L. (1992), "Comparisons of surface flux measurement systems used in FIFE 1989", *Journal of Geophysical Research* **97 D17**, 18,697–18,713.

65 Gao, W., Wesely, M.L., Cook, D.R. and Hart, R.L. (1991), "Dry air-surface exchange in hilly terrain", *V International Conference on Precipitation Scavenging and Atmosphere-Surface Exchange Processes*, Richland, WA, U.S.A, July 15th–19th.

66 Garratt, J.R. (1972), "Studies of turbulence in the surface layer over water (Lough Neagh). Part II: production and dissipation of velocity and

temperature fluctuations", *Quarterly Journal of the Royal Meteorological Society* **98**, 642–657.

67 Garratt, J.R. (1975), "Limitations of the eddy-correlation technique for the determination of turbulent fluxes near the surface", *Boundary Layer Meteorology* **8**, 255–259.

68 Garratt, J.R. (1982), "Observations in the nocturnal boundary layer", *Boundary Layer Meteorology* **22**, 21–48.

69 Garratt, J.R. (1983), "Surface influence upon vertical profiles in the nocturnal boundary layer", *Boundary Layer Meteorology* **26**, 69–80.

70 Garratt, J.R. and Brost, R.A. (1981), "Radiative cooling within and above the nocturnal boundary layer", *Journal of The Atmospheric Sciences* **38**, 2730–2746.

71 Goody, R.M. (1964), *Atmospheric Radiation*, Oxford at the Clarendon Press.

72 Goody, R.M. and Yung, Y.L. (1989), *Atmospheric Radiation*, 2nd ed., Oxford University Press.

73 Gradshteyn, I.S. and Ryzhik, I.M. (1980), *Table of Integrals, Series and Products*, Academic Press, San Diego.

74 Gudiksen, P. H., Leone Jr, J. M., King, C. W., Ruffieux, D. and Neff, W. D. (1992), "Measurments and modeling of the effects of ambient meteorology on nocturnal drainage flows", *Journal of Applied Meteorology* **31**, 1023–1032.

75 Herring, J.R., Schertzer, D., Lesieur, M., Newman, G.R., Chollet, J.P., Larcheveque, M. (1982), "A comparative assessment of spectral closures as applied to passive scalar diffusion", *Journal of Fluid Mechanics* **124**, 411–437.

76 Herring, J.R. and Métais, O. (1989), "Numerical experiments in forced stably stratified turbulence", *Journal of Fluid Mechanics* **202**, 97–115.

77 Hicks, B.B. (1972), "Propeller Anemometers as Sensors of Atmospheric Turbulence", *Boundary Layer Meteorology* **3**, 214–228.

78 Hicks, B.B. (1976), "Wind profile relationships from the Wangara experiment", *Quarterly Journal of the Royal Meteorological Society* **102**, 535–551

79 Hicks, B.B. (1981), "An Examination of Turbulence Statistics in the Surface Boundary Layer", *Boundary Layer Meteorology* **21**, 389–402.

80 Hicks, B.B. and Everett, R.G. (1979), "Comments on 'Turbulent exchange coefficients for sensible heat and water vapor under advective conditions' ", *Journal of Applied Meteorology* **18**, 381–382.

81 Hill, R.J. (1978), "Models of the scalar spectrum for turbulent advection", *Journal of Fluid Mechanics* **88**, 541–562.

82 Hill, R.J. (1989a), "Implications of Monin-Obukhov similarity theory for scalar quantities", *Journal of The Atmospheric Sciences* **46**, 2236–2244.

83 Hill, R.J. (1989b), "Structure functions and spectra of scalar quantities in the inertial-convective and viscous-convective ranges of turbulence", *Journal of The Atmospheric Sciences* **46**, 2245–2251.

84 Hinze, J.O. (1975), *Turbulence*, 2nd ed., McGraw-Hill.

85 Högström, U. (1988), "Non-dimensional wind and temperature profiles in the atmospheric surface layer: a re-evaluation", *Boundary Layer Meteorology* **42**, 55–78.

86 Högstrom, U. (1990), "Analysis of turbulence structure in the surface layer with a modified similarity formulation for near neutral conditions", *Journal of The Atmospheric Sciences* **47**, 1949–1972.

87 Hojstrup, J. (1981), "A simple model for the adjustment of velocity spectra in unstable conditions downstream of an abrupt change in roughness and heat flux", *Boundary Layer Meteorology* **21**, 341–356.

88 Holtslag , A.A.M. and Moeng, C. (1991), "Eddy diffusivity and counter gradient transport in the convective atmospheric boundary layer", *Journal of The Atmospheric Sciences* **48**, 1690–1698.

89 Houghton, J.T. (1986), *The Physics of Atmospheres*, Cambridge University Press.

90 Hunt, J.C.R. (1985), "Diffusion in the stably stratified atmospheric boundary layer", *Journal of Climate and Applied Meteorology* **24**, 1187–1195.

91 Hunt, J.C.R., Kaimal, J.C. and Gaynor, J.E. (1985), "Some observations of turbulence structure in stable layers", Quart. J. R. Met. Soc. **111**, 793–815.

92 Jayesh, Kyunghwan, Y. and Warhaft, Z. (1991), "Turbulent mixing and transport in a thermally stratified interfacial layer in decaying grid turbulence", *Physics of Fluids A*, **3**, 1143–1155.

93 Jenkins, G.M. and Watts, D. G. (1968), *Spectral Analysis*, Holden-Day.

94 Kader, B.A. (1993), "Determination of turbulent momentum and heat fluxtes by spectral methods", *Boundary Layer Meteorology* **61**, 323-347.

95 Kader, B.A. and Yaglom, A.M. (1990), "Mean fields and fluctuating moments in unstably stratified turbulent boundary layers", *Journal of Fluid Mechanics* **212**, 637–662.

96 Kader, B.A. and Yaglom, A.M. (1991), "Spectra and correlation functions of surface layer atmospheric turbulence in unstable thermal stratification" in: Métais, O. and Lesieur, M. (editors), *Turbulence and Coherent Structures*, 387-412, Kluwer Academic Publishers, Dordrecht.

97 Kaimal, J.C. (1973), "Turbulence spectra, length scales and structure parameters in the stable surface layer", *Boundary Layer Meteorology* **4**, 289–309.

98 Kaimal, J.C., Wyngaard, J.C., Izumi, Y. and Coté, O. R. (1972), "Spectral characteristics of surface-layer turbulence", *Quarterly Journal of the Royal Meteorological Society* **98**, 563–589.

99 Kaimal, J.C., Clifford, S.F. and Lataitis, R.J. (1989), "Effect of finite sampling on atmospheric spectra", *Boundary Layer Meteorology* **47**, 337–347.

100 Kaimal, J.C. and Wyngaard, J.C. (1990), "The Kansas and Minesotta experiments", *Boundary Layer Meteorology* **50**, 31–47.

101 Kaimal, J.C. and Kristensen, L. (1991), "Time series tapering for short data samples", *Boundary Layer Meteorology* **57**, 187–194.

102 Katul, G.G. and Parlange, M.B. (1992), "A Penman-Brutsaert model for wet surface evaporation", *Water Resources Research* **28**, 121–126.

103 Kikuchi, T. and Chiba, O. (1985), "Step-like temperature fluctuations associated with ramps in a stable surface layer", *Boundary Layer Meteorology* **31**, 51–63.

104 Kondo, J., Kanechica, O. and Yasuda, N. (1978), "Heat and momentum transfers under strong stability in the atmospheric surface layer", *Journal of The Atmospheric Sciences* **35**, 1012–1021.

105 Koshiek, W. (1982), "Measuring C_T^2, C_Q^2 and C_{TQ} in the unstable surface layer, and relations to the vertical fluxes of heat and moisture", *Boundary Layer Meteorology* **24**, 89–107.

106 Koshiek, W., De Bruin, H.A.R., The, H., Van der Hurk, B. (1993) "Estimation of the sensible heat flux a a semi-arid area using surface radiative temperature measurements", *Boundary Layer Meteorology* **63**, 213–230.

107 Kraichnan, R.H. (1970), "Convergents to turbulence fluctuations", *Journal of Fluid Mechanics* **41**, 189–217.

108 Kristensen, L, Panofsky, H.A. and Smith, S.D. (1981), "Lateral coherence of longitudinal wind components in strong winds", *Boundary Layer Meteorology* **21**, 199–205.

109 Kristensen, L., Lenschow, D.H., Kierkegaard, P. e Courtney, M. (1989), “The spectral velocity tensor for homogenenous boundary-layer turbulence”, *Boundary Layer Meteorology* **47**, 149–193.

110 Kunkel, K.E. and Walters, D.L. (1982), “Intermittent turbulence in measurements of the temperature structure parameter under very stable conditions”, *Boundary Layer Meteorology* **22**, 49–60.

111 Kurzeja, R.J., Berman, S. and Weber, A.H. (1991), “A climatological study of the nocturnal planetary boundary layer”, *Boundary Layer Meteorology* **54**, 105–128.

112 Kustas, W.P. and Brutsaert, W. (1987), “Virtual heat entrainment in the mixed layer over very rough terrain”, *Boundary Layer Meteorology* **38**, pp. 141–157.

113 Kyunghwan, Y. and Warhaft, Z. (1990), “The evolution of grid-generated turbulence under conditions of stable thermal stratification”, *Journal of Fluid Mechanics* **215**, 601–638.

114 Lamb, R.G. (1982), “Diffusion in the convective boundary layer”, in *Atmospheric Turbulence and Air Pollution Modelling*, (ed. Nieuwstadt F. T. M. and van Dop H.), D. Reidel.

115 Lang, A.R.G., McNaughton, K.G., Fazu, C., Bradley, E.F. and Ohtaki, E. (1983a), “Inequality of eddy transfer coefficients for vertical transport of sensible and latent heats during advective inversions”, *Boundary Layer Meteorology* **25**, 25–41.

116 Lang, A.R.G., McNaughton, K.G., Fazu, C., Bradley, E.F. and Ohtaki, E. (1983b), "An experimental appraisal of the terms in the heat and moisture flux equations for local advection", *Boundary Layer Meteorology* **25**, 89–102.

117 Launder, B.E. (1975), "On the effects of a gravitational field on the turbulent transport of heat and momentum", *Journal of Fluid Mechanics* **67**, 569–581.

118 Leavitt, E. (1975), "Spectral characteristics of surface-layer turbulence over the tropical ocean", *Journal of Physical Oceanography*, **5**, 143–156.

119 Leclerc, M.V. and Thurtell, G.W. (1990), "Footprint prediction of scalar fluxes using a markovian analysis", *Boundary Layer Meteorology* **52**, 247–258

120 Lee, X. and Black, T.A. (1993), "Atmospheric turbulence within and above a Douglas-Fir stand. Part I: statistical properties of the velocity field", *Boundary Layer Meteorology* **64**, 149–174.

121 Leuning, R. and King, K.M. (1992), "Comparison of eddy-covariance measurements of CO_2 fluxes by open- and closed-path CO_2 analyzers", *Boundary Layer Meteorology* **59**, 297–311.

122 Lesieur, M. (1990), *Turbulence in Fluids*, 2nd ed., Kluwer Academic Publishers.

123 Lloyd, C.R., Culf, A.D., Dolman, A.J. and Gash, J.H.C. (1991), "Estimates of sensible heat flux from observations of temperature fluctuations", *Boundary Layer Meteorology* **57**, 311–322.

124 Lumley, J.L. (1964), "Spectral energy budget in wall turbulence", *The Physics of Fluids* **7**, 190–196.

125 Lumley, J.L. (1965), "Interpretation of time spectra measured in high-intensity shear flow", *Physics of Fluids* **8**, 1056–1062.

126 Lumley, J.L. (1970a), *Stochastic Tools in Turbulence*, Academic Press.

127 Lumley, J.L. (1970b), "Toward a turbulent constitutive relation", *Journal of Fluid Mechanics* **41**, 413–434.

128 Lumley, J.L. (1992), "Some comments on turbulence", *Physics of Fluids A* **4**, 203–211.

129 Lumley, J.L. and Panofsky, H. A. (1964), *The Structure of Atmospheric Turbulence*, Interscience.

130 Mahrt, L. (1989), "Intermittency of Atmospheric Turbulence", *Journal of The Atmospheric Sciences* **46**, 79–95.

131 McBean, G.A. and Elliot, J.A. (1980), "Pressure and humidity effects on optical refractive–index fluctuations", *Boundary Layer Meteorology* **20**, 101–109.

132 Mellor, G.L. and Yamada, T. (1974), "A hierarchy of turbulence closure models for planetary boundary layers", *Journal of The Atmospheric Sciences* **31**, 1791–1806 ; and (1977), "Corrigenda", *Journal of The Atmospheric Sciences* **34**, 1482.

133 Métais, O. and Herring, J.R. (1989), "Numerical simulations of freely evolving turbulence in stably stratified fluids", *Journal of Fluid Mechanics* **202**, 117–148.

134 Moeng, C. (1984), "A large-eddy simulation model for the study of planetary boundary-layer turbulence", *Journal of The Atmospheric Sciences* **41**, 2052–2062.

135 Moeng, C. and Wyngaard, J.C. (1986), "An analysis of closures for pressure-scalar covariances in the convective boundary layer", *Journal of The Atmospheric Sciences* **43**, 2,499–2,513.

136 Moncrieff, J. B., Verma, S. B. and Cook, D. R. (1992), "Intercomparison of eddy correlation carbon dioxide sensors during FIFE-89", *Journal of Geophysical Research* **97 D17**, 18,725–18,730.

137 Monin, A. S. (1970), "The atmospheric boundary layer", *Annual Reviews of Fluid Mechanics* **19**, 225–250.

138 Moore, C.J. (1986), "Frequency response corrections for eddy correlation systems", *Boundary Layer Meteorology* **37**, 17–35.

139 Moraes, O.L.L. and Epstein, M. (1987), "The velocity spectra in the stable surface layer", *Boundary Layer Meteorology* **40**, 407–414.

140 Moraes, O.L.L. and Goedert, J. (1988), "Kaimal's isopleths from a closure model", *Boundary Layer Meteorology* **45**, 83–92.

141 Nagano, Y. and Tagawa, M. (1990), "A structural turbulence model for triple products of velocity and scalar", *Journal of Fluid Mechanics* **215**, 639–657.

142 Nappo, C. J. (1991), "Sporadic breakdowns of stability in the PBL over simple and complex terrain", *Boundary Layer Meteorology* **54**, 69–87.

143 Nieuwstadt, F.T.M. (1984), "The turbulent structure of the stable, nocturnal boundary layer", *Journal of The Atmospheric Sciences* **41**, 2202–2216

144 Obukhov, A.M. (1946, 1971), "Turbulence in an atmosphere with non-uniform temperature", *Boundary Layer Meteorology* **2**, 7–29.

145 Ohtaki, E. (1985), "On the similarity in atmospheric fluctuations of carbon dioxide, water vapor and temperature over vegetated fields", *Boundary Layer Meteorology* **32**, 25–37.

146 Olesen, H.R., Larsen, S.E. and Hojstrup, J. (1984), "Modelling velocity spectra in the lower part of the planetary boundary layer",*Boundary Layer Meteorology* **29**, 285–312.

147 Panofsky, H.A. and Dutton, J.A. (1984), *Atmospheric Turbulence*, John Wiley.

148 Pao, Y.H. (1965) "Structure of turbulent velocity and scalar fields at large wavenumbers", *The Physics of Fluids* **8**, 1063–1075.

149 Paquin, J.E. and Pond, S. (1971), "The determination of the Kolmogorov constants for velocity, temperature and humidity fluctuations from second- and third-order structure functions", *Journal of Fluid Mechanics* **50**, 257–269.

150 Parlange, M.B. and Katul, G.G. (1992), "An advection–aridity evaporation model", *Water Resources Research* **28**, 127–132.

151 Penman, H.L. (1948), "Natural evaporation from open water, bare soil, and grass", *Proceedings of the Royal Society,* London **A193**, 120–146.

152 Phelps, G.T. and Pond, S. (1971), "Spectra of the temperature and humidity fluctuations and of fluxes of moisture and heat in the marine boundary layer", *Journal of The Atmospheric Sciences* **28**, 918–928.

153 Press, W.H., Teukolsky, S.A., Vetterling, W.T. and Flannery, B.P. (1992), *Numerical Recipes in C*, 2nd ed., Cambridge University Press.

154 Priestley, J.T. and Hill, R.J. (1985), "Measuring high-frequency humidity, temperature and radio refractive index in the surface layer", *Journal of Atmospheric and Oceanic Technology* **2**, 233–251.

155 Priestley, C.H.B. and Taylor, R.J. (1972), "On The Assessment of Surface Heat Flux and Evaporation Using Large-Scale Parameters", *Monthly Weather Review* **100**, 81–92.

156 Raupach, M.R. (1978), "Infrared fluctuation hygrometry in the atmospheric surface layer", *Quarterly Journal of the Royal Meteorological Society* **104**, 309–322.

157 Raupach, M.R., Weng, W.S., Carruthers, D.J. and Hunt, J.C.R. (1992), "Temperature and humidity fields and fluxes over low hills", *Quarterly Journal of the Royal Meteorological Society* **118**, 191-225.

158 Rees, J.M. (1991), "On the characteristics of eddies in the stable atmospheric boundary layer", *Boundary Layer Meteorology* **55**, 325–343.

159 Roberts, R.E., Selby, J.E.A. and Biberman, L.M. (1976), "Infrared continuum absorption by atmospheric water-vapor in the 8–12 μm window", *Applied Optics* **15**, 2085–2090.

160 Rodgers, C.D. and Walshaw, C.D. (1966), “The computation of infra-red cooling rate in planetary atmospheres”, *Quarterly Journal of the Royal Meteorological Society* **92**, 67–92.

161 Schertzer, D. and Simonin, O. (1981), “A theoretical study of radiative cooling in homogeneous and isotropic turbulence”, *Turbulent Shear Flows III*, Springer-Verlag.

162 Schmitt, K.F., Friehe, C.A. and Gibson, C.H. (1981), “Structure of marine surface layer turbulence”, *Journal of The Atmospheric Sciences* **36**, 602–618.

163 Sellers, P.J., Hall, F.G., Asrar, G., Strebel, D.E. and Murphy, R.E. (1992), “An overview of the First International Satellite Land Surface Climatology Project ISLSCP Field Experiment (FIFE)”, *Journal of Geophysical Research* **97 D17**, 18,345–18,371.

164 Shaw, W.J. and Businger, J.A. (1985), “Intermittency and the organization of turbulence in the near-neutral marine atmospheric boundary layer”, *Journal of The Atmospheric Sciences* **42**, 2563–2584.

165 Sheppard, P.A., Tribble, D.T. and Garratt, J.R. (1972), “Studies of turbulence in the surface layer over water (Lough Neagh). Part I: instrummentation, programme, profiles”, *Quarterly Journal of the Royal Meteorological Society* **98**, 627–641.

166 Shved, G.M. (1978), “Influence of radiative transfer on certain types of motions in planetary atmospheres”, *Advances in Heat Transfer* **14**, 249–280.

167 Simonin, O., Coantic, M. and Schertzer, D. (1981), "Effet du rayonnement infrarouge sur la turbulence de témperature dans l'atmosphère: structule spectrale et taux de dissipation", *Comptes Rendus,* Acad. Sc. Paris **293**, 245–248.

168 Smedman-Högström, A.S. (1973), "Temperature and humidity spectra in the atmospheric surface layer", *Boundary Layer Meteorology* **3**, 329–347.

169 Smedman, A.S. (1988), "Observations of a multi-level turbulence structure in a very stable atmospheric boundary layer", *Boundary Layer Meteorology* **44**, 231–253

170 Smedman, A.S. (1991), "Some turbulence characteristics in stable atmospheric boundary layer flow", *Journal of The Atmospheric Sciences* **48**, 856–868.

171 Spiegel, E.A. (1957), "The smoothing of temperature fluctuations by radiative transfer", *Astrophysical Journal* **126**, 202–207.

172 Spiegel, M.R. (1992), *Mathematical Handbook of Formulas and Tables*, McGraw-Hill.

173 Stewart, R.W., Wilson, J.R. and Burling, R.W. (1970), "Some statistical properties of small scale turbulence in an atmospheric boundary layer", *Journal of Fluid Mechanics* **41**, 141–152.

174 Straka, J., Fiedler, F. and Hinzpeter, H. (1977), "Spectral transfer of turbulent energy and temperature variance", *Beiträge zur Physik der Atmosphäre* **51**, 60–85.

175 Stull, R.B. (1988), *An Introduction to Boundary Layer Meteorology*, D. Reidel.

176 Stull, R.B. (1991), “Static stability — an update”, *Bulletin of the American Meteorological Society* **72**, 1521–1529.

177 Sugita, M. and Brutsaert, W. (1990), “How similar are temperature and humidity in the unstable boundary layer?”, *Journal of Applied Meteorology* **29**, 489–497.

178 Sugita, M. and Brutsaert, W. (1991), “Daily evaporation over a region from lower boundary-layer profiles measured with radiosondes”, *Water Resources Research* **27**, 747–752.

179 Swinbank, W.C. and Dyer, A.J. (1967), “An experimental study in micrometeorology”, *Quarterly Journal of the Royal Meteorological Society* **102**, 494–500.

180 Tennekes, H. (1982), “Similarity Relations, Scaling Laws and Spectral Dynamics”, in *Atmospheric Turbulence and Air Pollution Modelling* (ed. Nieuwstadt F.T.M. and van Dop H.), D. Reidel.

181 Tennekes, H. and Lumley, J.L. (1972), *A First Course in Turbulence*, The M.I.T. Press.

182 Thorodsen, S.T. and Van Atta, C.W. (1992), “Exponential tails and skewness of density-gradient functions in stably stratified turbulence”, *Journal of Fluid Mechanics* **244**, 547–566.

183 Tillman, J.E. (1972), “The indirect determination of stability, heat and momentum fluxes in the atmospheric boundary layer from simple scalar

variables during dry unstable conditions", *Journal of Applied Meteorology* **11**, 783–792.

184 Tjemkes, S.A. and Duynkerke, P.G. (1988), "A new look at the Goody band model", *Beiträge zur Physik der Atmosphäre* **61**, 105–113.

185 Tjemkes, S.A. and Duynkerke, P.G. (1989), "The nocturnal boundary layer: model calculations compared with observations", *Journal of Applied Meteorology* **28**, 161–175.

186 Todorovic, P. (1992), *An Introduction to Stochastic Processes and Their Applications*, Springer Verlag.

187 Townsend, A.A. (1958), "The effects of radiative transfer on turbulent flow of a stratified fluid", *Journal of Fluid Mechanics* **4**, 361–375.

188 Tritton, D.J. (1988), *Physical Fluid Dynamics*, Oxford.

189 Van Atta, C.W. (1977), "Effect of coherent structures on structure functions of temperature in the atmospheric boundary layer", *Archives of Mechanics* **29**, 161–171.

190 Van Atta, C.W. (1977), "Second-order spectral local isotropy in turbulent scalar fields", *Journal of Fluid Mechanics* **80**, 609–615.

191 Van Atta, C.W. and Yeh, T.T. (1970), "Some measurements of multi-point time correlations in grid turbulence", *Journal of Fluid Mechanics* **41**, 169–178.

192 Verma, S.B., Rosenberg, N.J. and Blad, B. L. (1978), "Turbulent exchange coefficients for sensible heat and water vapor under advective conditions", *Journal of Applied Meteorology* **17**, 330–338.

193 Viswanadham, Y. (1982), "Examination of the empirical flux-profile models in the atmospheric surface boundary layer", *Boundary Layer Meteorology* **22**, 61–77.

194 Wang, J. and Mitsuta, Y. (1991), "Turbulence structure and transfer characteristics in the surface layer of the HEIFE Gobi area", *Journal of the Meteorological Society of Japan* **69**, 587–593.

195 Wang, J. and Mitsuta, Y. (1992), "An observational study of turbulent structure and transfer characteristics in Heife Oasis", *Journal of the Meteorological Society of Japan* **70**,

196 Warhaft, Z. (1976), "Heat and moisture flux in the stratified boundary layer", *Quarterly Journal of the Royal Meteorological Society* **102**, 703–707.

197 Warhaft, Z. (1981), "The use of dual heat injection to infer scalar covariance decay in grid turbulence", *Journal of Fluid Mechanics* **104**, 93–109.

198 Warhaft, Z. (1984), "The interference of thermal fields from line sources in grid turbulence", *Journal of Fluid Mechanics* **144**, 363–387.

199 Warhaft, Z. and Bolgiano Jr., R. (1984), "Moisture and heat transport in a stably stratified boundary layer over a water surface", in *Gas Transfer at Water Surfaces* (ed. Brutsaert, W. and Jirka, G. H.), 133–143, D. Reidel.

200 Weaver, H.L. (1990), "Temperature and humidity flux–variance relations determined by one-dimensional eddy correlation", *Boundary Layer Meteorology* **53**, 77–91.

201 Webb, E.K., Pearman, G.I. and Leunig, R. (1980), "Correction of flux measurements for density effects due to heat and vapor transfer", *Quarterly Journal of the Royal Meteorological Society* **106**, 85-100.

202 Webster, I.T. and Burling, R.W. (1981), "A test of isotropy and Taylor's hypothesis in the atmospheric boundary layer", *Boundary Layer Meteorology* **20**, 429–443.

203 Weinstock, J. (1978), "On the theory of turbulence in the buoancy range of stably stratified flows", *Journal of The Atmospheric Sciences* **33**, 634–649.

204 Wesely, M.L. (1976), "A comparison of two optical methods for measuring line averages of thermal exchanges above warm water surfaces", *Journal of Applied Meteorology* **15**, 1,177–1,188.

205 Wesely, M.L. and Hicks, B.B. (1978), "High–frequency temperature and humidity correlation above a warm wet surface", *Journal of Applied Meteorology* **17**, 123–128.

206 Wesely, M.L. (1983), "Turbulent transport of ozone to surfaces common in the eastern half of the United States", in: *Trace Atmospheric Constituents: Properties, Transformations and Fates*, (ed. Scharz, S.E.), John Wiley.

207 Wesely, M.L. (1988), "Use of Variance Techniques to Measure Dry Air-Surface Exchange Rates", *Boundary Layer Meteorology* **44**, 13–31.

208 Wetzel, P.J. (1982), "Toward parameterization of the stable boundary layer", *Journal of Applied Meteorology* **21**, 7–13.

209 Williams, A.G. and Hacker, J.M. (1993), "Interactions between coherent eddies in the lower convective boundary layer", *Boundary Layer Meteorology* **64**, 55–74.

210 Wittich, K.P. (1991), "The nocturnal boundary-layer over Northern Germany: an observational study", *Boundary Layer Meteorology* **55**, 47–66.

211 Woods, J.D. (1969), "On Richardson's number as a criterion for laminar-turbulent-laminar transition in the ocean and atmosphere", *Radio Science* **4**, 1289–1298.

212 Wyngaard, J.C. and Coté, O.R. (1971), "The budgets of turbulent kinetic energy and temperature variance in the atmospheric surface layer",*Journal of The Atmospheric Sciences* **28**, 190–201.

213 Wyngaard, J.C., Coté, O.R. and Izumi, Y. (1971) "Local free convection similarity, and the budgets of shear stress and heat flux", *Journal of The Atmospheric Sciences* **28**, 1,171–1,182

214 Wyngaard, J. C. and Coté, O. R. (1972), "Cospectral similarity in the atmospheric surface layer", *Quarterly Journal of the Royal Meteorological Society* **98**, 590–603.

215 Wyngaard, J.C. (1973), "On surface-layer turbulence", in *Workshop on micrometeorology*, Haugen, D.A. (ed.), American Meteorological Society, Boston.

216 Wyngaard, J.C. (1975), "Modeling the planetary boundary layer – extension to the stable case", *Boundary Layer Meteorology* **9**, 441–460.

217 Wyngaard, J.C., Pennell, W.T., Lenschow, D.H. and Lemone, M.A. (1978), "The temperature-humidity covariance budget in the convective boundary layer", *Journal of The Atmospheric Sciences* **35**, 47–58.

218 Wyngaard, J.C. and Clifford, S.F. (1978), "Estimating momentum, heat and moisture fluxes from surface structure parameters", *Journal of The Atmospheric Sciences* **35**, 1024–1211.

219 Wyngaard, J.C. (1982), "Boundary-layer modeling", in *Atmospheric Turbulence and Air Pollution Modelling* (ed. Nieuwstadt F. T. M. and van Dop H.), D. Reidel.

220 Wyngaard, J.C., Businger, J.A, Kaimal, J.C. and Larsen, S.E. (1982), "Comments on 'A reevaluation of Kansas mast influence on measurements of stress and cup anemometer overspeeding' ", *Boundary Layer Meteorology* **22**, 245–250.

221 Wyngaard, J.C. and Brost, R.A. (1984), "Top-down and bottom-up diffusion of a scalar in the convective boundary layer", *Journal of The Atmospheric Sciences* **41**, 102–112.

222 Wyngaard, J.C. (1988), "The effects of probe–induced flow distortion on atmospheric turbulence measurements: extension to scalars", *Journal of The Atmospheric Sciences* **45**, 3,400–3,412.

223 Wyngaard, J.C. (1988), "Flow-distortion effects on scalar flux measurements in the surface layer: implications for sensor design", *Boundary Layer Meteorology* **42**, 19–26.

224 Wyngaard, J.C. (1990), "Scalar fluxes in the planetary boundary layer-theory, modeling and measurement", *Boundary Layer Meteorology* **50**, 49–75.

225 Yaglom, A.M. (1977), "Comments on wind and temperature flux-profile relationships", *Boundary Layer Meteorology* **11**, 89–102.